Neutron and X-ray tomography as research tools for applied research in South Africa

Frederik C. De Beer
21663912

Thesis submitted in fulfillment of the requirements for the degree *Doctor Philosophiae* in Chemical Engineering
at the Potchefstroom Campus of the North-West University, South Africa.

Supervisor: Prof F Waanders (NWU)
Co-supervisor: Dr G Nothnagel (Necsa)

November 2017

Aan my geliefde vrou: Chevaune

en my kinders: Joalet, Elisna en Frikkie

DECLARATION

I, **Frederik Coenraad de Beer**, hereby declare that this thesis entitled:

"***Neutron and X-ray tomography as research tools for applied research in South Africa***",

submitted in fulfilment of the requirements for the degree Ph.D in Chemical Engineering is my own work and has not previously been submitted to any other institution in whole or in part. Written consent from authors had been obtained for publications where co-authors have been involved.

Signed at Brits on the 19th day of November 2017

Frikkie de Beer

PREFACE

Thesis Layout

This document is a thesis for a PhD by publication in the field of the use of penetrating radiation for non-destructive investigation, through the use of radiography and tomography techniques. Apart from the inclusion of a chapter in a book (Chapter 4 of this thesis), three further peer reviewed publications (Chapters 5, 6 and 7 of the thesis) were included in the same original format as in their respective journals. These publications were selected to cover some aspects of research facility design and to demonstrate the usefulness of the facilities and techniques to enhance research quality in a number of selected fields.

The book chapter, included here as Chapter 4, has been chosen because it provides a general overview of the wide scope of applications of radiography and tomography in the field of palaeontology, a vibrant research field in South Africa, with many local and international researchers that benefit from the facilities established through the initiative of the author and described in this thesis. Chapter 5 consists of a paper that shows how neutron radiography (NRAD) can be used to study aspects of hydrogen fuel cells, a sub-discipline of the field of Hydrogen Economy in general, which is a study area supported by the South African Department of Science and Technology. Chapter 6 consists of a publication that describes how X-ray and neutron radiography and tomography can be used as non-invasive diagnostics to study nuclear materials; another important area of interest when nuclear energy technology has to be localised as part of a future South African energy mix. Chapter 7 consists of a publication that describes aspects of the development of a new world-class neutron radiography facility at the SAFARI-1 research reactor, with emphasises on the use of local materials to design the radiation shielding.

Apart from these chapters the rest of the document has been prepared in the form of a self-consistent thesis, with an introduction and background, technical description of the principles of the techniques employed, a historical overview of developments in the field of radiography and tomography with reference to the contributions of the PhD candidate, hereafter referred to as “the author” and with a perspective on future developments. These chapters contain references, inter alia, to peer reviewed publications as author and co-author, other than those selected as requirements for the PhD by publication, which allows insight into his contributions towards the establishment of a valuable South African skills platform in radiography and tomography.

Thesis Format

The format of this thesis is a self-consistent description of a research capability development augmented with a series of original articles as allowed for in rule 5.1.1 of the General Academic Rules 2015, approved on the 18th November 2014. Other rules that are applicable to the publication of a doctoral thesis as a series of original articles are rules A.5.4.2.7; A.5.4.2.8 and A.5.4.2.9.

Rule 5.1.1 states:

> *"The structure of a doctoral degree is prescribed by faculty rules and may be acquired through the –*
>
> *5.1.1.1 writing of a thesis; or*
>
> *5.1.1.2 writing of a series of original articles; or*
>
> *5.1.1.3 registration of an internationally examined patent; or*
>
> *5.1.1.4 performance of a concert series; or*
>
> *5.1.1.5 compilation of a composition portfolio, or*
>
> *5.1.1.6 presentation of an art exhibition,*
>
> *provided that the research product submitted for examination makes a distinct contribution to the knowledge of and insight into a subject field and produces proof of originality, either by the revelation of new facts or by the exercising of an independent critical capacity."*

Rule ***A.5.4.2.7*** states:

> "*Where an author is permitted to submit a thesis in the form of a published research article or articles, or as an unpublished manuscript or manuscripts in article format and more than one such article or manuscript is used, the thesis must still be presented as a unit, supplemented with an inclusive problem statement, a focused literature analysis and integration and with a synoptic conclusion, and the guidelines of the journal concerned must also be included.*"

Rule ***A.5.4.2.8*** states:

> "*Where any research article or manuscript and/or internationally examined patent is used for the purpose of a thesis in article format to which other authors and/or inventors than the author contributed, the author must obtain a written statement from each co-author and/or co-inventor in which it is stated that such co-author and/or co-inventor grants permission that the research article or manuscript and/or patent may be used for the stated purpose and in which it is further indicated what each co-author's and/or co-inventor's share in the relevant research article or manuscript and/or patent was*."

Rule ***A.5.4.2.9*** states:

> *"Where co-authors or co-inventors as referred to in A.5.4.2.8 above were involved, the author must mention that fact in the preface and must include the statement of each co-author or co-inventor in the thesis immediately following the preface."*

Format of Numbering and Referencing

It should be noted that the formatting, referencing style, numbering of tables and figures, and general outline of the manuscripts were adapted to ensure uniformity throughout the thesis. The format of manuscripts which have been submitted and/or published adhere to the author guidelines as stipulated by the editor of each journal, and may appear in a different format to what is presented in this thesis. The headings and original technical content of the manuscripts were not modified from the submitted and/or published versions, and only minor spelling and typographical errors were corrected.

A list of references cited in each chapter is given at the end of that chapter.

STATEMENT FROM CO-AUTHORS

The following section contains all the statements of consent of the various co-authors of the various articles that are contained in this thesis.
(These letters of consent complies with rules *A.5.4.2.8 and A.5.4.2.9* of the academic rules, as stipulated by the North-West University).

The following is a list of all of the co-authors that contributed to the various publications:

Statement of consent: Dr. Dmitri Bessarabov

To whom it may concern

I, **DMITRI BESSARABOV**, hereby give FRIKKIE DE BEER consent to use the publication listed below, of which I am co-author, in the thesis entitled “Neutron and X-ray tomography as research tools for applied research in South Africa”. The thesis is submitted for the degree *Doctor Philosophiae in Chemical Engineering* at the Potchefstroom campus of the North-West University, South Africa:

- Frikkie de Beer, Jan-Hendrik van der Merwe and *Dmitri Bessarabov*, 2017. PEM water electrolysis: preliminary investigations using neutron radiography. *Physics Procedia,* 88, p19-26. (PA: 8th International Topical Meeting on Neutron Radiography, Beijing, China, 4-8 September 2016).

As Director: DST National Center of Competence: Hydrogen Infrastructure (HySA Infrastructure) located at the North West University (Potchefstroom Campus), I was responsible for recommendation of the hardware, selection of the PEM membrane (3M was selected) and joint discussion of the results used in the manuscript listed above. I was also responsible for significant proofing and editing of the manuscript, written by Frikkie de Beer, listed above.

This statement satisfies Rule A.5.4.2.8 and Rule A.5.4.2.9 of the General Academic Rules 2015 of the North-West University.

Signed at Potchefstroom on the 21th day of October 2017.

DMITRI BESSARABOV

Digitally signed by DMITRI BESSARABOV
DN: cn=DMITRI BESSARABOV, o=FACULTY OF ENGINEERING, HYSA INFRASTRUCTURE CENTRE OF COMPETENCE, ou=DIRECTOR, email=Dmitri.Bessarabov@nwu.ac.za, c=ZA
Date: 2017.10.23 11:06:31 +02'00'

D. Besserabov

Statement of consent: Dr. Nikolay Kardjilov

To whom it may concern

I, **NIKOLAY KARDJILOV**, hereby give FRIKKIE DE BEER consent to use the publication listed below, of which I am Editor of the Book, in the thesis entitled “Neutron and X-ray tomography as research tools for applied research in South Africa”. The thesis is submitted for the degree *Doctor Philosophiae in Chemical Engineering* at the Potchefstroom campus of the North-West University, South Africa:

- Chapter in book:
  Editors of the book: *Kardjilov, Nikolay*, Festa, Giulia (Eds.), Book Title: Neutron Methods for Archaeology and Cultural Heritage, Chapter 7: Paleontology: Fossilized Ancestors Awaken by Neutron Radiography, F.C. de Beer. Publisher Name: Springer International Publishing. Publisher Location: ChamSeries ID8141Series. Title: Neutron Scattering Applications and Techniques. Print ISBN: 978-3-319-33161-4, http://dx.DOI10.1007/978-3-319-33163-8, 2016

As Head of the neutron tomography group at HZB employed by the Helmholtz-Zentrum, Berlin Germany, I was responsible for selecting outstanding experts in neutron and X-ray imaging worldwide for contributing to the book. Frikkie de Beer accepted the invitation to contribute to the book and provided the manuscript in time and in good quality. I was also responsible for significant proofing and editing of the manuscript, written by Frikkie de Beer, listed above.

This statement satisfies Rule A.5.4.2.8 and Rule A.5.4.2.9 of the General Academic Rules 2015 of the North-West University.

Signed at Berlin on the 11th day of October 2017.

N. Kardjilov

Statement of consent: Dr. Burkhard Schillinger

To whom it may concern

I, **BURKHARD SCHILLINGER**, hereby give FRIKKIE DE BEER consent to use the publication listed below, of which I am co-author, in the thesis entitled “Neutron and X-ray tomography as research tools for applied research in South Africa”. The thesis is submitted for the degree *Doctor Philosophiae in Chemical Engineering* at the Potchefstroom campus of the North-West University, South Africa:

- F.C. de Beer, *M.J. Radebe*, B. Schillinger, R. Nshimirimana, M.A. Ramushu, T. Modise., 2015, Upgrading the Neutron Radiography Facility in South Africa (SANRAD): Concrete Shielding Design Characteristics. Physics Procedia, 69, p115-123. (PA: 10th World Conference on Neutron Radiography, Grindelwald, Switzerland, 5 - 9 October 2014)

As Instrument scientist for the ANTARES Neutron Imaging facility employed by the Technische Universität München - FRM II, Heinz Maier-Leibnitz Zentrum, Garching, Germany, I was responsible for the original development of the first ANTARES facility and it’s shielding at FRMII used in the manuscript listed above. I was also responsible for significant proofing and editing of the manuscript, written by Frikkie de Beer, listed above.

This statement satisfies Rule A.5.4.2.8 and Rule A.5.4.2.9 of the General Academic Rules 2015 of the North-West University.

Signed at Garching on the 23rd day of October 2017.

B. Schillinger

Statement of consent: Mr. M.A. Ramushu

To whom it may concern

I, **MOGOBI RAMUSHU**, hereby give FRIKKIE DE BEER consent to use the publication listed below, of which I am co-author, in the thesis entitled “Neutron and X-ray tomography as research tools for applied research in South Africa”. The thesis is submitted for the degree *Doctor Philosophiae in Chemical Engineering* at the Potchefstroom campus of the North-West University, South Africa:

- F.C. de Beer, *M.J. Radebe*, B. Schillinger, R. Nshimirimana, M.A. Ramushu, T. Modise., 2015, Upgrading the Neutron Radiography Facility in South Africa (SANRAD): Concrete Shielding Design Characteristics. Physics Procedia, 69, p115-123. (PA: 10th World Conference on Neutron Radiography, Grindelwald, Switzerland, 5 - 9 October 2014).

As a Civil Engineer employed by Necsa, I was responsible for the South African version of the development and design of the high density shielding concrete used in the manuscript listed above. I was also responsible for significant proofing and editing of the manuscript, written by Frikkie de Beer, listed above.

This statement satisfies Rule A.5.4.2.8 and Rule A.5.4.2.9 of the General Academic Rules 2015 of the North-West University.

Signed at Pretoria on the 23rd day of October 2017.

M.A. Ramushu

Statement of consent: Mr. Robert B. Nshimirimana

To whom it may concern

I, **ROBERT NSHIMIRIMANA**, hereby give FRIKKIE DE BEER consent to use the publication listed below, of which I am co-author, in the thesis entitled “Neutron and X-ray tomography as research tools for applied research in South Africa”. The thesis is submitted for the degree *Doctor Philosophiae in Chemical Engineering* at the Potchefstroom campus of the North-West University, South Africa:

- F.C. de Beer, *M.J. Radebe*, B. Schillinger, R. Nshimirimana, M.A. Ramushu, T. Modise., 2015, Upgrading the Neutron Radiography Facility in South Africa (SANRAD): Concrete Shielding Design Characteristics. Physics Procedia, 69, p115-123. (PA: 10th World Conference on Neutron Radiography, Grindelwald, Switzerland, 5 - 9 October 2014).

As a Scientist employed by the South African Nuclear Energy Corporation SOC Ltd. and co-worker on neutron radiography, I was responsible for the concrete homogeneity experiment and analysis used in the manuscript listed above. I was also responsible for significant proofing and editing of the manuscript, written by Frikkie de Beer, listed above.

This statement satisfies Rule A.5.4.2.8 and Rule A.5.4.2.9 of the General Academic Rules 2015 of the North-West University.

Signed at Pretoria on the 30th day of October 2017.

R.B. Nshimirimana

Statement of consent: Mr. Mabuti J. Radebe

To whom it may concern

I, **MABUTI RADEBE**, hereby give FRIKKIE DE BEER consent to use the publication listed below, of which I am co-author, in the thesis entitled “Neutron and X-ray tomography as research tools for applied research in South Africa”. The thesis is submitted for the degree *Doctor Philosophiae in Chemical Engineering* at the Potchefstroom campus of the North-West University, South Africa:

- F.C. de Beer, *M.J. Radebe*, B. Schillinger, R. Nshimirimana, M.A. Ramushu, T. Modise., 2015, Upgrading the Neutron Radiography Facility in South Africa (SANRAD): Concrete Shielding Design Characteristics. Physics Procedia, 69, p115-123. (PA: 10th World Conference on Neutron Radiography, Grindelwald, Switzerland, 5 - 9 October 2014).

As a Senior Scientist employed by the South African Nuclear Energy Corporation SOC Ltd. and co-worker on neutron radiography, I was part of the team to determine the homogeneity of the concrete composition, designed and built the experimental setup of concrete blocks for attenuation determination, as well as the fixed collimator to reduce the beam from 300 mm diameter to 50 mm diameter used in the manuscript listed above. I was also responsible for significant proofing and editing of the manuscript, written by Frikkie de Beer, listed above.

This statement satisfies Rule A.5.4.2.8 and Rule A.5.4.2.9 of the General Academic Rules 2015 of the North-West University.

Signed at Pretoria on the 30th day of October 2017.

M.J. Radebe

Statement of consent: Mr. Tankiso Modise

To whom it may concern

I, **TANKISO MODISE**, hereby give FRIKKIE DE BEER consent to use the publication listed below, of which I am co-author, in the thesis entitled “Neutron and X-ray tomography as research tools for applied research in South Africa”. The thesis is submitted for the degree *Doctor Philosophiae in Chemical Engineering* at the Potchefstroom campus of the North-West University, South Africa:

- F.C. de Beer, *M.J. Radebe*, B. Schillinger, R. Nshimirimana, M.A. Ramushu, T. Modise., 2015, Upgrading the Neutron Radiography Facility in South Africa (SANRAD): Concrete Shielding Design Characteristics. Physics Procedia, 69, p115-123. (PA: 10th World Conference on Neutron Radiography, Grindelwald, Switzerland, 5 - 9 October 2014).

As a Chief Scientist employed by the South African Nuclear Energy Corporation SOC Ltd. and appointed Project Leader of the upgrade of the neutron radiography facility at Necsa, I was responsible for the overall responsibility for the administration and execution of all activities related to the development of the concrete shielding used in the manuscript listed above. I was also responsible for significant proofing and editing of the manuscript, written by Frikkie de Beer, listed above.

This statement satisfies Rule A.5.4.2.8 and Rule A.5.4.2.9 of the General Academic Rules 2015 of the North-West University.

Signed at Pretoria on the 9th day of November 2017.

T. Modise

Statement of consent: Mr. Jan-Hendrik van der Merwe

To whom it may concern

I, **JAN-HENDRIK VAN DER MERWE**, hereby give FRIKKIE DE BEER consent to use the publications listed below, of which I am co-author, in the thesis entitled “Neutron and X-ray tomography as research tools for applied research in South Africa”. The thesis is submitted for the degree Doctor Philosophiae in Chemical Engineering at the Potchefstroom campus of the North-West University, South Africa:

- Frikkie de Beer, *Jan-Hendrik van der Merwe* and Dmitri Bessarabov, 2017. PEM water electrolysis: preliminary investigations using neutron radiography. *Physics Procedia*, 88, p19-26. (PA: 8th International Topical meeting on Neutron Radiography, Beijing, China, 4 - 8 September 2016).

As PhD researcher student at the DST National Centre of Competence: Hydrogen Infrastructure (HySA Infrastructure) located at the North West University (Potchefstroom Campus), I was responsible for the experimental and hardware setup as well as capturing the data which was used in the manuscript listed above. I was also responsible for significant proofing and editing of the manuscript, written by Frikkie de Beer, listed above.

This statement satisfies Rule A.A.5.4.2.8 and Rule 5.4.2.9 of the General Academic Rules 2015 of the North-West University.

Signed at Johannesburg on the 27th day of October 2017.

JHP van der Merwe

LIST OF PUBLICATIONS

The following chapter, on work conducted for this thesis, were published in a peer-reviewed book:

- Chapter in book:
  Editors: Kardjilov, Nikolay, Festa, Giulia (Eds.),
  Title: Neutron Methods for Archaeology and Cultural Heritage,
  Chapter 7: Paleontology: Fossilized Ancestors Awaken by Neutron Radiography, F.C. de Beer

  Publisher Name: Springer International Publishing. Publisher Location: ChamSeries ID8141Series. Title: Neutron Scattering Applications and Techniques. Book ID329974_1_En, Electronic ISBN: 978-3-319-33163-8 http://dx.DOI10.1007/978-3-319-33163-8, Copyright Holder NameSpringer International Publishing Switzerland Copyright Year 2016.

The following papers, on work conducted for this thesis, were presented at various conferences, and subsequently published in the applicable conference proceedings:

- Frikkie de Beer, Jan-Hendrik van der Merwe and Dmitri Bessarabov, “PEM Water Electrolysis: Preliminary Investigations using Neutron Radiography”, Physics Procedia 88:19-26, Proceedings of the 8th International Meeting in Neutron Radiography (ITMNR-8), Beijing, China, Sept 2016, http://dx.doi:10.1016/j.phpro.2017.06.002

- De Beer, F.C., Neutron- and X-ray radiography/ tomography: Non-destructive analytical tools for the characterization of nuclear materials. J. S. Afr. Inst. Min. Metall., Oct 2015, vol.115, no.10, p.913-924. ISSN 0038-223X. Nuclear Materials Development Network Conference, Oct 2015, Port-Elizabeth, South Africa.
  http://www.saimm.co.za/Journal/v115n10p913.pdf
  http://dx.doi.org/10.17159/2411-9717/2015/v115n10a3

- De Beer, F.C., Radebe, M.J., Schillinger, B., Nshimirimana, R.B., Ramushu, M.A. and T. Modise., 2015. “Upgrading the Neutron Radiography Facility in South Africa (SANRAD): Concrete Shielding Design Characteristics”, Physics Procedia, 69, (2015), 115 – 123, Proceedings of the 10th World Conference on Neutron Radiography (WCNR-10), Grindelwald, Switzerland, Sept 2014.
  http://dx.doi:10.1016/j.phpro.2015.07.017

ABSTRACT

SUMMARY

The use of penetrating radiation for non-destructive investigations, through the use of radiography and tomography, provides for powerful research tools. Development of such experimental facilities, and the establishment of a local core capability to utilise it optimally, can enrich the research scope of many scientific and engineering disciplines significantly. This thesis describes the design and development of such national facilities for both neutrons and X-rays at the South African Nuclear Energy Corporation SOC Ltd. (Necsa) and the subsequent building of capacity for research support to users of a number of disciplines. Aspects of localisation of the technology are described and the value proposition of the facilities and research capacity is demonstrated by three application examples from important South African research areas, namely palaeontology, a vibrant research field in South Africa, hydrogen fuel cell research, a sub-discipline of the field of a hydrogen economy in general, and in nuclear materials.

OPSOMMING

Die gebruik van deurpriemende straling vir nie-destruktiewe ondersoek deur middel van die tegnieke van radiografie en tomografie, gee toegang tot kragtige navorsingstegnieke. Plaaslike ontwikkeling van sulke eksperimentele fasiliteite en die vestiging van ’n sentrale vermoë om optimaal daarvan gebruik te maak, kan dus die navorsingsmoontlikhede van vele wetenskaplike- en ingenieurs-dissiplines aansienlik verryk. Hierdie tesis beskryf die ontwerp en ontwikkeling van sulke nasionale fasiliteite vir beide neutrone en X-strale by die Suid-Afrikaanse Kernenergiekorporasie (Necsa) asook die daaropvolgende bou van ’n vermoë om kundige navorsingsondersteuning te kan lewer aan gebruikers vanuit verskeie dissiplines. Ontwikkelingsaspekte eie aan plaaslike kondisies word uitgelig en die waardepotensiaal van die fasiliteite met hul navorsingskapasiteit word gedemonstreer deur middel van drie toepassings in belangrike Suid-Afrikaanse navorsingsvelde, naamlik palaeontologie wat ’n ryk Suid Afrikaanse geskiedenis het, navorsing op waterstofbrandstofselle wat van belang is vir ‘n waterstofekonomie en laastens toepassings in die veld van kernmateriale.

Keywords: South African Nuclear Energy Corporation SOC Ltd. (Necsa); SAFARI-1 nuclear research reactor; Neutron radiography (NRAD); X-Ray radiography (XRAD); Computed Tomography (CT); Micro-focus X-ray computed tomography (µXCT)

ACKNOWLEDGEMENTS

The author would like to thank and acknowledge the following people/institutions for their support and involvement during his 29 years of working at Necsa as well as for guidance with respect to completion of this PhD:

- First of all to my Heavenly Father, Jesus Christ, who gave me the wisdom and opportunities, but also the insight to realise the open doors to express myself to the full in all aspects of my work. Above all, glory to Him who gave me the physical health, strength and daily peace that goes beyond all understanding to complete my work in His name;
- My supervisor, Prof. Frans Waanders, for his supervision and for the opportunity to become part of his research area and interest;
- My co-supervisor, Dr. Gawie Nothnagel, who is also my Senior Manager in the Radiation Science Department, for his availability, supervision, encouragement and for making me passionate about research. Without his constant support and trust in my work and abilities, this would not have been possible;
- Close international collaborators and friends who introduced me and helped keeping me in touch with the international trends in my field of work: Dr. John Barton, Dr. Burkhard Schillinger and co-workers at TUM, Dr. Nikolay Kardjilov, Dr. Eberhard Lehmann and co-workers at PSI, Dr. Muhammed Arif and co-workers at NIST, Dr. Les Bennett, Dr. John Rogers, Dr. Ulf Garbe, Dr. Thomas Bücherl, Dr. Jack Brenizer and the late Dr. Mike Middleton;
- Former and current colleagues from Necsa who played a part in my career and supported me over many years: Dr. Johan Aspeling, Dr. Van Zyl de Villiers, Mr. Willie Jonker, Dr. Andrew Venter and NDIFF co-workers, Dr. Wessel Strydom, Dr. Chris Franklyn, Mr. Don Uytenbogaard, Dr. Willie Meyer, Mr. Tankiso Modise, Ms. Linda Reyneke, Ms. Mihloti Baloyi;
- Colleagues in the Radiography and Tomography Section who supported me in making my dreams come true in many aspects: Mr. Jacob Radebe, Mr. Kobus Hoffman, Mr. Lunga Bam and Mr. Robert Nshimirimana;
- All the national and international users of the radiography and tomography facilities located at Necsa and whom benefitted from using these research facilities;
- National and International Institutions/Societies who became part of my daily life in collaboration, support and participation: Necsa (Former AEC), International Atomic Energy Agency (IAEA), International Society for Neutron Radiology (ISNR), the National Research Foundation (NRF) of the Department of Science and Technology (DST), the Department of Energy (DOE), the South African Institute for Non-Destructive Testing (SAINT) and the South African Institute of Physics (SAIP);

- Last but not least to my wife Chevaune, my daughters Joalet and Elisna, my son Frikkie, my brothers Johannes and Pieter and my late Father and Mother who all played an immense role in my life and supported me wholeheartedly in my dedication to my work.

TABLE OF CONTENTS

CHAPTER 1

Introduction

This chapter contains a short condensed history of the discovery of X-rays and neutrons as well as the principles of radiography and tomography. This also includes a short history of radiography in South Africa with emphasis on the early neutron and X-ray radiography practices at the South African Nuclear Energy Corporation SOC Ltd. (Necsa).

"In fact it is not much of an exaggeration to say that what Hounsfield and I know about medicine and physiology could be written on a small prescription form!

I think that Alfred Nobel would have been pleased to know that an engineer and a physicist, each in his own way, have contributed just a little to the advancement of medicine."

Dr AM Cormack (Engineer & Nuclear Physicist):
In his banquet speech at the Nobel Banquet, Dec 10 1979. South African borne Nobel Prize winner for inventing the CAT scanner.

1.1 Background

The deployment of radiation beams (e.g. X-rays, neutrons) as research probes is a relative rare global phenomenon. However, the diversity of the research opportunities being created and made available at radiation based beam line laboratory facilities attracts multi-users from many scientific fields within institutional, regional, national and international contexts.

Pursuing the objectives of the South African National Research and Technology Infrastructure Strategy (July 2004) regarding research equipment infrastructure, enables the development of high level human capital and research for the purpose of the proliferation of new knowledge at the radiation beam line facilities located at the South African Nuclear Energy Corporation SOC Ltd. (Necsa).

This thesis describes the life-long career initiatives (29 years) of the author for the unique infrastructure development of X-ray and neutron radiography beam lines established at Necsa, a state funded R&D organisation promoting nuclear and radiation based science technologies. The work centred on design, construction, commissioning and/or acquirement of neutron and X-ray radiography and tomography instruments in support of the National System of Innovation (NSI) strategy which lead to exceptional research activities and the rendering of expert scientific support to users from many research fields.

1.2 Objective

The overall goal is to make Necsa's facilities, in particular the reactor based thermal neutron beams that are unique in the country, optimally available to Higher Educational Institutions (HEI) for pure and applied research towards the front end of the innovation value chain as part of a national drive towards a knowledge economy. As this and own's research related to nuclear materials are the two main goals of research with beam lines at Necsa, the work being presented here for consideration will be of this nature, namely development and research support oriented.

The objective of this thesis is to state the activities related to submiting evidence in fulfilling the requirements for a *PhD by publication*. These activities entail the publication, as the main author, of peer reviewed articles in national and international journals on:

- Infrastructure development and commissioning of unique penetrating radiation radiography and tomography equipment based at Necsa for the benefit of the HEI and in line with the NSI; and
- Utilisation of these infrastructures in unique research applications and projects.

1.3 Scope

The thesis reports on the published research output in a cohesive manner that will highlight:

- The radiography and tomography research facilities established at Necsa and the author's role in their establishment;
- The value of the research performed towards the improvement of neutron radiography and tomography in South Africa; and
- The value of radiography and tomography as a non-destructive research tools with reference to one's own current (and previous) research in a number of nationally important research disciplines, with emphasis on the paleo-sciences, nuclear related material science as well as the hydrogen economy as a renewable energy source.

1.4 Layout

Chapter 1 is a compendium of the objectives, scope, abstract and layout of this thesis. Chapter 2 briefly summarises the historical events of the discovery of X-ray and neutron radiation and its radiographic benefit including the invention of tomography (CT). This chapter also includes the neutron and X-ray radiography (NRAD and XRAD) initiatives since its application at Necsa until 1988, the year the author was employed at Necsa. Chapter 3 describes the ongoing work performed since 1988 to establish a unique state-of-the-art NRAD/CT capability at the SAFARI-1 nuclear research reactor to international standards. Furthermore, the development and utilisation, in parallel with the NRAD/CT capabilities, of the Micro-Focus X-ray CT (MIXRAD) facility at Necsa and of additional laboratories which also support the Palaeoscience research community, is being described. Summaries of the documented output in the form of post graduate dissertations and theses as well as peer reviewed articles, generated at the Necsa radiography and tomography facilities are provided. The four (4) peer reviewed chapter/articles on work conducted for this thesis are summarised and the full output is included in Chapters 4, 5, 6 and 7. Chapter 8 concludes the thesis with a summary of the thesis and a vision and outlook of the expansion of the current initiatives and user base of CT technology as a research tool in South Africa towards an important quality assurance (QA) and commercially viable tool. Appendix 1 summarises the relevant achievements of the author during his career at Necsa.

Each chapter will contain its own chapter references.

CHAPTER 2

Principles and Historical Overview

This chapter contains a short condensed history of the discovery of X-rays and neutrons as well as the principles of radiography and tomography. This also includes a short history of radiography in South Africa with emphasis on the early neutron and X-ray radiography practises at Necsa and concludes with a brief summary of the more recent developments in radiography and tomography.

"There is irony in this award, since neither Hounsfield nor I is a physician."

Dr AM Cormack (Engineer & Nuclear Physicist):
In his banquet speech at the Nobel Banquet, Dec 10 1979.

2.1 Introduction

Radiography has a long, rich and varied history of discovery, utilisation and value-adding developments in South Africa. In order to contextualise the research and development work presented in this thesis, this chapter contains a historical and theoretical overview of neutron and X-ray radiography and tomography techniques established and utilised at Necsa and more or less in line with the real historical development of these techniques in South Africa, and Necsa in particular. However, the material presented here is not intended to provide an in-depth and comprehensive theoretical background of the neutron and X-ray radiography techniques.

Emphasis will be on the complementary nature of neutron radiography (NRAD) and X-ray radiography (XRAD), their unique advantages and disadvantages, their roles as non-destructive analytic probes and their impact on society and industry. The chapter concludes with a rather brief discussion of more recent developments in radiography and tomography that will have to be considered for future developments at Necsa in order to keep local capabilities in touch with international practises.

Tomography is a more complex technique, which is built upon the principles of radiography. Thus, like elsewhere in the world, radiography was established at Necsa first. In the discussion that follows, the principles of each technique will be presented in the context of the development thereof in South Africa, and Necsa in particular.

The current state-of-the-art is a continuation of a proud South African legacy starting with the earliest (worldwide) developments in radiography, and later computed tomography (CT), during the period 1898 to 1979, followed in particular by applications with various penetrating radiation types at Necsa during the period 1965 to 1988. The description of the South African experience spans the full period, starting with the first introduction of medical XRAD in South Africa during the 2nd Anglo Boer War at the end of the 19th Century, includes the period of development of pioneering medical CT work by the South African born Nobel Laureate, Dr Allan Cormack, and ends with some of the key milestones of the South African Institute for Non-Destructive Testing (SAINT). The latter activities centred primarily on the development of industrial radiography as a non-destructive testing (NDT) technique in applications of importance to quality control, for example. The historical events concludes with the application and development of facilities for radiography at Necsa prior to 1988 and thus sets the baseline to view and evaluate the evidence provided in this thesis in fulfilment of the requirements for a *PhD by publication*.

2.2 An Abbreviated Historical Overview

X-rays were discovered by Röntgen in early January 1896 (Röntgen, 1896). As is almost invariably the case in scientific development, he made use of the knowledge of previous investigators and inventors such as Volta, Ampere, Ohm, Faraday, Crookes and Thomson, to name a few, to construct and use the Crooke's tube apparatus that retrospectively turned out to be the world's first known X-ray tube. Having noticed exposure of photographic plates when the apparatus was in operation, Röntgen further experimented and quickly realised that he discovered a new invisible kind of light, with hitherto unknown penetrative power, which he called X-rays. These later also became known as Röntgen rays and, for this discovery, he received the first Nobel Prize in Physics in 1901 "in recognition of the extraordinary services he has rendered by the discovery of the remarkable rays subsequently named after him." (The Nobel Prize, 1901)

Very soon after the discovery of X-rays, Röntgen took the first X-ray radiographs, which was of his wife's hand revealing her ring and skeletal structure (Glasser 1993) (Figure 2.1(a)), and so became the world's first "medical radiographer". With this, the enormous practical value of radiography was immediately evident.

Motivated by Röntgen's use of photographic emulsions to reveal invisible radiations, Henri Becquerel fortuitously discovered natural radioactivity in May 1896 for which he, his doctoral student, Marie Curie, and her husband, Pierre Curie, received the 1903 Nobel Prize in Physics. Some of the early pioneers of X-ray and neutron radiation studies are shown in Appendix 1 ('"All Nobel Prizes in Physics". Nobelprize.org. Nobel Media', 2014).

The medical benefits of X-rays, almost immediately realised by Röntgen, are now well understood to stem from the highly penetrating nature of electromagnetic radiation of extreme frequency (photon energy), such as X-rays and gamma-rays. Invisible, highly penetrating electromagnetic radiation, emanating from atoms and nuclei has thus been known, studied and beneficially utilised for more than 120 years. However, this highly energetic electromagnetic radiation is not the only penetrating radiation type in use today for radiographic studies of objects. The discovery of neutrons by Chadwick in 1932 (Chadwick, 1933), opened the door for the use of neutron beams to also generate radiographic information complementary to what can be achieved with X-rays. Kallman and Kuhn (Kallman, 1948) started their work on neutron radiography (NRAD) experiments in Berlin as early as 1935, but due to World War-2 they could only publish their results in 1948 and was thus preceded by Peter (Peter 1946) with an earlier publication in 1946 (Figure 2.1(b)).

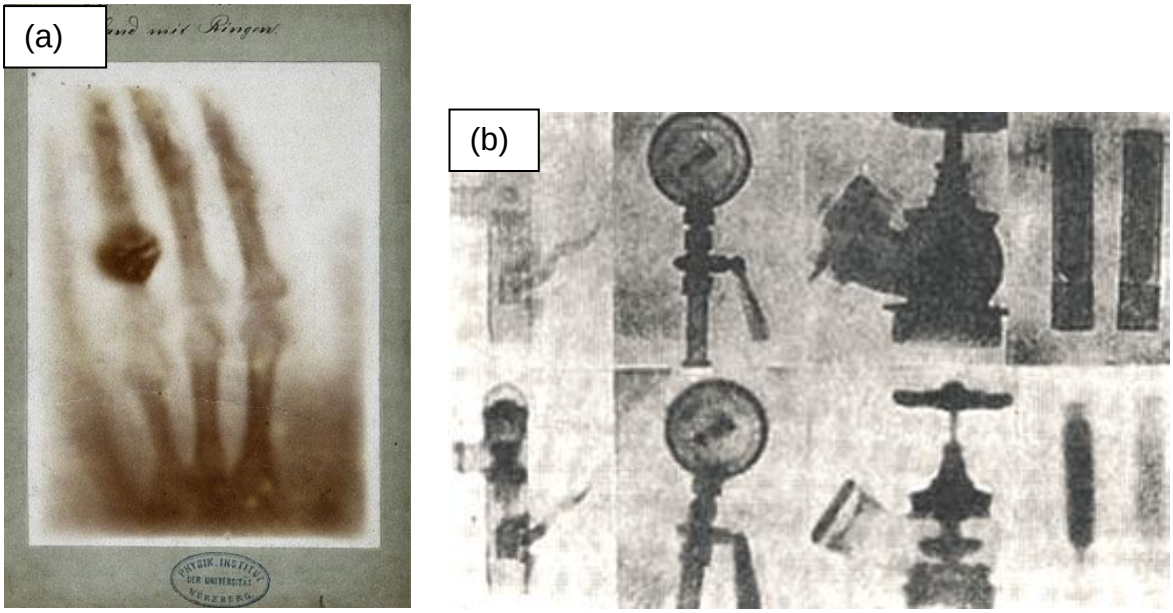

Figure 2.1: **Historical radiographic images: (a) X-ray radiographs taken by Röntgen of his wife's hand in Wurzburg. (Glasser, 1993) (b) Neutron radiographs taken by Peter in Berlin. (Peter, 1946).**

As with X-rays, the potential and advantage of neutrons as a new and additional probe for radiography, has been realised and explored shortly after the discovery of this new penetrating radiation type. NRAD only became fully on par with XRAD once nuclear research reactors were constructed from which a high flux of neutrons (in the order of ⟦10⟧^7 cm^(-2).s^(-1)) could be made incident onto study objects. However, the development in detection capability and resolution for NRAD lagged 40 years w.r.t. XRAD and only caught up with the advent of the digital era of detection from early 1990's. When used in a complementary fashion, X-rays and neutrons provide a powerful radiography and tomography diagnostic for a wide variety of objects.

Such dual capabilities have been developed at the SAFARI-1 nuclear research reactor at Necsa as well as at Necsa-based X-ray facilities and thus form the basis for the research and applications described in this thesis. Although radiography and tomography have become a vital quality-of-life technology for many people who undergo medical 3D-scans (also known as CAT scans), the full scope of its applications still remains unappreciated by the general public.

Through dissemination of parts of the work described in this thesis and, under the popular theme "Using the invisible to reveal the hidden" (Nothnagel, 2007), many additional benefits of the use of penetrating radiation has been made known to the general South African public over the years. The aim was to demonstrate the impact of radiation-based investigation techniques in many areas of modern human endeavour, such as to ensure safe living and working conditions,

good health, quality products and pure and applied research in many fields, should not be ignored nor be underestimated. As a result of the continuous development in the field of radiography, there was a growing awareness of the benefits of radiation methods over time which contributed towards the demystification of radiation and nuclear technology in general.

Although the first, and still the most well-known, applications of radiography was (and still is) in the medical field, the aim of this thesis is not to describe the impact of radiation applications in the medical diagnostic sciences. The focus is instead on the application of X-rays and neutrons as probes for research and specifically the role and activities of the author in a national and international context with respect to research and applications in the field of radiography and tomography from 1988 until the present.

2.3 The Principle of Radiography

The classical and conventional in-principle setup for radiography is the same for both X-ray and neutron radiography. The object under investigation is placed between the source and the detector so that the penetrating radiation passes through the sample and onto the detector. The detector forms an integrated radiographic image due to the attenuation (absorption / scattering) of the radiation beam by constituents (matrix including imbedded voids or inclusions) of the object during its propagation through the object, as illustrated schematically in Figure 2.2(a) for X-rays and Figure 2.2(b) for neutrons respectively.

The quasi pinhole geometry is shown with D the aperture size to the radiation source. In the case of X-rays, the aperture is equal to the size of the focal spot, which is in the order of a few millimetres (~ 5 mm) to microns (min 0.6 µm). For neutrons, the aperture ranges from 10 mm - 50 mm, but in extreme applications, specially designed apertures of 1 mm - 5 mm are used depending on the application (e.g. phase contrast imaging).

The effective angle of divergence (ϕ) of the collimator defines the maximum part of the source that can be viewed, thus contributing to radiation through the collimator. The narrower ϕ becomes, the smaller the utilisation of available source intensity. The optimum detector placement in the collimated beam occurs when the diverging beam precisely covers its full sensitive area (Flat Field (FF)). All work presented in this thesis was conducted with cone beam geometry. However, in the case of neutron radiography, the geometry is different and a cone beam is strictly speaking not applicable due to an aperture (D) to detector distance of several meters and a divergence of only a few tenths of a degree.

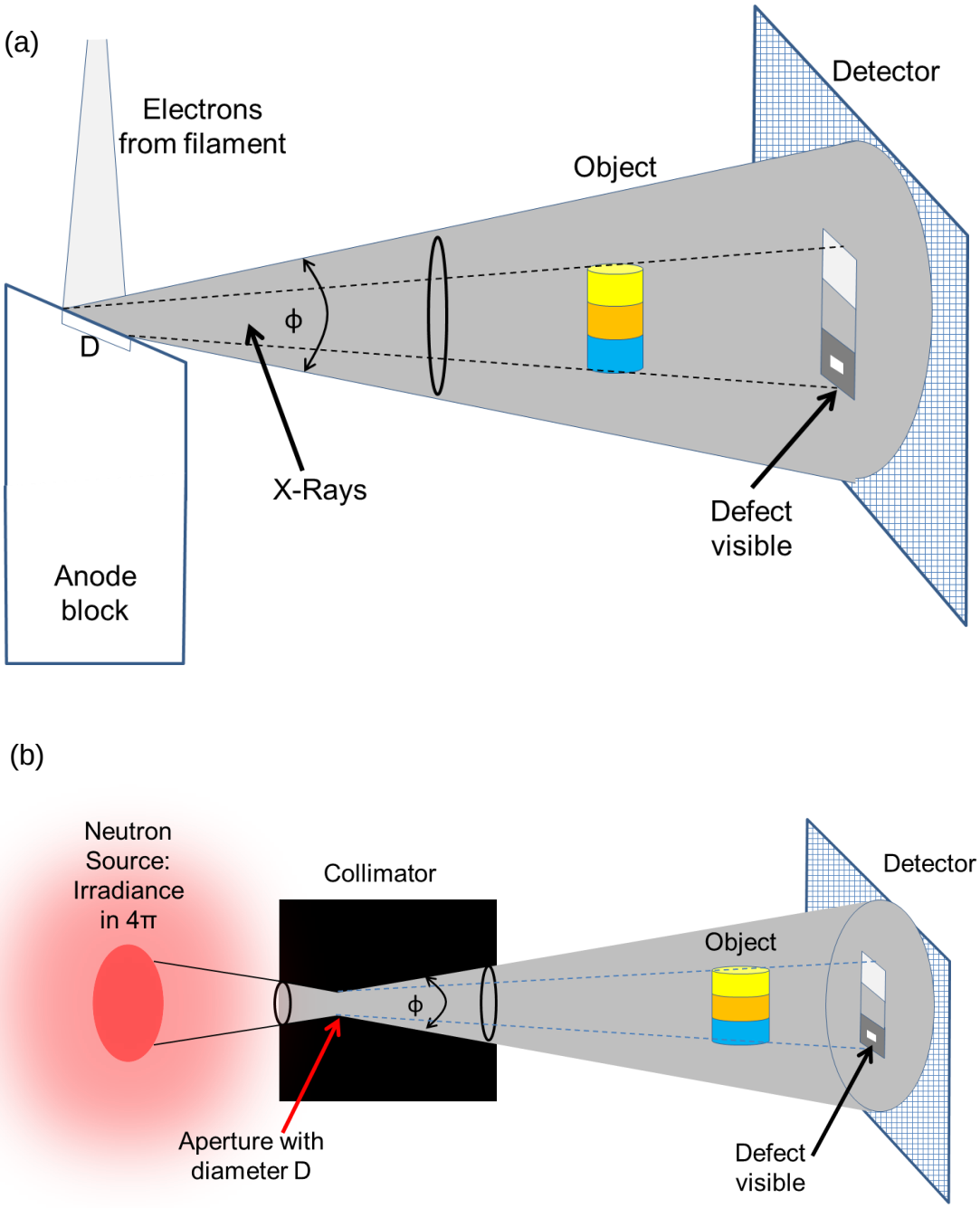

Figure 2.2: Schematic diagram of the classical principle and setup for (a) X-Ray and (b) neutron radiography each with a sample rotation capability for tomography application. (After: Halmshaw, 1988) (After: Domanus, 1987).

The ultimate aim of any radiography process is to obtain a high quality radiograph, which is defined by the visual characteristics of high contrast between the constituents of the object (good discrimination, e.g. large differences of grey scale values for digital detectors) and good geometric characteristics such as high spatial resolution (sharpness), which allows resolving of fine detail as well as distinction between these constituents. The following radiography set-up

parameters and their relationship, which are discussed further in detail below, define the quality of the radiograph; the size of the aperture (D), it's distance (L) from the sample (also refers as d_s: source-sample-distance), the size of the sample (2r in Figure 2.3) and it's placement between the aperture D and the detector (also refers as d_f: sample-detector-distance) (Figure 2.3).

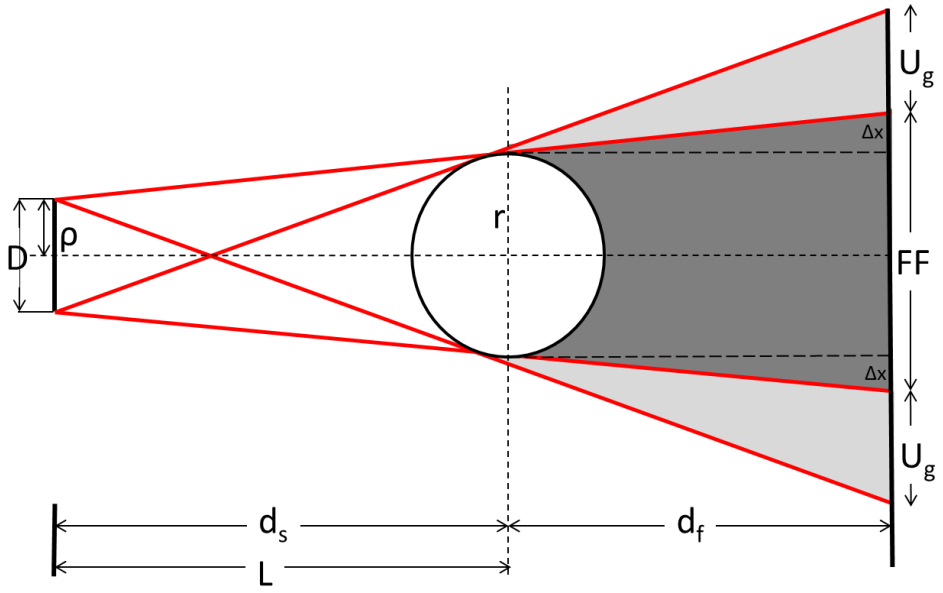

Figure 2.3: Schematic diagram of a radiography geometry setup. (Courtesy: Necsa).

L/D ratio:

For radiography, the size of the aperture, D, and the distance from the aperture to the sample, L, as shown in Figure 2.3, defines the ratio L/D and thus the degree of collimation of the radiation beam. The higher this ratio, the higher the quality of the radiographs that can be produced, but the lower will be the flux available for image formation and thus the longer the exposure times to achieve the same dynamic range and vice versa. Additionally, the size of the aperture D and the distances d_s, (source - sample) and d_f, (sample - detector), significantly affect the quality (sharpness) of the radiograph. A more comprehensive discussion will follow in Section 0.

Magnification:

According to the radiographic set-up parameters depicted in Figure 2.3, the magnification M, of any transmission radiography arrangement can be expressed as (with FF the Flat Field):

$$M = \frac{Image\ size}{Object\ size} = \frac{FF}{2r} = \frac{2r + 2\Delta x}{2r} = 1 + \frac{\Delta x}{r} \quad or \quad M = \frac{d_s + d_f}{d_s} = 1 + \frac{d_f}{d_s} \tag{1}$$

with Δx, the enlargement, defined as:

$$\Delta x = r\frac{d_f}{d_s}\left(1 - \frac{\rho}{r}\right) \tag{2}$$

The power of micro and nano-focus XRAD lies in the magnification (geometric enlargement) of an object up to 100 times or more while maintaining and achieving high spatial resolution. The aperture (D = 2ρ in Figure 2.3) is physically small (considered as a point source with sizes down to ~ 0.6 nm) and, with the sample placed as close as possible to the aperture ($<<d_s$) and far from the detector ($>>d_f$), Δx becomes large.

For NRAD, geometric magnification of an object is not an effective option to accomplish high spatial resolution. For NRAD spatial resolution rather lies within the beam geometry and detector setup. In particular, a desired pixel resolution (pixels per mm) for digital detection systems is governed by the inherent resolution of the neutron sensitive scintillator screen as well as the characteristics of the digital detector. (See Section 2.6.1.4 for a description of how the scintillator screen and CCD camera individually, and as a unit, contributes to spatial resolution). For conventional NRAD facilities the aperture is relatively large (5 mm to 40 mm) while the object is positioned as close to the detector as possible to render Δx and U_g (penumbra) as small as possible.

Penumbra (U_g):

The geometric blur, referred to as unsharpness (U_g), is an inevitable characteristic of any radiograph (Figure 2.3). It is the most important aspect of the radiograph to be minimised in order to obtain a high quality radiograph. From geometric principles, the unsharpness is defined by the size of the aperture, D, and the position of the object between the source and detector as follows:

$$U_g = D\left[\frac{d_f}{d_s}\right] \tag{3}$$

For neutron radiography setups with relative large apertures (D >> 1 mm), it is essential that the sample is positioned close to the detector ($d_f << d_s$) to minimise U_g, while, for the intrinsic small point source apertures of micro and nano focus X-ray sources, it is possible to place the sample at any position between the source and detector and still obtain a high quality sharp radiograph.

Each of the separate components of a radiography setup, which have an influence on the radiography outcome, is summarised in a little more detail below. However, the radiation shielding, flight tubes, sample translation table, beam limiters and radiation filters, which are normally important components of a particular radiography facility, are not described in this section, as they are of a practical nature and can differ significantly, depending on the specific radiation source and instrument geometries.

2.4 Sources of Radiation for Radiography

The two radiation sources currently being applied at Necsa as radiography probes, namely X-rays and neutrons, have different source geometries and characteristics, which are described separately below.

2.4.1 X-ray sources

Electrons are emitted through thermionic emission and accelerated from a heated cathode (filament) toward a metal anode by a potential difference in a vacuum tube. The basic design is still the same as for the cathode ray tube that was used by Röntgen, except that it became highly optimised in terms of efficiency of X-ray production. The intensity of the source can be arranged by changing the current, and thus the temperature, of the electron emitting filament while the maximum X-ray photon energy is determined by the potential difference across the tube. In modern devices, excellent stability and reproducibility of the X-ray intensity and X-ray energy spectrum can be achieved.

The X-ray spectrum produced and emitted from the cooled anode is of a general continuous nature with superimposed characteristic radiation determined by the anode material. The continuous part of the spectrum is the result of bremsstrahlung radiation due to deceleration of electrons upon collision with the anode material. The process is inherently statistical with the total emission composed of a superposition of radiation from a very large number of primary and random secondary collision steps, and therefore continuous in nature. The process is semi-classical in that the bremstrahlung can be described classically whereas the highest energy X-ray frequency is determined by equating the associated quantum energy $h\nu_{max}$ with the maximum electron energy (eV_{Tube}), where ν_{max} is the maximum radiation

frequency, h is Planck's constant, e is the electron charge and V_{Tube} is the potential difference between the cathode and anode of the tube. The superimposed characteristic spectral peaks are purely quantum mechanical in nature and due to a series $(e.g.\ K_n, L_n, n = 1,2,\ldots)$ of allowed quantum transitions from higher lying atomic orbitals into inner shell (e.g. K or L shell) vacancies, caused by collisions of the impinging electrons with the atoms of the anode material.

On average, more than 99% of the kinetic energy of impinging electrons is converted to heat on collision with the anode while the rest, < 1%, appears as the emitted X-ray spectrum. The anode target is typically placed at an angle of 45° so that the emitted X-rays can be viewed at an angle different from the incident electrons - reflection target mode. The heat generated at the anode is being dissipated through water cooling and/or a rotating anode.

From the description of the nature of X-ray production it follows that the peak wavelength of the X-rays decreases when the tube voltage increases, whereas the wavelength location of the characteristic peaks remains unaffected (Figure 2.4).

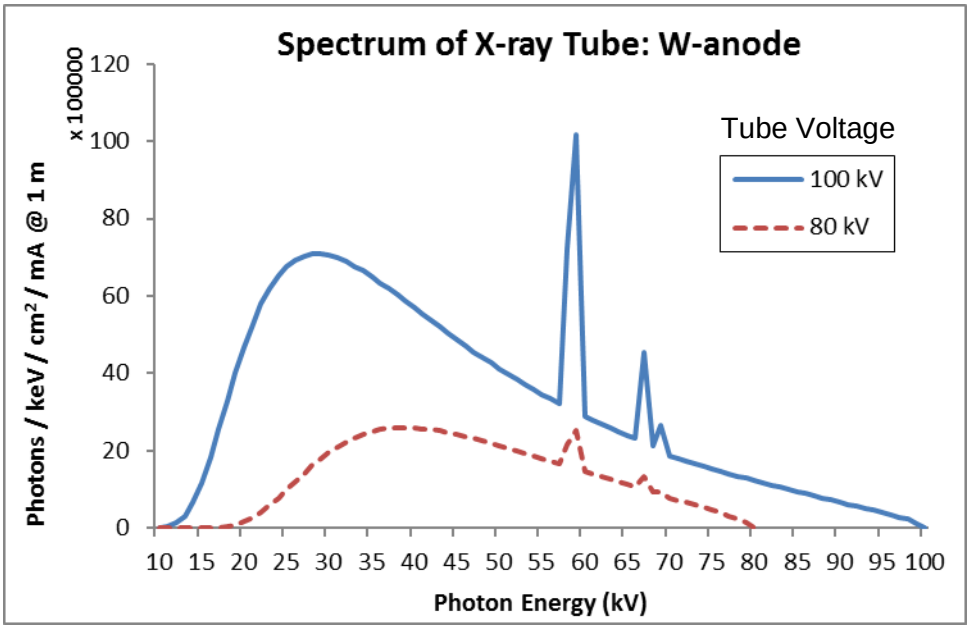

Figure 2.4: Spectrum of an X-ray tube with a tungsten anode for 2 different tube voltages calculated with SPEKCALC. http://spekcalc.weebly.com/free-version.html (Accessed on 4 Feb 2018).

2.4.2 Neutron sources

For the purpose of the research work presented in this thesis, neutrons produced at the SAFARI-1 research reactor have mostly been used with a few exceptions that will be mentioned

explicitly. The 235U inside the nuclear fuel has a high cross-section for fission when bombarded by thermal neutrons (meV energy range). The fast neutrons (MeV range), emanating from the fission process, are brought into thermal equilibrium through multiple scattering interactions with the moderator material inside the reactor core (light water in the case of SAFARI-1). The thermal neutrons inside the moderator scatter approximately isotropically because their transport mean free path in water is only about 2.5 cm.

In Figure 2.5, the blue shading represents an isotropic 4π source directly adjacent to a circular entrance window of radius R that allows neutrons to stream out into an evacuated or helium filled beam tube. The surface of the window itself then constitutes a half-plane (2π) source, which illuminates the beam tube from the left. The differential area element at an arbitrary radius r, as shown in the Figure 2.5 is $2\pi r dr$. The distance to an aperture of area A from all points on the differential source ring is ℓ and the projected aperture area perpendicular to the ray shown is Acosθ, representing a projected area in the horizontal direction.

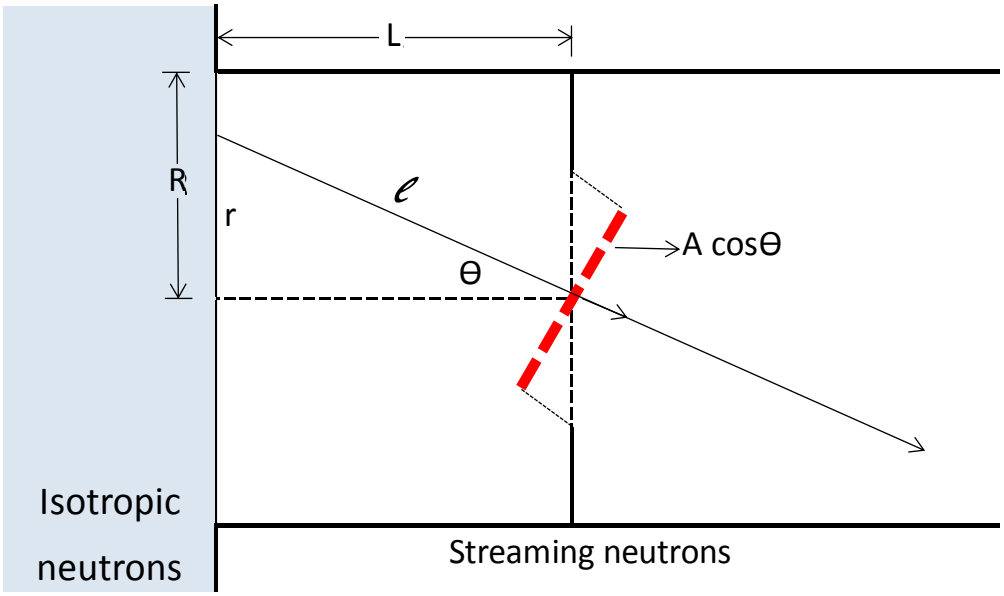

Figure 2.5: Thermal neutrons streaming down a reactor flight tube. (Courtesy: Necsa).

If the flux at the entrance window is ϕ_0, the number of particles dI streaming through the aperture in direction ℓ as a result of the differential ring source is:

$$dI = \phi_0 A \frac{Lrdr}{(r^2+L^2)^{3/2}} \quad (4)$$

After integration it follows that the flux through the aperture is:

$$\phi_A = \phi_0 \left[1 - \frac{1}{\sqrt{1+(R/L)^2}} \right] \quad (5)$$

A higher degree of collimation ($\mathrm{L/R}$) down the beam tube thus reduces the source strength. When the degree of collimation is as high as $\mathrm{L/D} = 800$, it follows from (Eq.5) that $\phi_\mathrm{A}/\phi_0 = 7.8 \times 10^{-7}$, which indicates an available flux of the order of $10^7\ \mathrm{cm^{-2}.s^{-1}}$ at the exit of the beam tube collimator, if the flux at the reactor side is of the order of $10^{13}\mathrm{cm^{-2}.s^{-1}}$. A flux of the order of $10^7\ \mathrm{cm^{-2}.s^{-1}}$ is typically expected from reactor beam tubes.

A beam tube in the biological shield of the reactor channels the neutrons and gamma-rays towards the sample and radiography instrument situated inside a shielded bunker outside the reactor vessel. For beam tubes such as those at SAFARI-1 that are axial to the radiation source, a full energy spectrum of neutrons and gamma-rays are available at the entrance of the instrument. The energies can be filtered to some degree by passing the beam through special filter materials (e.g. Bismuth, Sapphire) or velocity selecting chopper infrastructures. Characteristics of beam tubes tangential to the core as well as the generation of cold neutrons are described elsewhere (Banhart, 2008).

2.5 Collimation (Flight Path)

The collimator is a physical device that confines the radiation flight path into a beam with properties suitable for a given radiography set-up. Collimators consist of characteristic thick and high radiation absorption materials and are designed to minimise the arrival of radiation at the detector via routes other than through the object under study. The collimator also reduces the size of the outgoing radiation beam by limiting the size of the penumbra region which is unsuitable for use due to its reduced radiation intensity. For neutrons, in this manner, the collimator thus reduces also unwanted activation and secondary gamma production on the detector walls. The collimation relevant to the systems used in this work is in the form of a cone beam shape (near parallel “cone” for neutrons) with the collimator located between the source and sample.

For X-ray systems, the size of the focal spot effectively defines the aperture (D) and a collimator which typically consists of high density materials, such as depleted uranium or lead, is further utilised to restrict beam spread. For a D = 5 mm (Figure 2.2(a)) and sample close to the detector to minimise radiographic unsharpness and which is about 0.5 m – 1 m away from the source, an effective L/D = 200 can be achieved. For a D = 0.6 µm (typically for micro and nano focus X-ray systems) and the sample close to the aperture to allow maximum geometric

enlargement, an L/D = 16000 can be achieved resulting in high resolution. Due to the small spot size of micro-focus X-ray facilities, significant geometric enlargement of the sample is thus possible without introduction of a detrimental penumbra region (U_g) - which allows for radiography at very high resolution

Neutron radiography systems on the other hand, normally apply large apertures (D) (Figure 2.2(b)) in order to deliver sufficient radiation flux thus rendering the presence of a penumbra (Ug), which is inevitable. The penumbra has a detrimental effect on the quality of the radiograph but can however be minimized by placing the sample close to the detector system when sharpness of the image is a strict requirement. It implies that geometric magnification in NRAD systems cannot be achieved with a high quality radiographic result. Sharp high quality neutron radiographs depend inter alia on the degree of collimation. Most NRAD facilities operate with a L/D ratio between 250 – 800 with the higher desirable for radiographic quality as defined by high spatial resolution and high Signal-to-Noise ratio (SNR). Typical nuclear reactor based NRAD facilities normally operate at L/D ratios ranging from 100 – 800 and in extreme cases, such as for application of phase-contrast neutron radiography, at L/D = ~10000. A summary of the expected neutron radiographic outcomes with different sizes of D and L is shown in Figure 2.6 while in practice there is always a trade-off between the exposure time and resolution obtained for a specific experiment.

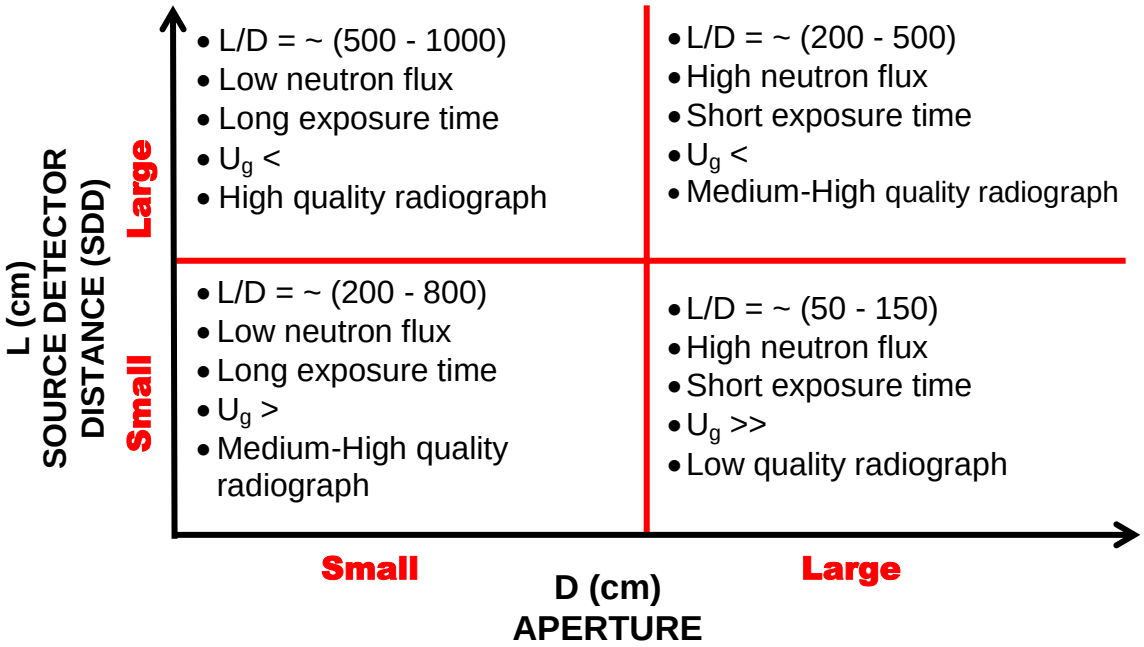

Figure 2.6: L/D characteristics and their consequences for neutron radiographic setups. (After: Domanus, 1987)

2.6 Detection / Recording of Radiation (Radiography Applications)

When a beam of radiation is transmitted through an object, it contains spatial variations in intensity, which represents the radiation image of the attenuation inhomogeneity in the object. As radiation is not directly perceptible by the eye, the transmitted beam needs to be converted into a visible recording of an image (radiograph) in different grey levels of shading (colouring).

X-ray radiographs can be recorded directly onto X-ray sensitive photographic emulsions or X-ray sensitive detector systems, or can be detected indirectly by first forming a visible light image via a scintillation screen.

For neutron radiographs a converter is needed because neutrons do not excite directly due to their lack of charge. Neutrons first convert their energy to secondary particles such as photons, conversion electrons or alpha particles, which are then captured by an emulsion or photosensitive electronic device such as a Charged Coupled Device (CCD) camera with digital performance, i.e. it consist of pixels in a square or rectangular array and have a linear response with respect to the radiation intensity in a particular intensity range.

Only those detection systems that are used at Necsa, namely, scintillator-electronic CCD camera based systems, amorphous-Silicon flat panel detectors, and photographic film used for both XRAD and NRAD, are briefly discussed here.

Other digital detection systems such as intensified real time camera systems, CMOS pixel detectors and imaging plates (IP) are used in radiography setups to great effect and are described in detail by Banhart (Banhart, 2010).

2.6.1 NRAD detectors

The analogue and digital neutron detector systems discussed in this section, were or are still, used at Necsa.

2.6.1.1 Direct technique: Analogue based X-ray film recording of thermal neutrons

Here the exposure is performed by placing an X-ray film (typically D4) in contact and directly in front of a Gadolinium (Gd) metal foil inside a light-tight cassette holder, which is under vacuum to ensure close contact between converter and film. The cassette is placed behind and close to the sample. Capture of neutrons by gadolinium results in production of prompt gamma rays, X-rays, conversion electrons and Auger electrons, exposure of the emulsion is primarily as a result

of the fast electron dose (187 keV). After receiving a thermal neutron fluence of typically ~10^9 neutrons per square centimetre, the X-ray film, after a waiting period of approximately ~15 - 20 minutes to allow radioactive decay of the cassette for safe handling, is unloaded and developed in a dark room. Spatial resolution is determined by the emulsion characteristics, which allows a spatial resolution of 20 - 50 µm with a dynamic range of 10^2 (non-linear response when evaluated on a transmission light scanner) (Lehmann, 2007). Optical film densities were not obtained during the exercise when neutron radiographs of water ingress into a helicopter main rotor blade were recorded by this method as shown in Figure 2.7 (F.C. De Beer, Coetzer, Fendeis, & Da Costa E Silva, 2004).

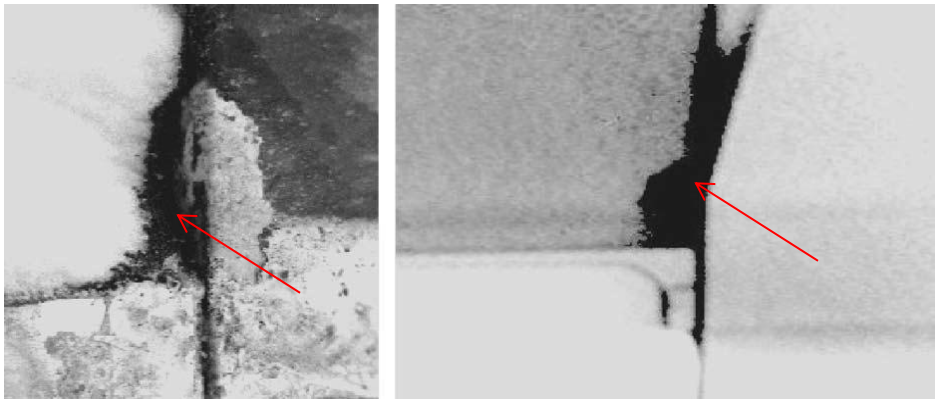

Figure 2.7: **Demonstration of the successful application of the direct technique in neutron radiography using Gd-metal foil and D4 X-ray film to reveal water ingress into the structure of a helicopter main rotor blade. Arrows indicate areas of water ingress. (Courtesy: Necsa).**

2.6.1.2 Indirect technique: Analog based X-ray film recording of neutrons

Here the X-ray film recording of neutrons takes place via radioactive Indium (In) foil transfer where the film is not directly exposed by the neutron beam. The exposure is performed by placing an Indium (In) foil closely behind the sample. After ~15 sec. neutron exposure, the activated foil is carefully and safely transported by hand to a darkroom and placed in close contact with an X-ray film for ~10 half-lives (~10 hours) for the foil to decay and form a latent neutron image. Thereafter the X-ray film is developed in a dark room (Figure 2.1).

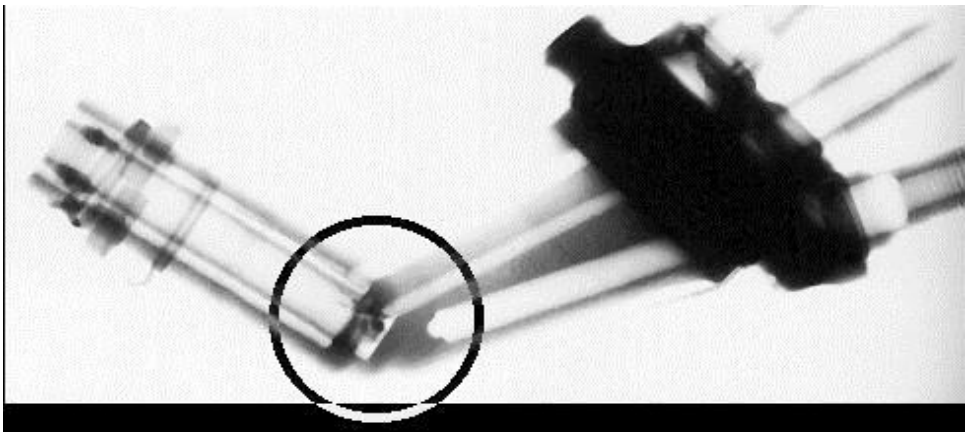

Figure 2.1: Blocked fuel line of aircraft by transfer technique using Indium foil. (Photo: Courtesy to Mr. Don Uytenbogaard)

2.6.1.3 Track-etch technique: Nitro-cellulose film recording of neutrons

In itself nitro-cellulose film (Kodak CN 85) is insensitive to neutrons, X-rays, gamma-rays and visible light. However, in combination with B-10 converters it is suitable to apply in the neutron radiography experimental setups for the post-irradiation examination of especially radioactive nuclear reactor spent fuel. Two Kodak B-10 re-usable converter foils (~ 50 µm thick) and enriched with boron-10, sandwich a single nitro-cellulose film (~ 100 µm thick) in a vacuum cassette. The cassette is placed closely and directly behind the radioactive sample in the neutron beam until a neutron fluence of ~ 2.0 x 10^7 neutrons / cm^2 has been achieved. Through the B-10 (n, α) reaction minute alpha particle tracks are created in the nitro-cellulose. Upon etching the film in a 10% NaOH bath for typically 45 minutes at 50 °C, the tracks are enlarged to form a conical hole with increased depth and thus create a visible image (neutron radiograph) of e.g. radioactive nuclear fuel pellets inside zirconium tubing (Figure 2.9). Low exposure in combination with longer etching provides a higher contrast radiograph while high exposure in combination with short etching results in a low contrast but sharper radiograph (Domanus, 1992).

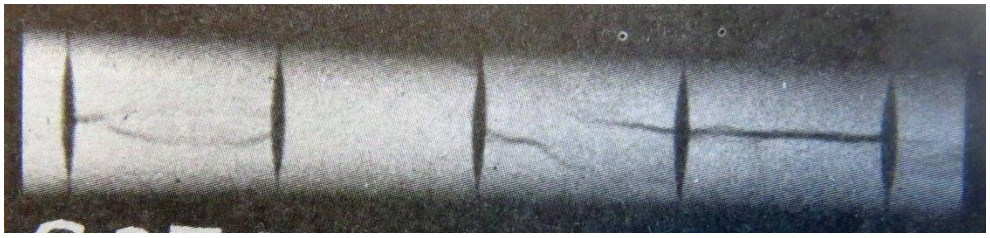

Figure 2.9: Demonstration of the application of the track-etch technique in neutron radiography using B-10 converter screens and nitro-cellulose film. A radiograph of post irradiation nuclear fuel pellets (10 mm long) inside a 10 mm diameter Zirconium-rod reveals shrinkage and crack formation. (Domanus 1987).

2.6.1.4 Digital neutron detection: Scintillation and CCD-camera based

A more thorough description of some aspects of the scintillator - front surface mirror - CCD camera based systems (see Figure 2.10) is provided in this section due to its prominent application at Necsa and a global trend to generally utilise these kinds of systems in neutron radiography setups.

The application of scintillation screens (conversion to visible light photons) with a high light yield and short light decay time are important for improving neutron efficiency, spatial resolution and detectability under high neutron flux (DOE, 2008). Whereas the exposure time to obtain a practical radiograph with the film technique is of the order of hours, scintillator screens reduce the exposure time to seconds and even down to micro seconds. A mirror is rotated 45° to the optical axis and reflects the visible-light image from the back of the scintillator screen towards the digital CCD camera via a suitable optical lens system.

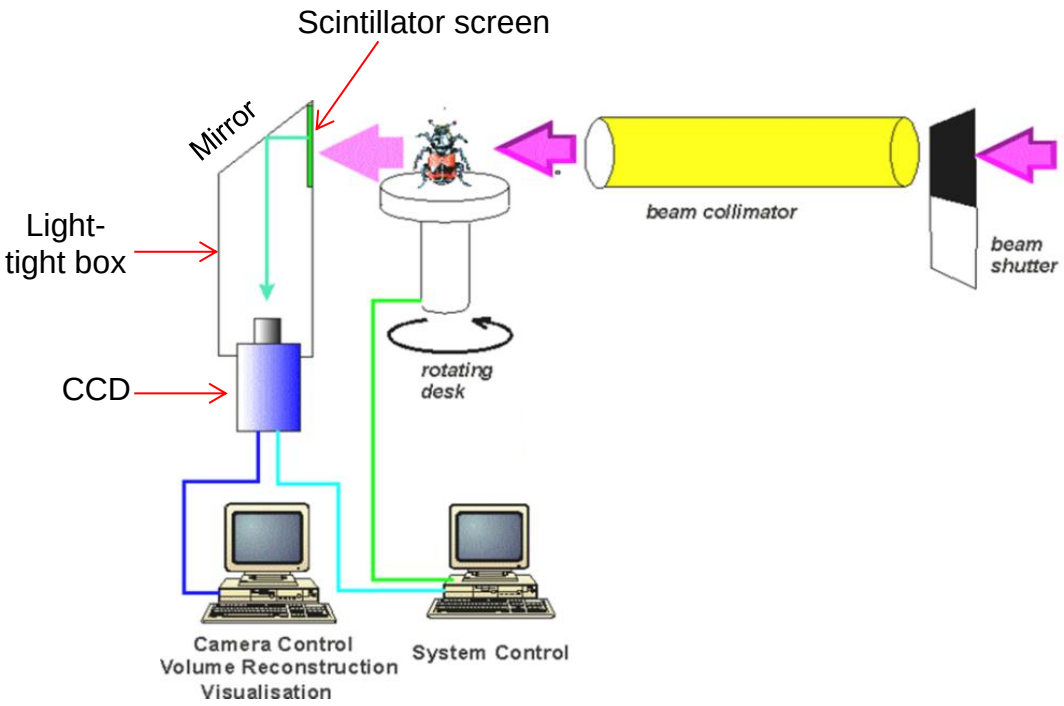

Figure 2.10: Scintillator screen and detector geometry of the radiation detection layout for digital neutron and X-ray radiography and tomography. (Courtesy: PSI).

Scintillator Screen Technology and Performance

A Lithium-fluoride-Zinc-Sulphide (LiF / ZnS) based scintillation screen is in use at Necsa. This device affects light production via a two-step conversion mechanism. Neutrons are firstly absorbed by ^{6}Li nuclei located within the LiF converter. Positively charged reaction products, ^{3}H and ^{4}He, emitted via the ^{6}Li(n,α)^{3}H reaction totalling 4.78 MeV, then react with the ZnS (Ag-

doped) grains to produce visible light. The ZnS crystals doped with copper (Cu) or gold (Au) emits green light and when doped with silver (Ag), blue light. The type of scintillator is thus chosen depending on the optimum CCD-camera sensitivity for blue (450 nm) or green (530 nm) light (TRITEC, 2018).

Alternatively, for either neutrons or X-rays, a single component system such as Gd_2O_2S:Tb, where Gd as the radiation absorbing species is incorporated into the fluorescent pigment, can be used as a scintillator. When X-ray photons are absorbed by the crystal grains, some electrons in the valence band are excited to the conduction band. When the excited electrons fall back into the holes previously left in the valence band, they emmit photons with energies equal to the width of the band gap. In un-doped crystallites the efficiency of the de-excitation process and bandgap widths do not allow emittance of light suitable for fast CCD detection. Doping of scintillators with rare-earth elements such as europium (Eu), terbium (Tb) or cerium (Ce) overcome these problems with increased light yield, fast decay time and minimal self-absorption.

^{6}LiF/ZnS provides the highest light output while Gd-based phosphors have the highest resolution due to the high neutron capture cross section (smaller mean free path to capture). New developments in scintillator technology allows production of screens containing the combination ^{6}LiF / Gd_2O_2S:Tb with maximum emission at 549 nm (green light) and with a 30 – 50 % higher brightness, while the same resolution as with conventional Gd_2O_2S:Tb screens can be achieved. Research to improve the performance of neutron scintillators in the light yield, light decay time and neutron capture efficiency is ongoing.

The intensity of the photons generated by scintillators are normally of low intensity relative to ambient background light levels, thus requiring the whole system to be contained inside a secured light-tight box with the inside painted black.

Digital Detector Technology

Ideally, a digital neutron radiograph should have as many pixels as possible (the smaller the pixel size the better) in both directions with equal performance of each to obtain a high spatial-pixel resolution in the digital radiograph. Flexible camera-box systems that have different positional options for the CCD camera w.r.t. the scintillator screen, provides flexible field-of-view (FOV) selections that ranges from 5 x 5 cm up to 35 x 35 cm. Subsequent pixel resolutions for CCD cameras with pixel arrays of 2048 x 2028 pixel elements ranges from 0,024 – 0,170 mm/pixel.

Using the digital neutron detector system at the SANRAD facility in South Africa, a spatial resolution of 100 µm was achieved at an L/D of 250 on a digital radiograph taken with the purpose to perform quality control on a SAFARI-1 cadmium containing control rod (Figure 2.11). However, development of digital NRAD detection systems during the past decade, and already available at international facilities[1] now also allows for spatial resolution down to 5 micron available at which matches the resolution performance of micro-focus XRAD detection systems. Apart from the time needed for the acquisition of the radiograph, which is a function of the radiation flux, the efficiency of the radiation conversion and subsequent detection, as well as the electronic read out time from the arrays of pixel elements that forms the detector, determines the time resolution of the acquisition system.

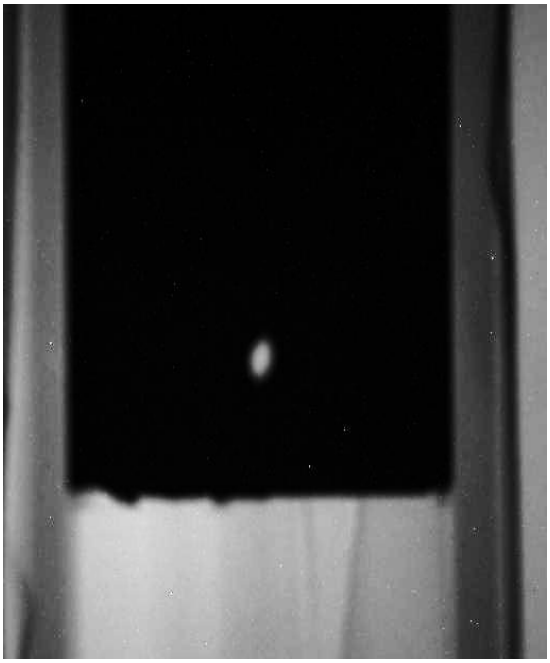

Figure 2.11: Demonstration of the successful application of a digital neutron radiography / tomography detection system using a LiF/ZnS(Ag) neutron sensitive scintillator and digital CCD camera: Quantitative quality inspection of a SAFARI-1 nuclear reactor control rod containing Cadmium (Black) could be achieved. (Courtesy: Necsa).

Spatial resolution

The spatial resolving power of an imaging system is its ability to distinguish separation between two objects very close to each other in space. More generally, it is its ability to distinguish spatial frequency information accurately. In practice the final image is produced by the digital detection

[1] Neutron radiography facilities: PSI (Switzerland); Helmholtz-Berlin (Germany); TUM (Germany); NIST (USA).

system. The system spatial resolution is derived from this final image and therefore includes contributions of all optical elements along the complete radiography system, such as, collimation ratio (Section 2.5), object-to-detector-distance (Section 2.3), scanning parameters such as the number of projections for tomography (Section 2.8.2), the scintillation screen effect, characteristics of the digital detector and subsequent image processing. Perturbing effects by secondary radiation and object stability is discussed elsewhere (Lehmann, 2007) and shall not be addressed in this section, which addresses spatial resolution determination in general and mention considerations to improve and optimise resolution through ongoing scintillator and CCD-camera detection development. Spatial resolution is commonly defined in terms of full width at half maximum (FWHM) and also nowadays in terms of the contrast modulation transfer function (MTF).

Consider an equally spaced series of narrow strips (say thin wires) with well-defined straight edges. Let the spaces between the wires be large compared to the wavelength of the radiation, so that a real image rather than a diffraction pattern is produced upon illumination by a beam of radiation. The images of the wires will not exhibit perfectly sharp edges. They will instead have a continuous half-shadow transition region from total absorption to total transmission (over full gray scale range) whilst the wires are still clearly resolved, provided the spacing exceeds the resolution limit of the imaging system. As the spacing between wires becomes smaller the resulting image will eventually gain the appearance of a sine wave. Should the spacing decrease even further the waves start to overlap and no regions of total transmission will be seen in the image. When the spacing between two lines becomes so small that the sine waves, which constitute their images, overlap at half the value of their original amplitude, the corresponding spacing is known as the full width at half maximum. The FWHM, also known as the Rayleigh criterion, is often used as the definition for the spatial resolving power of the imaging system.

In the MTF approach the system's response to a periodic sine wave, as a function of spatial frequency, is specified. Formally the MTF is defined as the Fourier transform of the Line Spread Function (LSF), which is the derivative of the Edge Spread Function (ESF). In practice the latter is obtained by taking a radiograph of (typically) a sharp straight gadolinium edge and determining the line profile perpendicular to the edge by averaging over a number of pixels (Lehmann, 2007) (Gonsalves, 2007). The Fourier transform of the LSF, the MTF, provides the system response amplitude as a function of spatial frequency. This allows for a more comprehensive definition of the ability of the system to resolve high spatial frequencies. In terms of the MTF, spatial resolution is defined in terms of the spatial frequency where the MTF drops to 10% of its maximum value.

For CCD-scintillator setups, the available range of active scintillator material thickness from 50 µm to 400 µm allows researchers to optimize either for resolution or high light output respectively. Thicker scintillation material produces more chance for neutron capture and light production but also more opportunity for the effects of energy transfer to spread out. The material becomes more absorbing to, and scatters its own light more strongly, and thus contributes to the blur in the radiograph.

Spatial resolution in digital images depends, inter alia, on the number of pixels defining the image. Images with higher spatial resolution are composed of a greater number of pixels than those of lower spatial resolution. There is a constant effort to improve the time resolution as well as image quality (higher S/N ratio) of digital systems, an effort that entails development of detectors with higher pixel element density and with lower electronic noise (detector optimisation) as well as developments to increase neutron flux, whilst reducing background.

2.6.2 XRAD detectors

Two X-ray detector systems utilised at Necsa are discussed:

2.6.2.1 Digital X-ray detection: Scintillation and CCD-camera based

A similar approach as described for the neutron scintillation-CCD setup (Par 2.6.1.4) applies, with the difference that an X-ray sensitive gadolinium-oxysulfide (Gd2O2S:Tb) (Gadox) scintillator is now used. A focal spot size of 1 mm together with the maximum sample to detector distance of ~ 1000 mm and detector 2D array of 1024 × 1024 pixel elements, allowed only for a spatial pixel resolution of ~100 µm and relatively high unsharpness (Ug). A resolution 2D-radiograph and corresponding 3D-tomogram of a PBMR fuel sphere, taken under these conditions, are shown in Figure 2.12. These results illustrate the limitations of low L/D's in radiographs and tomograms using this configuration of source characteristics and source - detector setup. Despite the limitations a tomographic reconstruction was done in an attempt to see if the presence of coated particles in the fuel free zone could in principle be detected. In a radiograph this will only be possible if the orientation fortuitously allows detection. As can be seen from the tomographic slice in Figure 2.12, this will be highly unlikely for the particulat radiography system used.

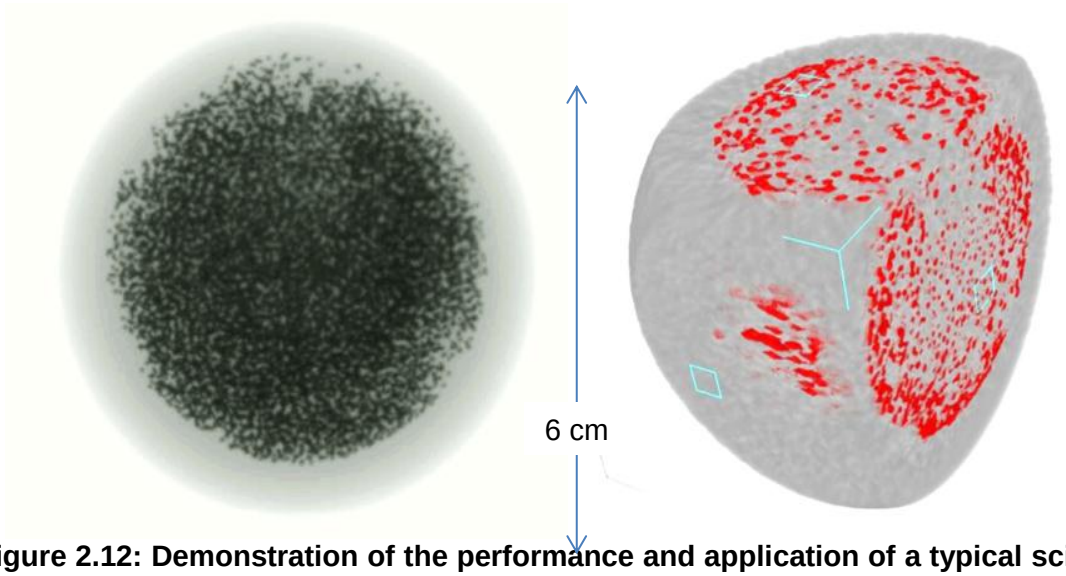

Figure 2.12: Demonstration of the performance and application of a typical scintillator - CCD-camera based digital setup with a 1 mm X-ray focal spot on a PBMR fuel sphere: LEFT: Low quality X-ray radiograph with low definition of the TRISO particles, but ability to visualise the fuel containing core and fuel free zone. RIGHT: Corresponding low quality sliced X-ray tomogram. (Courtesy: Necsa).

2.6.2.2 Digital X-ray detection: Amorphous silicon 2D flat panel

The current Micro-focus X-ray tomography (MIXRAD) facility is equipped with the PerkinElmer amorphous silicon (a-Si) X-ray flat panel detector (PerkinElmer, 2017). The detector has a 2D array of 2048 × 2048 pixel elements - each with a physical dimension of 0.2 mm x 0.2 mm and allows for a 16 bit grey scale dynamic range. Due to the extremely small X-ray focal spot of 3 - 5

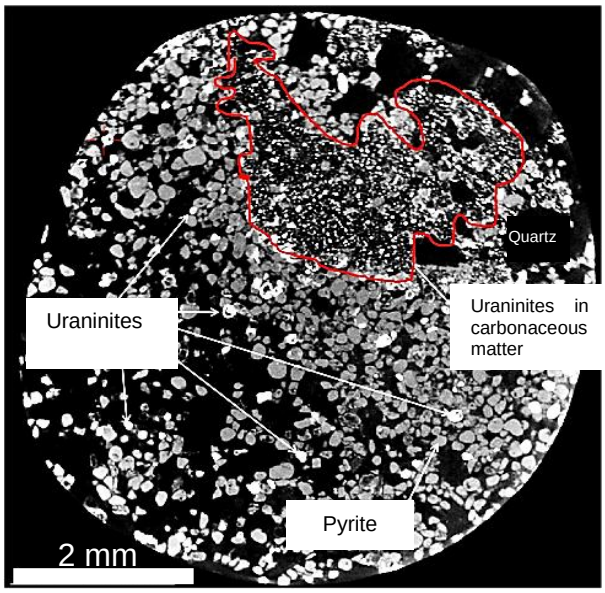

Figure 2.2: Demonstration of the performance of the PerkinElmer Amorphous Silicon X-ray flat panel detector. Large geometric magnification resulted in high pixel resolution in the 2D slice of a µXCT tomogram showing small uraninite grains, quartz-pyrite matrix and carbonaceous matter but with sharp defined edges. (Courtesy: Necsa).

µm, geometric enlargement is possible to obtain, a theoretical best resolution of ~5 µm / pixel. In practice the resolution achievable depends on the total object size to be imaged and sample to source distance. Figure 2.13 illustrates the high practical resolution of the detector. The figure reveals micro-millimetre high quality and well defined edges of grains in a typical 8 mm diameter large and geometrically magnified geological sample.

2.7 Attenuation of Radiation by the Object

The physics of photon interaction with materials is a well-established field (Jackson and Hawkes, 1981), and in this chapter, only the basic principles of relevance to radiography, and especially with respect to differences between X-rays and neutrons will be discussed briefly.

The difference in attenuation of radiation passing through the object makes the process of radiography possible. Attenuation of a thin parallel, monochromatic beam in slab geometry is described by the Beer-Lambert law (Banhart, 2008) (Eq.6):

$$I = I_0 e^{-\mu\rho x} \tag{6}$$

With:
- I_0 = Impinging radiation flux (particles.cm^{-2}.s^{-1})
- I = Transmitted flux (particles.cm^{-2}.s^{-1})
- μ = Mass attenuation coefficient (cm^2/g)
- ρ = Density (g/cm^3)
- x = Thickness of object (cm)

The difference in attenuation mechanisms for X-rays and neutrons stem from the fact that X-rays undergo electromagnetic interaction with the electrons in matter, whereas neutrons undergo point-like scattering from, or are absorbed by, the nuclei. The cross-section for X-ray attenuation thus increases monotonically with the atomic number.. For neutrons, on the other hand, there is no such simple rule. A graphical comparison of the attenuation characteristics of some elements for neutrons and X-rays are depicted in Figure 2.14 (PSI, 2017). Note in particular that the neutron attenuation coefficient for lead is very small compared to that for X-rays. The complementary nature of X-ray and neutron radiography stems from these intrinsic attenuation differences.

When used and applied in radiography, the two techniques complement each other and provide different insight into the same object. Comparison of advantages of neutrons and X-rays over each other, are summarised below:

- Some light elements such as hydrogen and boron can be detected by neutrons, but not by X-rays – to allow inter alia, detection of water within a high density concrete sample.
- Better penetration by neutrons of high Z-elements such as lead and bronze to inter alia support the study of some cultural heritage artefacts.
- Neutrons are more sensitive for defect detection in a hostile environment containing, for example, gamma-rays and other radiation. NRAD's first dedicated application was the radiography of highly radioactive power reactor fuel pins in the NDE-investigation of their structural integrity.
- Neutrons differentiate between isotopes of certain elements, i.e. U-235 and U-238.
- As the X-ray scattering and absorption of elements increase gradually with an increasing Z, the contrast between neighbouring elements on the periodic table is very small. In many cases, such elements can be better distinguished between by neutrons.

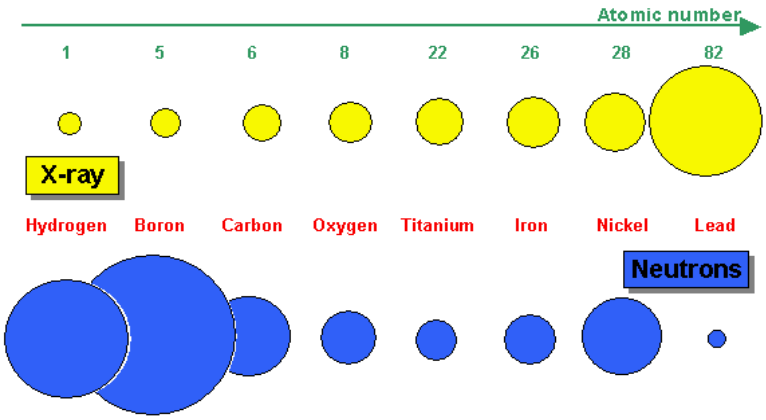

Figure 2.14: Graphical comparison of neutron and X-ray attenuation for some elements. (Courtesy: PSI).

A comprehensive compilation of linear attenuation coefficients (cm^{-1}) for thermal neutrons and X-rays (150kV) are listed by PSI, Switzerland (PSI, 2017).

Attenuation involves absorption, incoherent as well as coherent scattering. In coherent scattering the neutron waves can undergo Bragg reflection off crystal planes, whereas there are no such material induced systematic phase relationships for incoherent scattering. Attenuation due to coherent scattering is exploited with great effect in cold neutron radiography and tomography where wavelengths on different sides of a Bragg edge of the materials in the study object result in a significant change in attenuation, allowing inter alia texture to be visualised (See Section 2.11 for more on Bragg-reflection).

2.8 History and Principle of Tomography

Here only a brief history and some basic principles of tomography are described.

2.8.1 History of tomography

Computed Tomography (CT) imaging is also known as "CAT scanning" (Computerized Axial Tomography or Computer Assisted Tomography). Tomography is from the Greek word "tomos" meaning "slice" or "section" and "graphia" meaning "describing" (IMAGINIS, n.d.).

The basic principle entails that, from a large series of 2D radiographs obtained along a single rotation axis and at many equally spaced rotation angles around a sample, cross sectional slices of an object and consequently a three-dimensional virtual representation of the object can be computed (reconstructed). The first mathematical model, the Radon transform, defined by an Austrian mathematician Johann Radon in 1917, is an integral transform whose inverse forms the basis for reconstruction of 3D images (Weisstein n.d.). It was first used in the medical field in the form of XCT scans and still forms the mathematical basis of a host of different numerical reconstruction techniques used today.

The principle of CT was mutually invented (made public) in 1972 by the British engineer Godfrey Hounsfield and by the South African-born American physicist Allan Cormack (Vaughan, 2007). The enormous contribution of the discovery to the health of humankind was immediately obvious and as a consequence Cormack and Hounsfield were awarded the 1979 Nobel Prize in Medicine for their contributions to medicine and science (Cormack, 1979) (Hounsfield, 1979) (See Appendix 1).

However, much earlier in October 1971, the 1st medical clinical 3D-scan in history was produced and computerized at the Atkinson Morley Hospital, England. The object was a slice of the brain as shown in Figure 2.15(a) (Impactscan, 2013). The first clinical CT scanners, dedicated to 3D head imaging only, was commercially produced in 1973 by the Electric and Music Industries (EMI) Company in England and were installed in England between 1974 and 1976 (see Figure 2.15(b)). The "whole body" 3D CT systems also became available in 1976 and globally by about 1980.

The first tomography EMI head scanner, in the South African medical CT-context, was acquired by the Groote Schuur Hospital in Cape Town in 1976 and was located on the ground floor of the J-block, in the Neuro radiology unit. The first “whole body CT scanner” was purchased by the “Volkshospitaal” in 1977, with Groote Schuur Hospital receiving theirs in 1981 (Beningfield, 2017).

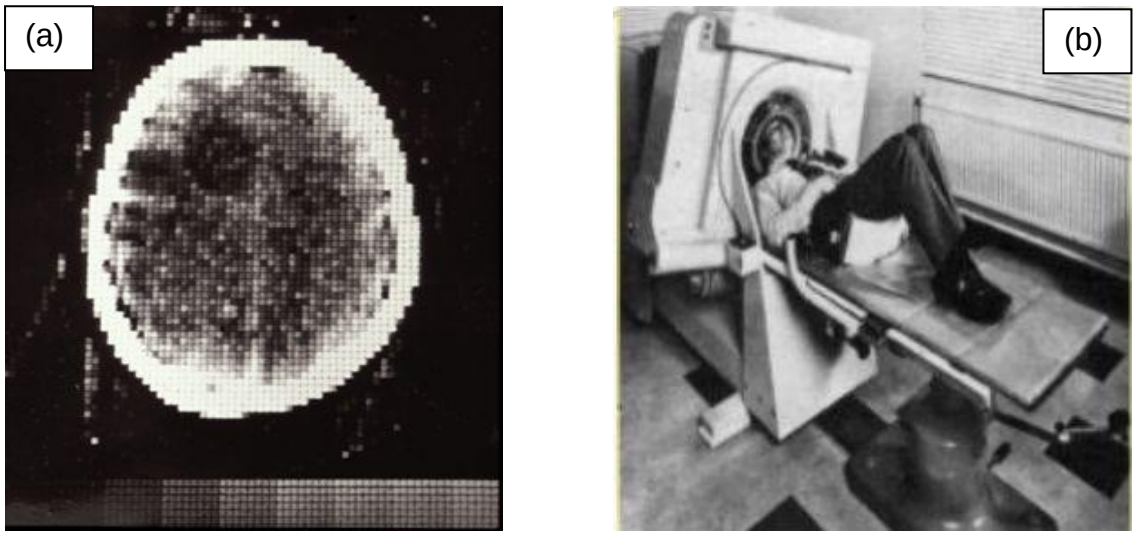

Figure 2.15: (a): A slice from the first clinical CT scan performed at the Atkinson Morley Hospital: Oct 1971. (b): First Generation of CT scanners – scanning only the head section. (Impactscan, 2013)

2.8.2 Tomography process

The basic principles of each of the key actions/methodologies within the tomography process, namely data acquisition (scanning), reconstruction and evaluation (analysis), are briefly discussed. Detail descriptions can be studied with reference to the UTCT X-ray laboratory in

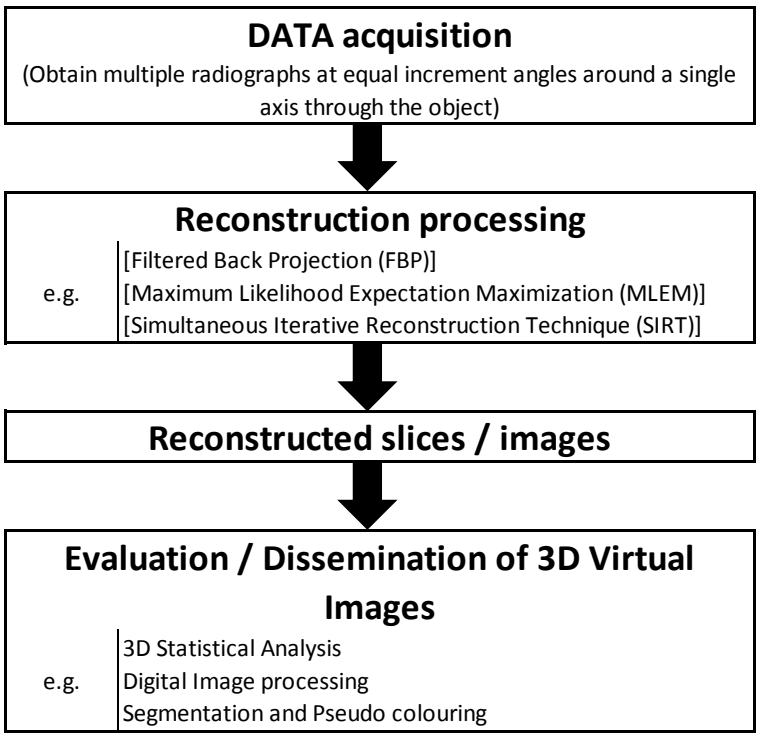

Figure 2.16: Basic 3D tomography steps.

Austin Texas, USA (UTCT, 2017) and the ANTARES neutron radiography facility at FRMII, TUM, Garching, Germany (Lorenz, 2007). The basic steps to obtain a 3D virtual volume of a sample under investigation are depicted in Figure 2.16.

Data Acquisition (Scanning):

Only the cone beam geometry that results from using the collimator geometry explained in Section 2.5, in combination with object rotation and a 2D planar area detector is used at Necsa. A more detailed explanation of alternative beam geometries has been described elsewhere (Ketcham, 2017) and is depicted in Figure 2.17.

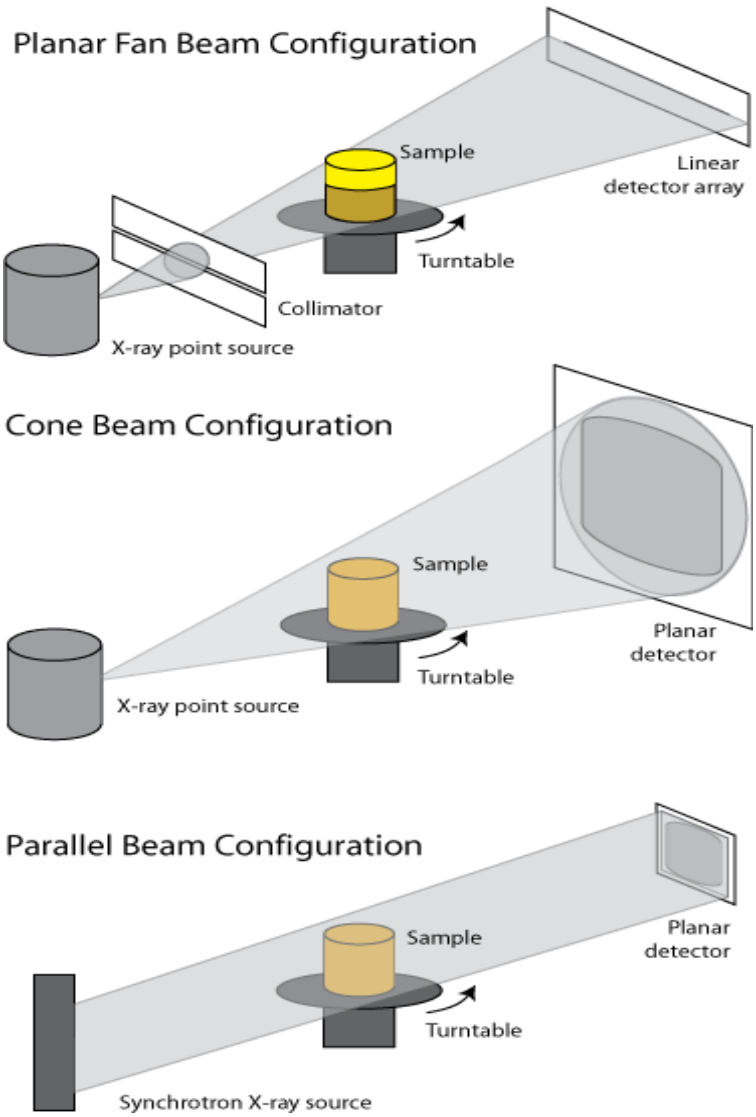

Figure 2.17: Tomography beam geometries.

For successful implementation, the experimental setup parameters have to be arranged carefully in line with the principles discussed in Section 2.3 for X-rays and neutrons. In addition, other practical aspects to be considered during the scanning process are (a) the neutron activation of samples, (b) number of projections for an optimized quality tomography result and (c,d) collection of additional radiographs for their application in quantitative evaluations.

(a) Neutron activation of the sample

For all samples subjected to a thermal neutron beam a degree of induced radioactivity is expected, depending on the elemental composition, their concentration within the object, and the time of exposure to neutrons. Just after exposure there is some emission of secondary radiation due to the decay of activated nuclides but most of the involved material activity is short-lived and background radiation levels are reached after 3-7 days at most. Special care has to be taken to limit exposure of or even avoiding the study of samples consisting of large concentration of elements such as Co, Eu, Ni or Ag since their decay half-lives are long and the activation cross section high. For valuable objects, it may be prudent to make a brief exposure to verify the degree of activation before an extended tomographic investigation is attempted.

(b) Number of projections

To reduce artefacts and optimise for spatial resolution in both X-Ray and neutron detection systems, the total sample, part of the sample or region of interest (ROI) within a sample, should be visible on the detector from any viewing angle. Additionally, the number of projections in 180° to optimise for spatial resolution is described by the Nyquist-Shannon theorem that states that details with high spatial frequency will not be accurately represented in the final digital image when scanned with a fewer number of projections as defined by equation 7.

$$N_{projection} = \pi/2 * OW \quad (7)$$

Where:

- $N_{projection}$ is the minimum number of projections required in 180°.
- OW is the object width defined by the number of pixels that constitutes the widest horizontal dimension of the object to be radiographed.

(c) Normalisation for uniformity of the radiation beam, scintillator screen and CCD chip: Acquisition of open beam (OB) projections

A set of radiographs of a sample under investigation, acquired over a longer period of acquisition, requires normalization due to possible temporal intensity variations resulting from potential radiation beam fluctuation and detector system inconsistency. A number of open beam (OB) radiographs at the beginning and end of an acquisition period are acquired without sample in the beam. The average OB radiograph then obtained, contains spatial variations in beam intensity and detector sensitivity. The OB radiograph is normally used as the un-attenuated intensity of the beam, I_0, in each pixel to solve for (μpx) as depicted in Eq-6 (Section 2.7) during quantitative analysis. Additionally, during the tomography reconstruction process, in order to reduce artefacts in the resultant tomogram, all projections are normalised to the OB resultant radiograph by using the same small field of un-attenuated open beam area in all projections.

(d) Correction for internal camera noise: Acquisition of dark-current (DC) projections

CCD cameras have intrinsic thermal generated noise known as *dark-current* (DC) noise originating from electron hole pairs thermally generated inside the silicon of the CCD chip (The CCD off-set). The pixel wells are filled by these electrons and thus contribute in a negative manner to the grey scale value. Although the CCD chip can be thermoelectrically (Peltier cooling) cooled through air or water to reduce the dark current effect, the dark current offset (per pixel) can further be corrected for by taking a number of “dark field” radiographs with no radiation beam present. The average CCD off-set per pixel is then used in the correction of each of the 2D radiographs and is subtracted from all projections as well as the open beam (OB) radiographs used for beam normalisation. After the normalization (including DC and OB corrections) and cleaning of the “white spots”, which is caused by unwanted gamma evens on the CCD chip, the projection data is ready for reconstruction into a 3D virtual data set.

3D Reconstruction from 2D projections

Radon (Radon, 1917) provided a proof that the density of an object can be reconstructed from observations along many lines and for many angles of observation, a brief discussion of which will be provided below. Here “density” is meant in the abstract sense of the attenuation ability at each point in the (x,y) plane of the object slice.

Principle of reconstruction from line integrated information

Consider a cylindrically symmetric object for which the density varies radially only, such as shown in Figure 2.18. For such an object, the density profile $\rho(r)$ can be deduced from parallel rays passing through the object at different distances p from the centre for only one angle of observation. It follows from Figure 2.18 that (Eq. 8):

$$f(p) = \int_{-\infty}^{\infty} \frac{\rho(r)r}{\sqrt{r^2-p^2}}\, dr \qquad (8)$$

The inverse of this integral is known as the Abel inverse and is given by (Eq 9):

$$\rho(r) = -\frac{1}{\pi}\int_{r}^{\infty} \frac{df}{dp}\frac{dp}{\sqrt{r^2-p^2}} \qquad (9)$$

Thus, if many rays are measured to determine a projected profile f(p) on the detector (also known as a sinogram), the density profile can be found by evaluation of (Eq 9).

Thus, even for cylindrical symmetry, many rays are required for a good reconstruction of the density features of the object.

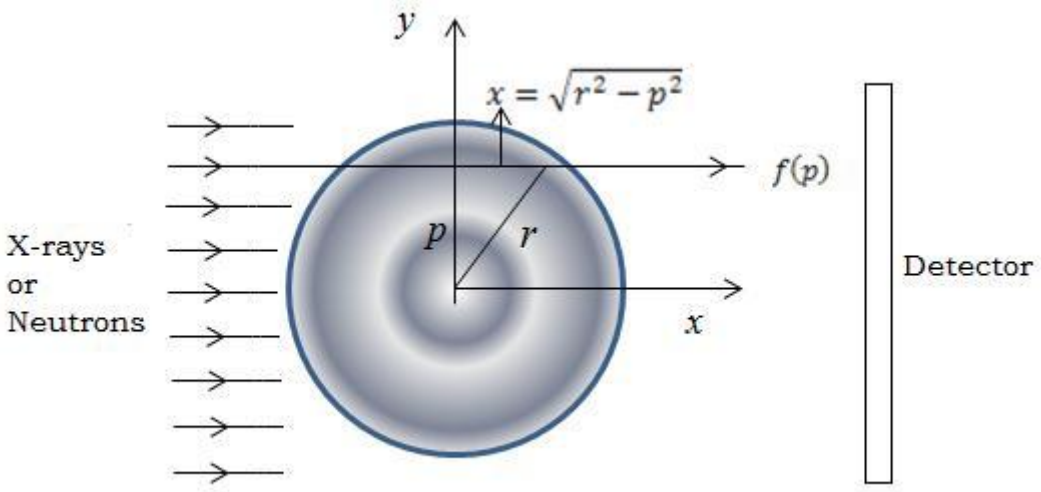

Figure 2.18: Reconstruction of a cylindrically symmetric object slice. (Courtesy: Necsa).

Now consider an object which has angular and radial distribution $\rho(r,\theta)$. It is obvious that apart from as many parallel rays as before, many angular orientations also need to be recorded to reconstruct the density distribution in sufficient detail. The geometry is shown in Figure 2.19.

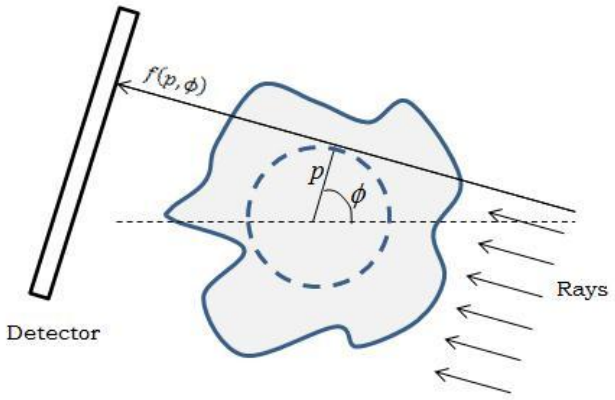

Figure 2.19: Reconstruction geometry for a general 2D density distribution. (Courtesy: Necsa).

The sinograms on the detector have the form:

$$f(p,\phi) = \int_{-\infty}^{\infty} \rho(r,\theta)\, dl \qquad (10)$$

Here dl is a line element along the ray direction. The question then arises whether a formal reconstruction of $\rho(r,\theta)$ can be achieved through information acquired for many p and ϕ values. That such a reconstruction can be done is not obvious unless formally proven. If the object is rotated around some rotation point O, the angularly averaged sinogram can be determined and represents a quasi-cylindrically symmetric quantity as:

$$f(p,\phi) = -\frac{1}{\pi}\int_{0}^{2\pi} f(p,\phi)\, d\phi \qquad (11)$$

Radon has formally shown that an inverse, analogous to the Abel inverse, exists that provides the density at the origin of rotation as:

$$\rho(O) = -\frac{1}{\pi}\int_0^{\infty}\frac{d\bar{f}}{p} = -\frac{1}{\pi}\int_0^{\infty}\frac{d\bar{f}}{dp}\frac{dp}{p} \qquad (12)$$

Equation 12 proves the existence of a true reconstructed density from line integrated angular and distance information, but does not provide for a direct practical way to construct $\rho(r,\theta)$ for the object. A practical means to perform the Radon inverse was first reported by Hounsfield & Cormack (See Section 2.8.1). A 3-dimensional (3D) virtual object can be assembled consisting of many vertically stacked cross-sectional slices reconstructed in such a manner. Each slice has a thickness of the spatial resolution obtained during the scanning process and can be of the order of 3 - 500 microns thick. Over the years, a number of different computational schemes have been developed to perform the reconstruction conveniently in practice. One such technique is the filtered back projection method.

Consider a two dimensional slice of an object in the Cartesian XY plane as shown in Figure 2.20(a). The two-dimensional slice has in fact a narrow width in the third dimension due to a thin slab of radiation traversing it. Let the object function of the material in the plane be represented by f(x,y), which represent an effective attenuation field, due to material properties in combination with physical density as mentioned above.

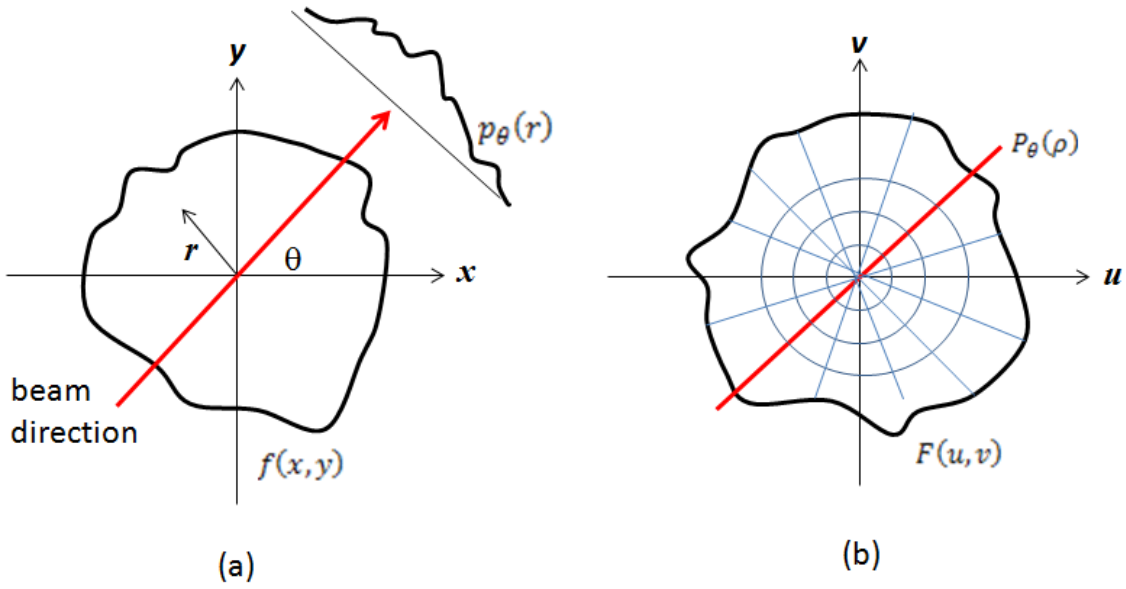

Figure 2.20: (a) Graphical representation of a 2-dimensional slice $f(x,y)$ in the Cartesian plane. (b) Fourier transform of $f(x,y)$ in the spatial frequency space (u,v). (Courtesy: Necsa).

A projected transmission profile $p_\theta(r)$, also known as a sinogram, is recorded on a detector. This is also sometimes referred to as the detector function. A sinogram can be recorded for as many

angles as desired and as many z-slices can be taken as desired for a given resolution. Note that the angle is labelled as a parameter rather than a variable, which emphasises that a sinogram is a one-dimensional function of the radial distance r parametrised by the angle of observation.

In tomography, many sinograms at different angles are recorded and the object function f(x,y) has to be derived from the resulting data. As the sinograms are one-dimensional and the object function is two-dimensional, this cannot be achieved in a direct manner. However, an ingenious method, known as the Filtered Fourier Back Projection Method, has been devised to achieve this via fast Fourier transform routines. The method relies on the fact that the Fourier transform of the object function $f(x,y)$, namely $F(u,v)$, can be constructed from the information contained in the one-dimensional Fourier transform $P_\theta(\rho)$ of the one-dimensional sinogram $p_\theta(r)$. From the Fourier slice theorem (Kak and Slaney, 1988), it follows that the Fourier transform $P_\theta(\rho)$ represents a slice through the origin of $F(u,v)$ in Fourier space at the same angle as the original angle of observation in object space. This is explicitly indicated in Figure 2.20(b) by the profile $P_\theta(\rho)$ in red. A few other hypothetical $P_\theta(\rho)$ profiles in Fourier space are also shown. All of them run through the origin of Fourier space and represent Fourier transforms of their respective θ-equivalent sinograms in real space, as proven by the Fourier slice theorem. It is now possible to simply perform a Fourier back projection of $F(u,v)$ to find the object function, $f(x,y)$. This is the principle behind Fourier back projection. However, without first performing a filtering of the data points in the Fourier domain, such a raw reconstruction will result in inadequate resolution of small features (high frequency) detail. This can be seen as follows from Figure 2. 20(b). Regularly sampled data points in the XY plane of the object function translates to Fourier space as non-regularly spaced data points, represented by the crossings of radial lines and circles in Figure 2.20(b). In particular it can be seen that there is a higher density of data points near the centre than towards the edge of the Fourier transformed object. As the direct and Fourier coordinates are inversely related, this implies that low frequencies is sampled much more densely than high frequencies. The relative shortage of high frequency data will cause a loss of detail in the Fourier back projection. To correct for this phenomena, a filter needs to be applied to the data in Fourier space. Effectively this partially restores balance between data density in the central and outer regions of $F(u,v)$. As more data is taken to achieve sufficient data everywhere, the final result is a more even data spread across Fourier space. A common filter used in X-ray CT is due to Ramachandran & Lakshminarayanan (Ramachandran, 1971) and is referred to as the Ram-Lak filter. In practice interpolation routines are also used to provide a rectangular (u,v) data grid, which is required for Fast Fourier Transform routines, after which the back projection can be performed to yield a

much improved object function with respect to clarity of detail, thus the name Filtered Back Projection.

Analysis: View and interpretation

The 3D virtual data sets, generated from the reconstruction process, now allow that the physical information of an object at the spatial resolution level is available for analysis, segmentation and dissemination. At Necsa these functions are performed by making use of commercially available software products. Table 2.1 summarises the different software packages currently commercially available and normally utilised worldwide within the tomography research community.

Table 2.1: Different PC software packages available for 3D data analyses.

Name of product	Company	WWW	Discussion
2D IMAGE ANALYSIS SOFTWARE			
ImageJ	Open Source software on internet	https://imagej.nih.gov/ij	Image processing program designed for scientific multidimensional images.
IPPLUS	MediaCybernetics	http://www.mediacy.com	Image analysis software makes it easy to acquire images, count, measure, classify objects and automate analysis.
3D IMAGE ANALYSIS SOFTWARE			
VGStudioMAX	Volume Graphics	https://www.volumegraphics.com	Leading analysis and visualisation software for industrial CT data and is a pioneer in digital workflow management using data from all common measuring methods.
Amira - Aviso	FEI – part of Thermo Fisher Scientific	https://www.fei.com	Amira and Avizo are the leading high-performance 3D visualisation and analysis software for scientific and industrial data.

2.9 Radiography in South Africa: A Short Historical Overview

To make an assessment about the author's contribution in radiography within the South African context and in time, it is necessary to also paint the picture of the history of the early (1st of) radiography applications within South Africa in the medical and non-destructive analysis fields.

2.9.1 Early days of medical radiography in South Africa

The medical application of the "new" X-rays within 5 years after its discovery showed its acceptance as a diagnostic tool during the Anglo Boer war (1899 – 1902). The first X-ray apparatus was installed in Johannesburg as early as 1897 and is thoroughly described by Hahn (Hahn, 1973).

At least five sets of apparatus were fully operational and utilised at Jacobsdal, Springfontein, Krugersdorp, Johannesburg and Pretoria, servicing the Boers. In addition, about

ten systems, including those on the hospital ships were in operation on the British side (Edwards, 1901). Dr Hall Edwards (1858 - 1926), the “father” of British radiology who championed the new discovery, was in charge of the apparatus in the Imperial Yeomanry Hospital in Pretoria but tragically lost his fingers years later from irradiation necrosis as a result of his pioneering work. The crudeness of the early apparatus together with a lack of knowledge about the hazards of radiation exposure at the time was to blame for his loss. In those early days (Figure 2.21), care was taken to protect the patient from electrical shocks by connecting wires, but no consideration was given to the safety of the operator (Hahn, 1973). Apart from medical use of X-rays, the people also flocked to see and experience the new wonder of radiography displayed at exhibitions (Figure 2.22).

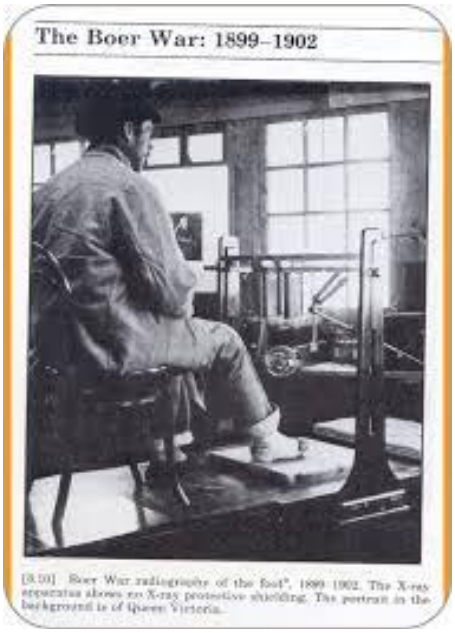

Figure 2.21: X-ray apparatus and unsafe X-ray medical practice during the Boer War. (Hahn, 1973)

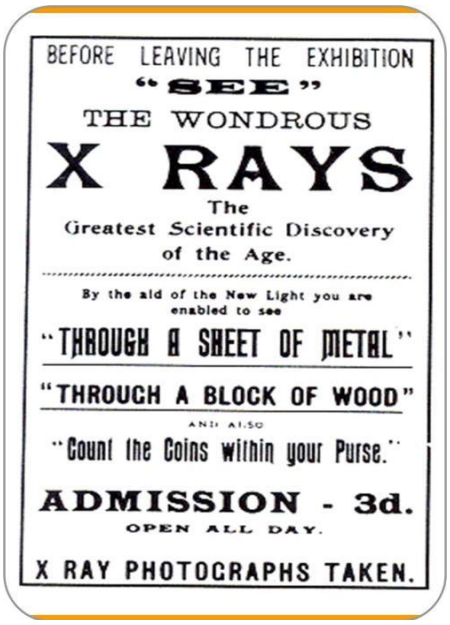

Figure 2.22: Advert to the public to experience the wonder of X-rays early in 1900's. (Click Americana memories & memorabilia, 2017)

2.9.2 Radiation based techniques in the NDE industry in South Africa

When the Boer war was over and things had returned to normal, X-ray apparatus were duly delivered to the Jagersfontein Mine to be used on all diamond diggings. When the State Alluvial Diggings were opened in 1929 at Alexander Bay, the Government installed a very large X-ray unit for the same purpose (Hahn, 1973). Thus radiography became a standard non-destructive (NDE) quality assurance and analytical technique in the South African industries which led to the founding of the South African Institute for Non-Destructive Testing (SAINT) in 1968. A time-

line of important activities of SAINT is tabled in Table 2.2 with the participation of the author in some activities of SAINT added to the list. (SAINT, 2016)

Table 2.2: Main activities of the SAINT.

1968	**SAINT: The Institute was founded on 28 September 1968.**
1985	SAINT in conjunction with the SA Institute of Welding (SAIW) launched the South African Qualification and Certification Committee (SAQCC).
1991	Professional co-operation agreement signed between SAINT and the American Society for Non-Destructive Testing (ASNT).
1995	SAINT appoints a manager, Neville Budd.
1996	First newsletter known as IMAGES, was launched.
1996	**Frikkie de Beer receives the Reisener Award for best Lecture at a SAINT evening meeting**.
1997	The Institute hosted the 2nd African Convention for NDT in Johannesburg. **Frikkie de Beer participated.**
2000	SAINT launches the predecessor of the SAINT Professional Body for NDT i.e. the South African Certification Body for NDT (SACBNDT) – disbanded in 2003.
2002	SAINT receives the H Rohloff Trophy for Progress in NDT from the H Rohloff company to award as they see fit.
2003	In conjunction with the Engineering Council of South Africa (ECSA) in an effort to register NDT practitioners, council members in particular Manfred Johannes compiled NDT standards, Level I and II UT and PT.
2003	SAINT launched its first Website – designed and managed by the late Mark Mason.
2004	The Institute won the bid for the 18th World Conference on NDT (WCNDT) in Durban at the 17th WCNDT in Montreal, Canada.
2004	SAINT hosted the 1st National NDT Conference at the CSIR in Pretoria. **Frikkie de Beer participated.**
2012/2013	The 1st edition of the SAINT Yearbook, was published.
2012	SAINT hosted the 18th World Conference for NDT in Durban. **Frikkie de Beer participated.**
2013	Indaba held with members and interested parties in February – SAINT was given the mandate to establish a Professional Body for NDT Practitioners.
2013	Steering Committee starts operating on SAINT Professional Body. The Annual General Meeting receives unanimous acceptance to proceed with the Professional Body. **Frikkie de Beer fulfils the role of the vice-chairman of PBNDT.**
2014	SAINT President attended the European Federation for NDT (EFNDT) conference in Prague.
2014	SAINT President - Keith Cain – presents the Reisener Award to Phil Kilfoil for the best paper presented at a technical evening during the year.
2015	SAINT receives a huge acknowledgement for its WCNDT with the request from the ASNT President during his visit to South Africa to please provide him with a summary of what SAINT's WCNDT local organising Committee did, in order to hold such a successful conference.
2015	SAINT confers Honourary Memberships on Butch Davies and Professor Arthur Every for their enormous efforts towards making the WCNDT the success that it was.
2015	The SAINT Professional Body (SPBNDT) awarded professional status and registered by the SA Qualifications Authority (SAQA) with the authority to issue designations to NDT Operators (Level I) and NDT Technicians (Level II).
2017	**SAINT President - Keith Cain – presents the H Rohloff trophy to Frikkie de Beer for the best research project conducted in 2016.**

2.10 Radiography at Necsa (Early Years: 1970 – 1988)

All the radiography activities practiced at Necsa and which set the baseline of activities before the contribution of the Author are briefly described below.

2.10.1 X-ray and gamma-ray radiography at Necsa

As one of the key capabilities within the nuclear energy sector, industrial film-based radiography has been applied since the early years of the Atomic Energy Board (AEB) along with ultrasonic, magnetic particle and liquid penetrant testing as quality control Non-destructive Examination (NDE) techniques. Many years later, the National Nuclear Manufacturing Centre at Necsa obtained accredited competence status in NDE Level-I and Level-II in X-ray- and gamma-ray radiography with American Society of Mechanical Engineers (ASME) III Nuclear Certification, ASME VIII accreditation and ISO 9001 certification.

2.10.2 Neutron radiography at Necsa

2.10.2.1 Van de Graaff and RFQ-linac accelerator based neutron sources

Necsa's 4 MV Van de Graaff accelerator accelerates protons, deuterons and a range of other positively charged species for application in Particle Induced X-ray Emission (PIXE) and Rutherford Backscattering Spectroscopy (RBS) experimental Ion Beam techniques. In particular, neutrons can be generated through d(Be,n) or p(Li,n) reactions. A Radio Frequency Quadrapole (RFQ) accelerator system that can accelerate D+ ions to 3.7 – 5.1 MeV or protons to 1.8 – 2.5 MeV is also available at Necsa. Depending on the beam target used, these two accelerators can produce fast neutrons with energies of up to 14 MeV (and associated gamma-rays) at a rate of 10^{6} - 10^{12} $n.cm^{-2}.s^{-1}$, ideally suited for neutron radiography (Franklyn & Daniels, 2012).

2.10.2.2 SAFARI-1 nuclear research reactor as neutron source

The South African 20 MW nuclear research reactor, which is based on the Oak-Ridge open pool type design, was commissioned in 1965. This research reactor is located at Pelindaba about 30 km west of Pretoria. This reactor, named the South African Fundamental Atomic Research Installation No 1, also known as SAFARI-1, is currently still operated by the state-owned South African Nuclear Energy Corporation SOC Ltd. (Necsa) (Figure 2.23). The purpose of the reactor is to be used as a Material Testing Reactor (MTR) with in-pool and out-of-pool irradiation capabilities.

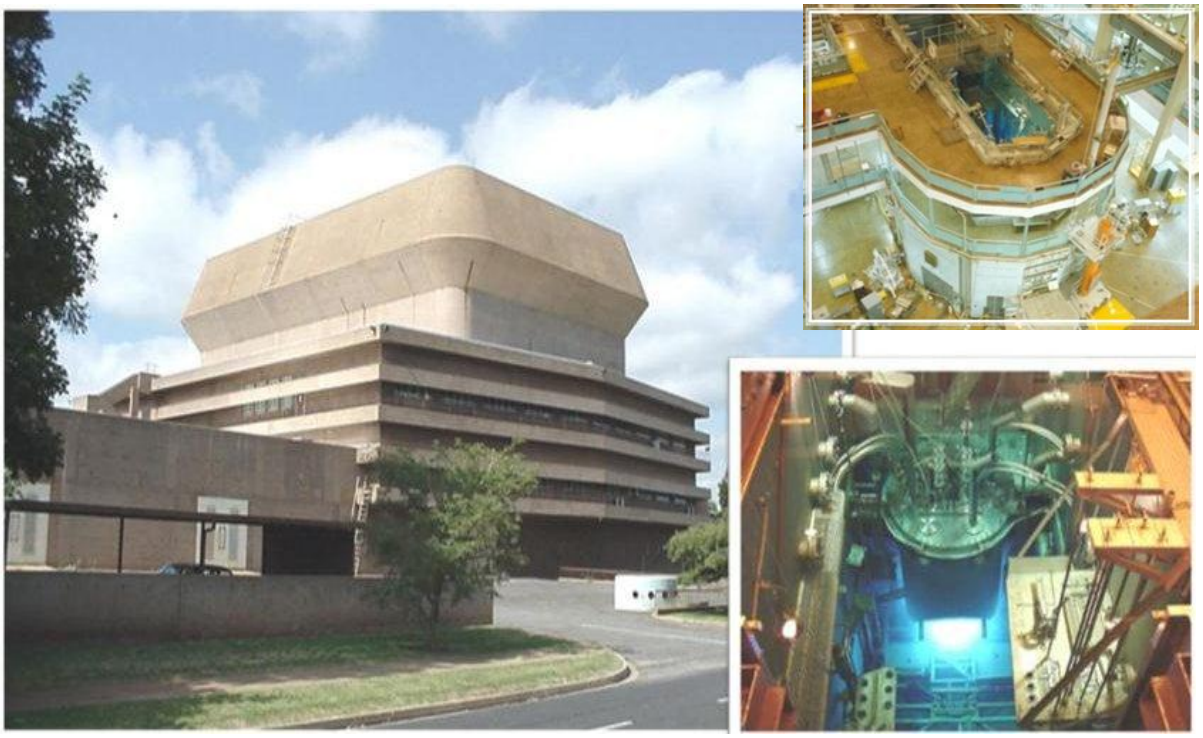

Figure 2.23: Necsa's SAFARI-1 nuclear research reactor at Pelindaba. (Courtesy: Necsa).

The splitting (fission) of enriched U-235 nuclei within the core of SAFARI-1, releases neutron and gamma-ray radiation. In-core irradiation capabilities include Neutron Activation Analysis (NAA) and the production of medical isotopes as commercial products. Neutron transmutation doping of silicon or irradiation of, for example, Topaz to enhance its commercial value is performed in-pool and close to the reactor core (Position A in Figure 2.24). Neutrons are also channelled from the reactor core via six (6) axially aligned beam tubes, either 7 inch or 10 inch diameter wide, through the biological shield of the reactor to the beam port hall (Position C in Figure 2.24).

The beam ports are equipped with experimental infrastructure for such applications as prompt gamma neutron activation analysis (PGNAA), neutron diffraction (NDIFF), currently at Beam Tube no-5 (BT5), or neutron radiography (NRAD), currently at BT2.

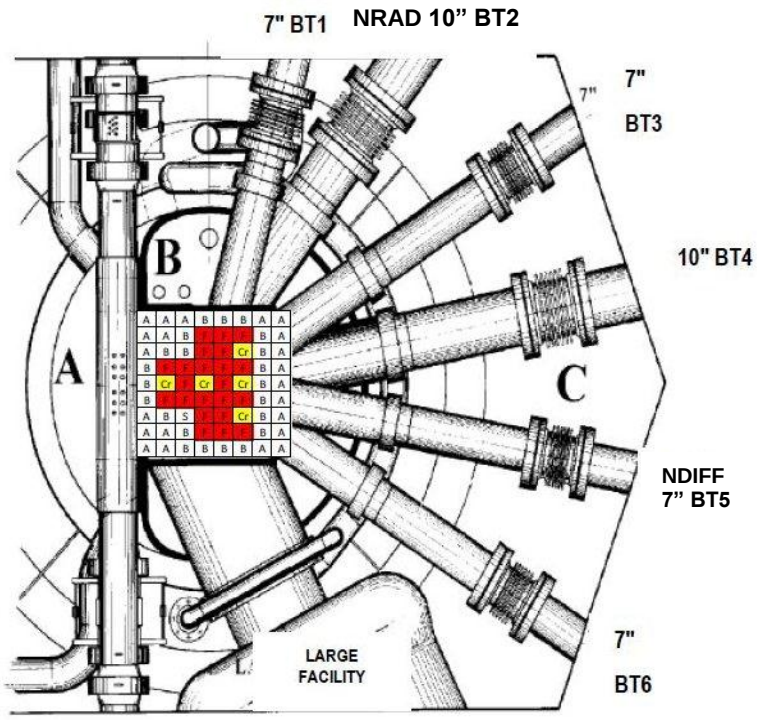

Figure 2.24: Radiation beam lines from the reactor core towards the beam port hall. Beam Tube 5 (BT5) and BT2 currently host the Neutron Diffraction (NDIFF) and Neutron Radiography (NRAD) facilities respectively. (Courtesy: Necsa).

(a) In-pool neutron radiography

During the early days (from 1965), SAFARI-1 was used as a source of neutrons for the very first research activities during the 1960's, which included an in-pool NRAD as a non-destructive analytical technique (Newby-Fraser 1979). The integrity of the nuclear fuel (Figure 2.25) of the Pelindaba Deuterium Uranium Sodium (Na) (PELINDUNA) power reactor concept was investigated in an in-pool NRAD configuration installed inside specialised "chouca rigs" (Uytenbogaard, 2017).

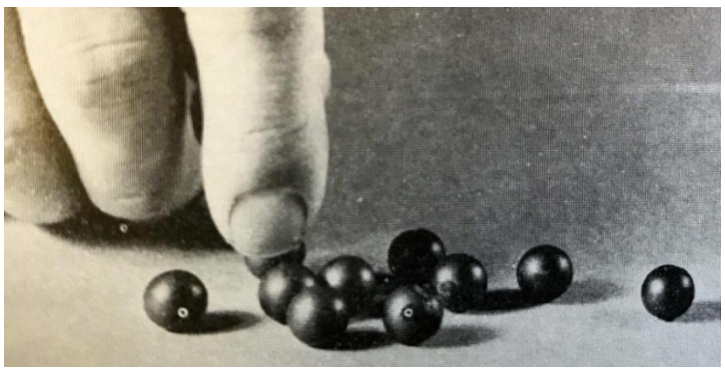

Figure 2.25: Fuel spheres from the PELINDUNA project. (Newby-Fraser 1979)

Apparatus, similar to what was used at SAFARI-1, are illustrated in Figure 2.26 (Domanus & Markgraf, 1987). Unfortunately, no permanent record of the very first NRAD investigations at SAFARI-1 could be located.

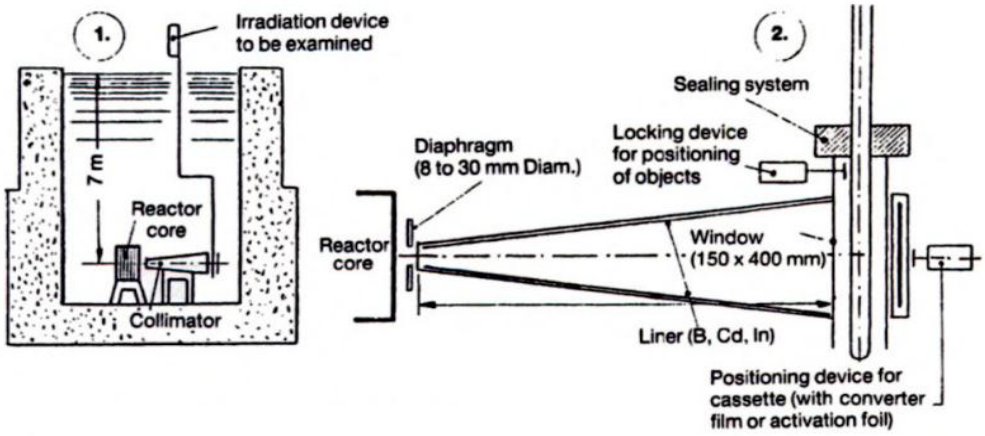

Figure 2.26: In-pool collimator set-up for neutron radiography.(Domanus, 1987).

(b) Out-of-pool (Beam lines)

One of the 6 beam lines of SAFARI-1 was equipped early in the 1970's with a pin-hole collimator for neutron radiography. From the late 1970's, the direct film technique (see Section 2.6.1.1) was applied[2] to obtain several neutron radiographs for inter alia the detection of blockages in aircraft fuel lines (Figure 2.27).

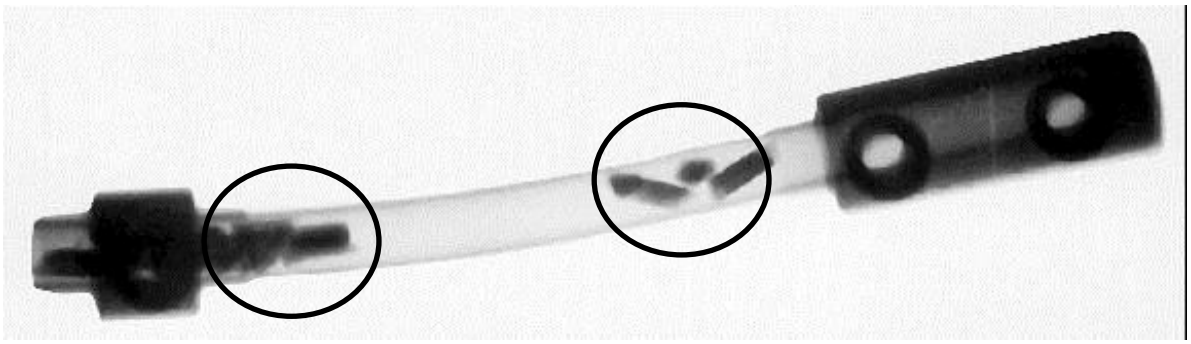

Figure 2.27: Film neutron radiograph of the blockage (encircled) of aircraft fluid flow components. (Photo: Courtesy of Mr. Don Uytenbogaard).

During the early 1980's, a Post Irradiation Examination (PIE) program for the performance validation and testing of Necsa-manufactured Koeberg nuclear fuel pins (Lead Test Assemblies

[2] Mr. Don Uytenbogaard: Engineer at SAFARI-1.

(LTA)) was launched. A hot cell complex[3] that hosts several analytical techniques was developed for the PIE program. At SAFARI-1, the NRAD facility at BT2 was equipped[4] with a neutron film camera especially to image[5] the highly radioactive fuel pins as an important non-destructive analytic technique to study the physical behaviour and performance of the fuel within the Zirconium fuel cladding.[6]

New Neutron Radiography Innovations - a Future Perspective for South Africa.

During the last few decades, development of new methods in radiography world-wide increased the scope of the method significantly. Neutron scattering and imaging have not only started to overlap in terms of accessible structure sizes, but also have been merged in several techniques taking advantage of diffraction and scattering while probing macroscopic variations with real space image resolution (Strobl and Grazzi, 2015). These developments include probing the small angle scattering regime through dark-field contrast imaging (Strobl, 2008) and utilizing coherent scattering through spatially resolved Bragg edge signatures of crystalline materials in the transmitted beam. Such methods naturally require both imaging detection and wavelength resolution and therefore the best available neutron phase space densities. Due to inherent limitations none of these techniques are currently assessable at Necsa, but clearly should be considered in future planning for radiography and tomography expansion in South Africa. The following paragraphs briefly describe utilisation of a number of contrast mechanisms in neutron radiography/tomography beyond traditional attenuation contrast, which allows various mechanical, micro-structural and magnetic properties of materials to be studied.

Neutron Bragg-edge Imaging

Energy dispersive attenuation measurements, which are straightforward at pulsed neutron sources through time-of-flight measurements, enable access to a wealth of additional information in imaging. This is in particular the case for crystalline materials where the coherent elastic Bragg scattering dominates the attenuation of the beam at the lattice planes in the wavelength range of cold neutrons. Correspondingly the transmitted wavelength resolved spectrum provides insights with respect to the crystalline structures in the sample.

Neutron energy selective imaging is applied in the investigation of polycrystalline materials. Kardjilov et al. (Kardjilov, 2017) describe the technique of diffraction contrast based neutron

[3] Program Manager of the Hot Cell Complex: Dr. Johan Aspeling.
[4] Manager: Mr. Willie Jonker; NRAD Beam Line Technicians: Ms. Clara Dyason and Mr. Paul Thomson; Electronic Program IT Technician: Mr. Gordon Proctor.
[5] See PAR 2.6.1.3 for the discussion of the nitro-cellulose film imaging technique.
[6] See PAR 2.6.1.3 for a NRAD radiograph of nuclear fuel.

imaging in terms of its history, theory and instrumentation and further applied the technique, inter alia, successfully into studying aspects of cultural heritage artefacts –an area of great interest to South Africa. The principle is based on the phenomena that the neutron attenuation coefficient of a polycrystalline material changes suddenly for certain well-defined neutron wavelengths in the cold neutron spectrum, thereby causing discreet edges in the transmitted intensity profile as a function of wavelength. The attenuation sensitivity afforded by neutron diffraction under Bragg edge conditions can be used to detect presence of residual stress by measuring the shift of the Bragg edges due to lattice distortions. Additionally, texture in metallurgical samples as well as some information about grain size becomes available. Bragg edge recording thus allows for additional contrast enhancement (e.g. Fe and Cu in the same sample) as well as crystallite (grain) phase separation and segregation (e.g. Fe_2O_3 and Fe_3O_4) (Strobl, 2015).

As long as the overall attenuation effect of the final transmitted information can be written in the form of the radon transform, it should be able to visualise the effects through reconstruction. Quantitative CT image reconstruction of crystalline structural information (e.g., crystal lattice strain, crystallographic texture, crystallite size and crystalline phase) in a bulk material by using the Bragg-edge neutron transmission spectroscopy is one of the final goals of technical developments in the energy-resolved neutron imaging field. The development is of obvious importance to materials science and engineering, and means that a useful new tool for “three-dimensional” crystalline structure analysis may be available to complement diffraction (a non-imaging technique).

Grating interferometry (Dark Field Imaging)

Dark field imaging is similar to phase contrast imaging in that features that would otherwise be invisible (transparent) due to inadequate contrast in transmission mode, can be rendered visible through analysis of the scattered part of the radiation field only. The name dark field has its origin in optical microscopy and comes from the fact that the direct transmitted radiation field is excluded, leaving an image formed only by scattered radiation against an otherwise dark background. Likewise, dark-field images are formed by small-angle scattering of X-rays or neutrons. Because the small-angle scattering signal is sensitive to density fluctuation on much smaller length scales ($d \sim \theta / \lambda$) than what can be achieved with direct imaging, the result is improved image resolution. The dark-field image thus visualizes the scattering properties of samples in the small-angle and ultra-small-angle scattering range. These angles correspond to correlation lengths from several hundred nano meters up to several tens of micro meters.

Noteworthy developments in dark field imaging (Strobel, M. et. Al 2008) with grating interferometers promises to make it possible to get information about small angle scattering

combined with three dimensional spatial resolution via direct imaging, even at lab-based X-ray and neutron sources (Strobel, 2014). Whereas imaging provides visualisation (through attenuation) of individual structures at typically micrometer size and larger, small angle scattering provides the ability to use the distribution of scattered radiation at small forward angles to derive information about the statistical distribution and nature of the scattering medium at a smaller scale. The latter is normally achieved by probing relatively homogeneous samples, such as solutions of colloids or defects in materials. Investigation of small angle scattering from regions of heterogeneous samples requires a technique that can spatially resolve such regions, whilst being able to provide small angle scattering information relating to the regions at the same time.

The introduction of grating interferometers for dark-field contrast imaging provided two orders of magnitude improvement in efficiency with respect to the possibility of accessing some structural information in the small angle scattering regime at the same time. In practise neutron dark field imaging with grating interferometers make use of three gratings (Strobel et.al., 2008; Hilger A. et. al., 2010). The first grating is an absorption slit grating positioned behind the aperture, which defines together with the distance to the sample, and the sample to detector distance, the geometrically achievable resolution of the imaging instrument. The source grating, provides a number of partially coherent beams, which form an interference pattern behind a second phase grating due to periodical phase shifts, $\phi=\pi$. The geometry is arranged to allow for constructive superposition of the beams at the first Talbot distance. There a third grating, which is an absorption analyzer grating with a period corresponding to the interference pattern, is placed. The interference pattern cannot be directly resolved by the detection system, but can be resolved in each imaging pixel by a stepwise scan of the analyzer grating. This way, the angular and spatial resolution is decoupled (Kardjilov, 2011) (Kardjilov, 2009) (Grünzweig, 2008).

Applications of dark-field contrast with neutrons are of considerable practical importance to assist with improved understanding of, and thus development of advanced technologies in, engineering materials. It also becomes possible to diagnose fundamental aspects of magnetic materials, of great importance to information technology, due to the magnetic moment of neutrons. It's value is realised in the investigation of micro and nano heterogeneity of structures in the scale range of 0.1 µm to 10 µm. and thus the visualization of microstructural changes (e.g. areas of porosity) in metallurgical samples such as archaelogical bronzes and iron. X-ray dark-field contrast imaging renders soft tissue open to detailed scrutiny with direct medical applications, such as for instance in the investigation of breast cancer (Ando, 2005). All of these areas are of interest to the ambitions of South Africa to become an advanced knowledge driven economy.

Phase-contrast Radiography

The simplest tomography set-up to perform phase contrast with neutrons (and X-rays) is to exploit propagation based contrast. Provided the distance between the sample and detector is appropriately selected, phase contrast can be recorded in the image without the need for analyser crystals or any form of additional phase shift. The setup is therefore the same as for conventional radiography, except for an increased sample-to-detector distance. It is essential though to utilise a small aperture for the incoming beam and to place the sample far from the aperture to have a radiation field with near plane wave character and high transverse (perpendicular to the optical axis) coherence. The variation in refractive index of the sample cause the outgoing waves to have small but differing angular deviations.

If the detector is too close to the sample the waves cannot interfere as phase information must have time to spread out an overlap. In such a case only the normal attenuation contrast will be observed by the detector. This represents the normal neutron radiography set-up.

As the detector is moved further back from the sample, diffraction effects start to appear around the edges of the image of small features in the object, thereby enhancing the edge definition and contrast. If the detector is placed too far away the Fourier transform of the sample, rather than a projection of its features, is recorded. In practice the set-up can be empirically arranged to provide an optimally sharp image of the features of the object. The phase-contrast method is thus actually an edge-enhancement method to visualize very fine structures where conventional radiography provides unsatisfactory results. Intensity is sacrificed by the stringent aperture reduction and distance requirements, which makes the method practical only for high flux primary sources (Kardjilov, 2004).

Polarized Neutron Radiography

The neutron possesses a magnetic moment, which makes it sensitive to magnetic fields in free space and inside the bulk materials. Polarized neutron radiography is possible through the spatially resolved measurement of the final precession angles of a polarized monochromatic cold neutron beam that transmits a magnetic field. When using polarized neutrons, detection of polarization changes in the transmitted beam is possible after it has passed through a spin analyser onto an area detector, thus allowing visualization of the magnetic fields. A double crystal monochromator device is commonly used to select a defined wavelength from a cold neutron spectrum together with one spin polariser device and one spin analyser device. The resulting transmitted polarised beam is of low intensity and therefore the background interference of other radiation such as high energy gammas and fast neutrons must be kept as

low as possible. The high penetrability advantage of neutrons allows thus the investigation of magnetism in the bulk of e.g. superconductor materials (Kardjilov, 2009).

Bibliography

Ando, M. et al., 2005. Attempt at Visualizing Breast Cancer with X-ray Dark Field Imaging. Jpn. J. Appl. Phys. 44, 528–531.

Anon, 2014. 'All Nobel Prizes in Physics'. Nobelprize.org. Nobel Media. Available at: http://www.nobelprize.org/nobel_prizes/physics/laureates/%3E [Accessed September 4, 2017].

Banhart, J., 2008. *Advanced Tomographic Methods in Materials Research and Engineering* 1st ed. J. Banhard, ed., Berlin: Hahn-Meittner Institute, Berlin, Germany.

Beningfield, S. (Prof), 2017. Personal Communication: Head of Radiology at Groote Schuur Hospital and UCT.

Chadwick, J., 1933. The Nobel Prize in Physics 1935: James Chadwick. 'The Neutron and its Properties'. *British Journal of Radiology*, 6, pp.24–32. Available at: http://www.nobelprize.org/nobel_prizes/physics/laureates/1935/chadwick-facts.html

Click Americana memories & memorabilia, https://clickamericana.com/eras/1800s/1890s/x-ray-wonders-1896/2. (Accessed May 20, 2017)

.

Cormack, A.M., 1979. The Nobel Prize in Physiology or Medicine 1979: Allan Cormack, Godfrey Hounsfield. 'Early Two-Dimensional Reconstruction and Recent Topics Stemming from it.' Nobelprize.org. Available at: http://www.nobelprize.org/nobel_prizes/medicine/laureates/1979/cormack-bio.html [Accessed June 13, 2017].

De Beer, F.C. et al., 2004. Neutron Radiography and Other NDE Tests of Main Rotor Helicopter Blades. Applied Radiation and Isotopes, 61(4), pp.609–616. Available at: http://linkinghub.elsevier.com/retrieve/pii/S096980430400185X.

DOE–report: Next Generation Neutron Scintillators Based on Semiconductor Nanostructures, Final Report 6/30/2008, DOE Award: DE-FG02-07ER84884

Domanus, J.C. & Markgraf, J.F.W., 1987. *Collimators for Thermal Neutron Radiography an Overview*, D.Reidel Publishing Company.

Domanus, J.C., 1992. Practical Neutron radiography, Kluwer Academic Publications.

Edwards, J., 1901. The Roentgen Rays in South Africa. Lancet 1, (1), pp.1755–1756.

Franklyn, C. & Daniels, G.C., 2012. Characterization Methods for an Accelerator Based Fast-Neutron Facility. Journal of *Instrumentation*, 7(2), pp.C02043–C02043. Available at: http://iopscience.iop.org/article/10.1088/1748-0221/7/02/C02043/pdf [Accessed November 2, 2017].

Glasser, O., 1993. *Wilhelm Conrad Röntgen and the Early History of the Roentgen Rays*., Norman Publishing.

Gonsalves, M.J., Lopes, R.T., Silvani,M.I., De Almeida, G.L. and Fureiri, R.C.A.A., 2005. Development of a CCD-based Image Acquiring System for Neutrons at the Argonauta Reactor, Brazil Journal of Physics, Vo. 35, No 3b.

Grünzweig, C., Pfeiffer, F., Bunk, O., Donath, T., Kühne, G., Frei, G., Dierolf, M. and David, C., Design, 2008. Fabrication, and Caracterization of Diffraction Gratings for Neutron Phase Contrast Imaging. Review of Scientific Instruments 79.

Hahn, O.H., 1973. Some Historical Notes on South Africa's Pioneer Radiographer. S.A. Medical Journal, (22 Dec 1973), pp.2428–2430.

Halmshaw, R., 1988. Introduction to the Non-Destructive Testing of Welded Joints. Crampton & Sons, UK.

Hilger, A., Kardjilov, N., Kandemir, T., Manke, I, Banhart, J., Penumadu, D., Manescu, A. and Strobl, M., 2010. Revealing microstructural inhomogeneities with dark-field neutron imaging, Journal of Applied Physics 107, 036101, p107.

Hounsfield, G.N., 1979. The Nobel Prize in Physiology or Medicine 1979: Godfrey N. Hounsfield. 'Computed Medical Imaging'. Nobleprize.org. Available at: https://www.nobelprize.org/nobel_prizes/medicine/laureates/1979/hounsfield-bio.html [Accessed June 17, 2017].

IMAGINIS, Brief History of CT. *IMAGINIS*. Available at: http://www.imaginis.com/ct-scan/brief-history-of-ct. [Accessed June 17, 2017].

Impactscan, 2013. *A Brief History of CT*. Available at: http://www.impactscan.org/CThistory.htm [Accessed June 17, 2017].

Jackson, D.F. and Hawkes, D.J., 1981. X-ray attenuation coefficients of the elements and mixtures. *Physics Reports*, 70, 169.

Kak and Slaney, 1988. *Principles of Computerized Tomographic Imaging 1st ed*., New York: IEEE Press.

Kallman, H., 1948. Neutron Radiography. Research 1, p.254.

Kardjilov, N., Lehmann, E., Steichele, E. and Vontobel, P., 2004. Phase-contrast radiography with a polychromatic neutron beam. Nuclear Instruments and Methods in Physics Research Section A: Accelerators, Spectrometers, Detectors and Associated Equipment 527, 519-530; published online Epub7/21/.

Kardjilov, N., Hilger, A., Manke, I., Strobl, M., Dawson, M. and Banhart, J., 2009. New trends in neutron imaging. Nuclear Instruments and Methods in Physics Research Section A: Accelerators, Spectrometers, Detectors and Associated Equipment 605, 13-15.

Kardjilov, N., Hilger, A., Manke, I., Strobl, M., Dawson, M. and Banhart, J., 2011. Neutron imaging in materials science. Materials Today 14, 248.

Kardjilov, Nikolay, Festa, Giulia (Eds.), 2016. Book Title: Neutron Methods for Archaeology and

Cultural Heritage, Chapter 16: Neutron Imaging, N. Kardjilov, E. Lehmann, M. Strobl, R. Woracek and I Manke. Publisher Name: Springer International Publishing. Publisher Location: ChamSeries ID8141Series. Title: Neutron Scattering Applications and Techniques. ISBN: 978-3-319-33161-4, http://dx.DOI10.1007/978-3-319-33163-8.

Ketcham, R., 2017. X-Ray Computed Tomography (CT). *Geochemical Instrumentation and Analysis.* Available at: https://serc.carleton.edu/research_education/geochemsheets/techniques/CT.html [Accessed July 23, 2017].

Lehmann, E.H., Frei, G., Kuhne, G. And Boillat, P. 2007. The Micro-setup for Neutron Imaging: A major step forward to Inprove the Spatial Resolution, NIM-A, 576, p389-396.

Lorenz, K., 2007. Antares (Advanced Neutron Tomography and Radiography Experimental System). Available at: http://einrichtungen.ph.tum.de/antares/ [Accessed July 25, 2017.

Newby-Fraser, A.R., 1979. *CHAIN REACTION.*

Nothnagel, G., 2007. Personal Communication, 'Using the Invisible to Reveal the Hidden'.
.

PSI - Paul-Sherrer-Institute, Neutrons: Comparison to X-ray. What is neutron imaging? Available at: https://www.psi.ch/niag/comparison-to-x-ray [Accessed July 20, 2017].

PerkinElmer : https://perkinelmer.com. [Accessed July 22, 2017].

Peter, O., 1946. Neutronen-Durchleuchtung. Naturforsch, I(10), p.557.

Radon, J., 2017, "On the Determination of Functions from their Integrals Along Certain Manifolds". Über die Bestimmung von Funktionen durch ihre Integralwerte längs gewisser Mannigfaltigkeiten. Berichte Sachsische Akademie der Wissenchaften, Leipzig, Mathematische-Physikalische Klasse, vol. 69, pp. 262-267.

Ramachandran, G.N. and Lakshminarayanan, A.V., 1971. Proc. Natl. Acad. Sci. USA., 68(9):2236-40.

Röntgen, C.R., 1896. On a New Kind of Rays. Nature, 53, p.274.

SAINT: YEARBOOK 2016/2017: Cornerstone of South African Non-Destructive Testing

Strobl, M., et al., 2008. Neutron dark-field tomography. Physical Review Letters, 101(12).

Strobl, M., 2014. General solution for dark field imaging with grating interferometers. Scientific Reports. 4 : 7243. DOI: 10.1038/srep07243.

Strobl, M. and Grazzi F., 2015. From Scattering in Imaging to Prospects at Pulsed Sources, Neutron News 26:2.

Strobl, M., 2015. The Scope of the Imaging Instrument Project ODIN at ESS, Physics Procedia, 69, p18 – 26.

"The Nobel Prize in Physics 1901". Nobelprize.org. Nobel Media AB 2014. Web. 3 Apr 2017. <http://www.nobelprize.org/nobel_prizes/physics/laureates/1901/>

TRITEC, 2018. http://www.rctritec.com/en/scintillators/products.html (Visited on 5 March 2018).

UTCT, 2017. University of Texas at Austin CT Lab. *TEXAS Geosciences*. Available at: http://www.ctlab.geo.utexas.edu/ [Accessed July 25, 2017].

Uytenbogaard, D., 2017. Personal Communication: Engineer at SAFARI-1 and NRAD Practitioner.

Vaughan, C.L., 2007. Imagining the Elephant: Biography of Allan MacLeod Cormack C. L. Vaughan, ed., ICP.

Weisstein, E.W., RadonTransform. MathWorld--A Wolfram Web Resource. Available at: http://mathworld.wolfram.com/RadonTransform.html [Accessed June 18, 2017].

CHAPTER 3

Development and Utilisation of Necsa Facilities

This Chapter summarises the activities of the author from 1988 over a period of 29 years in the development of research radiography and tomography facilities at Necsa. It also includes a comprehensive summary of the research output generated at the established facilities by all visiting post graduate students and researchers. The complete research output of the author is mentioned with reference to the four research outputs for the requirement of this PhD.

"Anyone who has never made a mistake has never tried anything new"
Albert Einstein

3.1 Introduction

This chapter summarises the development and utilisation of advanced neutron and X-ray radiography and tomography facilities, of which the former being the first in the southern Hemisphere. The author has been instrumental in these developments, has subsequently promoted the research potential thereof, and rendered expert scientific instrument support to researchers from diverse fields of application. For these reasons, a short overview of research collaborations, user group growth and some research outputs relevant to the requirements of this thesis are presented. This compilation helps to indicate to what extent the establishment and expert utilisation of these facilities supported the goals of the South African National System of Innovation (NSI), and the role the author played in this regard. This chapter further allows visualisation of how the publications selected to form part of this thesis fits into a larger number of local activities and applications of neutron and X-ray radiography and tomography.

3.2 Development of Radiography and Tomography Facilities at Necsa

Both neutron and X-ray radiography and tomography research facilities have been developed because of the complementary nature of the techniques and for the benefit of offering both analytical services to users.

3.2.1 Development of neutron based radiography research facilities

The author's role in the development of the Neutron Radiography (NRAD) facilities at Necsa will be discussed in the context of three different periods, each mandated by affordability, practicality and user needs at the specific time.

3.2.1.1 Post irradiation examination (PIE) of PWR fuel (1980 – 1994): SAFARI-1 reactor beam tube 4

Hot cell facilities were developed at the South African Nuclear Energy Corporation SOC Ltd. (Necsa) as part of its Pressurised Water Reactor (PWR) fuel development and reactor surveillance programme. The PWR post-irradiation examination (PIE) programme at Necsa, which included neutron radiography (NRAD) investigations on six Lead Test Assemblies (LTA's), managed to provide a good overall picture of locally produced PWR fuel behaviour (Klopper et al. 2007).

The author, who had just joined Necsa at the time, worked as part of a team[7] assisting with the commissioning of a neutron radiography facility at beam port No. 4 at SAFARI-1 (Figure 3.1). The basic infrastructure was minimal, but effective, and constituted a crane, flask, beam stop, NRAD chamber and nitrocellulose film camera system. Development work entailed testing and parameter optimisation for the nitro-cellulose film based camera system, including the film development and the analysis aspects. The author completed the necessary quality assurance documentation (e.g. standardised work procedures) before the arrival of the first LTA fuel rods for PIE in 1992. Termination of the LTA testing program in 1994 led to partial decommissioning of the NRAD facility with the existing shielding and door infrastructure available for future NRAD utilisation. The demonstration of the usefulness of neutron radiography for non-destructive testing of fuel test assemblies provided strong motivation and impetus for the development of a general purpose NRAD facility at SAFARI-1.

3.2.1.2 General purpose NRAD (1994 – 2013): SAFARI-1 reactor - Beam tubes 4 and 2

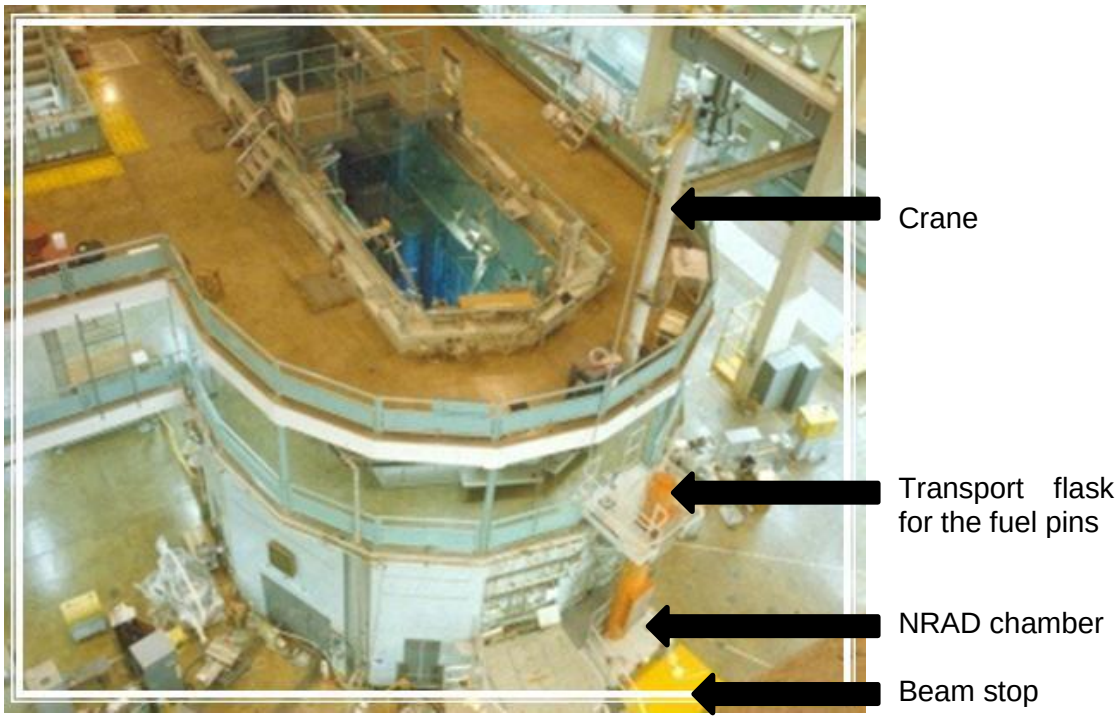

Figure 3.1: Neutron radiography set-up at beam tube 4 on the beam port floor of the SAFARI-1 nuclear research reactor for PIE of LTA fuel pins.

The primary detection methods on the first NRAD instrument were limited to nitro-cellulose and X-ray film. Both direct and transfer neutron radiography techniques could however be utilised to

7 Mr. Paul Thompson and Ms. Clara Dyason as co-workers; Mr. Gordon Proctor and Mr. Ben van Staden as Engineers and Mr. Willie Jonker as Project Leader and Supervisor.

produce an image on film. A limited space of less than 0.5 x 0.5 x 0.5 m for sample placement was available, which restricted sample size and made the facility unsuitable for general purpose neutron radiography.

About 30 years after film techniques for neutron radiography were successfully developed and applied, electronic neutron imaging methods that would eventually largely replace film techniques were developed abroad and reported in several World Conferences on Neutron Radiography (WCNR) proceedings (WCNR-2: Barton 1986) (WCNR-3: S. Fugine 1991) (WCNR-4: Barton 1993).

Within a short time period, the author and co-workers[8] expanded the experimental chamber to a 2 m x 2 m x 2 m enclosure in a cost-effective manner, using the old door as a beam stop for the new system. In addition, the first electronic camera with a zoom capability to obtain higher spatial resolution and with a frame rate of 25 fps was developed, installed and commissioned in collaboration with Betascan (SA)[9]. This system produced dynamic neutron radiographs and, in comparison with the film method, was flexible and boasted direct quantitative as well as qualitative imaging capabilities (Figure 3.2).

Figure 3.2: LEFT: First neutron radiography facility at beam port 4. MIDDLE: Electronic camera box partially covered with borated wax and B_4C materials as radiation shield. RIGHT: First electronic neutron radiography camera system.

This upgrade was planned, not only for applied research related investigations (Strydom, Venter, Franklyn, & De Beer, 2002), but also to conduct contract research and non-destructive testing for industrial clients on a commercial basis (F.C. De Beer & Strydom, 2001) (WCNR-6: Fujine et al. 2001).

8 Dr. Wessel Strydom: Necsa: Specialist Nuclear Scientist and Line Manager.
9 Mr. Wouter van der Berg: BetaScan Electronics CC (Now Stinger Electronics).

The first NRAD facility installed at beam tube 4 was relocated to beam tube 2 due to the development and expansion of the adjacent Neutron Diffraction (NDIFF) facility at beam tube 5 (Figure 3.3). The existing NRAD shielding components and electronic camera system were also relocated to beam tube 2 while a new replica NRAD collimator was manufactured. This was necessary due to a corroded front end of the old collimator that resulted in water leakage and associated interference with free streaming neutron transport through the tube. A description of the proposed South African Neutron Radiography (SANRAD) facility with tomography capability (F.C. de Beer & Lehmann, 2005) and its current performance in relation to other NRAD facilities on the African continent (F.C. de Beer et al., 2005) were presented by the author in 2002 at the WCNR-7 in Rome, Italy.

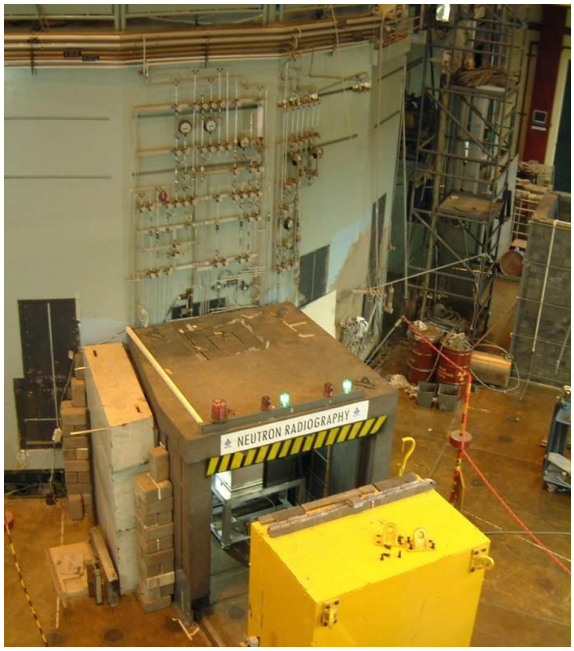

Figure 3.3: Relocation of the neutron radiography facility at beam port no. 2 of the SAFARI-1 reactor.

Three dimensional (3D) Neutron Computed Tomography (NCT) imaging concepts were demonstrated as early as 1986 at the 2nd World Conference on Neutron Radiography (WCNR-2), but were only advanced into full application as one of the highlights of the 4th International Topical Meeting on Neutron Radiography (ITMNR-4) in 2001 at Penn-State University, Pennsylvania, USA. From attending his first conference of the ITMNR-series, the author initiated a scientific collaboration with the NRAD team[10] at the Paul-Scherrer Institute (PSI) in Switzerland for the development of a NCT capability at SAFARI-1. The characteristics of the proposed new NCT capability for South Africa was presented in 2002 at the WCNR-7 (F.C. de Beer & Lehmann, 2005). The author installed and commissioned the very first neutron

10 PSI collaborators: Dr. Eberhard Lehmann, Mr. Peter Vontobel and Dr. Gabriel Frei.

tomography detection infrastructure in South Africa, Africa and the southern Hemisphere at the SANRAD facility located at beam port No. 2 of the SAFARI-1 research reactor in January 2003 and reported its operational characteristics and performance in Munich at the ITMNR-5 in 2005 (F.C. De Beer, 2005), (Figure 3.4).

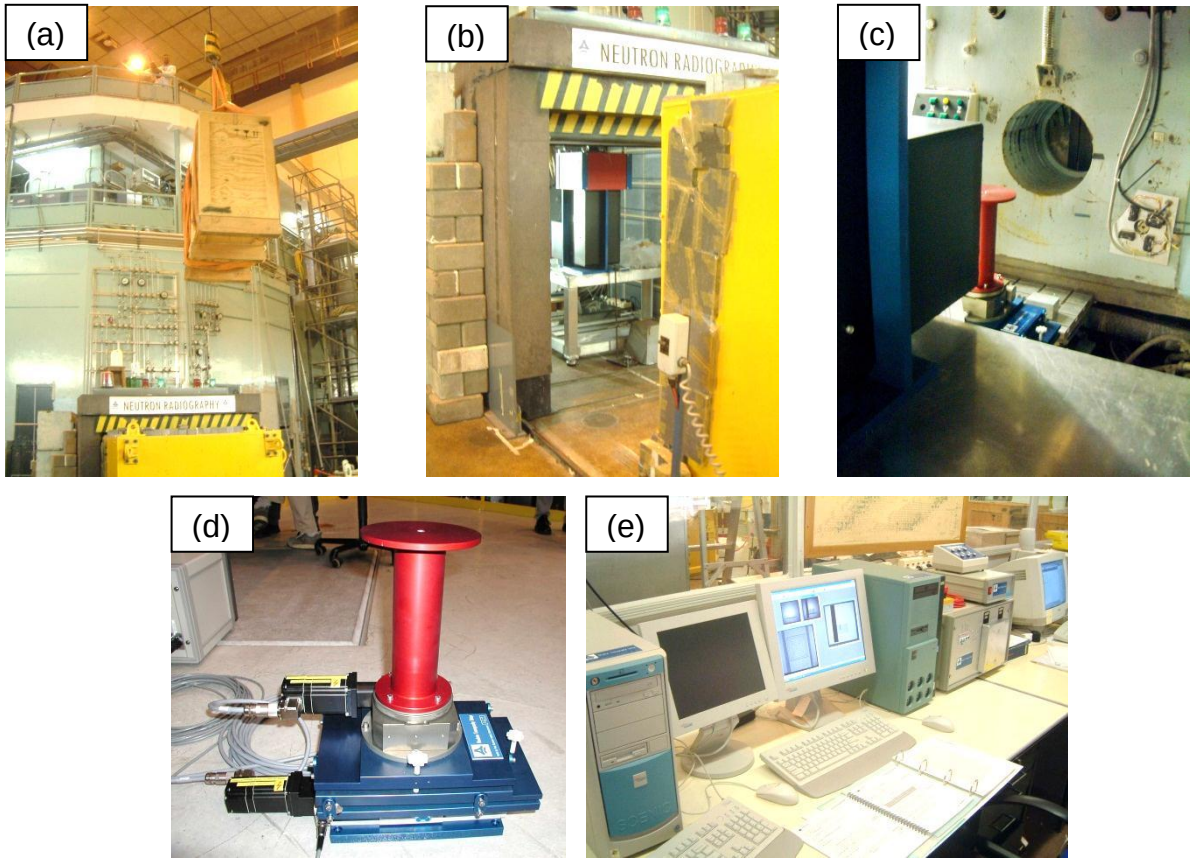

Figure 3.4: (a) Delivery of the neutron CT system from PSI in January 2003. (b) Outside view: CT system installed inside the NRAD bunker at beam port 2. (c) *Inside view:* Camera box – translation table – radiation beam port alignment. (d) Translation-rotation table, a key CT component required for acquisition of the projections at high angular resolution. (e) Computer infrastructure supporting CT acquisition and capturing of 2D projections at specific angular increments.

The South African research community was informed about this new capability through the publishing of an overview article describing the characteristics of the new neutron tomography facility at Necsa including a comprehensive description of the major fields of application with all-inclusive 3D tomographic illustrations (F.C. De Beer, 2008).

The upgrade to a 3D neutron tomography capability, managed to place South Africa on par with international trends in NRAD infrastructure development and resulted in South Africa being considered as one of the 15 highly rated and advanced facilities in the world as recorded in 2010 (Figure 3.5) (Lehmann, Vontobel, Frei, Kuehne, & Kaestner, 2011).

Figure 3.5: South Africa hosting one of the 15 advanced neutron radiography and tomography facilities in the world in 2010. (Lehmann et al. 2011).

The author and his co-scientists[11] participated in several high level initiatives in collaboration with international experts to improve aspects such as the development of quantitative digital NRAD and NCT as accepted Non-Destructive Testing (NDT) techniques. The focus was to address the problem of neutron scattering effects on quantitative analysis using digital neutron detector systems due to multiple neutron scattering in samples placed close to the scintillator screen of the detector system.

From 2003 to 2006, the International Atomic Energy Agency (IAEA) actively supported the international development of neutron radiography systems and facilities. Through an IAEA Collaborative Research Program (CRP)[12] (Paranjpe, 2008), the author collaborated, as the main author, with a post graduate (PhD) student[13,] (Hassanein 2006) and an international recognised NRAD expert scientist and co-worker[14] in a research program[15] on corrections of neutron radiographs due to neutron scattering (F.C. De Beer, Kardjilov, Lehmann, & Hassenein, 2007). Together with these international experts, the principle and method of the data correction, especially when strong thermal neutron scattering materials such as water are imaged, were described (Kardjilov, De Beer, Hassanein, Lehmann & Vontobel, 2005) (Kardjilov, De Beer, Middleton, et al., 2005). The author tested a Monte Carlo computer algorithm implemented in Interactive-Data-Language (IDL) computer software developed by the post-doctoral fellow[19]

11 Necsa co-workers: Mr. Mabuti Radebe, Mr. Jakobus Hoffman, Mr. Lunga Bam and Mr. Robert Nshimirimana.
12 CRP program entitled: “Neutron Imaging: A Non-Destructive Tool for Materials Testing”.
13 Mr. Rene Hassanein: PhD student located at PSI, Switzerland.
14 Dr. Nikolay Kardjilov: Hahn-Meitner Institute (now Helmholtz-Berlin institute), Berlin, Germany.
15 IAEA-CRP research program entitled: “Neutron Scattering Corrections for Neutron Radiography”.

entitled ***"Quantitative Neutron Imaging"*** (QNI) (Vontobel, 2008) also at the SAFARI-1 NRAD facility (R. Hassanein, de Beer, Kardjilov & Lehmann, 2006). The significance of this algorithm is that the principle of quantitative determination of characteristic parameters of porous media[16], by using neutron radiographs and high neutron scattering contrast agents such as water and/or hydrocarbons, can be determined with improved accuracy and in good agreement with the bulk total amount of water measured by weighing. The additional advantage of QNI is that the spatial distribution of the water inside such porous media can be quantified. It was shown that the neutron scattering effect can also be reduced using a compact poly-capillary neutron collimator (Tremsin et al., 2015) and that no scattering corrections are needed when the samples are placed close (<0.1 cm) to the detector/scintillator (Nshimirimana, Radebe & De Beer, 2015). See Section 3.3 for applications where these corrections are applicable within Civil Engineering and Geosciences.

Initiatives on the international level entailed the testing of the functionality of the QNI corrections in porous media with the aim to establish a standardisation method for digital neutron radiography and tomography (M.J. Radebe, De Beer & Nshimirimana, 2011). Part of the work entailed a Round Robin exercise in partnership with international facilities[17] for the optimisation and testing of spatial resolution and contrast standards as part of an IAEA-CRP[18] (M.J. Radebe, De Beer, Kaestner, Lehmann & Sim, 2013) as well as a setup of neutron radiography facilities and respective procedures for the characterisation and standardisation for porous media applications (M.J. Radebe & De Beer, 2015). Additionally, an international co-worker[19] in collaboration with a Necsa colleague[20] designed a collection of test objects to quantify neutron tomography facility performance in terms of spatial resolution and material contrast in tomograms (Kaestner et al., 2013) as well as pixel and voxel size, resolution and beam divergence of digital neutron imaging systems (Kaestner et al., 2017).

3.2.1.3 SAFARI-1 reactor - Beam tube no 2 SANRAD facility upgrade (Since 2005)

In 2003 Necsa entered into a Technical Cooperation (TC) program[21] for 4 years with the IAEA to assist in the upgrade of the NRAD beam line facilities at SAFARI-1 (Frikkie de Beer, 2003). The author's established international network with various experts and role players in the

16 Porosity, percentage saturation.
17 PSI-Switzerland, IPEN-Brazil, KFKI-Hungary, KAERI-Korea, Portugal.
18 IAEA-CRP research program entitled: "Standardisation in Neutron Radiography".
19 Dr. Andreas Kaestner: PSI, Switzerland.
20 Mr. Mabuti Radebe: Necsa co-worker and PhD student.
21 IAEA-TC entitled: "Establishment of a Versatile Neutron Radiography Facility at Beam Line No. 2 of the SAFARI-1 Research Reactor".

international arena of NRAD, allowed for an IAEA expert mission to South Africa by two NRAD experts[22] during 2005 (Figure 3.6).

Figure 3.6: (a) Dr. Burkhard Schillinger (Germany), (b) Dr. Reynaldo Pugliesi (Brazil) and (c) Dr. Florian Grunauer (Germany) at work during their respective IAEA expert missions to Necsa in 2005.

The outcome of the IAEA expert mission proposed significant changes in the basic infrastructure of the current SANRAD facility. The suggested design parameters for the intended SANRAD facility upgrade were incorporated into a Monte Carlo neutron transport model[23] (Grunauer, 2005) (Grünauer, 2009). The latest state-of-the-art neutron optics infrastructure and instrumentation were incorporated into the new design and a final layout of the upgraded NRAD facility at SAFARI-1 was established (Figure 3.7) by the author in negotiation with experts during several IAEA sponsored scientific visits to several world leading NRAD facilities[24] (Figure 3.8).

Based on this state-of-the-art design and the expanded research scope, a successful application was submitted by the author to the National Equipment Fund (RISP – NEP) of the DST-NRF in 2009. Funding of MR13.18 was provided for the finalisation of the upgrade of the NRAD facility.

Concepts of the proposed upgrade of the South African NRAD facility were communicated by the author and co-worker[25] at various international forums to the NRAD community. General descriptions of the anticipated upgraded facility were presented at an International Youth Nuclear Congress (IYNC) in Interlaken, Switzerland (M.J. Radebe & De Beer, 2008), an IAEA meeting during 2012 in Rabat, Morocco (F.C. de Beer, Franklyn, Venter, & Nothnagel, 2012)

22 Dr. Burkhard Schillinger (Germany) and Dr. Reynaldo Pugliesi (Brazil).
23 Dr. Florian Grunauer (Germany): MCNP-X software simulation expert.
24 Dr. Burkhard Schillinger at FRMII in Garching, Germany; Dr. Nikolay Kardjilov at Helmholtz-Berlin (Previously Hahn-Meitnner Institute) in Berlin, Germany; Dr. Eberhard Lehmann at PSI, Switzerland; Dr. Muhammad Arif at NIST, Gaithersburg, USA.
25 Mr. Mabuti Radebe: (Necsa - South Africa): NRAD Instrument Scientist.

and at the 18th World Conference on Non-Destructive testing (WCNDT-18) during 2012 in Durban, South Africa (Frikkie C. De Beer & Radebe, 2012)

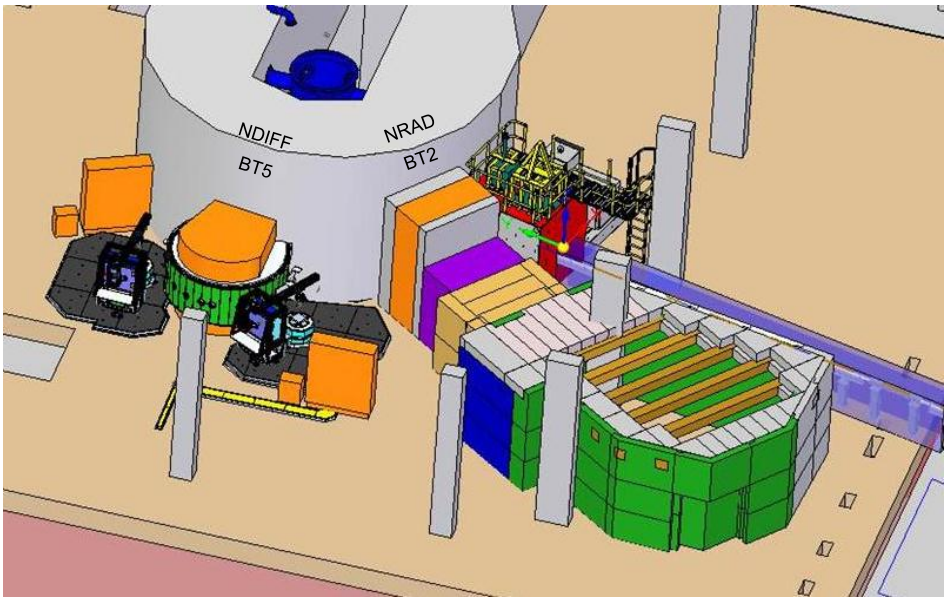

Figure 3.7: Monte Carlo model of the upgraded SANRAD facility at beam tube-2 in relation to the NDIFF (BT-5) and SANS (BT-1) facilities.

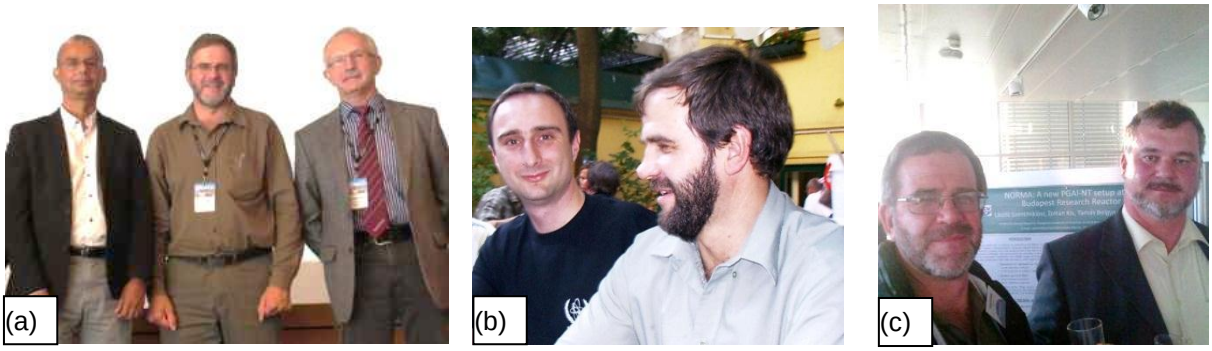

Figure 3.8: (a) Dr. Mohammud Arif (USA) Left, Frikkie de Beer and Dr. Eberhard Lehmann (Switzerland) Right, (b) Dr. Nikolay Kardjilov (Germany) Left and Frikkie de Beer and (c) Dr. Burkhard Schillinger (Germany) Right with Frikkie de Beer.

A description of the scientific design of the upgrade of the NRAD facility has been delivered at the ITMNR-7 in 2012 in Kingston, Canada (F.C. De Beer, Gruenauer, Radebe, Modise & Schillinger, 2013) and the concrete shielding design characteristics (F.C. De Beer, Radebe, Schillinger, Nshimirimana & Ramushu, 2015) and Au foil activation characterisation of the shielding capability of the proposed concrete (M.J. Radebe, Korochinsky, Strydom & De Beer, 2015) at the WCNR-10 in 2014 in Grindelwald, Switzerland. Chapter 7 contains a detailed description of the peer reviewed article submitted to WCNR-10 and forms part of the requirements for this PhD.

The author and other international experts were invited to an IAEA consultancy meeting (IAEA-CM) in 2016 in Vienna, Austria for technical support to compile and publish, with the author elected as rapporteur of the meeting, a comprehensive IAEA publication on internationally accepted guidelines for the upgrade and design of new NRAD facilities (F.C. De Beer, 2016).

Several in-depth post graduate studies supporting the initiative of the upgrade of the NRAD facility were conducted. Special care was taken on several aspects of the upgrade and involved post-graduate students in the development of the models which include the He-filled flight tube (Du Preez 2011), radiation beam filtering concepts and mechanism (Maartens 2011), translation table (Cloete 2012) and the beam catcher (Van der Merwe 2015) – all co-supervised by the author.

Status of the SANRAD upgrade at Dec 2017:

The user requirements and specifications for the upgraded SANRAD facility were compiled by the RADTOM section under the leadership of the author for the project manager[26] to perform the necessary project scheduling and planning activities, some of them mentioned below:

- **Shielding infrastructure:**

  Although the main component recipe of the NRAD radiation shielding was adopted from the ANTARES facility at FRMII, Germany and formed the basis of the SANRAD upgrade shielding design, a civil engineering study determined the complete concrete mix and composition for South African conditions (Ramushu, 2014). After the design and manufacturing, 70% of the containers were cast during 2013. Completion of the remainder awaits National Nuclear Regulator (NNR) quality assurance approval (Figure 3.9).

Figure 3.9: Cast inter connected shielding steel blocks filled with high density concrete.

26 Mr. Tankiso Modise: Necsa: NRAD Upgrade Project Manager.

- **Collimators:**

  The author adopted, through an agreement with German experts and colleagues[27,28], the design of their collimators to be used at the new SANRAD facility. The manufactured collimators were inspected and declared suitable for use in the SANRAD upgrade by the author while in Germany on a scheduled visit and were delivered to Necsa during 2014 (Figure 3.10).

Figure 3.10: Three collimators manufactured in Germany ready for installation.

- **NNR approved documentation:**

  Following NNR final approval, the following actions can proceed: Manufacturing of instrumentation and components; installation of the shielding blocks; implementation of the control and instrumentation hardware and software and lastly the cold and hot commission phases.

The commissioning of the SANRAD upgrade is anticipated for April 2019. The facility will be unique in the sense that it will allow fast and epithermal neutrons, thermal neutrons and gamma-rays to be used as penetrating radiation sources for radiography and tomography.

27 Dr. Burkhard Schillinger: NRAD Specialist at the ANTARES NRAD Facility based at FMRII.
28 Mr. Elbio Calzada: Engineer at FRMII, Germany.

3.2.2 Development of X-ray based radiography research facilities

The development of two X-ray tomography facilities based at Necsa and initiated by the author, one at the SAFARI-1 SANRAD facility utilising the NRAD detection infrastructure and the other, a separate micro-focus X-ray tomography facility in building P1500, are described.

3.2.2.1 Cone beam X-ray tomography at the SANRAD facility

The need to radiograph Pebble Bed Modular Reactor (PBMR) fuel spheres to assess the coated particle distribution within, necessitated the establishment of an X-ray tomography facility complementary to the neutron facility. Not only do neutrons activate fuel spheres, but the spatial resolution is also inadequate to reliably observe coated particles that may be present in the fuel free boundary zone of fuel spheres, an important quality assurance (QA) test for PBMR fuel.

An X-ray radiography facility was established by installing a variable energy (30 kV to 100 kV) X-ray source inside the neutron radiography facility and by utilising parts of the neutron detection system. Apart from being able to record radiographs on X-ray film, a gadolinium oxysulfide (Gd_2O_2S or Gadox) scintillator screen was introduced in order to directly utilise the back–end detection system of the neutron tomography facility to produce 3D X-ray tomography images of the fuel spheres (F.C. De Beer, 2005).

3.2.2.2 Micro-focus X-ray tomography

The cone beam X-ray system, described above, with a minimum of 1 mm focal spot could not serve the goals for high resolution X-ray tomography on smaller samples. However, at the 1st tomography symposium in South Africa organised by SAIMM on 25 July 2008 at DEBTECH, DeBeer's mining company premises in Johannesburg, the local HEI need for such research instrumentation was expressed and the capability of neutron and X-ray tomography was demonstrated by the author (F.C. De Beer, 2008). A successful application to the 2009 DST-NEP call for national infrastructure development was made.[29] The X-Tek (now NIKON) micro-focus X-ray tomography facility (MIXRAD), earmarked to serve the national research community, was commissioned and officially launched in 2011 (Figure 3.11 and Figure 3.12).
A public announcement of the commissioning of the MIXRAD facility at Necsa was made through "Necsa Today" (Mulane & De Beer, 2011) and "Engineering News" (Burger, 2011) with a full characterisation description of the instrument performance at the 18th WCNDT in Durban (J. Hoffman & De Beer, 2012). Optimal research availability of the system is made possible

29 Main Applicant: Dr. Andrew Venter: Necsa (South Africa) Neutron Diffraction Section Manager.

through a maintenance agreement with X-Sight, the supplier of the MIXRAD facility and local representative and technician of NIKON in South Africa[30]

Figure 3.11: MIXRAD: (a) Delivery of the MIXRAD facility to Necsa. (b) Installed MIXRAD facility in Building P1500. (c) Facility notice board on the wall of building P1500.

Figure 3.12: Official launch of the Micro-focus X-ray tomography facility (MIXRAD) in 2011 at Necsa. L to R: Mr. De Beer (Necsa), Dr. De Villiers (Necsa), Dr. Nothnagel (Necsa), Mr. Keanly (X-Sight, South Africa), Ms. Stofile (DST - NRF), Mr. Claustre (NIKON – UK), Dr. Rudolph (NIKON - UK). (Photo: Necsa Today)

3.2.3 Development of other facilities

The author extended his involvement in support of user communities and in particular the Heritage community, by assisting with the planning and establishment of auxiliary or support infrastructure. In addition, his expertise in imaging analysis techniques was utilised to assist with the development of online particle size distribution analyses for the coal mining industry.

3.2.3.1 Mechanical and chemical fossil preparation laboratory (PREPLAB) at Necsa

The author obtained extensive experience in using neutron and X-ray tomography on fossils and fossil bearing rock (F.C. De Beer, Prevec, Cisneros & Abdala, 2008) (Fornai, 2009). As a

30 Mr Paul Keanly: NIKON Representative.

result, a healthy collaborative relationship was established with several local[31] and international palaeo-scientists[32] working in South Africa, curators at both the DITSONG Museum for Natural History (DMNH)[33] and at the fossil repository at the University of the Witwatersrand (WITS)[34].

High density calcite rock (breccia) is a hindrance for palaeo-scientists to obtain access to their object of study, namely the imbedded fossil itself. Mechanical and chemical preparation techniques are required to release the embedded fossil. DMNH has a limited chemical breccia preparation processing capability of ~35 blocks of breccia per annum while WITS hosts only a mechanical preparation laboratory. These facilities do not have the capacity to deliver clean and clear fossils from breccia materials at the rate required by the research community.

To make study objects and scanning facilities conveniently available in one location, the author initiated a project to establish communal fossil preparation and storage facilities at Necsa, near the X-ray and neutron tomography facilities (Necsa-Corporate-communications, 2014). This laboratory is envisaged be funded, managed and operated by a consortium of users and stakeholders together with Necsa, such as the Department of Science and Technology (DST), University of the Witwatersrand (WITS), South African Heritage Research Association (SAHRA) and the University of Johannesburg (UJ). Necsa supports the cultural heritage community of South Africa with the mechanical and chemical preparation of fossilised materials and at the same time with availability of its neutron and X-ray tomography capabilities. The combined effect promises to increase the quality and quantity of palaeo science research in the country. Pilot chemical preparation instrumentation was already commissioned in Sept 2017 and is planned to become operational early 2018.

3.2.3.2 WIPFRAG: Imaging system

Early in the 1990's the Atomic Energy Corporation (AEC - now Necsa) developed the Kangela dual gamma coal-ash monitor and installed several systems at South African coal mines as on-line ash monitors in coal processing operations. Augmentation of the coal ash values with coal particle size data provided information for a comprehensive coal management system. For this reason, the AEC, established in 1995, a particle size analyser to be used in conjunction with the Kangela ash monitor. This system, known as WipFrag made use of photo-analysis techniques in a computer and imaging technology environment to compute sample size distributions online. Furthermore the system is not limited to coal mining, but is also effective in other on-line mining

31 Dr. Francis Thackeray (DITSONG and WITS); Dr James Brink (Florisbad, OFS.,); Dr Teresa Kearney (DITSONG).
32 Dr. Jose Braga (France); Dr Justin Adams (Australia).
33 Ms. Stephany Potze (DITSONG): Curator of hominin collection.
34 Dr. Bernhard Zipfel (WITS) Curator; Dr. Bruce Rubidge Palaeonscientist.

related particle size distribution applications. The author supported the testing and installation of the WipFrag systems at various South African coal and platinum mines during the period of 1996 – 1999 (Von Gogh, 1999). In this way, the mining industry could also benefit from technology know-how originally established for image analysis in X-Ray and NRAD radiography.

3.2.4 Summary of facility development

The radiography and tomography facilities, auxilliary facilites, as well as the spin-off technologies discussed above are summarised in a tabular time line format in Table 3.1 below. This Table serves to indicate the prolonged and persistant efforts on the part of the author to establish radiography and tomography facilities to benefit the research output of a number of SA research communities, as will be briefly discussed in the remainder of this chapter.

Table 3.1: Facilities at Necsa under the planning, commissioning and operation responsibilities of the author.

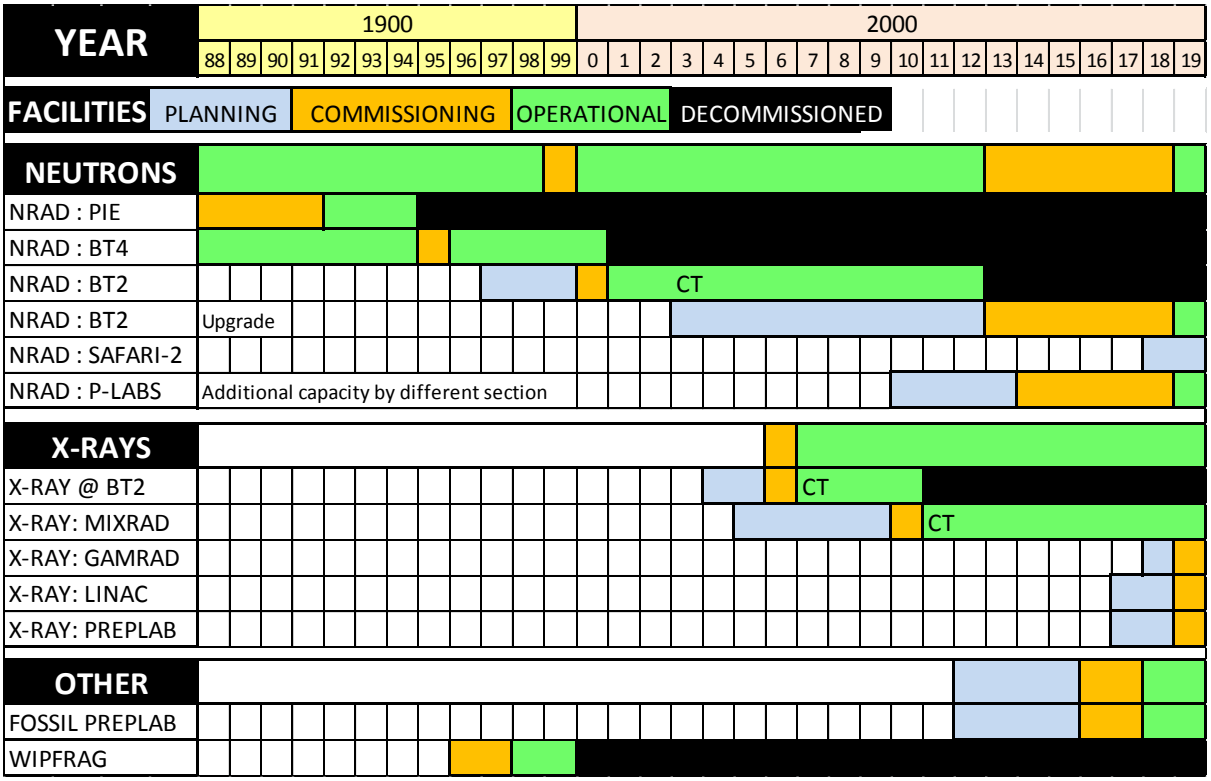

PIE: Post Irradiation Examination (PIE) of Koeberg fuel – Lead test assemblies (LTA).
BT2 & BT4: Beam tubes on the beam port floor of the SAFARI-1 research reactor.
P-LABS Pelindaba Laboratories for Accelerator Based Science.
MIXRAD : Micro-focus X-ray radiography and tomography Laboratory.
GAMRAD: Gamma-ray radiography and tomography Laboratory.
LINAC: Linear accelerator.
PREPLAB: Chemical and Mechanical Fossil Preparation Laboratory.
WIPFRAG: In-line software using real time imaging for sieve size analysis.

3.3 Topical Utilisation of the Facilities as per User Interest

Necsa, which is one of the state owned entities falling within the ambit of the Department of Energy (DOE), is mandated to undertake and promote research and development (R&D) in the field of nuclear energy and radiation sciences and technology, subject to the Safeguards Agreement and to make these generally available (Necsa-Corporate-communications, 2014).

The research benefits originating from the use of modern neutron and X-ray CT instrumentation at Necsa can best be seen by reference to a number of selected applications in the respective research fields of the more regular users of the Necsa facilities. Some such application examples will be briefly mentioned in the following paragraphs with reference to post graduate theses and dissertations as well as peer reviewed articles that resulted from the work. All work referenced were made possible due to the availability of the X-ray and/or neutron tomography facilities at Necsa. The author and his co-workers[35] were either a main author or co-author of a publication, and the tomography facilities at Necsa were explicitly acknowledged or not.

3.3.1 Energy

The Energy sector includes fields of application in nuclear, coal and renewable energy and is discussed below. A summary of the output generated in each field is reflected in Figure 3.13.

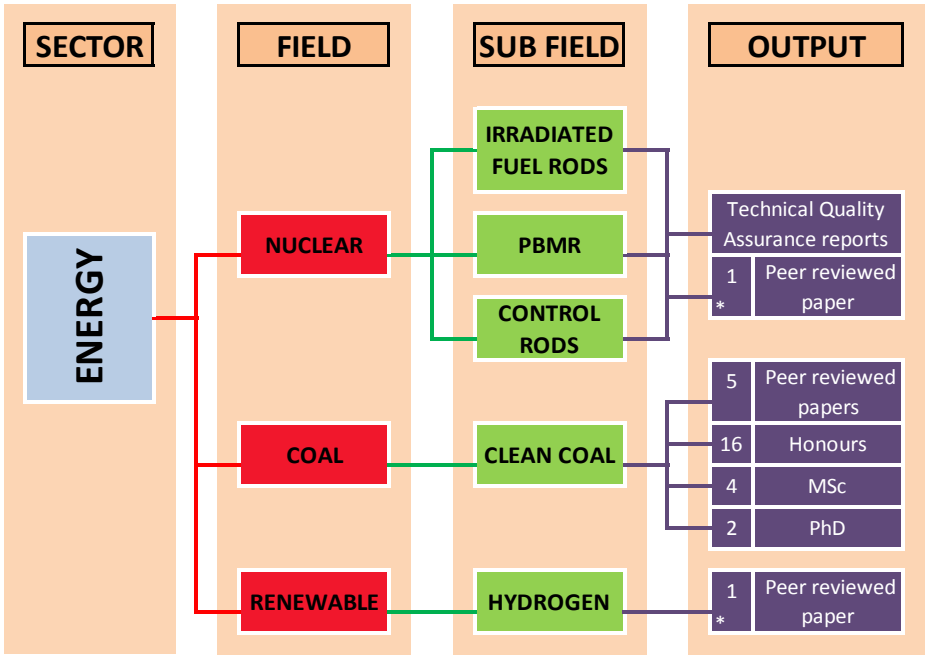

*** Author is the main author: Full peer reviewed articles submitted as requirement for this PhD by publication.**

Figure 3.13: Schematic and summary of outputs generated in the Energy sector.

35 Co-workers: Mr. Kobus Hoffman, Mr. Mabuti Radebe, Mr. Lunga Bam, Mr Robert Nshimirimana.

3.3.1.1 Nuclear materials

Necsa's mission to develop nuclear technology was embraced by the author from 1988 and culminated in the successful development and utilisation of the beam line research facilities at Necsa. The utilisation of these facilities can best be seen by reference to a number of selected applications in the respective research fields of the more regular users of the Necsa facilities. The peer reviewed article submitted as requirement for this PhD (See Chapter 4) summarises the work performed by the author on Koeberg LTA and PBMR nuclear fuel at Necsa, but also the role and potential of neutron and X-ray tomography at several sectors within the nuclear fuel cycle (F.C. De Beer, 2015b).

3.3.1.2 Coal

South Africa is the 4th largest coal producer in the world (2013/2014) utilising coal as its primary energy source.[36] As a result, coal research requires ongoing attention.

Work done[37] at the Micro-focus X-ray Computed Tomography (MIXRAD) facility of Necsa summarised the opportunities in coal research afforded by µXCT as a new and important analytical tool for South Africa (Hoffman 2012). This study comprised a number of coal research opportunities for researchers and post graduate students using µXCT as an analytical technique. The EXXARO coal mining company, co-sponsor of the MIXRAD facility at Necsa, immediately realised the potential of this technology as an important research tool in order to understand the crushing behaviour of coal as well as the mechanism of char production through pyrolysis and gasification (Naude, Hoffman, Theron & Coetzer, 2013).

The North-West University (NWU) realised the power of µXCT in coal research and committed itself to use the technology on a regular basis since the inauguration of the MIXRAD system at Necsa. To date, fifteen 4th year students[38] have conducted post graduate research studies on the behaviour of coal during processes such as pyrolysis and gasification. Additionally, post-graduate studies were conducted on the thermal fragmentation behaviour of coal (Badenhorst 2013) and were extended to quantify the fragmentation of coal due to pressure build-up of volatiles during the rapid heating of samples (Badenhorst 2016).

Swelling and caking behaviour of South African large coal particles, influenced by potassium carbonate, was another phenomenon studied through the use of µXCT and the results

36 http://www.statssa.gov.za/?p=4820

37 Mr. Kobus Hoffman (Necsa) : Qualified Chemical Engineer on Coal and MIXRAD Instrument Scientist.

38 Luzaan Van Schalkwyk; Belinda Du Preez; Johandri Vosloo; Werner Koekemoer; Adrian Seconds; Ernest Mokoisa; Joanna Skoczynski; Jeanique van der Westhuizen; Joani van Rooyen; Hardus Louw; Mosele Tsemane; Wynand Breytenbach; Nomsa Tsabalala; Jacobus Hermanus Kemp; Danie le Roux.

contributed to an improved understanding of large coal sample behaviour during de-volatilisation processes (Coetzee 2015). Image analysis of the coal samples also revealed the different phases of plastic behaviour during these processes (Coetzee, Neomagus, Bunt, Strydom & Schobert, 2014). In addition, the best suited combination of breakage modes of coal were investigated to optimise the liberation of coal in order to attain a certain yield, to optimise liberation at the coarsest possible coal particle size, and to keep fines generation to a minimum (Potgieter 2014).

Using µXCT, qualification of coal degradation, which normally occurs at many steps during beneficiation or utilisation processes, revealed that lower density macerals contributed more to breakage and the production of unwanted fines in comparison to higher density macerals. It could further be established that pre-existing cracks, lithotype boundaries and mineral boundaries potentially initiate cracks, change the direction of, or can stop crack propagation (Jacob Viljoen, Campbell & Le Roux, 2014). The study towards the fundamental understanding of coal breakage continues with the aim to minimise the production of unwanted fines. To clarify the complex nature of coal breakage, an analysis of the slow compression breakage of South African Waterberg coal, applying µXCT, concluded that inherent crack distribution within coal dominate breakage and breakage patterns (Viljoen, Campbell, Le Roux & Hoffman, 2015). A follow-up investigation on coal originating from the same colliery focusing on the bedding-plane orientation, and the consequential influence on the degradation characteristics, revealed that propagation of cracks is a function of the orientation of the bedding planes in relation to the impact surface with deeper crack propagation when the impact force was applied along the bedding plane (Viljoen, Campbell, Le Roux & Hoffman, 2016). The complete study on coal degradation with a main and significant contribution of µXCT that highlights the potential and the usability of the MIXRAD facility in this sector, was summarised in a comprehensive PhD-thesis[39] (Viljoen 2016).

3.3.1.3 Renewable Energy

The application of neutron radiography and tomography in the development and optimisation of hydrogen fuel cell technology at a number of international facilities[40] has been reported from 2004 and onwards at all the WCNR- and ITMNR-series of international conferences. The relatively high neutron scattering by hydrogenous materials, such as water, makes neutron radiography an ideal research method to optimise the water management within fuel cells (Lehmann, Boillat, Scherrer & Frei, 2009) (Yasuda et al., 2011) (Manke et al., 2008).

39 Japie Viljoen: PhD graduate (at NWU) Thesis entitled: “A tomographic exploration of the internal structure of coal and its role in single particle breakage”.

40 PSI in Switzerland; NIST in USA; TUM and Helmholtz in Germany; KAERI in South Korea.

National and international research output in Polymer Electrolyte Membrane (PEM) electrolysers, which enable electrical energy storage in the form of hydrogen gas to produce on-demand electricity using fuel cells, needs to be accelerated. The South African Department of Science and Technology initiated a high priority research and development focus in fuel cell technology. The author initiated the first South African related studies of this kind using neutrons in 2015 in collaboration with researchers[41] from Hydrogen South Africa (HySA-NWU) in a preliminary study of electrolysers at the NIST-NI facility in USA. The outcome of this study is presented in the peer reviewed article submitted as requirement for the PhD (See Chapter 5) (De Beer, Van der Merwe & Bessarabov, 2017).

3.3.2 Biosciences

Contributions made by the Necsa radiography and tomography facilities in the Biosciences can be subdivided into the fields of Humanities and Zoology. A summary of the output generated in each field is reflected in Figure 3.14 and briefly discussed below.

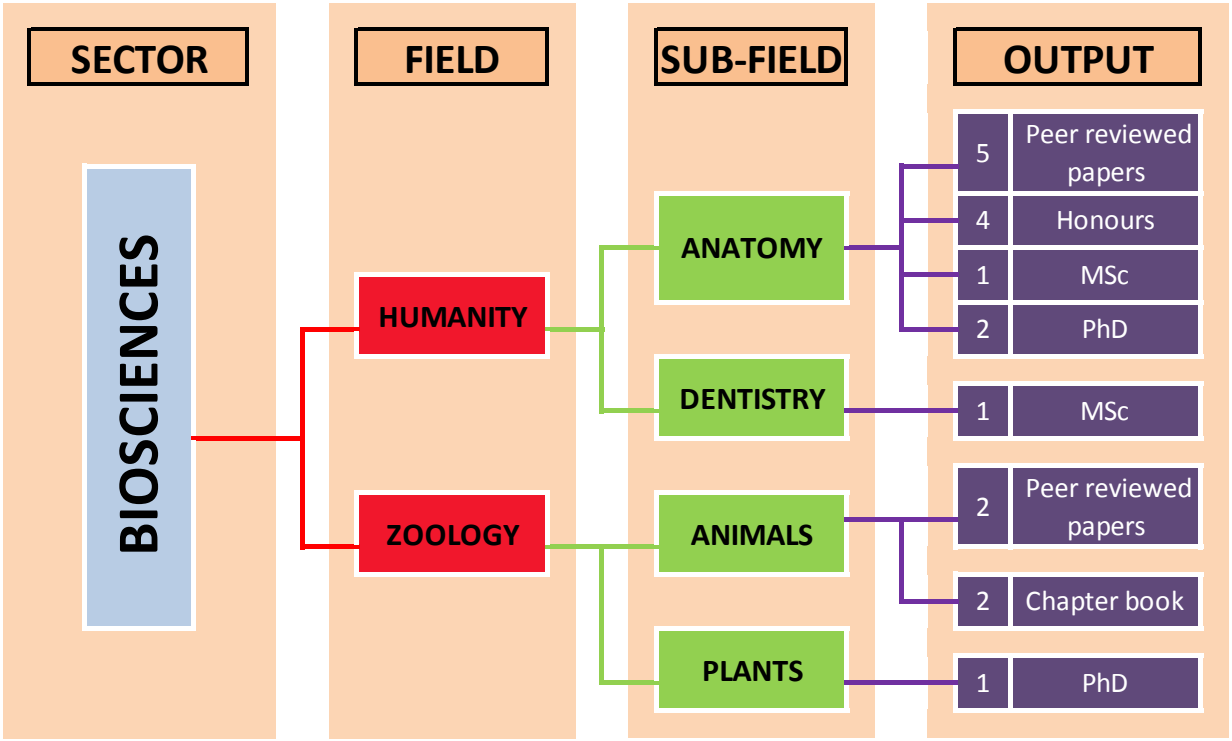

Figure 3.14: Schematic and summary of outputs generated in the Biosciences sector.

3.3.2.1 Anatomy applications

Ever since its discovery, X-rays were used for non-invasive study of the human body and specifically for the morphology of the human skeleton. The first extensive cone beam XCT

41 HySA- NWU South Africa: Dr. Dmitri Bessarabov & Mr. Jan-Hendrik van der Merwe.

investigations of the human skeleton structures, which were conducted at Necsa, were initiated by a researcher at the University of Pretoria (UP).[42] This work later culminated in the "Pelindaba - Pretoria skull collection" program between UP and Necsa. The human bone collection at UP[43] was successfully researched, using µXCT, and more specifically the human skull collection where µXCT allowed 3D visualisation of previously hidden morphological structures such as belonging to the cochlea. Consequently, a former student[44] and now researcher at the Anatomical Sciences Institute of the University of the Witwatersrand (WITS) was persuaded to utilise the µXCT facility at Pelindaba more frequently as a research tool.

Several Honours student research studies were performed which entailed the first 3D visualisations through µXCT movies of the pterygopalatine fossa (Hills 2011) and ventricles of the brain (Dorfling 2010)(De Jager 2016) for educational purposes.

The traumatic effect of a lightning strike on the morphology and ultrastructure of human bone (Bacci, 2016) was evaluated while the effects of adult mandibular morphology due to dental loss in South Africans (Oettlé, 2014) with additional focus to determine if midline mandibular dental implants pose a risk for the midline lingual canal (Oettlé, Fourie, Human-Baron & Van Zyl, 2015), were determined. The human mandibular development and growth across the life span was assessed (Hutchinson, 2017) with specific aims to record the changes in the morphology of the immature mandible canal during early growth (Florentino 2013) (Hutchinson, Florentino, Hoffman & Kramer, 2016) and how the bone density vary across the body of the immature human mandible (Hutchinson, Farella, Hoffman & Kramer, 2017).

The enormous wealth of information that can be extracted through the use of µXCT is evident from the selection of work highlighted here.

3.3.2.2 Dentistry

The 3D data collected by µXCT scanning of complete skulls from the depository at UP allow for the individual analysis of the maxilla and mandible. In particular, high resolution µXCT scanning of a single tooth allows for the assessment of the success of µXCT application in using several different instrumentations in the root canal glide path and measurement of the enlargement of extracted human mandible molars (Paleker, 2015).

It was possible to use µXCT to investigate the effectiveness of implant-abutment designs, by allowing the axial bite force on two different implant sizes to be compared for a number of

42 Dr. Anna Oettle: Anatomy Department – University of Pretoria.
43 Mr. Marius Loots and Ms. Gabriele Kruger: Bone collection at University of Pretoria.
44 Ms. Erin Hutchinson: Anatomical Sciences – WITS.

different implant systems. These results contributed to an improved understanding of how to best engineer the implants (Van Zyl, 2017).

3.3.2.3 Animal applications

The ostrich which is the largest (up to 2.75 m and 155 kg) bird in the world and also lays the largest egg of all living birds (up to 15 cm long) ('Ostrich', 2017). The evolution of such large birds and eggs pose some enigmatic questions that can partly be addressed through a study of the egg itself. Gas exchange mechanisms, in particular, are of interest. Through µXCT, pore structures and pore distribution of ostrich egg shells were studied to cast more light on possible gas exchange mechanisms. Also using µXCT, defects and deficiencies of egg shells were studied to improve the understanding of underlying causes in order to mitigate against large economic losses in ostrich farming (Willoughby et al., 2016) (Willoughby, 2015). A complete scientific study of the ostrich, including these µXCT results on the egg shell, were extensively documented in a book[45] (Maina, 2017). Eggshells laid in different conditions, handled differently during incubation and those possessing different physical characteristics, were investigated to help explain the functional design of the ostrich eggshell.

Bats, the second largest mammalian order, capture the attention of evolutionary biologists due to their important role in ecosystems, disease and conservation. Their unique cochlear abilities can be studied by means of µXCT. Investigations focused on the elucidation of relationships between bite force, echolocation frequency and the three-dimensional shape of their skulls (Jacobs, Bastian & Bam, 2014). Differentiation of bat species is normally done on cranial, dental, noseleaf morphology as well as echolocation call frequencies. µXCT studies of the function of cochlea morphology showed that it is possible to distinguish in this way between 10 southern African Horseshoe bat species (Rhinolophidae) (Nobrego, 2012). Furthermore, it was shown that differences in skull shapes and mandible morphology across localities and between sexes applying Canonical Variate Analysis (CVA) on µXCT data (Mutumi, 2016) can also be used to distinguish between species. These and other Micro-CT results of the study of bats were compiled and included in a chapter of a book[46] (Jacobs, Mutumi, Maluleke & Webala, 2016).

45 Book: J.N. Maina (ed.), "The Biology of the Avian Respiratory System", DOI 10.1007/978-3-319-44153-5_9.

46 Book: Pierre Pontarotti (ed.), "Evolutionary Biology: Convergent Evolution, Evolution of Complex Traits, Concepts and Methods".

3.3.2.4 Plants

In the study of maize, which is used for human and animal consumption throughout the world, the presence and time dependant expansion of voids and airspaces in the microstructure of the maize kernels, caused by the infection by different fungi processes and thus showing the effect of fungal damage, could be studied using µXCT (Williams, 2013).

3.3.3 Heritage Studies

Heritage studies are of great importance in South Africa because of, inter alia, our rich fossil beds.

> ***"Heritage is our legacy from the past, what we live with today, and what we pass on to future generations. Our cultural and natural heritages are both irreplaceable sources of life and inspiration. Places as unique and diverse as the wilds of East Africa's Serengeti, the Pyramids of Egypt, the Great Barrier Reef in Australia and the Baroque cathedrals of Latin America make up our world's heritage. What makes the concept of World Heritage exceptional is its universal application. World Heritage sites belong to all the peoples of the world, irrespective of the territory on which they are located."*** –quoted from UNESCO website[47].)

The Radiation Science (RS) Department of the Research and Development Division of Necsa actively supports productive research cooperation within the NSI as one of the institutional obligations of Necsa. A core focus area of the R&D Department is to render support to the local and international Heritage research community as one of the internationally recognised areas of expertise in South Africa (Tshelane, 2015).

The author took a leading role in an IAEA-CRP project that included participants from 18 countries[48]. He was elected as the chairperson for the 1st Research Coordinated Meeting (1st-RCM in 2012) in Vienna, Austria (De Beer, 2012) and rapporteur of proceedings for both the 2nd-RCM in Munich, Germany (De Beer, 2013) and 3rd-RCM in Firenze, Italy (De Beer, 2015a).

One of the major benefits of cultural heritage studies is the non-destructive and non-invasive nature of penetrating radiation. Three dimensional quantitative, qualitative and morphological information can be obtained from valuable and precious artefacts, sometimes the only one of their kind showing the potential of transmission tomography as a tool for dealing

47 (http://whc.unesco.org/en/about/ http://www.unesco.org/archives/multimedia/?pg=44&sj=World+heritage

48 IAEA-CRP entitled: "Application of 3D Neutron Imaging and Tomography in Cultural Heritage Research".

with problems presented by heritage objects that are too valuable for any kind of destructive testing.

Heritage studies can broadly be divided into archaeology and palaeontology and some µXCT applications in each sector are briefly discussed below. A summary of the output generated in each field is reflected in Figure 3.15.

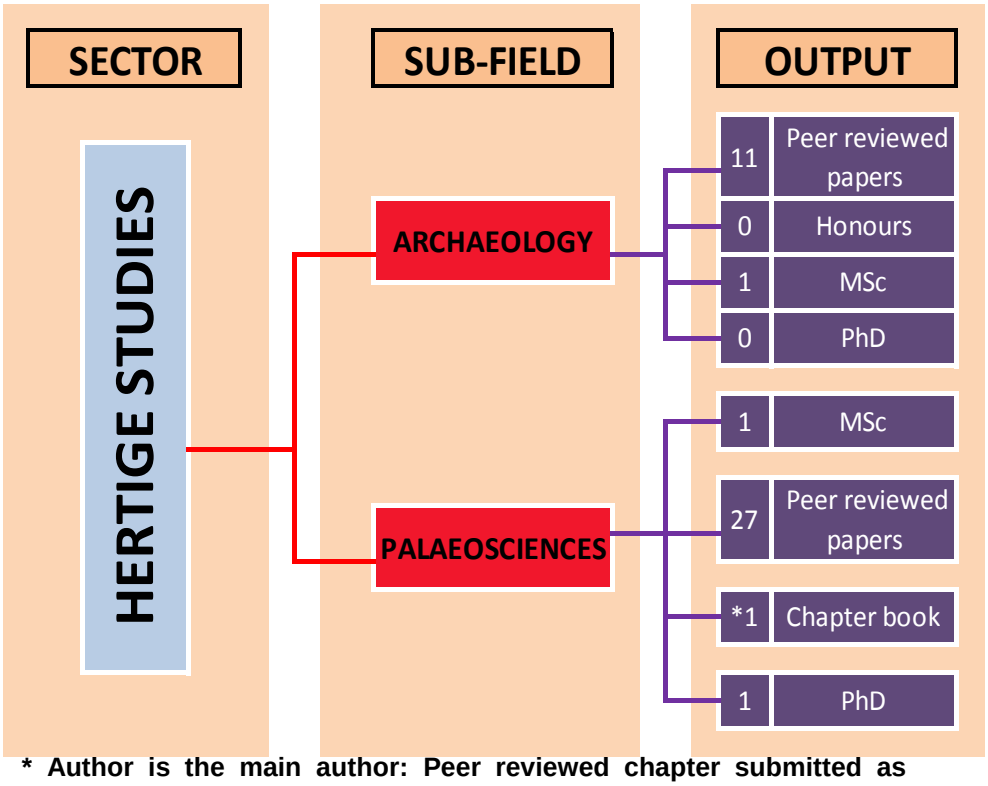

*** Author is the main author: Peer reviewed chapter submitted as requirement for this PhD by publication.**

Figure 3.15: Schematic and summary of outputs generated in the Heritage Studies sector.

3.3.3.1 Archaeology

Complementary to X-rays, neutron penetration through thick and dense materials allows for the successful neutron radiography of cultural objects usually made from, for example, bronze, lead, iron or copper.

In collaboration with the South African National Museums of Cultural History (NMCH), the first neutron tomography investigations of its kind in South Africa on an Egyptian bronze falcon as well as some Horus statuette artefacts were performed (De Beer, Botha, Ferg, Grundlingh & Smith, 2009). By being able to use X-ray tomography as well, value was added to the Museum's collections through work performed in collaboration with local researchers focusing on several different artefacts (Smith, Botha, De Beer & Ferg, 2008) (Smith, Botha, De Beer & Ferg, 2011)

(Masiteng, De Beer, Nshimirimana & Segonyana, 2010). Additionally, an attempt was made to verify the authenticity, provenance, probable date of origin as well as the proper cultural context of a gilded bronze Osiris statuette originating from the Middle Kingdom Period by also using neutron tomography scanning (Gravett, 2011).

A successful verification of the potential of μXCT in the study of the ancient bone tool function (arrow heads) revealed evidence for stress-related damage in bone that is not yet mineralised and provided unique insights into the mechanical stresses experienced during the arrow head's usage (Bradfield, Hoffman & De Beer, 2016) .

The use of X-ray and neutron tomography in the NDE evaluation of ceramic pottery sherds, originating from the site of Leokwe Hill, Shashe-Limpopo Valley, Limpopo Province, provided an alternative means of analysis for their provenance (Jacobson, De Beer & Nshimirimana, 2011).

The high penetration capability of neutrons through dense rock matrixes, allowed for the successful visualisation of ironstone slabs found in a late Earlier Stone Age context (dated to greater than 180,000 years ago) at the back of the Wonderwerk Cave, Northern Cape Province, South Africa. It was formerly believed that markings (reminiscent of incised lines) on the surface might be anthropogenic and therefore would provide insight into the development of early human symbolic behaviour. Neutron tomography was, however, able to reveal that the lines are natural rather than artificial, and are in fact surface expressions of natural internal fractures in the rock (Jacobson, De Beer, Nshimirimana, Horwitz & Chazan, 2012).

With the aim on conservation, metal artefacts from the Mapungubwe museum were studied using neutron tomography. An internal structure were visualised that allowed an estimation of physical stability and at the same time revealed signs of how those artefacts were manufactured. Not only was it possible to retrace the fabrication methods used in heavily corroded and encrusted artefacts, but additional information was obtained that could be used for proper conservation and maintenance planning (Koleini, De Beer, et al., 2012). Additionally, a re-evaluation of several cupreous conical tubes, using neutron tomography, stereomicroscope and SEM-EDS, revealed that the funnels date to the period of the rise of Mapungubwe as a town and centre of a powerful state (during the Iron Age). Additionally, it was found that the simple ordinary conical tubes were most probably used in iron strip-drawing to produce wire by drawing a thin strip of iron or copper through them – probably the earliest practice of its kind in southern Africa (Koleini, Schoeman, Pikirayi & Chirikure, 2012). Previous quantification of the percentage corrosion of the artefacts by neutron radiography lead to further characterisation of those corrosion layers on the iron archaeological artefacts by means of SEM-EDS, XRD and micro-Raman spectroscopy to retrace the corrosion history during burial and long term storage as well (Koleini, Prinsloo, Schoeman, Pikirayi & Chirikure, 2013).

Forensic investigations, using µXCT, of naturally mummified inhumations of termite-infested burials from the Magogwe Anglo-Boer War cemetery, Mafikeng, North-West Province revealed in particular the role of insect faunas as an agent of modification of soft and hard tissues (Parkinson et al., 2010).

3.3.3.2 Palaeontology

A first-in-the-world documented application of neutron radiation based imaging technology in palaeoanthropology research focused on the cranial bone of the celebrated “Mrs Ples” hominin fossil from the Sterkfontein site (Sts 5). Neutron radiography, located at the SAFARI-1 nuclear research reactor at Necsa, South Africa, was used on the parietal, frontal and occipital bone of Sts 5, but was unsuccessful for the identification of temporal lines (Le Roux, De Beer & Thackeray, 1997).

The multidisciplinary contributions of various researchers in specific thematic areas of the palaeosciences are highlighted below:

Dental studies as early hominin specimen indicators

A study on the metrics and morphology of the upper third molar (M^3) of an adult fossil hominin, from the late Middle Pleistocene, found at Florisbad showed that the fossil falls within the size range of the African *Homo erectus* (recent black South Africans) (Smith, et al., 2015).

The hypothesis of the “second Australopithecine species” for the South African site of Sterkfontein was tested, as new evidence, by the geometric morphometric analysis of maxillary molar teeth obtained by µXCT from South African Plio-Pleistocene hominids (Fornai, 2009) (Fornai, et al., 2010). Inadequate preservation, difficult interpreted stratigraphy and mostly no association of the cranial, dental, and postcranial remains of the Australopithecus species at Sterkfontein Member 4 and Makapansgat, make species identification very difficult. However, the variability of Australopithecus second maxillary molars from Sterkfontein Member 4 could be evaluated through 3D geometric morphometrics to establish markers for distinction. It was found that Homo is differentiated from both Australopithecus and Paranthropus, and Neanderthals from modern humans, but there is no statistical confirmation and proof that the Australopithecus distribution represents two distinct groups. (Fornai, Bookstein & Weber, 2015)

Craniodental remains form fossil papionin and colobine taxa originating from Makapansgat, Sterkfontein, Swartkrans, and Kromdraai stratigraphic units were detailed by µXCT for their subtle morphology to effectively discriminate amongst extant hominid and fossil hominin taxa. The tooth endostructural organisation as well as the morphology of the bony labyrinth, the inner facial skeleton and endocranium was assessed and it was also concluded that the structures are time-sensitive and show evolutionally changes in fossil taxa (Beaudet, et al., 2014).

Samples from the same sites were used in a follow-up study of the upper third molar internal structural organisation and semicircular canal morphology of these Plio-Pleistocene South African cercopithecoids for discrimination of fossil cercopithecoid species. It was concluded that enamel-dentine junction morphology could be useful for discerning highly autapomorphic taxa such as Theropithecus, while the possibility to use semicircular canal shape as an efficient criterion for diagnosing Dinopithecus ingens should be considered with caution (Beaudet, Dumoncel, Thackeray, et al., 2016).

In addition to classical descriptions, µXCT quantitative analysis on a fragmentary lower third molar crown and of a maxillary fragment of a cercopithecoid dentognathic specimen, was shown and thus it was possible to assess its taxonomic assignment (Beaudet, et al., 2015).

The first successful virtual extraction and analysis of the preserved dentognathic structural morphology of a Cercopithecoid Partial Cranium (STS 1039) from Sterkfontein Member 4 (South Africa) from hard rock breccia materials were performed using neutron microtomography (µNCT). The analysis of the morphological, dimensional and structural dentognathic features and specifically enamel thickness and topographic thickness variations demonstrated the capability of µNCT as a new analytical technique for fossil remains still imbedded in breccia materials (Amélie Beaudet, Braga, et al., 2016) (Beaudet, 2016)[49]

Three-D µXCT allows for the evaluation of the enamel thickness and Enamel-Dentine junction (EDJ) morphology among the mandibular postcanine dentitions of South African early hominins and extant Homo sapiens and found that early Homo showed a similar enamel thickness distribution pattern to modern humans. The study suggests that a dietary shift occurred between australopiths and the origin of the Homo family and confirms that some dental morphological patterns occurred early in the Homo lineage rather than in later Homo (Pan et al., 2016). The taxonomic value of premolar EDJ morphology in the hominin species found continued in a follow-up study of the intra-individual metameric variation expressed at the enamel dentine junction (Pan, et al., 2017).

In the question of if the deciduous/permanent molar-enamel thickness ratio is a taxon-specific indicator in extant and extinct hominids, the results do not provide a clear-cut picture as might otherwise have been expected on the basis of some ontogenetic and morphological studies on sequential teeth. µXCT results, however, suggest complex patterns that probably result from the influence of a number of interactive factors that should be exploited in further studies (Zanolli, et al., 2017).

49 Beaudet conclusion in a summary of her research within a PhD-thesis entitled: “Characterization of the internal cranio-dental structures of the cercopithecoids and diachronic study of their morphological variations in the South African Plio-Pleistocene sequence”.

Long Bones:

A µXCT study comparing Paranthropus and Homo in terms of the inner structural organisation of their distal humerus concludes that the two distinct patterns of organisation found in the South African and the Ethiopian specimens have biomechanical significance in terms of distal humeral strength (Cazenave, et al., 2017).

Skull / Endocast / Cochlea studies:

Characterisation was performed on the patterns of external brain morphology in a study comprising the morpho-architectural variation in South African fossil cercopithecoid endocasts originating from the famous South African fossil sites[50]. Potential phylogenetic and taxonomic implications can be derived from results obtained on variations in the sulcal pattern of Theropithecus oswaldi subspecies as well as the neuroanatomical condition of the colobine taxon Cercopithecoides williamsi (Beaudet, Dumoncel, De Beer, et al., 2016).

From a virtual imprint from µXCT data of the endocranial surface of fossils, their subsequently created endocasts provided significant information for tracing both structural and morphological changes in the brain. A potential identification of the cerebral reorganisation with implications for speech capacity was made in correlation with similar studies within the hominin family (Beaudet, 2017).

Kromdraai B is one of the rich fossil sites in South Africa and was the focus of many palaeoscientists in the past. Recent excavations lead to the first discoveries of the earliest hominins (Braga, Thackeray, Bruxelles, Duranthon, Couzens & De Beer, 2014) which includes a new partial temporal bone of a juvenile hominin, KB 6067 (Braga, et al., 2013). By using 3D µXCT, inconsistent cochlear lengths in Genus Homo was also found and it shows a unique "hypertrophied" cochlea with a significantly high phylogenetic signal, indicating its usefulness to aid in the investigation of homologies and monophyletic groups in the hominid fossil record (Braga, et al., 2015). Braga summarized the current hominin findings at Kromdraai with an updated portrayal of differences between Australopithecus africanus and Paranthropus robustus in a book.[51] (Braga, et al., 2016).

Fossil evidence for disease:

Animal fossil specimens of the cynodonts and the rocephalians (mammal-like reptiles) were investigated using tomography to explore their nasal and cerebral cavities (De Beer, et al., 2008). Successful neutron CT-scans of nearly complete vertebrae and limb fossil bones (tibia)

50 Fossil sites of Makapansgat, Sterkfontein, Swartkrans, and Taung.
51 Book entitled: "Kromdraai. A birthplace of Paranthropus in the cradle of humankind".

of an archosaur carnivorous reptile from the Lower Triassic of the South African Karoo revealed a spondarthritis condition, the oldest instance of this pathology hitherto known and a possible indirect cause of death (Cisneros, et al., 2010).

The re-analysis through 3D imaging of a hominin metatarsal specimen (SK 7923 dated to 1.8–1.6 million years old) from a cave site in South Africa[52] identified the earliest detectable case of malignant neoplastic disease from an early human ancestor (Odes, et al., 2016).

Database for 3D data:

Necsa's 3D-data generation capability contributes significantly to the new open-access database of 3D-surface scan and tomographic data of inter alia the non-hominin primate specimens curated in the Plio-Pleistocene Palaeontology Section of the DNMNH (Adams, et al. 2015).

As invited contributor, the author summarised several previously published research performed by neutron radiography and tomography on fossilised specimens in a book entitled "***Neutron Methods for Archaeology and Cultural Heritage***". The contribution of Chapter 7 entitled "***Paleontology: Fossilized Ancestors Awaken by Neutron Radiography***" describes the utilisation of neutron radiography and tomography to assist with answering palaeontology questions. This book chapter is included as Chapter 7 as partial fulfilment of the requirements for this **PhD** (De Beer, 2017).

52 Fossil site: Swartkrans in the Cradle of Humankind.

3.3.4 Material Science

The Materials Science sector includes the fields of application in the various Engineering fields. A summary of the output generated in each field is reflected in Figure 3.16 and is briefly discussed below.

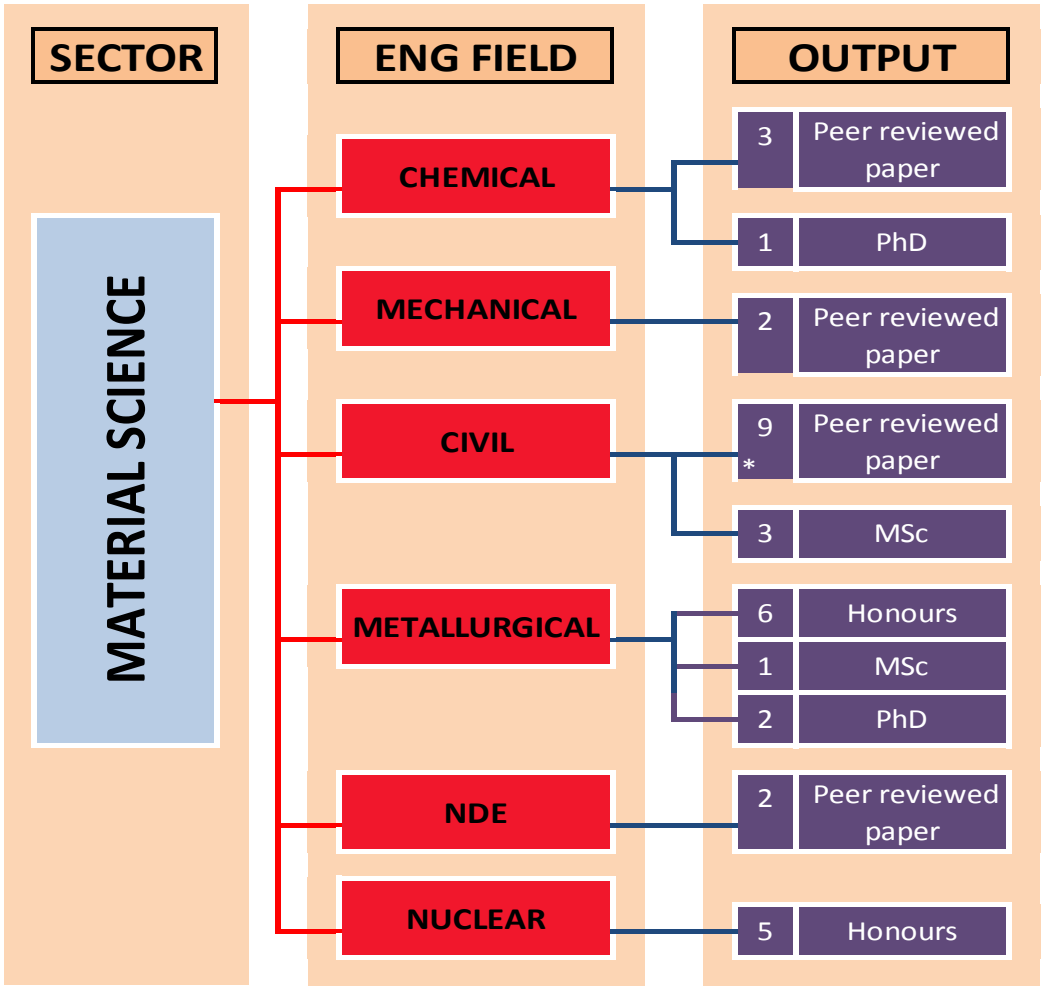

*** Author is the main author: Full peer reviewed articles submitted as requirement for this PhD by publication.**

Figure 3.16: Schematic and summary of outputs generated in the Material Science sector.

3.3.4.1 Chemical engineering

Evaluation of the internal Ba-doped water saturation dynamics of alumina catalyst particles using XCT concluded that the time to catalyst saturation may be as long as 24 hours. It could thus be recommended that catalysts in reactors where a liquid phase is present be soaked for at least a day prior to use (Van Der Merwe, Nicol & De Beer, 2006). The saturation condition of the catalysts also influences the multi-phase trickle flow in porous media such as in packed beds. XCT investigations of the trickle flow regime under various conditions concluded that CT

techniques offer exceptional potential for detailed examinations of trickle flow hydrodynamics (Van der Merwe, Nicol & De Beer, 2007a). By using the developed CXT techniques together with 2D X-ray Radiography, new insights into flow patterns as well as the stability and uniformity of trickle flow encountered in multiple hydrodynamic states was obtained (Van der Merwe, Nicol & De Beer, 2007b). The understanding of trickle flow was enhanced by the use of X-ray radiography and tomography to study the hydrodynamic multiplicity phenomena successfully (Van der Merwe, 2007).

Eight different packed bed test sections containing Perspex cylinders and acrylic spheres were evaluated by XCT with the focus on the positions of the spheres in each packed bed and the subsequent morphology and porosity for each packed bed (Du Toit & Rosslee, 2012).

3.3.4.2 Civil engineering

A ground breaking first quantitative neutron radiography observation of the drying process of concrete was in reasonable agreement with the gravimetric bulk analysis of water content and porosity with the additional advantage of visualising porosity distribution (De Beer, Strydom & Griesel, 2004). The existence of a receding drying front (Fijał-Kirejczyk, Milczarek, Radebe, De Beer & Żołądek-Nowak, 2011) with particular focus on the existence and time evolution of the inner wet core (Fijał-Kirejczyk, et al., 2012) in capillary-porous media during the drying process as researched through a bilateral scientific and technical cooperation[53] between South Africa[54] and Poland[55]. The scientific basis of this cooperation was supported by in-house research into the quantification of porosity, sorptivity and permeability of concrete at different water to cement ratios and curing times (De Beer, Le Roux & Kearsley, 2005) as well as an Australian[56]-South African collaboration with an application in water transport through cement-based barriers, designed for low level nuclear waste disposal (Brew, et al., 2009) (McGlinn, et al., 2010) (Payne, Aldridge, Brew & Mcglinn, 2012) (Mcglinn, De Beer, Brew, Radebe & Nshimirimana, 2013).

A study to identify chlorides and their effects on steel reinforcement within laboratory concrete samples concluded that NRAD is superior to XRAD in detecting the effect that chlorides have on concrete and that NCT-visualisation of the rate of deterioration of steel imbedded in concrete is possible (Radebe, 2007). An in-depth study in the quantification of porous media in terms of particle size, particle shape, tortuosity, surface area and porosity also

53 SA-Poland NRF-TC entitled: “Neutron Radiography/Tomography of Porous Media”.
54 Dr. Gawie Nothnagel: NRAD section, SAFARI-1 nuclear research reactor, Necsa, Pretoria, South Africa.
55 Dr. Jacek Milckzarek: NRAD section, MARIA nuclear research reactor, POLATOM, Swierk, Poland.
56 Peter McGlinn, Dan Brew and Laurence Aldridge: Australian Nuclear Science & Technology Organisation (ANSTO), NSW, Australia.

revealed that the pixel resolution and contrast achieved in a tomogram is key in the determination of the kind of quantitative information that can be retrieved (Nshimirimana, 2008). The role that the SANRAD facility can play in quantitative and morphology investigations of porous media are summarised (Nshimirimana, De Beer & Radebe, 2011). The characterisation of manufacturing processes of building bricks, used in rural areas of South Africa, and their resistance to moisture uptake demonstrated the practical application of NCT in Civil Engineering of low-cost structures (Maweza, 2011).

3.3.4.3 Metallurgical engineering

Evolution of porosity in metal injection moulding and direct powder rolling were compared using µXCT and traditional microscopy. Spatial variations in densities and the existence of characteristic moulding and roll compaction defects, obtained from µXCT, were shown to be in agreement with traditional microscopic microstructural analysis (Muchavi, Bam, De Beer, Chikosha, & Machaka, 2016).

Glass flakes incorporated into epoxy composite coatings as a possible composite barrier, to limit the leakage of radioactive gases generated by irradiated graphite can successfully reduce helium gas permeability. The morphology of the modified composite barrier, especially the orientation of the flakes to the substrate surface, was characterised, amongst others, by µXCT (Van Rooyen, Karger-Kocsis, Vorster & Kock, 2013). It was found that incorporation of graphene nanoplatelets and the influence of preparation techniques improve the helium gas barrier properties of the epoxy coatings (Van Rooyen, Karger-Kocsis & Kock, 2015). µXCT assisted further in characterisation of the improvement of the barrier by adding a oxyfluorination filler to the graphene nanoplatelets which resulted in better dispersion of the graphene nanoplatelets compared to the unmodified ones and subsequent reduction of helium gas permeability of the polytetrafluoroethylene (PTFE)/graphene nanocomposites (Van Rooyen, Bissett, Khoathane & Karger-Kocsis, 2016). In formulating a guideline for the preparation of PTFE/graphene nanocomposites by compression moulding and free sintering, µXCT has shown the potential to optimise processing parameters and to determine the void content of the billet and to visually assess how the pre-form pressure influenced the billet structure (Van Rooyen, Bissett, Khoathane & Karger-Kocsis, 2016) (Van Rooyen 2017).

The relationship between iron ore granulation mechanisms, granule shapes, and sinter bed permeability were tested (Nyembwe, Cromarty & Garbers-Craig, 2017) and the complete modelling of the characteristics of iron ore granules formed during the granulation process of mixtures that contain concentrate and micropellets were described. µXCT comparison of the

experimental and predicted[57] granule size distribution of iron ore was performed to distinguish between the different phases in the granules and allowed the predicted model to be benchmarked after which it could predict the mean granule size of sinter mixtures (Nyembwe, Cromarty & Garbers-Craig, 2016) (Nyembwe, 2017).

3.3.4.4 Non-destructive examination (NDE)

The benefit of radiography and tomography as intrinsic non-destructive examination (NDE) techniques for industrial applications, can add tremendous value.

One example is the qualitative industrial application of neutron radiography to image main rotor helicopter blades. Deficiencies such as oil or water ingress, corrosion, delamination and resin build-up or lack thereof were successfully detected (De Beer, Coetzer et al., 2004).

Several components of an IS-60 Rover Gas turbine engine have been successfully explored through neutron tomography as a reverse engineering tool, particularly for complex internal geometries (Roos, Quin, De Beer & Nshimirimana, 2011).

3.3.5 Geosciences

The Geoscience sector of interest to Necsa users including the fields of geology and petrophysics and are briefly discussed separately. A summary of the output generated in each field is reflected in Figure 3.17 and will be discussed briefly below.

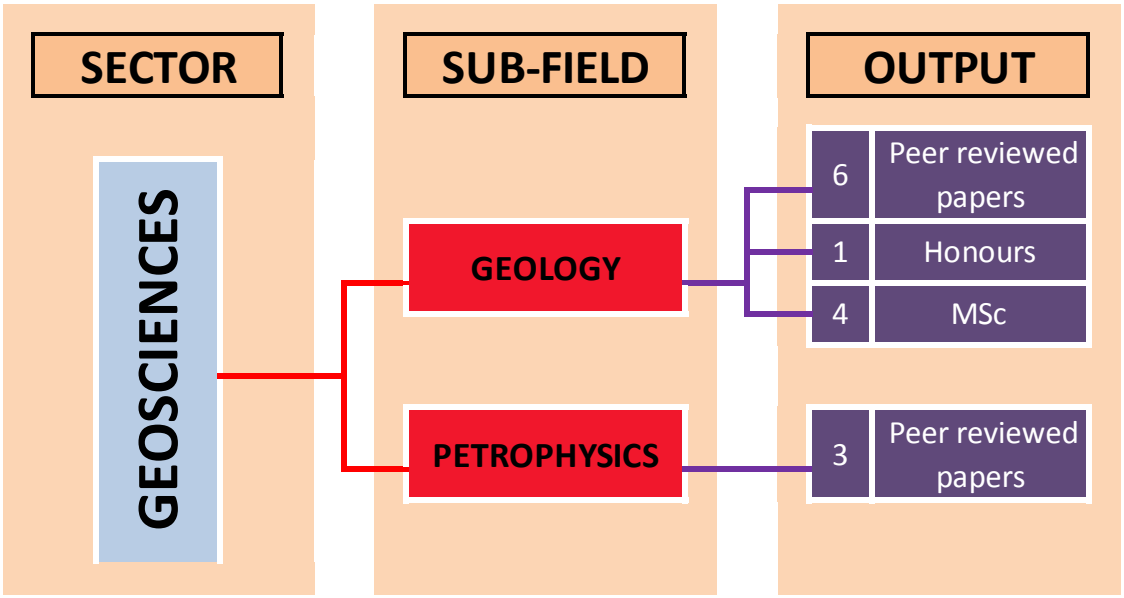

Figure 3.17: Schematic and summary of outputs generated in the Geosciences sector.

57 Prediction of granule size distribution using the model developed by Litster.

3.3.5.1 Geology

The quantification and qualification of the morphological and physical characteristics of geo-materials through high resolution 3D tomography adds value to the rich South African geoscience record. In the first utilisation at Necsa, the capabilities of neutron tomography and X-ray tomography were compared with respect to their ability to identify different minerals and examining the shape and size of fractures in geological samples (Mahlatji, 2004).

Understanding of the formation, genesis and evolution of Vaalputs[58] soils provides an opportunity to gain insights into the past climates that have shaped the palaeosoils at Vaalputs. Significant qualification and quantification by µXCT of the vertically and horizontally (box-shaped) laminated structures of the soil, often associated with barite accumulations, was achieved (Majodina, 2013) with further investigations revealing that the barite is closely associated with the calcite/clay laminae and in general follows the topography of the wavy laminae (Clarke, Majodina, Du Plessis & Andreoli, 2016).

The µXCT analysis of gold in exploration drill cores from the Witwatersrand showed that the method can be used to evaluate drill cores successfully (Deshenthree, Nshimirimana & De Beer, 2011) and assess the potential of the ores for heap leaching (Nwaila, et al., 2013) (Nwaila, 2014). Gold identification in drill cores could be made due to the high X-ray attenuation and the resulting contrast with surrounding materials. For simulation reasons, a better understanding of the formation and deposition of uranium-bearing minerals in the Vaal Reef through analysis of drill core samples using, inter alia, µXCT, was possible (Sebola, 2014).

The mineralogy and morphological properties of inclusions present in megacrysts originating from Marion Island[59], as studied by means of µXCT, contributed to the understanding of the geological evolution of the island (Keabetswe, 2016).

The quantification of total and effective porosity in porous rocks and iron ore was shown to provide sufficient information to assess resource availability of petroleum and iron ore, respectively. A robust methodology using µXCT to validate iron ore mineralogy and geometry was furthermore developed that meets the requirements of geo-metallurgical testing for application in minerals processing (Bam, Miller, Becker, De Beer & Basson, 2016). Neutron radiography characterisation developments by the author (De Beer, Middleton & Hilson, 2004) lead to the visualisation and the generalisation of the characterisation of fluid flow in porous media (De Beer & Middleton, 2006) (De Beer, Schoeman, Nshimirimana, Ledwala & Middleton, 2007) (De Beer & Middleton, 2009).

58 Depository for low and medium nuclear waste in the Karoo, Northern Cape Province, South Africa.
59 Marion Island: South African Island ~ 2100 km South of Cape Town in the Atlantic Ocean.

3.3.5.2 Petrophysics

The physical characteristic of spontaneous uptake of water (imbibition) in Australian reservoir rock (Mardie Greensand and Barrow group) was dynamically visualised using neutron radiography for the collaborators[60,61] to conclude, applying the *Li and Horne* model, that the water permeability and the capillary pressure-water saturation gradient are constant throughout most of the imbibition process (Middleton, Li & De Beer, 2005). Furthermore, neutron radiography data of tar deposits[62] in sandstone contributed to form a spatial interpretation of how hydrocarbon migrated into, and was preserved within, a specific geological habitat (Middleton, De Beer, Haines & Mory, 2007). Development of a calibration procedure of digital neutron radiographs resulted in the accurate and correct quantification of hydrocarbons in oil bearing rocks (De Beer & Middleton, 2005).

3.4 Summary and Conclusions

In many instances, the author introduced researchers and post graduate students for the first time to the utilisation of neutron and X-ray radiography and tomography as a unique non-destructive analytic research technique. In this Chapter, the author provided a brief overview of the research stimulation, growth and diversification that resulted from his establishment of state-of-the-art radiography and tomography research hubs at Necsa. At the same time, the powerful contribution that radiography and tomography can make towards qualitative and quantitative understanding of mechanisms and processes in many areas of research has been illustrated through a number of selected examples.

Establishment of research and development partnerships with researchers from many different fields, locally and abroad, formed the basis of the establishment of a strong local capability. The research hubs at Necsa afford an ideal platform for multi-disciplinary research as workers from different fields interact and exchange ideas. The facilities also offer an excellent platform for post graduate research and training as illustrated in Table 3.1 by the research networks established.

The contributions of the author towards the establishment of an internationally recognised radiography and tomography capability in Africa did not go unnoticed and he was elected as vice-president of the International Society for Neutron Radiology (ISNR) in 2004 and he was elected President in 2008. In 2010 he hosted the 9th World Conference on Neutron Radiography

60 Australian petro-physicist: The late Prof. Mike Middleton from Curtin University, Perth, Australia.
61 American researcher: Prof. Kewen Li, Stanford University, USA.
62 Worral Formation: Pillara Formation: Grant Formation from Western Australia.

(WCNR-9) in South Africa. In addition, the author assisted in the publications of peer reviewed publications in national and international journals.

A bird's eye view of several collaborations established by the author which lead to research programs and output such as peer reviewed published articles in national and international journals is depicted in Table 3.2 below.

Table 3.2: Summary of the activities and collaborations lead and driven by the author.

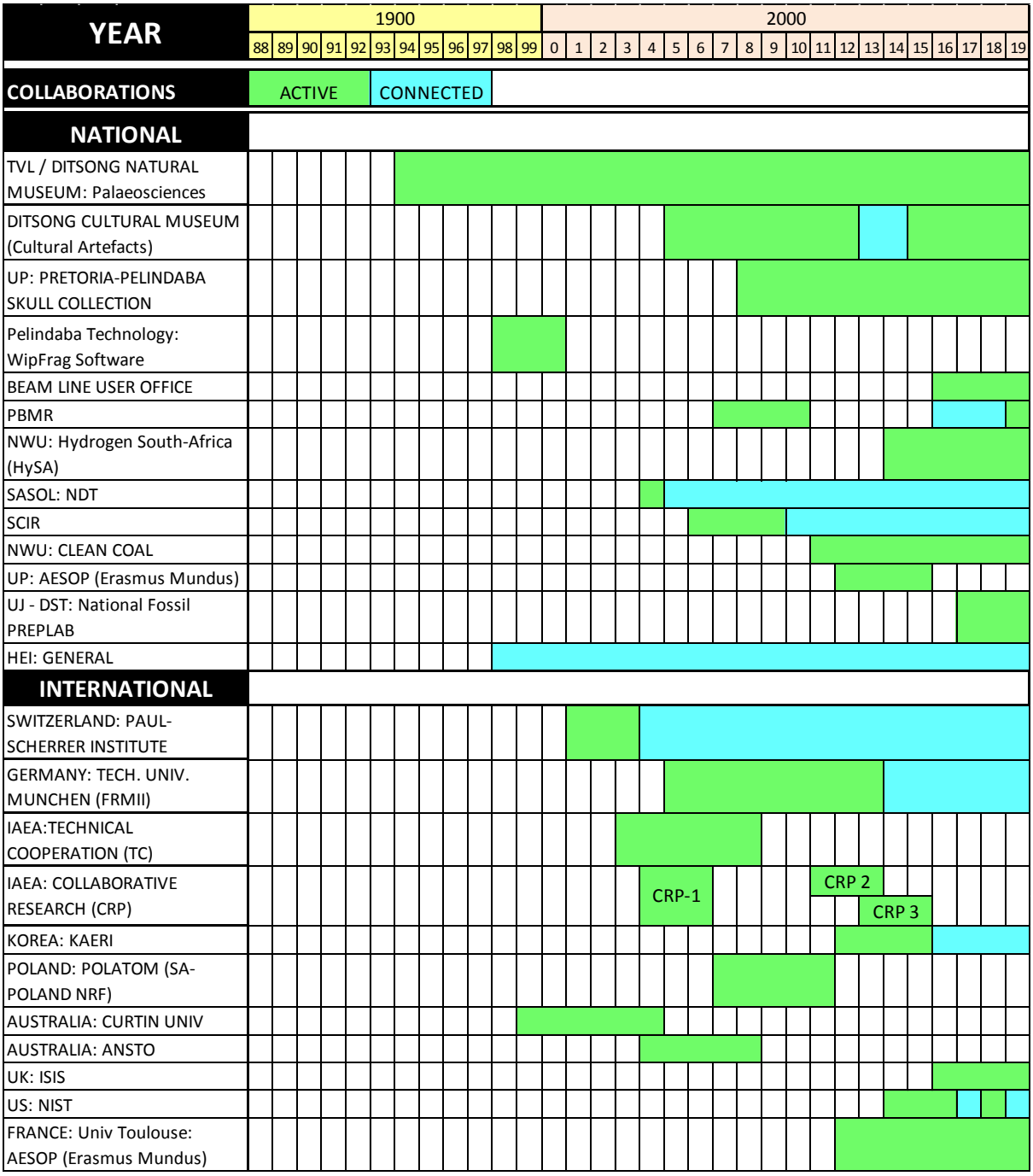

Figures 3.18 and 3.19 show the growing number per annum of peer reviewed articles (123 in total to date) and graduation of post graduate students, respectively (57 in total). The scientific research community began to show maturity in the tomographic research modality as, from 2012, 76 (62% of the total) peer reviewed articles were published and 44 (77% of the total) higher educational degrees were obtained based upon work done at Necsa's radiography and tomography facilities.

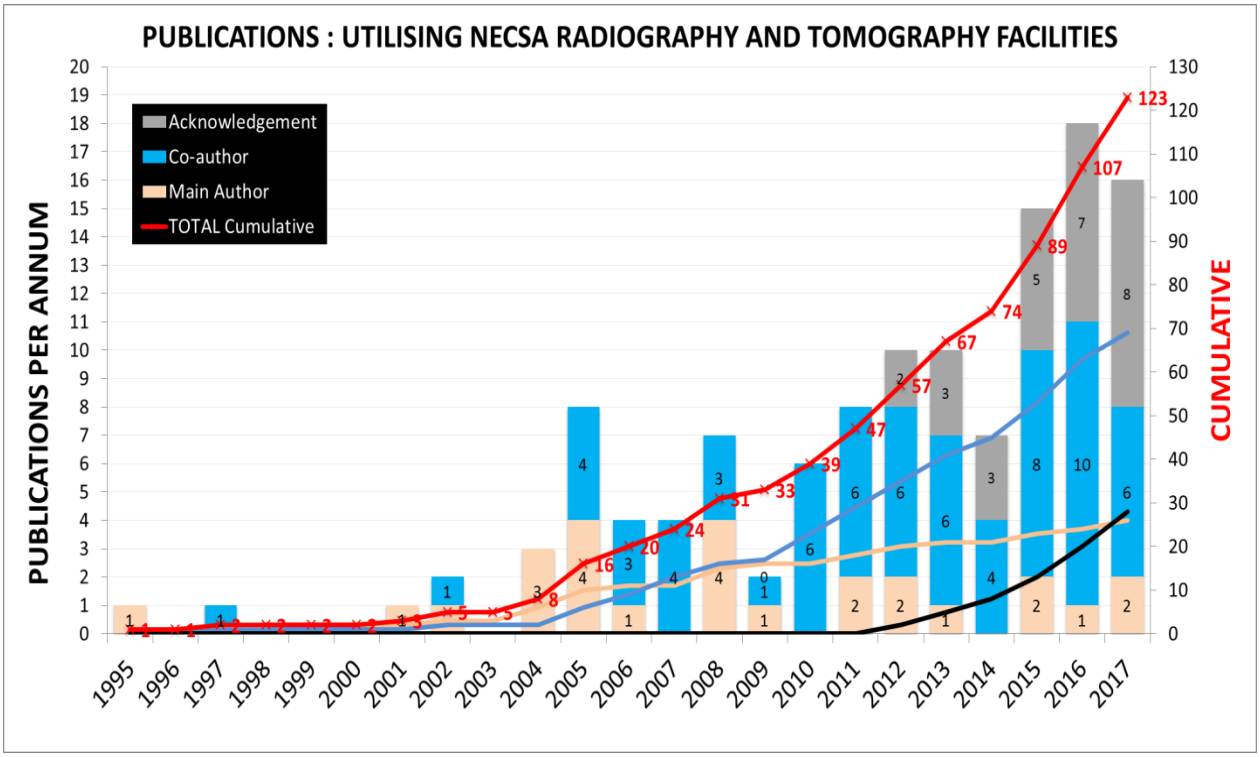

Acknowledgement: Necsa Colleagues are co-authors or Necsa only acknowledged; Author in supportive role.
Co-Author: Author is added as a co-author to the publication; Author in active and highly supportive role.
Main Author: Author initiated research and is fully responsible for publication of results.
TOTAL Cumulative: Cumulative number of all the different output per annum.

Figure 3.18: Number of publications resulted from utilising Necsa's tomography facilities.

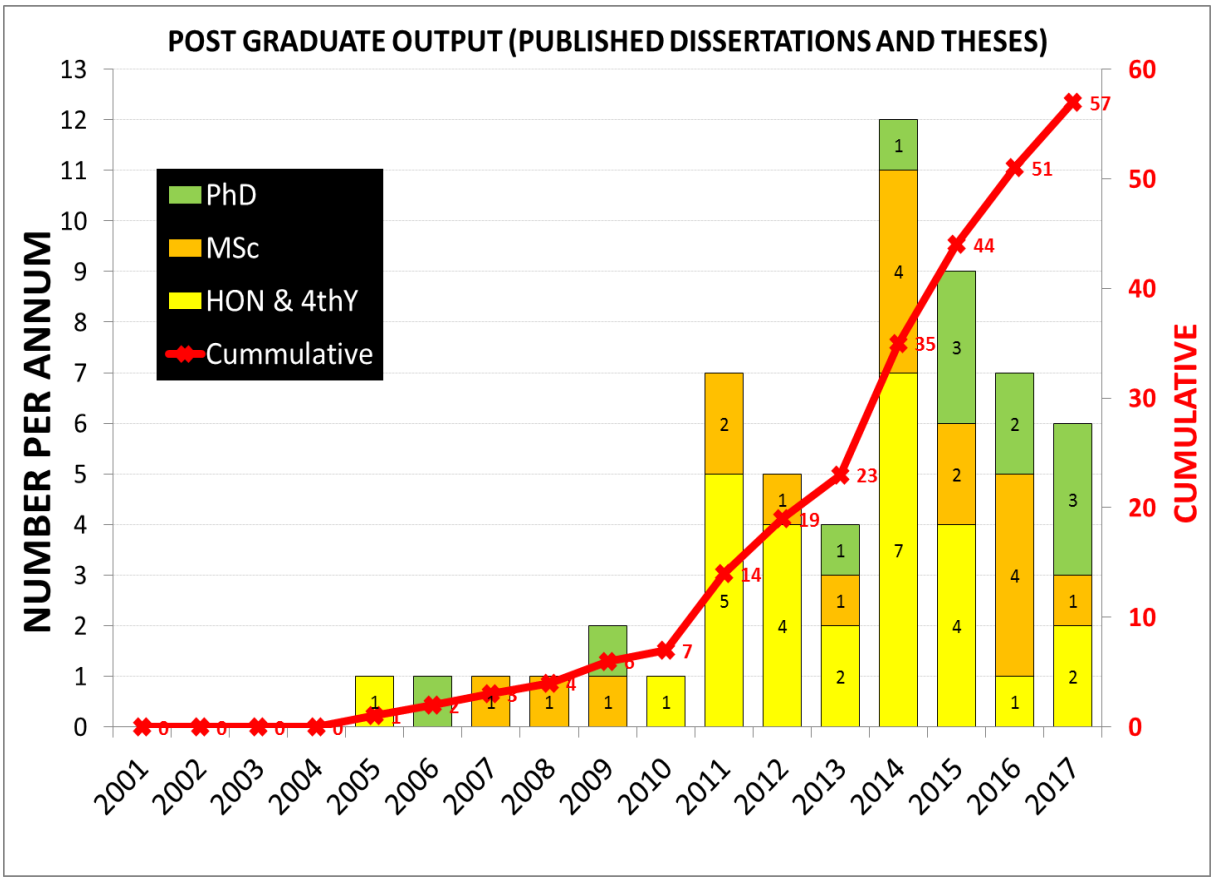

PhD: Doctoral.
MSc: Masters.
HON & 4thY: Honours and 4th Year (Normally 4th year Engineering Projects).
Cumulative: Cumulative output number of Post Graduate dissertations and theses per annum.

Figure 3.19: Number of completed post graduate studies at Necsa's facilities per annum.

Figure 3.20 summarises the diverse scientific areas covered in all the output generated to date.

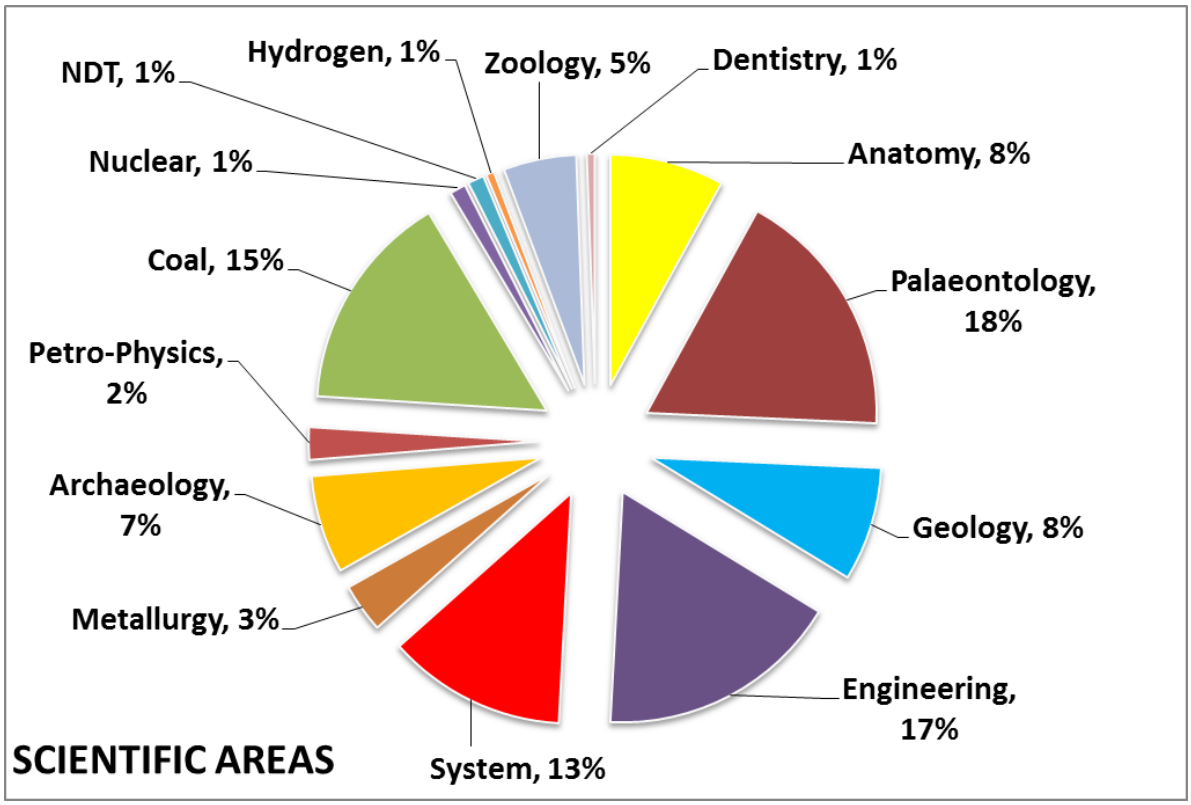

Figure 3.20: Miscellaneous scientific areas covered in the total output generated at the Necsa's radiography and tomography facilities to date.

Chapter 3 Bibliography:

'All Nobel Prizes in Physics'. Nobel prize.org. Nobel Media. (2014). Retrieved 4 September 2017, from http://www.nobelprize.org/nobel_prizes/physics/laureates/%3E.

Bacci, N. (2016). *Traumatic Effects of Lightning Strike on Human Bone Morphology and Ultrastructure*. Master's - WITS.

Badenhorst, C. J. (2013). *Study on the Thermal Fragmentation Behaviour of Coal by Using Tomography*. Honours - NWU.

Badenhorst, C. J. (2016). *Primary Fragmentation of Large Coal Particles.* Master's - NWU.

Bam, L. C., Miller, J. A., Becker, M., De Beer, F. C. & Basson, I. (2016). X-ray Computed Tomography – Determination of Rapid Scanning Parameters for Geometallurgical Analysis of Iron Ore. In *The Second AUSIMM International Geometallurgy Conference* (pp. 15–16).

Banhart, J. (2008). *Advanced Tomographic Methods in Materials Research and Engineering*. (J. Banhard, Ed.) (1st ed.). Berlin: Hahn-Meittner Institute, Berlin, Germany.

Barton, J. P. (Ed.). (1986). *Neutron Radiography (2) (1986)*. Paris, France: D. Reidel Publishing Company, Dordrecht, Holland.

Barton, J. P. (1993). *Neutron Radiography (4) (1991)*. (J. P. Barton, Ed.). San Francisco, California, USA: Gordon & Breach Science Publishers Ltd (1 Nov. 1993).

Beaudet, A. (2015). *Characterization of the Internal Cranio-Dental Structures of the Cercopithecoids and Diachronic Study of their Morphological Variations in the South African Plio-Pleistocene Sequence. French: Caracterisation des Structures Cranio-dentaires Internes des ce*. Doctorate - Doctorate - Univ Toulouse Paul Sabatier.

Beaudet, A. (2017). The Emergence of Language in the Hominin Lineage: Perspectives from Fossil Endocasts, *11*(August), 1–4. http://doi.org/10.3389/fnhum.2017.00427.

Beaudet, A., Braga, J., De Beer, F., Schillinger, B., Steininger, C., Vodopivec, V. & Zanolli, C. (2016). Neutron Microtomography-based Virtual Extraction and Analysis of a Cercopithecoid Partial Cranium (STS 1039) Embedded in a Breccia Fragment from Sterkfontein Member 4 (South Africa). *American Journal of Physical Anthropology*, *159*(4), 737–745. http://doi.org/10.1002/ajpa.22916.

Beaudet, A., Bruxelles, L., Macchiarelli, R., Dumoncel, J., Thackeray, J. F., De Beer, F. & Braga, J. (2014). Time-related Changes in fossil cercopithecoid inner Craniodental Structures and Chronological Seriation of South African Hominin-Bearing Sites. In *Proc. Europ. Soc. Hum. Evol.*

Beaudet, A., Dumoncel, J., De Beer, F., Duployer, B., Durrleman, S., Gilissen, E., Hoffman, J., Tenailleau, C., Thackeray, J. and Braga, J. (2016). Morphoarchitectural Variation in South African Fossil Cercopithecoid Endocasts. *Journal of Human Evolution*, *101*, 65–78. http://doi.org/10.1016/j.jhevol.2016.09.003.

Beaudet, A., Dumoncel, J., Thackeray, J. F., Bruxelles, L., Duployer, B., Tenailleau, C., Bam, L., Hoffman, J., De Beer, F. and Braga, J. (2016). Upper Third Molar Internal Structural Organization and Semicircular Canal Morphology in Plio-Pleistocene South African Cercopithecoids. *Journal of Human Evolution*, *95*, 104–120. http://doi.org/10.1016/j.jhevol.2016.04.004.

Beaudet, A., Zanolli, C., Redae, B. E., Endalamaw, M., Braga, J. & Macchiarelli, R. (2015). A New Cercopithecoid Dentognathic Specimen Attributed to Theropithecus from the Late Early Pleistocene (c. 1 Ma) Deposits of Simbiro, at Melka Kunture, Ethiopian Highlands. *Comptes Rendus - Palevol*, *14*(8), 657–669. http://doi.org/10.1016/j.crpv.2015.07.003.

Bradfield, J., Hoffman, J. & De Beer, F. (2016). Verifying the Potential of Micro-focus X-ray Computed Tomography in the Study of Ancient Bone Tool Function. *Journal of Archaeological Science: Reports*, *5*(2016), 80–84. http://doi.org/10.1016/j.jasrep.2015.11.001.

Braga, J., Loubes, J. M., Descouens, D., Dumoncel, J., Thackeray, J. F., Kahn, J. l., … Gilissen, E. (2015). Disproportionate Cochlear Length in Genus Homo Shows a High Phylogenetic Signal during Apes' Hearing Evolution. *PLOS ONE*, *10*(6), e0127780. http://doi.org/10.1371/journal.pone.0127780.

Braga, J., Thackeray, Francis Bruxelles, L., Duranthon, Francis Couzens, R. & De Beer, F. C. (2014). New Excavations Reveal First Discoveries of the Earliest Hominins from Kromdraai B. In *The African Human Fossil Record*. http://doi.org/10.13140/2.1.2285.64.

Braga, J., Thackeray, J. F., Dumoncel, J., Descouens, D., Bruxelles, L., Loubes, J.-M., … Spoor, F. (2013). A New Partial Temporal Bone of a Juvenile Hominin from the Site of Kromdraai B (South Africa). *Journal of Human Evolution*, *65*(4), 447–456. http://doi.org/10.1016/j.jhevol.2013.07.013.

Braga, J., Thackeray, J. F., Dumoncel, J., Duployer, B., Tenailleau, C., De Beer, F. & Thackeray, J. F. (2016). The Kromdraai Hominins Revisited with an Updated Portrayal of Differences Between Australopithecus Africanus and Paranthropus Robustus. In J. Braga & J. F. Thackeray (Eds.), *Kromdraai. A birthplace of Paranthropus in the cradle of humankind*.

Brew, D. R. M., De Beer, F. C., Radebe, M. J., Nshimirimana, R., McGlinn, P. J., Aldridge, L. P. & Payne, T. E. (2009). Water Transport Through Cement-Based Barriers—A Preliminary Study Using Neutron Radiography and Tomography. *Nuclear Instruments and Methods in Physics Research Section A: Accelerators, Spectrometers, Detectors and Associated Equipment*, *605*(1–2), 163–166. http://doi.org/10.1016/j.nima.2009.01.146.

Burger, S. (2011, August 19). Corporation Launches Microfocus X-Ray Machine. *Engineering News: August*, p. 57. Retrieved from http://www.engineeringnews.co.za/print-version/microfocus-x-ray-machine-for-sa-scientific-community-2011-08-19.

Cazenave, M., Braga, J., Oettlé, A., Thackeray, J. F., De Beer, F., Hoffman, J., … Macchiarelli, R. (2017). Inner Structural Organization of the Distal Humerus in Paranthropus and Homo. *Comptes Rendus Palevol*, *16*(5–6), 521–532. http://doi.org/10.1016/j.crpv.2017.06.002.

Chadwick, J. (1933). The Nobel Prize in Physics 1935: James Chadwick. 'The Neutron and its Properties'. http://doi.org/10.1259/0007-1285-6-61-24.

Cisneros, J., Cabral, U.G., De Beer,F.C., Damiani, R., Fortier, D.C. (2010). Spondarthritis in the Triassic. PLOS ONE, https://doi.org/10.1371/journal.pone.0013425.

Clarke, C. E., Majodina, T. O., du Plessis, A. & Andreoli, M. A. G. (2016). The Use of X-ray Tomography in Defining the Spatial Distribution of Barite in the Fluvially Derived Palaeosols of Vaalputs, Northern Cape Province, South Africa. *Geoderma*, *267*(2016), 48–57. http://doi.org/10.1016/j.geoderma.2015.12.011.

Cloete, D. (2012). *NRAD Translation Table*. Honours - Univ Pretoria.

Coetzee, S. (2015). The Caking and Swelling of South African Large Coal Particles, (October). Doctoral - NWU

Coetzee, S., Neomagus, H. W. J. P., Bunt, J. R., Strydom, C. A. & Schobert, H. H. (2014). The Transient Swelling Behaviour of Large (À 20 + 16 mm) South African Coal Particles During Low-Temperature Devolatilisation. *FUEL*, *136*, 79–88. http://doi.org/10.1016/j.fuel.2014.07.021.

Cormack, A. M. (1979). The Nobel Prize in Physiology or Medicine 1979: Allan Cormack, Godfrey Hounsfield. 'Early Two-Dimensional Reconstruction and Recent Topics Stemming from it.' Retrieved 13 June 2017, from http://www.nobelprize.org/nobel_prizes/medicine/laureates/1979/cormack-bio.html.

De Beer, F. (2003). *IAEA TC Application for Beam Lines - NRad*.

De Beer, F. C. (2005). Characteristics of the Neutron/X-Ray Tomography System at the SANRAD Facility in South Africa. *Nuclear Instruments and Methods in Physics Research, Section A: Accelerators, Spectrometers, Detectors and Associated Equipment*, *542*(1–3), 1–8. http://doi.org/10.1016/j.nima.2005.01.003.

De Beer, F. C. (2008). Neutron and X-Ray Tomography at Necsa. *Journal of the South African Institute of Mining and Metallurgy*, *108* (October), 1–8.

De Beer, F. C. (2012). *F1-RC-1219.1: Application of 3D Neutron Imaging and Tomography in Cultural Heritage Research. Report of the 1st Research Coordinated Meeting (RCM), Vienna, Austria: 07 - 11 May 2012*. Vienna, Austria.

De Beer, F. C. (2013). *F1-RC-11018.2: IAEA CRP on Application of 3D Neutron Imaging and Tomography in Cultural Heritage Research. Report of the 2nd Research Coordinated Meeting (RCM) in Garching, Germany 3-6 Sept 2013.* Garching, Germany.

De Beer, F. C. (2015a). *F1-RC-1219-3: Application of 3D Neutron Imaging and Tomography in Cultural Heritage Research.* Report of the 3rd Coordinated Meeting (RCM) in Firenze, Italy 20 - 24 April 2015. Florance, Italy.

De Beer, F. C. (2015b). *Neutron and X-ray Radiography/Tomography: Non-destructive Analytical Tools for the Characterization of Nuclear Materials.* Journal of the Southern African Institute of Mining and Metallurgy (SAIMM), 115(10), 913–924. http://doi.org/http://dx.doi.org/10.17159/2411-9717/2015/v115n10a3.

De Beer, F. C. (2016). *Development of Guidelines for Major Upgrades and New Design of Neutron Imaging Facilities*. Vienna. Retrieved from IAEA Ref. F1-CS-53685.

De Beer, F. C. (2017). Paleontology: Fossilized Ancestors Awaken by Neutron Radiography. In Kardjilov N. & Festa, G. (Eds.), *Neutron Methods for Archaeology and Cultural Heritage. Neutron Scattering Applications and Techniques.* (pp. 141–171). Springer, Cham. http://doi.org/10.1007/978-3-319-33163-8_7.

De Beer, F. C., Botha, H., Ferg, E., Grundlingh, R., & Smith, A. (2009). Archaeology Benefits from Neutron Tomography Investigations in South Africa. *Nuclear Instruments and Methods in Physics Research A*, *605*, 167–170. http://doi.org/10.1016/j.nima.2009.01.213.

De Beer, F. C., Coetzer, M., Fendeis, D. & Da Costa E Silva, A. (2004). Neutron Radiography and other NDE Tests of Main Rotor Helicopter Blades. *Applied Radiation and Isotopes*, *61*(4), 609–616. http://doi.org/10.1016/j.apradiso.2004.03.088.

De Beer, F. C., Franklyn, C. B., Venter, A. M. & Nothnagel, G. (2012). Utilisation And Upgrading Of The Neutron Beam Lines. In *International Conference on Research Reactors: Safe Management and Effective Utilization, 14-18 November 2011,* (pp. 1–8). Rabat, Morocco: IAEA. Retrieved from http://www-pub.iaea.org/MTCD/publications/PDF/P1575_CD_web/datasets/papers/A10 de Beer.pdf.

De Beer, F. C., Gruenauer, F., Radebe, M. J., Modise, T. & Schillinger, B. (2013). Scientific Design of the New Neutron Radiography Facility (SANRAD) at SAFARI-1 for South Africa. *Physics Procedia*, *43*, 34–41. http://doi.org/10.1016/j.phpro.2013.03.004.

De Beer, F. C., Kardjilov, N., Lehmann, E. H. & Hassenein, R. (2007). Neutron Scattering Corrections for Neutron Radiography. 2nd IAEA-RCM of Materials and Neutrons, Vienna.

De Beer, F. C., Le Roux, J. J. & Kearsley, E. P. (2005). Testing the Durability of Concrete with Neutron Radiography. *Nuclear Instruments and Methods in Physics Research Section A: Accelerators, Spectrometers, Detectors and Associated Equipment*, *542(1–3), 226–231.* http://doi.org/10.1016/j.nima.2005.01.104.

De Beer, F. C. & Lehmann, E. (2005). Proposed Neutron tomography Facility in South Africa. (*P. Chirco & R. Rosa, Eds.) Proceedings of the 7th World Conference on Neutron Radiography (WCNR-7), Rome, Italy 15 - 21 Sept 2002. (WCNR-7). Rome, Italy: ENEA*.

De Beer, F. C. & Middleton, M. F. (2005). Calibration of neutron imagary for petrolium engineering application. *In WCNR-7 (2002). Rome, Italy.*

De Beer, F. C. & Middleton, M. F. (2006). Neutron Radiography Imaging, Porosity and Permeability in Porous Rocks. *South African Journal of Geology*, *109*, 525–534.

De Beer, F. C., Middleton, M. F. & Hilson, J. (2004). Neutron Radiography of Porous Rocks and Iron Ore. *Applied Radiation and Isotopes,* 61(4), 487–495. http://doi.org/10.1016/j.apradiso.2004.03.089.

De Beer, F. C., Prevec, R., Cisneros, J. & Abdala, F. (2008). Hidden Structure of Fossils Revealed by Neutron and X-Ray Tomography. *Neutron Radiography (8), 452–461.*

De Beer, F. C. & Radebe, M. J. (2012). Neutron Imaging – Practice and Role as a Complementary NDE Technique to X-Ray Imaging, (April), *Proceedings of the 18th World Conference on Non-Destructive Testing, Durban, South Africa,* 16–20.

De Beer, F. C., Radebe, M. J., Schillinger, B., Nshimirimana, R. & Ramushu, M. A. (2015). Upgrading the Neutron Radiography Facility in South Africa (SANRAD): Concrete Shielding Design Characteristics. *Physics Procedia*, (October 2014), 1–9.

De Beer, F. C. & Strydom, W. J. (2001). Neutron Radiography at SAFARI-l in South Africa. *Nondestructive Testing and Evaluation*, *16*(2–6), 163–176. http://doi.org/http://dx.doi.org/10.1080/10589750108953073.

De Beer, F. C., Strydom, W. J. & Griesel, E. J. (2004). The Drying Process of Concrete: a Neutron Radiography Study. *Applied Radiation and Isotopes*, *61*(4), 617–623. http://doi.org/10.1016/j.apradiso.2004.03.087.

De Beer, F. C., Zidi, T., Abd El Salam, T. M., Khafki, F., Motlauthi, G. M. D. & Guzek, J. (2005). Facilities for Neutron Radiography in Africa: Description, Performance and Application. In P. Chirco & R. Rosa (Eds.), *Proceedings of the 7th World Conference on Neutron Radiography (WCNR-7), Rome, Italy 15 - 21 Sept 2002. (WCNR-7)*. ENEA.

De Beer, F. & Middleton, M. (2009). Neutron Imaging in South Africa Adds Value to Geosciences and Petrophysics. In *ESEG* (pp. 1–4).

De Beer, F., Schoeman, C., Nshimirimana, R., Ledwala, J. & Middleton, M. (2007). Penetrating Neutron Radiation Enhances Physical Properties of Rock. In *South African Geological Association (SAGA)* (pp. 5–8).

De Beer, F., Van der Merwe, J-H. & Bessarabov, D. (2017). PEM Water Electrolysis: Preliminary Investigations using Neutron Radiography. *Physics Procedia*, *88,*(September 2016), 19–26. http://doi.org/10.1016/j.phpro.2017.06.002.

De Jager, E. (2016). *Visualisation of the Ventricles of the Brain: A Microfocus X-Ray Study*. Honours - Univ Pretoria.

Deshenthree, C., Nshimirimana, R. & De Beer, F. (2011). The Use of 3D X-Ray Computed Tomography for Gold Location in Exploration Drill Cores. In *Proceedings, 10th International Congress for Applied Mineralogy (ICAM)* (pp. 1–5).

Domanus, J. C.,& Markgraf, J. F. W. (1987). *Collimators for Thermal Neutron Radiography an Overview*. D.Reidel Publishing Company.

Dorfling, F. (2010). *Exploring Methodologies to Three Dimensionally Represent the Ventricular System of the Brain for Educational Purposes*. Honours - Univ Pretoria.

Du Preez, M. (2011). *Design of Flight Tube and Vacuum Pump System for a Neutron Radiography Facility*. Honours - University of Pretoria.

Du Toit, C. G. & Rosslee, P. J. (2012). Analysis of the Porous Structure of Packed Beds of Spheres using X-ray Computed Tomography. In *Eighth South African Conference on Computational and Applied Mechanics SACAM2012* (pp. 3–5).

Edwards, J. (1901). The Roentgen Rays in South Africa. *Lancet 1*, (1), 1755–1756.

Elert, G. (n.d.). The Physics Hypertextbook. Retrieved 9 July 2017, from https://physics.info/x-ray/.

Fijał-Kirejczyk, I. M., Milczarek, J. J., Radebe, M. J., De Beer, F. C. & Żołądek-Nowak, J. (2011). Neutron Radiography Applications in Studies of Drying of Capillary-Porous Systems. *European Drying Conference - EuroDrying'2011*, (October), 26–28.

Fijał-Kirejczyk, I. M., Milczarek, J. J., Żołądek-Nowak, J., De Beer, F. C., Radebe, M. J. & Nothnagel, G. (2012). Application of Statistical Image Analysis in Quantification of Neutron Radiography Images of Drying. *Acta Physica Polonica A*, *122*(2), 410–414. http://doi.org/10.12693/APhysPolA.122.410.

Florentino, G. (2013). *An Evaluation of the Development and Growth of the Mandibular Canal in Relation to the Developing Juvenile Dentition*. Honours - WITS.

Fornai, C. (2009). *Testing the Second Australopithecine Species Hypothesis for the South African Site of Sterkfontein: Geometric Morphometric Analysis of Maxillary Molar Teeth*. Masters - University of the Witwatersrand.

Fornai, C., Bookstein, F. L. & Weber, G. W. (2015). Variability of Australopithecus Second Maxillary Molars from Sterkfontein Member 4. *Journal of Human Evolution*, *85*, 181–192. http://doi.org/10.1016/j.jhevol.2015.05.013.

Fornai, C., Clarke, R. J., Moggi-Cecchi, J., Hemingway, J., De Beer, F. C. & Radebe, M. J. (2010). Testing the‘ Second Australopithecine Species Hypothesis’ for Sterkfontein Member 4, South Africa. In *American Journal of Physical Anthropology* (pp. 105–106). Wiley-Liss Div John Wiley & Sons Inc.

Franklyn, C. & Daniels, G. C. (2012). Characterization Methods for an Accelerator Based Fast-Neutron Facility. *Journal of Instrumentation*, *7*(2), C02043–C02043. http://doi.org/10.1088/1748-0221/7/02/C02043.

Fujine, S., Kobayashi, H. & Kanda, K. (Eds.). (2001). *Neutron Radiography (6) (1999)*. Osaka, Japan: Gordon and Breach.

Glasser, O. (1993). *Wilhelm Conrad Röntgen and the Early History of the Roentgen Rays.* Norman Publishing.

Gravett, V. F. (2011). *A Critical Analysis of Selected Egyptian Bronze Artefacts in the National Cultural History Museum (NCHM)*. Masters - UNISA.

Grunauer, F. (2005). *Design, Optimization, and Implementation of the New Neutron Radiography Facility at FRM-II*. Techische Universitat Munchen. Retrieved from https://mediatum.ub.tum.de/doc/603112/document.pdf.

Grünauer, F. (2009). *RS-RAD-REP-14001:* Monte Carlo Simulations for the SAFARI-1 Reactor and its Instrumentation: *Part C: Neutron Radiography Facility.*

Hahn, O. H. (1973). Some Historical Notes on South Africa’s Pioneer Radiographer. *S.A. Medical Journal*, (22 Dec), 2428–2430.

Hassanein, R., De Beer, F., Kardjilov, N. & Lehmann, E. (2006). Scattering Correction Algorithm for Neutron Radiography and Tomography Tested at Facilities with Different Beam Characteristics. *Physica B*, *385–386*, 1194–1196. http://doi.org/10.1016/j.physb.2006.05.406.

Hassanein, R. K. (2006). *Correction Methods for the Quantitative Evaluation of Thermal Neutron Tomography*. Doctorate - Swiss Federal Institute Of Technology Zurich.

Hills, R. (2011). *Three Dimensional Visualisation of the Pterygopalatine Fossa by Microfocus Imaging*. Honours - Univ Pretoria.

Hoffman, J. & De Beer, F. (2012). Characteristics of the Micro-focus X-Ray Tomography Ffacility (MIXRAD) at Necsa in South Africa. In *www.ndt.net*. Durban: *18th World Conference on Nondestructive Testing. Retrieved from http://www.ndt.net/article/wcndt2012/papers/37_wcndtfinal00037.pdf.*

Hoffman, J. W. (2012). *Ionizing Radiation As Imaging Tool for Coal Characterization and Gasification Research*. Masters - North-West University.

Hounsfield, G. N. (1979). The Nobel Prize in Physiology or Medicine 1979: Godfrey N. Hounsfield. ‘Computed Medical Imaging’. Retrieved 17 June 2017, from https://www.nobelprize.org/nobel_prizes/medicine/laureates/1979/hounsfield-bio.html.

Hutchinson, E. F. (2017). *Aspects Of Mandibular Development and Growth at Different Stages Across the Lifespan*. Doctorate - WITS.

Hutchinson, E. F., Farella, M., Hoffman, J. & Kramer, B. (2017). Variations in Bone Density Across the Body of the Immature Human Mandible. *Journal of Anatomy*, *230*(5), 679–688. http://doi.org/10.1111/joa.12591.

Hutchinson, E. F., Florentino, G., Hoffman, J. & Kramer, B. (2016). Micro-CT Assessment of Changes in the Morphology and Position of the Immature Mandibular Canal During Early Growth. *Surgical and Radiologic Anatomy*, *39*, 185–194. http://doi.org/DOI 10.1007/s00276-016-1694-x.

IMAGINIS. (n.d.). Brief History of CT. Retrieved from http://www.imaginis.com/ct-scan/brief-history-of-ct.

Impactscan. (2013). A Brief History of CT. Retrieved 17 June 2017, from http://www.impactscan.org/CThistory.htm.

Jacobs, D. S., Bastian, A. & Bam, L. C. (2014). The Influence of Feeding on the Evolution of Sensory Signals: A Comparative Test of an Evolutionary Trade-Off Between Masticatory and Sensory Functions of Skulls in Southern African Horseshoe Bats (Rhinolophidae). *Journal of Evolutionary Biology*, *27*(12), 2829–2840. http://doi.org/10.1111/jeb.12548.

Jacobs, D. S., Mutumi, G. L., Maluleke, T. & Webala, P. W. (2016). Convergence as an Evolutionary Trade-Off in the Evolution of Acoustic Signals: Echolocation in Horseshoe Bats as a Case Study. In P. Pontarotti (Ed.), *Evolutionary Biology: Convergent Evolution, Evolution of Complex Traits, Concepts and Methods* (pp. 89–103). Cham: Springer International Publishing. http://doi.org/10.1007/978-3-319-41324-2_6.

Jacobson, L., De Beer, F. C. & Nshimirimana, R. (2011). Tomography Imaging of South African Archaeological and Heritage Stone and Pottery Objects. *Nuclear Inst. and Methods in Physics Research, A*, *651*(1), 240–243. http://doi.org/10.1016/j.nima.2011.02.093.

Jacobson, L., De Beer, F. C., Nshimirimana, R., Horwitz, L. K. & Chazan, M. (2012). Neutron Tomographic assessment of Incisions on Prehistoric Stone Slabs: A Case study from Wonderwerk cave, South Africa. *Archaeometry*, *55*(1), 1–13. http://doi.org/10.1111/j.1475-4754.2012.00670.x.

Kaestner, A. P., Kis, Z., Radebe, M. J., Mannes, D., Hovind, J., Grunzweig, C., … Lehmann, E. H. (2017). Samples to determine the resolution of neutron radiography and tomography. *Physics Procedia*, *88* (September 2016), 258–265. http://doi.org/10.1016/j.phpro.2017.06.036.

Kaestner, A. P., Lehmann, E. H., Hovind, J., Radebe, M. J., De Beer, F. C. & Sim, C. M. (2013). Verifying Neutron Tomography Performance Using Test Objects. In *Physics Procedia* (Vol. 43). http://doi.org/10.1016/j.phpro.2013.03.016.

Kak and Slaney. (1988). *Principles of Computerized Tomographic Imaging* (1st ed.). New York: IEEE Press.

Kallman, H. (1948). Neutron Radiography. *Research 1*, 254.

Kardjilov, N., De Beer, F. C., Middleton, M. F., Lehmann, E., Schillinger, B. & Vontobel, P. (2005). Corrections for Scattered Neutrons in Quantitative Neutron Radiography. In P. Chirco & R. Rosa (Eds.), *Neutron Radiography (7) (2002)* (pp. 521–528). Rome: ENEA.

Kardjilov, N., De Beer, F., Hassanein, R., Lehmann, E. & Vontobel, P. (2005). Scattering Corrections in Neutron Radiography Using Point Scattered Functions. *Nuclear Instruments and Methods in Physics Research A*, *542*, 336–341. http://doi.org/10.1016/j.nima.2005.01.159.

Keabetswe, D. L. (2016). *Inclusions in Clinopyroxene Megacrysts from Marion Island*. Master's - University of Pretoria.

Koleini, F., de Beer, F., Schoeman, M. H. A., Pikirayi, I., Chirikur, S., Nothnagel, G. & Radebe, J. M. (2012). Efficiency of Neutron Tomography in Visualizing the Internal Structure of Metal Artefacts from Mapungubwe Museum Collection with the Aim of Conservation. *Journal of Cultural Heritage*, *13*(3), 246–253.

Koleini, F., Prinsloo, L. C., Schoeman, M. H. A., Pikirayi, I. & Chirikure, S. (2013). Characterization of the Corrosion Layer on iIron Archaeological Artefacts from K2 (825–1220 AD), an Archaeological Site in South Africa. *Studies in Conservation*, 58(3), 274-282.

Koleini, F., Schoeman, M. H. A., Pikirayi, I. & Chirikure, S. (2012). Evidence for Indigenous Strip-drawing in Production of Wire at Mapungubwe Hill (1220–1290 AD): Towards an Interdisciplinary Approach. *Journal of Archaeological Science*, *39*(3), 757–762. http://doi.org/10.1016/j.jas.2011.11.012.

Le Roux, S. D., De Beer, F. C. & Thackeray, J. F. (1997). Neutron Radiography of Cranial Bone of Sts 5 (Australopithecus Africanus) from Sterkfontein, South Africa. *South African Journal of Science*, *93*(4), 176.

Lehmann, E. H., Boillat, P., Scherrer, G. & Frei, G. (2009). Fuel Cell Studies with Neutrons at the PSI's Neutron Imaging Facilities. *Nuclear Instruments and Methods in Physics Research Section A: Accelerators, Spectrometers, Detectors and Associated Equipment*, *605*(1–2), 123–126. http://doi.org/10.1016/j.nima.2009.01.143.

Lehmann, E. H., Vontobel, P., Frei, G., Kuehne, G. & Kaestner, A. (2011). How to Organize a Neutron Imaging User Lab ? 13 Years of Experience at PSI, CH. *Nuclear Inst. and Methods in Physics Research, A*, *651*(1), 1–5. http://doi.org/10.1016/j.nima.2010.12.135.

Lorenz, K. (2007). Antares (Advanced Neutron Tomography And Radiography Experimental System). Retrieved 25 July 2017, from http://einrichtungen.ph.tum.de/antares/.

Maartens, J. C. (2011). *Neutron Beam Filter Machanism*. Honours - Univ Pretoria.

Mahlatji, N. M. (2004). *Comparison of the Capabilities of Neutron Tomography with X-Ray Tomography on Geological Samples*. Honours - University of the Witwatersrand.

Maina, J. N. (2017). Chapter 9: Structure and Function of the Shell and the Chorioallantoic Membrane of the Avian Egg: Embryonic Respiration. In J. N. Maina (Ed.), *The Biology of the Avian Respiratory System: Evolution, Development, Structure and Function* (pp. 219–248). Springer. http://doi.org/10.1007/978-3-319-44153-5.

Majodina, T. O. (2013). *Geochemical and Mineralogical Characterisation of Vaalputs Palaeosols: Inference of Paleoclimates*. Master's - Univ of Stellenbosch.

Manke, I., Hartnig, C., Kardjilov, N., Messerschmidt, M., Hilger, A., Strobl, M., … Banhart, J. (2008). Characterization of Water Exchange and Two-Phase Flow in Porous Gas Diffusion Materials by Hydrogen-Deuterium Contrast Neutron Radiography. *Applied Physics Letters*, *92*, 2–4. http://doi.org/10.1063/1.2946664.

Masiteng, I., De Beer, F. C., Nshimirimana, R. B. & Segonyana, P. (2010). X-Ray Tomography, Neutron Tomography and Eenergy Dispersive X-Ray Spectroscopy Investigations of Selected Ancient Egyptian Artefacts. *NCHM Research Journal*, *5*, 1–18.

Maweza, E. L. (2011). *On the Investigation of the Properties of Building Materials for Low Cost Housing*. Master's - Univ Fort Hare.

McGlinn, P. J., De Beer, F. C., Aldridge, L. P., Radebe, M. J., Nshimirimana, R. B., Brew, D. R. M., … Olufson, K. P. (2010). Appraisal of a Cementitious Material for Waste Disposal: Neutron Imaging Studies of Pore Structure and Sorptivity. *Cement and Concrete Research*, *40*(8), 1320–1326. http://doi.org/10.1016/j.cemconres.2010.03.011.

Mcglinn, P. J., De Beer, F. C., Brew, D. R. M., Radebe, M. J. & Nshimirimana, R. B. (2013). Interaction of Water with Cement Based Repository Materials — Application of Neutron Imaging. *IAEA-TECDOC-CD--1701*, 1–19. Retrieved from www.iaea.org/inis/collection/NCLCollectionStore/_Public/44/122/44122410.pdf.

Middleton, M. F., De Beer, F., Haines, P. & Mory, A. (2007). Evaluation of Tar Deposits Using Neutron Tomography, Canning Basin, Western Australia. *ASEG Extended Abstracts*, *2007*(1), 1. http://doi.org/10.1071/ASEG2007ab093.

Middleton, M. F., Li, K.,& De Beer, F. C. (2005). Spontaneous Imbibition Studies of Australian Reservoir Rocks with Neutron Radiography. *Pretorium Engineers*, (SPE 93634), 1–9.

Muchavi, N. S., Bam, L. C., De Beer, F. C., Chikosha, S. & Machaka, R. (2016). X-Ray Computed Microtomography Studies of MIM and DPR Parts. *IEEE Transactions on Nuclear Science*, *116*(October), 973–980. http://doi.org/dx.doi.org/10.17159/2411-9717/2016/v116n10a13.

Mulane, E., & De Beer, F. (2011). New Era for Radiation iImaging Research in South Africa. *Necsa Today Issue 3*.

Mutumi, G. (2016). Geographic Variation in the Phenotypes of Two Sibling Horseshoe Bats Rhinolophus Simulator and R.Swinnyi. Doctorate - UCT.

Naude, G., Hoffman, K., Theron, S. J. & Coetzer, G. (2013). The Use of X-Ray Computed Tomography in the Characterization of Coal and Associated Char Reductants. *Minerals Engineering*, *52*(October 2013), 143–154. http://doi.org/10.1016/j.mineng.2013.05.012.

Necsa-Corporate-Communications. (2014). *Necsa Annual Report: 2014*.

Newby-Fraser, A. R. (1979). *Chain Reaction*.

Nobrego, C. (2012). *Investigation of the Utility of Cochlea Morphology to Distinguish Between Species of 10 Southern African Horseshoe Bat (Rhinolophidae)*. Honours - Univ Pretoria.

Nothnagel, G. (2007). Personal Communication, 'Using the Invisible to Reveal the Hidden'.

Nshimirimana, R. (2008). *Quantification of Porous Media Using Tomography Imaging*. Master's - Univ Western Cape.

Nshimirimana, R., De Beer, F. & Radebe, M. (2011). The Role of SANRAD Facility in Quantitative and Morphological Investigation. *Nuclear Inst. and Methods in Physics Research, A*, *651*(1), 305–311. http://doi.org/10.1016/j.nima.2011.02.067.

Nshimirimana, R., Radebe, M. & De Beer, F. (2015). Precision of Porosity Calculation from ' Material Stopping Power' Using Neutron Radiography. *Physics Procedia*, *69*(October 2014), 358–365. http://doi.org/10.1016/j.phpro.2015.07.050.

Nwaila, G. (2014). *Application of HPGR and X-Ray CT to Investigate the Potential of Witwatersrand Gold Ore for Heap Leaching: A Process Mineralogy Approach*. Master's - University of Cape Town.

Nwaila, G., Becker, M., Ghorbani, Y., Petersen, J., Reid, D. L. & Bam, L. C. (2013). A Geometallurgical Study of the Witwatersrand Gold Ore at Carletonville, South Africa, Proceedings of the Second AUSIMM International Geometallurgy Conference / Brisbane, QLD, 30 September - 2 October 2013.

Nyembwe, A. M. (2017). Modelling of the Characteristics of Iron Ore Granules Formed During the Granulation Process of Mixtures that Contain Concentrate and Micropellets. Doctorate - Univ Pretoria.

Nyembwe, A. M., Cromarty, R. D. & Garbers-Craig, A. M. (2016). Prediction of the granule size distribution of iron ore sinter feeds that contain concentrate and micropellets. *Powder Technology*, *295*, 7–15. http://doi.org/10.1016/j.powtec.2016.03.010.

Nyembwe, A. M., Cromarty, R. D. & Garbers-Craig, A. M. (2017). Relationship Between Iron Ore Granulation Mechanisms, Granule Shapes, and Sinter Bed Permeability. *Mineral Processing and Extractive Metallurgy Review*, *38*(5), 298–303. http://doi.org/10.1080/08827508.2017.1323750.

Odes, E. J., Randolph-Quinney, P. S., Steyn, M., Throckmorton, Z., Smilg, J. S., Zipfel, B., … Berger, L. R. (2016). Earliest Hominin Cancer: 1.7-Million-Year-Old oOsteosarcoma from Swartkrans Cave, South Africa. *South African Journal of Science*, *Volume 112*(Number 7/8), 7–11. http://doi.org/10.17159/sajs.2016/20150471.

Oettlé, A. C. (2014). Effects of Dental Loss and Senescence on Aspects of Adult Mandibular Morphology in South Africans. Doctoratre in Anatomy. Univ Pretoria.

Oettlé, A. C., Fourie, J., Human-Baron, R. & Van Zyl, A. (2015). The Midline Mandibular Lingual Canal : Importance in Implant Surgery. *Clinical Implant Dentistry and Related Research*, *17*(1), 93–101. Retrieved from https://repository.up.ac.za/bitstream/handle/2263/44111/Oettle_Midline_2015.pdf?.

Ostrich. (2017). Retrieved 14 October 2017, from https://onekindplanet.org/animal/ostrich/.

Paleker, F. (2015). *Comparison of Canal Transportation and Centering Ability of K-files , the ProGlider file and G-Files : A Micro- Computed Tomography Study of Curved Root Canals*. Master's - Univ. of Pretoria.

Pan, L., Dumoncel, J., De Beer, F., Hoffman, J., Thackeray, J. F., Duployer, B., … Braga, J. (2016). Further Morphological Evidence on South African Earliest Homo Lower Postcanine Dentition: Enamel Thickness and Enamel Dentine Junction. *Journal of Human Evolution*, *96*, 82–96. http://doi.org/10.1016/j.jhevol.2016.05.003.

Pan, L., Thackeray, J. F., Dumoncel, J., Zanolli, C., Oettlé, A., De Beer, F., … Braga, J. (2017). Intra-Individual Metameric Variation Expressed at the Enamel-Dentine Junction of Lower Post-Canine Dentition of South African Fossil Hominins and Modern Humans. *American Journal of Physical Anthropology*, *163*(4), 806–815. http://doi.org/10.1002/ajpa.23240.

Paranjpe, S. K. (2008). *Neutron Imaging: A Non-Destructive Tool for Materials Testing*. (S. K. Paranjpe, Ed.)*IAEA-TECDOC-1604: Neutron Imaging: A Non-Destructive Tool for Materials Testing (IAEA-TECDOC Series)*. Vienna: IAEA. http://doi.org/978–92–0–110308–6.

Parkinson, A. H., Van der Walt, S., Randolph-Quinney, P. S., Dirks, P., Billings, B., Steyn, M., … Esterhuysen, A. (2010). Application of Forensic Taphonomy and Entomology to the Analysis of South African Burial Systems. *14th Congress of the Pan African Archaeological Association*.

Payne, T. E., Aldridge, L. P., Brew, D. R. M., & Mcglinn, P. J. (2012). Mechanisms of Cement Leaching and Degradation - Integration of Neutron Imaging Techniques. Retrieved from http://www.iaea.org/inis/collection/NCLCollectionStore/_Public/46/133/46133944.pdf.

Peter, O. (1946). Neutronen-Durchleuchtung. *Naturforsch*, *I*(10), 557.

Potgieter, W. (2017). *The Effect of the Mode of Applied Breakage on Coal Yield*. Master's - NWU.

Radebe, M. J. (2007). *Exploration of Several Radiation-based Analytical Techniques to investigate Chlorides and Chlorides Effects within Concrete.* Master's - Univ West. Cape.

Radebe, M. J. & De Beer, F. C. (2008). Current Radiography and Tomography Applications at Necsa and an Envisaged Upgrade Towards a Proposed South African National Centre for Radiography and Tomography, (460), 20–26. http://doi.org/doi: 10.1016/j.phpro.2015.07.055.

Radebe, M. J. & De Beer, F. C. (2015). Use of Neutron Beam Line Facilities for Nuclear Materials Related R&D with Emphasis on International Benchmarking of the Technique. *IAEA-TECDOC-1773*, 62–70.

Radebe, M. J., De Beer, F. C., Kaestner, A., Lehmann, E. & Sim, C. M. (2013). Evaluation Procedures for Spatial Resolution and Contrast Standards for Neutron Tomography. *Physics Procedia*, *43*, 138–148. http://doi.org/10.1016/j.phpro.2013.03.017.

Radebe, M. J., De Beer, F. C.,& Nshimirimana, R. (2011). Evaluation of QNI Corrections in Porous Media Applications. *Nuclear Inst. and Methods in Physics Research, A*, *651*(1), 282–285. http://doi.org/10.1016/j.nima.2011.02.023.

Radebe, M. J., Korochinsky, S., Strydom, W. J. & De Beer, F. C. (2015). Au Foil Activation Measurement and Simulation of the Concrete Neutron Shielding Ability for the Proposed New SANRAD Facility. *Physics Procedia*, *69*(October 2014), 392–398. http://doi.org/10.1016/j.phpro.2015.07.055.

Ramushu, M. A. (2014). *High Density Shielding Concrete for Neutron Radiography*. Master's - University of the Witwatersrand (WITS).

Röntgen, C. R. (1896). On a New Kind of Rays. *Nature*, *53*, 274.

Roos, T. H., Quin, R. L., De Beer, F. C. & Nshimirimana, R. B. (2011). Neutron Tomography as a Reverse Engineering Method Applied to the IS-60 Rover Gas Turbine. *Nuclear Instruments and Methods in Physics Research Section A: Accelerators, Spectrometers, Detectors and Associated Equipment*, *651*(1), 329–335. http://doi.org/10.1016/j.nima.2011.02.104

S. Fugine (Ed.). (1991). *Neutron Radiography (3) (1989)*. Kluwer Publishers (1990).

Sebola, T. P. (2014). *Characterisation of Uranium-Mineral-Bearing Samples in the Vaal Reef of the Klerksdorp Goldfield, Witwatersrand Basin*. Master's - University of the Witwatersrand.

Smith, A., Botha, H., De Beer, F. C. & Ferg, E. (2008). The Examination, Analysis and Conservation of an Egyptian Bronze Horus Statuette. *NCHM Research Journal*, *3*, 73–92.

Smith, A., Botha, H., De Beer, F. C., & Ferg, E. (2011). The Examination, Analysis and Conservation of a Bronze Egyptian Horus Statuette. *Nuclear Inst. and Methods in Physics Research, A*, *651*, 221–228. http://doi.org/10.1016/j.nima.2011.02.087.

Smith, P., Brink, J. S., Hoffman, J. W., Bam, L. C., Nshimirimana, R. & De Beer, F. C. (2015). The Late Middle Pleistocene Upper Third Molar from Florisbad: Metrics and Morphology. *Transactions of the Royal Society of South Africa*, *70*(3), 233–244. http://doi.org/10.1080/0035919X.2015.1065930.

Strydom, W. J., Venter, A. M., Franklyn, C. B. & De Beer, F. C. (2002). The Role of SAFARI-1 in Industry and Academia. *Physica Scripta*, *T97*(0), 45–49. http://doi.org/doi.org/10.1088/1402-4896/74/6/E01.

Tremsin, A. S., Lehmann, E. H., Mcphate, J. B., Vallerga, J. V., Siegmund, O. H. W., White, B., … Kockelmann, W. (2015). Quantification of Cement Hydration Through Neutron Radiography with Scatter Rejection. *IEEE Transactions on Nuclear Science*, *62*(3), 1288–1294. http://doi.org/10.1109/TNS.2015.2428231.

Tshelane, G. (2015). RS-MNG-PLN-15001 Business Plan for The Radiation Science Department R&D Vision.pdf.

UTCT. (2017). University of Texas at Austin CT Lab. Retrieved 25 July 2017, from http://www.ctlab.geo.utexas.edu/.

Uytenbogaard, D. (2017). Personal Communication: Engineer at SAFARI-1 and NRAD Practitioner.

Van der Merwe, L. (2015). *Development of a Radiation Beam Stop for a Neutron Radiography Facility*. Honours - Univ Pretoria.

Van der Merwe, W. (2007). *Trickle Flow Hydrodynamic Multiplicity*. Doctorate - Univ Pretoria.

Van der Merwe, W., Nicol, W. & De Beer, F. (2007a). Three-Dimensional Analysis of Trickle Flow Hydrodynamics: Computed Tomography Image Acquisition and Processing. *Chemical Engineering Science*, *62*(24), 7233–7244. http://doi.org/10.1016/j.ces.2007.08.009.

Van der Merwe, W., Nicol, W. & De Beer, F. (2007b). Trickle Flow Distribution and Stability by X-Ray Radiography. *Chemical Engineering Journal*, *132*(1–3), 47–59.

Van Der Merwe, W., Nicol, W. & De Beer, F. (2006). Internal Wetting Dynamics of Catalyst sSpheres Using X-Ray Computed Tomography. *South African Journal of Science*, *102*(December), 585–588.

Van Rooyen, L. J. (2017). *Polytetrafluoroethylene/Functionalised Graphene Nanocomposites with Improved Tribological and Gas Barrier Properties*. D-Tech - TUT.

Van Rooyen, L. J., Bissett, H., Khoathane, M. C. & Karger-Kocsis, J. (2016). Gas Barrier Properties of Oxyfluorinated Graphene Filled Polytetrafluoroethylene Nanocomposites. *Carbon*, *109*, 30–39. http://doi.org/10.1016/j.carbon.2016.07.063.

Van Rooyen, L. J., Bissett, H., Khoathane, M. C. & Karger-Kocsis, J. (2016). Preparation of PTFE/graphene Nanocomposites by Compression Moulding and Free Sintering: A Guideline. *Journal of Applied Polymer Science*, *133*(17), n/a-n/a. http://doi.org/10.1002/app.43369.

Van Rooyen, L. J., Karger-Kocsis, J. & David Kock, L. (2015). Improving the Helium Gas Barrier Properties of Epoxy Coatings Through the Incorporation of Graphene Nanoplatelets and the Influence of Preparation Techniques. *Journal of Applied Polymer Science*, *132*(39), n/a-n/a. http://doi.org/10.1002/app.42584.

Van Rooyen, L. J., Karger-Kocsis, J., Vorster, O. C. & Kock, L. D. (2013). Helium Gas Permeability Reduction of Epoxy Composite Coatings by Incorporation of Glass Flakes. *Journal of Membrane Science*, *430* (March), 203–210. http://doi.org/10.1016/j.memsci.2012.11.083.

Vaughan, C. L. (2007). *Imagining the Elephant: Biography of Allan MacLeod Cormack*. (C. L. Vaughan, Ed.). ICP.

Viljoen, J. (2016). A Tomographic Exploration of the Internal Structure of Coal and its Role in Single Particle Breakage, Doctorate - NWU.

Viljoen, J., Campbell, Q. P. & Le Roux, M. (2014). An Analysis of the Slow Compression Breakage of Coal Using Microfocus X-Ray Computed Tomography. *International Journal of Coal Preparation and Utilization*, *35*, 1–13. http://doi.org/10.1080/19392699.2014.907283.

Viljoen, J., Campbell, Q. P., Le Roux, M. & Hoffman. W.J. (2016). The Influence of Bedding-Plane Orientation on the Degradation Characteristics of a South African Waterberg Coal *International Journal of Coal Preparation and Utilization*, *37*(4), 179–194. http://doi.org/10.1080/19392699.2016.1143369.

Viljoen, J., Campbell Quentin, P., Le Roux, M. & Hoffman, J. (2015). The Qualification of Coal Degradation with the Aid of Micro-Focus Computed Tomography. *South African Journal of Science*, *111*(9), 1–10. http://doi.org/http://dx.doi.org/10.17159/ sajs.2015/20140025.

Von Gogh, R. (1999). You Can Only Manage What You Can Measure. *S.A. Industrial Solutions: Newsletter from Pelindaba Technology*, *8*(2), 3.

Vontobel, P. (2008). Quantification in Neutron Imaging. Paul Ascherrer Institute. Retrieved from indico.psi.ch/conferenceDisplay.py/getPic?picId=20&confId=3679.

Williams, P. J. (2013). *Near infrared (NIR) Hyperspectral Imaging and X-Ray Computed Tomography Combined with Statistical and Multivariate Data Analysis to Study Fusarium Infection iIn Maize*. Doctorate - Univ of Stellenbosch.

Willoughby, B. (2014). *Morphological and Morphometric Study of the Ostrich Egg-Shell with Observations on the Chorioallantoic Membrane: A Micro-CT, Scanning Electron Microscope and Histological Study.* Honours - University of Johannesburg.

Willoughby, B., Steyn, L., Bam, L., Olivier, A. J., Devey, R. & Maina, J. N. (2016). Micro-Focus X-Ray Tomography Study of the Microstructure and Morphometry of the Eggshell of Ostriches (Struthio Camerus). *The Anatomical Record*, *1026* (September 2014), 1015–1026. http://doi.org/10.1002/ar.23354.

Yasuda, R., Nittoh, K., Konagai, C., Shiozawa, M., Takenaka, N., Asano, H. & Murakawa, H. (2011). Evaluation of Water Distribution in a Small Operating Fuel Cell Using Neutron Color Image Intensifier. *Nuclear Inst. and Methods in Physics Research, A*, *651*(1), 268–272. http://doi.org/10.1016/j.nima.2011.01.175.

Zanolli, C., Bayle, P., Bondioli, L., Dean, M. C., Le Luyer, M., Mazurier, A., … Macchiarelli, R. (2017). Is the Deciduous/Permanent Molar Enamel Thickness Ratio a Taxon-Specific Indicator in Extant and Extinct Hominids? *Comptes Rendus Palevol*, *16*(5–6), 702–714. http://doi.org/10.1016/j.crpv.2017.05.002.

CHAPTER 4

PUBLICATION OF A CHAPTER IN A BOOK:

Chapter 7 Paleontology: Fossilized Ancestors Awaken by Neutron Radiography

South Africa, in particular, has a rich fossil heritage that is in principle irreplaceable and requires special care to protect, whilst making it available for scientific study. The information extracted, lifts the veil on our historical natural history and paints a picture that becomes a source of inspiration for future generations of researchers. Special care therefore needs to be taken during the examination of specimens in order to preserve their integrity at all cost. The non-destructive and non-invasive tomographic techniques, based on neutrons and complementary X-rays, allow detailed 3-dimensional virtual representation of the objects with consequential visualisation capability of normally hidden morphology of the specimen such as trabecular details of bone structures, and details of the cochlea and sinuses that are not possible using invasive methods. As more state-of-the-art international neutron and X-ray CT research facilities are being commissioned, palaeontologists make ever increasing use of radiation based analytical techniques to investigate critical internal details of valuable fossilised specimens without causing damage.

Because of South Africa's rich fossil treasure, the X-ray and neutron radiography and tomography techniques at Necsa have been utilised in the study of a range of paleontological fields of study. As a result, a significant level of expertise has been established to assist researchers to extract relevant information effectively. As recognition of this expertise, vested in South Africa, the writer of this thesis has been invited to write a review chapter in an IAEA book entitled "Neutron Methods for Archaeology and Cultural Heritage" [1] on the topic of neutron radiography applications in palaeontology. The current chapter contains the review chapter in the IAEA publication, which attempts to highlight palaeontology applications with reference to the main findings of several national and international peer reviewed publications.

[63]Chapter 7
Paleontology: Fossilized Ancestors Awaken By Neutron Radiography

Frikkie C. de Beer

Abstract Fossils and fossil bearing materials are in principle irreplaceable and are globally a scarce commodity. Countries with natural fossil collections and known fossil sites, which are only a few, thus do take special care of their "heritage" and fossil findings and in the process enhances the role of non-destructive testing and related examination procedures on these findings. This chapter summarizes the documented research utilizing neutron radiography and tomography and the penetrating power of neutrons in a combined effort with other non-destructive analytic techniques to find answers from the "past". In the quest to "solve the past", the role of neutron radiography as a modern, unique, non-invasive and non-destructive analytic technique is being described through several full length article case studies to assist to answer modern palaeontology questions.

7.1 Introduction

The palaeosciences are a unique combination of all the scientific disciplines that tell us the story of life on Earth, including the story of humankind (SA Strategy 2011). Palaeosciences denote thus to the fields of palaeontology, palaeo-anthropology, archaeology, and related disciplines. It is a complex saga, where the many layers of knowledge and understanding of what were in the past and how it proceeded and played a role in history and modern existence, are increasingly being revealed through research and discovery.

"Fossils" as being described within this chapter, refers to the remains of animal, plant or hominid remnants typically imbedded in a kind of matrix such as sedimentary rocks that preserved it over thousands to millions of years. Fossils are generally rare as the landscape/area must have the right conditions to stimulate fossilization. It has been assessed that for every animal that dies, its chances of becoming fossilized in this way are less than one in a million (Maropeng 2015a).

F.C. de Beer (✉)
Radiation Science Department, South African Nuclear Energy Corporation, SOC Ltd. (Necsa),
Pretoria, South Africa
e-mail: Frikkie.debeer@necsa.co.za

N. Kardjilov and G. Festa (eds.) *Neutron Methods for Archaeology and Cultural Heritage*, Neutron Scattering Applications and Techniques,
DOI 10,1007/978-3-319-33163-8_7

Fossils are formed when minerals such as calcium carbonate, over time, envelope and/or replace bones and other organic matter. The covering hardens and casts them into the rock matrix, called breccia, which remains untouched and thus unchanged for millions of years. Breccia is a conglomerate rock consisting of cave infill that forms when material – bones, rocks, and vegetation falls into the cave. Mineralization of the bones and organic materials is also possible, making them as hard as rock once the sediment contains the ideal mineral constituents.

Some evidence of neutron radiography being applied in the study of bones or remnants of dinosaurs was found in the open literature and thus also forms part of the discussion within this chapter. Fossils usually represent the hard parts, such as bones or shells of animals and leaves, seeds, or woody parts of plants. Fossils occur on every continent and on the ocean floor. Through the scientific study of fossils and their stratigraphy, it is somehow possible to recreate ancient communities of living organisms and to suggest the evolution of species (Fossil and Fossilization 2015).

Unsurprisingly, the fossils become uncovered again after millions of years through either human activities (limestone mining or dedicated cave exploration) or natural occurrences (erosion, earthquakes). The history of the past then becomes unlocked through scientists (Palaeo-scientists and palaeo-anthropologists) who actively study cave formations and -morphologies, landscape morphologies that support palaeo related findings and others to reveal a window to our past.

In the process to find the truth about the existence of life through the palaeo-sciences, various modern scientific analytical methods are applied to reveal the contents of these breccia materials which are in a form of blocks of limestone with imbedded possible fossil materials (See Figure 7.1).

As the fossil materials are imbedded into the breccia matrix, it was actually impossible to perform a study of the physical structure and the morphological nature of the fossil. Time consuming and long pain staking mechanical- and/or chemical preparation processes are applied, both with their own advantages and disadvantages in order to reveal the fossil materials in the best original form possible for further study.

Fig. 7.1 The fossilised tooth of a sabre-toothed cat embedded in breccia. *Photo* Tara Turkington (Maropeng 2015b)

7.2 Preparation of Fossils for Scientific Evaluation

Once the fossil blocks are recovered from their location which is again thoroughly documented, careful planning to expose the fossil material is made as each sedimentary block has its own morphology and material composition. Normally mechanical- (see Figure 7.2) and/or acid preparation (see Figure 7.3) is being performed to reveal the fossil materials depending on the nature of the breccia materials. It is normally unknown to the palaeoscientist or preparator of the blocks if any "one in a kind" fossil material could possibly be "hidden" within the breccia blocks. Thus, the process to expose the target of study e.g. the fossils from the breccia material in both preparation mechanisms takes painstaking long. On average for a breccia block of 25kg the average preparation time applying mechanical preparation is up to 1 – 2 years and a couple of months using a weak chemical acid process. In many cases the fossil materials are only partially revealed once the surrounding breccia materials are removed and important information regarding e.g. dental- and cochlea morphologies or even brain cavity volume can-not be determined – even when the total fossil has been recovered from the breccia materials.

Fig. 7.2. Mechanical preparation - Preparator at work. Fossils are prepared in a laboratory using small, pointed chisels and light-weight hammers. Fine cleaning of important fossils is done under a microscope with dental picks and air scribes (Maropeng 2015c).

Fig. 7.3. DITSONG Natural Heritage Museum: Chemical Preparation Laboratory with fossils imbedded in acetic acid within plastic buckets – operational as from 2012 (Gommery and Potze 2013).

Once most breccia materials are removed, morphological analyses and other speciation assumptions of the fossil materials can be performed through visual inspection (the normal scientific practice as from early 1900) also taking into consideration the location of the finding, the sedimentology as well as stratigraphic information of the surrounding rocks.

The disadvantages of both preparation processes where either smaller bone losses occur or long term effects of acid could have a detrimental effect on the recovered fossil, the modern era of computational palaeontology started in the late 20th century, where computers and associated technologies began to play a more prominent and highly exiting role, saving time and costs in not only revealing the fossilized materials inside the breccia materials but also non-invasively accurately visualize the inner morphology structure of prepared fossils (Ashraf 2011).

7.3 Radiation Based Non-Invasive Analytical Techniques

From about 2000, with the introduction of highly sophisticated electronic analytical techniques, palaeo-scientists gave preference to radiation based non-invasive and non-destructive techniques to recover hidden information of fossilized materials even when the fossils are still imbedded within the breccia blocks. These techniques do not harm or destroy the fossil materials evidence or information which, in many cases, are imbedded in/on a single recovered/found breccia fossil sample. Modern radiation based analytical techniques, such as 3D tomography using X-rays or neutrons became available to be used to investigate either the untreated breccia materials or the recovered fossils after treatment. These non-invasive techniques became, as from about 2005 state-of-the-art analytical investigation tools to researchers from the palaeosciences. Hidden information such as fossil position and location within the breccia block to assist with speeding up of the recovery process, became a state of the art activity. Morphological data of the fossil materials became possible and thus added value to the investigation process even before they were recovered from the breccia blocks. The relative availability of e.g. neutron tomography as an unique analytic technique made it possible for researchers worldwide to access, through beam time submitted proposals, these highly sophisticated instruments. These are well established facilities and are being described and discussed elsewhere in this book.

For many years the unique nature of X-ray penetrating radiation, found at many X-ray tomography facilities around the globe, was the favourite amongst researchers due to its relative very high resolution, of up to a few microns, which is being achieved. Although the focus of this chapter is on the application of the relative unknown application of neutron radiography/tomography within the palaeo-sciences, reference to XCT is only made for the comparison and enhancement of the complementary benefit of neutron radiography/tomography. The nature of neutron radiography/tomography within this unique application and specifically the contrast obtained between the fossil and the breccia materials are being generalized and first order theoretically described, however neutron radiography principles and techniques are been described in detail in Chapter 14.

No formal studies were conducted in breccia materials where the only focus is to compare X-ray- and neutron radiography with respect to the contrast that can be obtained between the breccia and fossilized materials. The problem is the vast different composition of breccia

materials to predict which contrast could be reached with either one of the techniques. However, a generalized approach is taken in the following paragraphs by assuming hydroxyapatite as the most abundant fossilized materials present in the calcified rock and the composition of the breccia materials that originated from Bolts Farm and from the Taung child as listed in Table 7.1:

Table 7.1 General % elemental composition of hydroxyapatite and the breccia materials.*

Hydroxyapatite % in composition.[7]	$Ca_5(PO_4)_3(OH)$												
Element	SiO_2	Al_2O_3	Fe_2O_3	FeO	MnO	MgO	CaO	Na_2O	K_2O	TiO_2	P_2O_5	Cr_2O_3	NiO
% Range: Breccia materials:[64]	11.9 - 47.1	1.1 - 4.5	0.1 - 0.3	0.4 - 2.4	0.1 - 0.7	0.3 - 1.3	16.6 - 82.3	0 - 0.1	0.2 - 0.6	0.1 - 0.3	0.5 - 3.9	0.01 - 0.036	0 - 0.04

* Average percentages used in further calculations.

From the table and the respective composition and densities of these materials, the relative linear attenuation coefficients for X-Rays and neutrons are compiled through 1st-order calculations as being listed in Table 7.2:

Table 7.2 First order calculated linear attenuation coefficients of breccia (theoretical CaCO3) and hydroxyapatite by X-rays and neutrons.

Sample		**Radiography technique using**	
Description	**Density (g/cm^3)**	**X-ray (cm^{-1}) (* 5 g/cc)**	**Thermal Neutrons at 0.05eV (cm^{-1})**
Hydroxyapatite	3.156*	0.95 @ 200kV 1.10 @ 160kV 1.49 @ 100kV	0.48
Breccia materials calcite ($CaCO_3$)	5.0* Calc: 2.71	1.43 @ 200kV 1.63 @ 160kV 2.18 @ 100kV	0.34 Max for Pure $CaCO_3$

* = Theoretical density

Penetration capabilities of breccia materials by X-rays and neutrons are predicted and listed in Table 7.3. Penetration of radiation through the breccia is needed for any success in radiography. As an unwritten rule, 10% transmission or radiation in all angles through the breccia sample is preferred for tomography to be successful without major artifacts being created in the virtual volume reconstructed data set.

In a first order assumption about breccia materials it is taken to be pure CaCO3 mineral. It is evident from Table 7.3 that neutron penetration through breccia material is about 100% better than with X-rays. However, we can generalize and through assumptions, a difference and

[64] J.F. Thackeray for 13 x breccia samples from Taung ; J.F. Thackeray, Dominique Gommery, Sandrine Prat, Stephany Potze and Lazarus Kgasi for 7 x breccia samples from Bolts Farm.

comparison in the investigations of fossil containing breccia materials using X-ray- and neutron tomography is being obtained.

Table 7.3 Thickness of breccia for 10% transmission of X-ray- and neutron radiation. (Theoretical)

Sample	Radiography technique using:	
	X-ray (120kV) (cm)	Thermal Neutrons at 0.05eV (cm)
Breccia materials	2.95 [32] 10 – 20 cm @ 225kV	6.77

7.4 Fossil Locations/Areas

Although many fossils and fossil bearing rock exist in many places around the globe and many books were published describing fossils from their existence many years ago – making assumptions based on visual inspection of some findings - this chapter only describes the application of neutron radiography and -tomography in the non-destructive investigation of fossils and fossil bearing rock. In general, most hominid fossil materials are found in Africa while a higher abundance of dinosaur fossils are found in the Americas. More reading can be found in (Franco 2011, List of fossil sites, List of human evolution fossil and Dinofossils locations).

7.5 X-Ray Tomography

It will be unfair not to mention as well the possibilities and complementary nature of micro-focus X-ray tomography (XCT) to neutron tomography as an application in the palaeo-sciences. Braga et al. investigated in breccia free pre-prepared fossil samples the cochlear morphological features associated with hearing capacities across 22 living and 5 fossil catarrhine species. The goal was to look at reliable indicators of auditory capacities by investigating the phylogenetic signal of cochlear features, which is also taxonomically useful among apes' main lineages (Braga et al. 2013). The study provides evidence to improve classifications of fossil hominid species into true monophyletic groups in that evidence was found that body mass-dependent and non-homoplasious changes of cochlear elongation in apes contribute mainly but not only to their evolutionary history (Figure 7.4).

Because this chapter focuses on the application of neutron tomography in this field, other XCT applications in this field are only referenced for further reading (Braga et al. 2015 and Sutton 2008).

To illustrate why neutron radiography/tomography should be considered as complementary techniques to X-ray tomography within the Palaeosciences, the results of the X-ray acquisition of the breccia block embedding the specimen STS 1039 from Sterkfontein, South Africa, has been compared with neutron tomography results as shown in Figure 7.5. While the enamel tissue is slightly better discriminated from the dentine material on X-Ray sections, the distinction

between bone/matrix (1) and between dental tissues/matrix (2) is definitely more accurate in neutron-based images and allows a virtual reconstruction of the specimen (Beaudet et al. 2015). The following sections of this chapter discuss the development and showcase with some case studies the role of NRAD in the Palaeosciences.

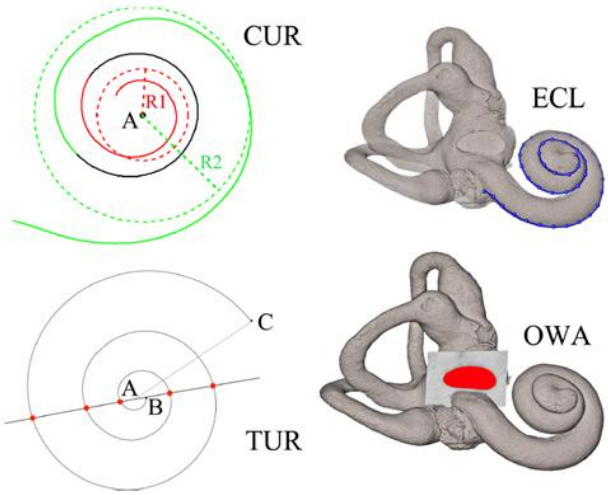

Fig. 7.4. Illustrations of the five cochlear features expressed as continuous variables. The external cochlear length (ECL, in mm), number of turns (TUR, expressed as the sum of full circle rotations and the angle between lines "AB"—center to apex—and "AC"—center to base), and relative length (RECL = ECL/TUR, in mm), the curvature gradient (CUR, expressed as a dimensionless ratio between the radii of the larger first—noted "R2"—and the smaller last spiral turns—noted "R1"), and the oval window area (OWA in mm2) Courtesy: (Braga et al. 2013).

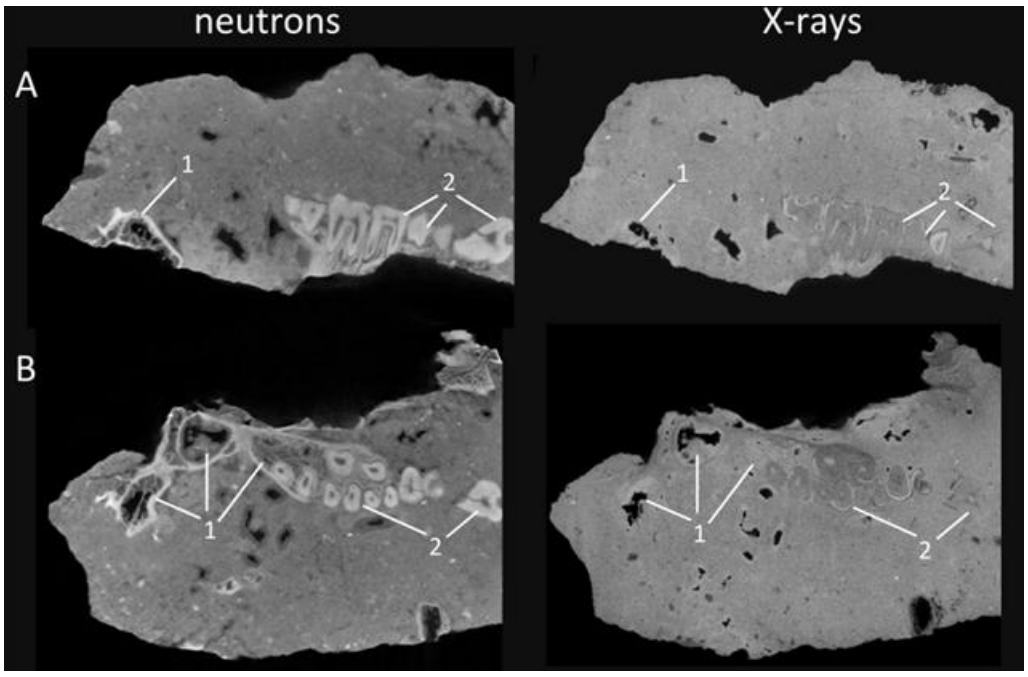

Fig. 7.5. Comparison of sagittal (A) and traverse (B) sections of the breccia block embedding STS 1039 obtained by neutron-based and X-Ray acquisitions performed at a similar resolution. While traditional X-Ray microtomography fails to fully discriminate bone from matrix (1) and dental tissues from matrix (2), the neutron-based microtomography successfully separates the biological and mineral materials.

7.6 Film Based Neutron Radiography and Fossils – Early Days

The power of neutron radiography also in the field of fossil evaluations was realized by Berger et al. as early as in 1962 (Berger 1962).

With the very first known published article of this kind in 1997, Le Roux et al. focused on the use of neutron radiography, as non-destructive technique, to facilitate the identification of structures in the STS 5 fossil specimen found at the Cradle of Human Kind, Sterkfontein, South Africa.

The aim was to facilitate the identification of structures in the fossil specimen, as indicated in Figure 7.6, and to investigate methods used to obtain planar neutron radiographs and evidence of damage (cracks and breaks) at the time of discovery or preparation of the specimen (Le Roux 1997). The H-rich clue lines in-between the fractured parts of the cranium could easily been identified. This study reports the results of groundbreaking research in South Africa utilizing the neutron radiography facility at the SAFARI-I nuclear research reactor at Pelindaba. The focus of the study was on fossils from Sterkfontein, including cranial bone of the celebrated 'Mrs Ples' (STS 5), representing Australopithecus africanus.

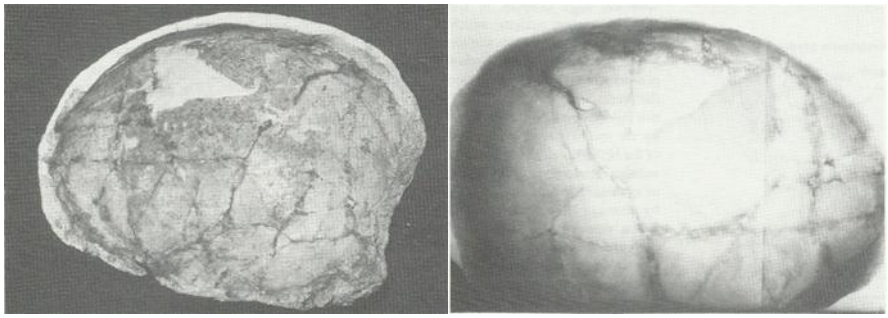

Fig. 7.6. *Left*: Photo of the top of the cranium of STS 5 (Mrs Ples) *Right*: Subsequent film based neutron transmission radiograph.

7.7 Digital Radiography: Neutron Radiography Experience

With the introduction of digital neutron radiography/tomography, the value added by neutron radiography (NRad) related research to the palaeosciences increased dramatically. It took many years before the connection between the palaeoscience and NRad communities was made and the value added by NRad could be practically experienced by the palaeoscience community. The selected examples in this section of the chapter are from full length research publications trying to capture the capabilities, advantages and possibilities of neutron radiography/tomography within the palaeosciences as from the first known publication to the latest in Dec 2015.

7.8 Examples of Neutron Studies of Palaeontological Samples

7.8.1 Souropod Vertaebrae

7.8.1.1 Scientific Question

The main goal for this investigation was the comparison of neutron tomography (NT) as a research tool in the investigation of fossilized sauropod vertebrae and the comparison with corresponding CT images. Comparisons between X-ray tomographic and neutron tomographic scans were made to identify: i) if NT is an appropriate method for the investigation of diagenetically altered bone fragments; ii) the benefits and limits of NT analyses of vertebrate remains; iii) advantages and differences between CT and NT images; and iv) how differential preservation and preparation of the specimens affect both techniques.

7.8.1.2 Materials and Methods

The Neutron Transmission Radiography Station (NEUTRA http://neutra.web.psi.ch/) of the Paul-Scherrer-Institute (PSI) in Villigen/Switzerland has been available since 1997 also for the nondestructive testing of fossilized materials.

The Saurier-Museum Aathal/Switzerland provided remains of diplodocid sauropods from the Late Jurassic (Kimmeridgian) Morrison Formation of Wyoming for the NT and CT analyses. The sample investigated consisted of five cervical vertebrae and one cervical rib each belonging to juvenile individuals. One caudal vertebra was scanned both with CT and NT to compare with a vertebra without internal cavities. In order to preserve the fossils, internal cavities, openings and foramina are filled with siliciclastic mud characterized by calcareous cement (Ayer 2000). The bones are badly fractured and most fractures and cracks were filled with quick drying cyano-acrylate resin and missing parts of the vertebrae have been remodeled with polyester cast resin.

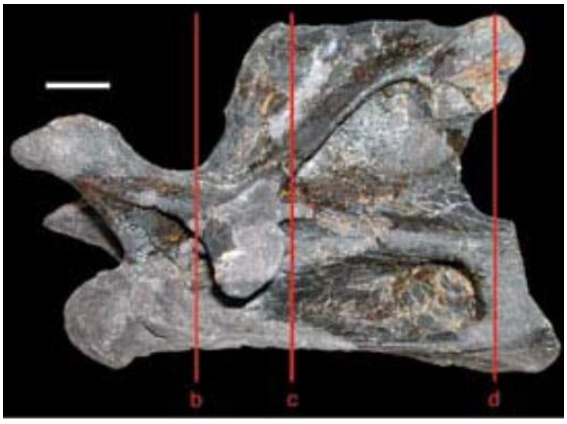

Fig. 7.7. Photo of the fourth cervical vertebra (No. H25-2) of an undetermined diplodocid sauropod with broken parts of vertebral body and diapophysis modelled in polyester cast resin in left lateral view - *red bars* indicate axial cross-sections displayed in Figure 7.8 *Courtesy*: Schwartz et al. (2005).

Samples were scanned with a neutron flux of about 3.6 x 10^6 [n/cm^2/s], collimation ratio (L/D) of 550 and rotated over 180^o while up to 300 transmission projections were taken. A relative large neutron path length of 12 cm through the specimen was achieved.

7.8.1.3 Results

Neutrons are sensitive to detect small differences in the concentration of some light materials such as hydrogen. This study demonstrates through 3-D visualization and characterization of internal structures of vertebrate remains this unique ability of neutrons. The quality of the 3D neutron tomograms of the sauropod vertebrae was unfortunately decreased due to several aspects such as the density of the fossil bones, the within openings of the bones that was filled with high a amount of marly sediment matrix as well as glue inserted into the multiple fractures of the specimens. Unfortunately NT results are strongly influenced by the resins used for preservation and preparation of these fossilized objects. However, the advantage of neutron tomography lies in the fact that the distribution of glue within the fossil remains can be evaluated at a spatial resolution achieved at PSI of 0.1 mm - 0.27 mm. The complementary nature of XCT and NT data supported knowledge generation about the internal structure of sauropod vertebrae (Figure 7.8).

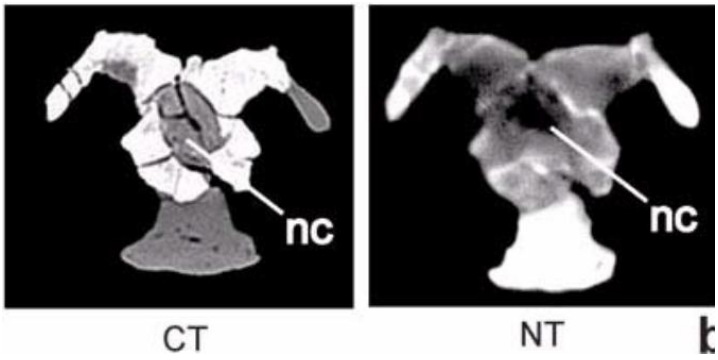

Fig. 7.8. Axial section in the cranial third of the vertebra: both in the CT image (*left*) and the NT image (*right*), the polyester cast resin can be distinguished from bone, but only in the NT image the resin has a different colour than the matrix; nc = neural canal (Schwartz et al. 2005)

This study confirms that NT would be an adequate or even better 3D analytical technique than XCT:

- when objects contain metal inclusions;
- when the distribution of sediment in unprepared fossil bones in their internal cavities needs to be investigated, and
- when the authenticity of fossils in a forensic or historical context needs to be investigated. E.g. the nature of historical preparation of museum fossilized specimens (e.g., identifying the resin materials used to glue individual parts – See the white marks in Figure 7.8 on the NT slice).

7.8.2 Dinosaur Eggs

7.8.2.1 Scientific Question

Investigation of the capabilities of NT to reveal the concealed information of a partially opened dinosaur egg.

7.8.2.2 Materials and Methods

A 9 cm diameter dinosaur egg (Figure 7.9) was found at the Aptian–Albian Algui Ulaan Tsav site, Mongolia. In 2008 an egg specimen NSM60104403-20554450, with a few visually detected embryonic bones, was denoted by the Public Procurement Service of South Korea to the National Science Museum of Korea. Over time the egg was diagenetically altered into a hollow calcite geode. The embryonic bones partially condensed on the egg surface and below within a thin layer. The egg is also eroded away in the one section revealing a hollow egg that reveals the calcite geode. The surface of the remaining eggshell present does not show any fractures, suggesting that minimum compression had occurred after the egg was buried. The neutron tomography study was performed at the Neutron Radiography Facility of HANARO, KAERI, Korea which allows for a spatial resolution of 0.228 mm for the reconstructed egg when scanned through 180° and a total of 600 sequential images.

7.8.2.3 Results

The anterior surface of the 18.8 mm long humerus, the most diagnostic bone among those visible on the surface (Figure. 7.9) is partly exposed. It is found with neutron imaging (Figure 8.10), that the humerus becomes totally visible and extends diagonally into the calcitic matrix.

The femur, a 29.17 mm long bone in posterior view is also noticeable, which, similar to the humerus, is partially encased in a thin calcitic matrix. Although the proximal section of the femoral head is absent, the application of NT revealed the full extent of the bone also within the calcitic matrix.

Fig. 7.9. Photo of egg with **a)** calcite crystals and **b)** embryo skeleton surfaces (*Courtesy*: Grellet-Tinner et al. 2011).

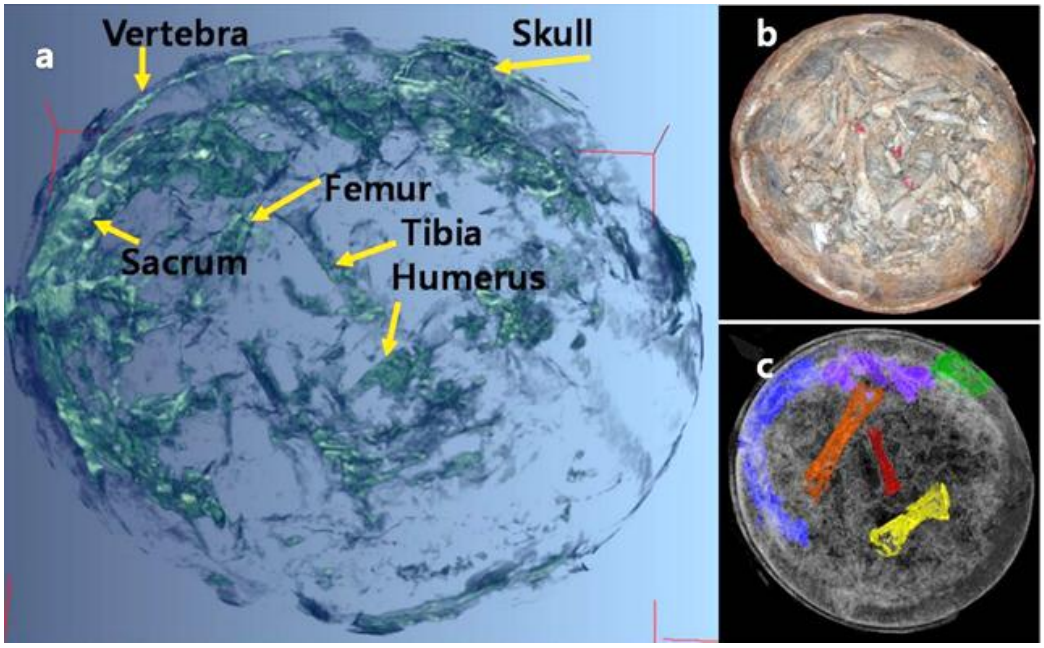

Fig. 7.10. Neutron image of dinosaur embryo, (a) Skull, sacrum, limbs and vertebra preserved in the layer identified by neutron tomography (X-Z view), (b) Embryonic skeleton settled down at the unopened pole of the egg (red arrows on limbs), (c) Pseudo colouring Skull, sacrum, limbs and vertebra preserved in the layer identified by neutron tomography (X-Z view) (Courtesy: Grellet-Tinner et al. 2011).

7.8.2.4 Conclusive Remarks Related to the Study

The aim was to complement X-CT with NT to fully expose and identify the various bones partially imbedded into the calcite structure. Additionally, NT could provide successfully accurate dimensional measurements of the humerus, femus and tibia of the embryo. Fossil embryos are difficult to study due to their small size and fragility – an advantage for and only feasible using NT. Unique and specific taphonomic and diagenetic processes should work together for their preservation thus making fossil embryos not common in the fossil record. NT as non-destructive analytical technique could successfully be utilized in this study where it was difficult to categorize this fossil embryo, adding valuable information to the current knowledge of fossil embryos but also in general to fossil research.

7.8.3 Ichthyosaurus in Iron Block

7.8.3.1 Materials and Methods

More than 100 million years old saurian fossils, and specially ichthyosaurus, which is a relatively large fossil, was studied due to its structure and specific finds. The fossil, embedded into the stone slab and partially hidden in the rock (Figure 7.11) could not be totally cleaned out from the breccia material.

Fig. 7.11. A 1.4 m long ichthyosaurus fossil imbedded into the rock matrix.

Only the head section of this fossil could be successfully scanned at the Neutron Transmission Radiography Station (NEUTRA http://neutra.web.psi.ch/) of the Paul-Scherrer-Institute (PSI) in Villigen/Switzerland.

7.8.3.2 Results

The penetration capability of neutrons and the ability to differentiate between different materials although with similar densities, allowed for the head of the ichthyosaurus fossil to be easily distinguished from the stone. Within Figure 7.12, a zoomed in view of the photograph of the head section under investigation and imbedded into the stone, is shown. The neutron transmission radiograph of the eye area, which is being magnified due to the high spatial resolution achieved at the NR station at PSI is shown in the centre while a full 3D reconstructed neutron tomogram of the head of the fossil, with relative detailed information preserved, is shown on the right.

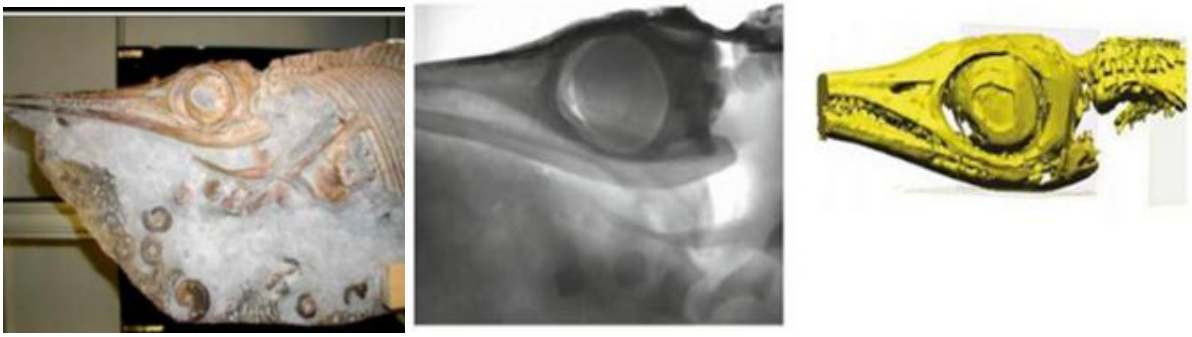

Fig. 7.12. : *Left*: Photo of the head section; *Middle*: Transmission neutron radiograph; *Right*: 3D printed model based on neutron tomography data of the head section (*Courtesy*: PSI and Liang et al. 2008).

7.8.3.3 Conclusive Remarks Related to the Study

Fossils has no organic materials present within but its structures deliver quite a high contrast compared to the surrounding and embedding breccia materials when subjected to neutron radiography/tomography investigations. The study shows that NR permits non-destructive evaluation of large fossil materials. Morphological information is easily extracted in a non-invasive manner through high quality segmentation of the skeleton from the rock matrix that gives insight into the development of the fossil through a study of its brain cavity and other distinct features.

7.8.4 Spondarthritis in the Jurassic

7.8.4.1 Scientific Question

The South African Karoo, a semi desert area, is known for numerous findings of fossil materials and especially those from the Lower Triassic (~245 million years old) period. The study focused on the vertebral series that belonged to a carnivorous archosaurian reptile and reports some evidence of spondarthritis, a form of arthritis found in pre-Cenozoic vertebrates especially regarding reptiles which, is not yet well documented.

7.8.4.2 Materials and Methods

South Africa and some neighbouring countries contain the "Karoo Basin", an area that has produced an unmatched wealth of past life. The area provided a detailed record of fossil vertebrates that highlight the Permo-Triassic biotic crisis. One such record is the vertebral remains of a carnivorous reptile from the Lower Triassic, that shows macroscopic signs of severe bone pathology.

Three articulated anterior caudal vertebrae of a large, basal archosaurian reptile (Figure 7.13), specimen BP-1-5796, collected at Driefontein District, Free State Province, South Africa and stored at the Bernard Price Institute for Palaeontological Research, Johannesburg was scanned. The nearly complete specimen comprises out of three nearly complete, fused vertebral bodies and partial zygapophyses (Fig. 7.13) with a total length of 116 mm and with no signs of taphonomical alteration. Evaluating the size of these vertebrae, it is assumed that they could originate from a large and probably old individual.

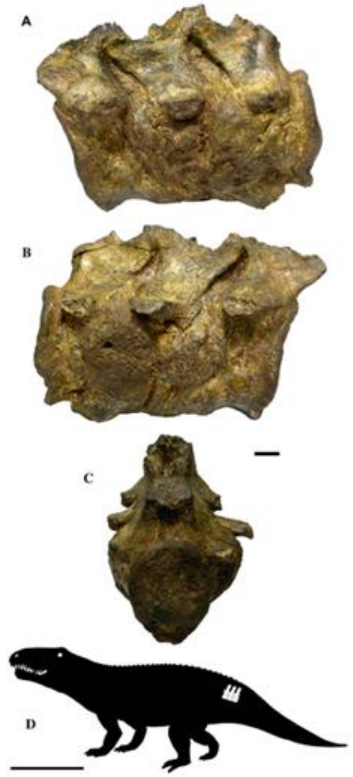

Fig. 7.13. External views of vertebrae BP-1-5796. A. Left lateral view. B. Right lateral view. C. Posterior view. D. Schematic drawing of a basal archosaurian reptile, showing the likely placement of the vertebral series within the caudal region of the column. *Scale bars* represent 10 mm for (A–B), and 1 m for (D) (*Courtesy*: Cisneros et al. 2010).

Neutron tomography was performed at the SANRAD facility at the SAFARI-1 nuclear research reactor and operated by the South African Nuclear Energy Corporation SOC Ltd. (Necsa) near Pretoria. A total of 180 neutron radiography projections in 180 angular degrees were made with a resultant spatial resolution of 100 micron. Good neutron penetration through the specimen was achieved that eliminated ring and beam hardening artifacts in the 3D virtual tomograms of the specimen.

7.8.4.3 Results

The neutron tomography (Figure 7.14) revealed no traces of fracture or trauma in the vertebral series. Through the tomography we observed that the intervertebral disc spaces (both annulus fibrosus and nucleus pulposus) are totally ossified, producing the complete ankylosis of the vertebrae (Figure 7.14F and G). In this way, it is not possible to distinguish the limits of each vertebral element. No evidence of zygapophyseal ankylosis, however, was found through the tomography (Figure 7.14E and H), thus, confirming what was recognized by the external exam of the specimen. Neutron images also showed that in the innermost layer of the vertebral bodies the trabecular bone forms trabecular bridges that follow a regular pattern across the ankylosed areas (Figure 7.14G). The absence of an irregular pattern of trabecular bone allows discarding the hypothesis of an infectious process or tumor (Cisneros et al. 2010).

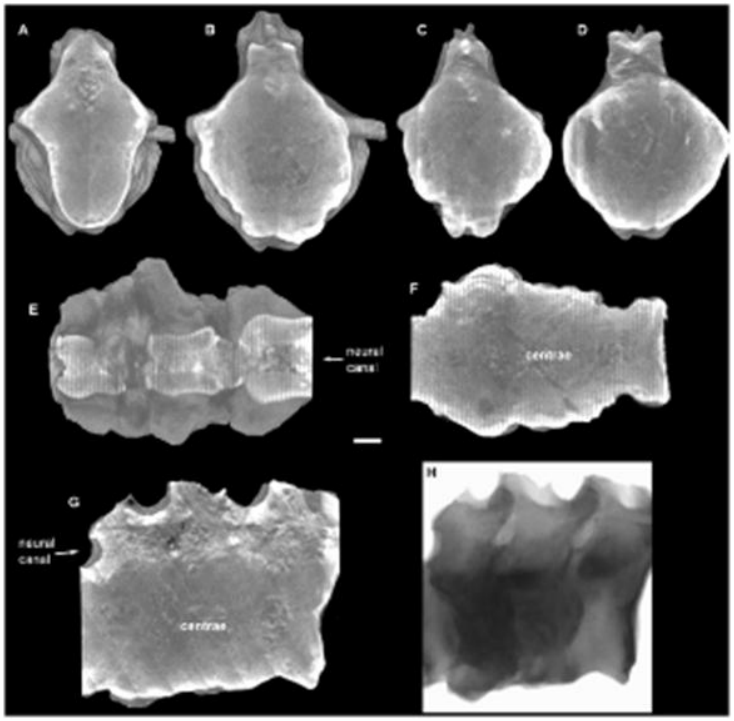

Fig. 7.14. Neutron tomographies of vertebrae BP-1-5796. **A.** First (anterior to posterior direction) preserved vertebrae. **B**. Second vertebrae. **C–D**. Third vertebrae. **A–C**. Transversal slices, in anterior view, at level of anterior border of the transverse process. **D**. Transversal slice, in anterior view, at level of maximum thickness of inflammation. **E–F**. Coronal slices of the vertebral series in dorsal view, (**E**) at level of the neural canal, (**F**) at level of the centrae, anterior to the left. **G**. Sagittal slice of the vertebral series in right view. **H**. Raw neutron image in right lateral view. Scale bar represents 10 mm. (*Courtesy*: Cisneros et al. 2010).

7.8.4.4 Conclusive Remarks Related to the Study

A severe pathology was recognized in both macroscopic examination and neutron tomography data that revealed features that are diagnostic of the condition, spondarthritis which comprises a diverse group of related inflammatory arthritides. This finding represents the earliest example of this pathology in the fossil record. It is postulated that spondarthritis was probably the indirect cause of the death of the animal.

Neutron tomography confirmed the macroscopic collected data, revealing the ossification of the entire intervertebral disc space which supports the diagnosis of spondarthritis.

7.8.5 Breccia of Sterkfontein

7.8.5.1 Scientific Question

Sterkfontein, a Plio-Pleistocene karstic complex site in the Gauteng Province, South Africa, is located within the well-known and so-called "Cradle-of-Humankind". Within this region, numerous australopithecine remains, as well as evidence of early Homo were discovered including more cercopithecoid remains than any other fossiliferous site in South Africa. The aim of the study include the successful virtual extraction through micro neutron tomography of a cercopithecoid partial cranium (STS 1039) which is still embedded within breccia material.

7.8.5.2 Materials and Methods

A sedimentary breccia block prior to preparation towards revealing possible concealed imbedded fossil materials, with an uncertain taxonomic attribution, was the focus of the study (Figure 7.15). The block of breccia is permanently stored at the DITSONG National Museum of Natural History, Pretoria, South Africa and contains the partial cranium STS 1039 (c. 13.5 x 7 x 3 cm). To reveal the presence of any possible diagnostic element preserved in the hardened sediment, microfocus X-ray tomography, as preliminary investigation (Figure 7.5), was applied at the MIXRAD facility at Necsa, South Africa.

Fig. 7.15. Photograph of a block of breccia materials with cercopithecoid partial cranium (STS 1039) imbedded into the rock matrix (Beaudet et al. 2015).

The specimen has been detailed by micro neutron CT at the ANTARES Imaging facility of the Heinz Maier-Leibnitz Center (FRM II) of Technische Universität Munchen, Germany. Scanning parameters include a collimation ratio of L/D 550 (ratio between sample-detector distance and collimator aperture), a neutron intensity of 6.43 10^7 n/cm^{2}s and a final voxel spatial resolution of 75.0 μm.

7.8.5.3 Results

XCT partially failed due to the extremely low contrast between the breccia and bony/tooth elements as no reliable information of taxonomic value could be obtained. However, micro neutron tomography (μNCT), whose results are depicted in Figures 7.16 & 7.17, clearly reveals that the specimen preserves several bony structures. Morphological information of the maxillary bones, the pterygoid bones and part of the left temporal bone, including the mastoid process and the external acoustic meatus, up to the level of the canine jugum (Figure 7.17B) could be obtained.

Through the utilization of μNCT, more detailed information of the concealed fossil materials became available. Apart from the relatively complete right and left upper post canine dentition, the crown of the left maxillary canine and a small root fragment of the right canine could be revealed. Due to the occlusal wear of both third molars as well as the completely developed roots, fossil STS 1039 is postulated to represent an adult, more likely a young adult individual.

From Figure 7.17 (A,B) it can be seen that the third and fourth premolar, as well as the first molar crowns have lost most of their enamel. Additionally, it is observed that the roots of the left post-canine teeth are perfectly preserved while some of the right row, are broken.

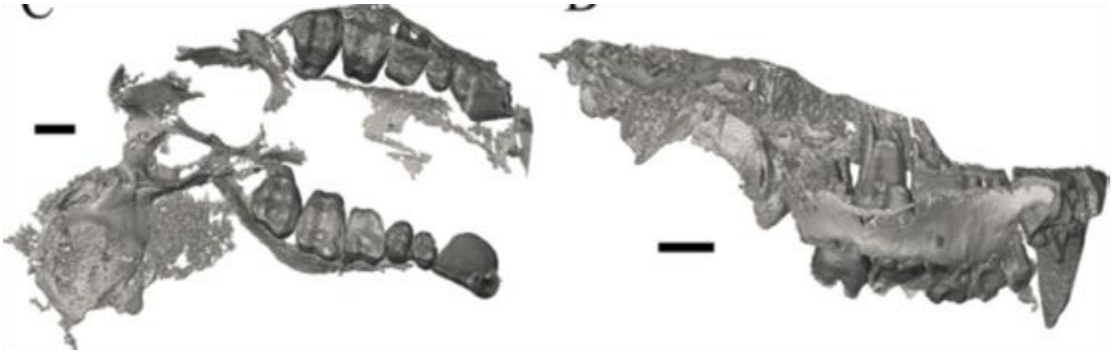

Fig. 7.16. The 3D neutron tomography reconstruction of the virtually extracted maxilla is shown in occlusal (*Left*) and right lateral (*Right*) views. Scale bars: 1 cm (*Courtesy*: Beaudet et al. 2015).

Neutron micro CT also allows for cartography of the enamel thickness distribution across the overall M3 crowns in STS 1039 and clearly reveals relatively thin enamel across the entire crown.

7.8.5.4 Conclusive Remarks Related to the Study

The ability of μNCT to provide an accurate picture of all the elements contained in the breccia block makes it a valuable probe for palaeoscientists to use in similar situations of concealed fossilized materials. It reveals data previously impossible to access (e.g. bone morphology, enamel thickness across the crown, EDJ shape, etc.) using μXCT.

The use of micro neutron tomography (μNCT) to inspect the STS 1039 breccia block embedding the partial monkey cranium from Sterkfontein was successful. This study, providing the excellent neutron tomography results on micron scale, is the first to be documented to virtually disclose and 3D render the content of breccia with enclosed primate remains from the South African hominin-bearing cave sites.

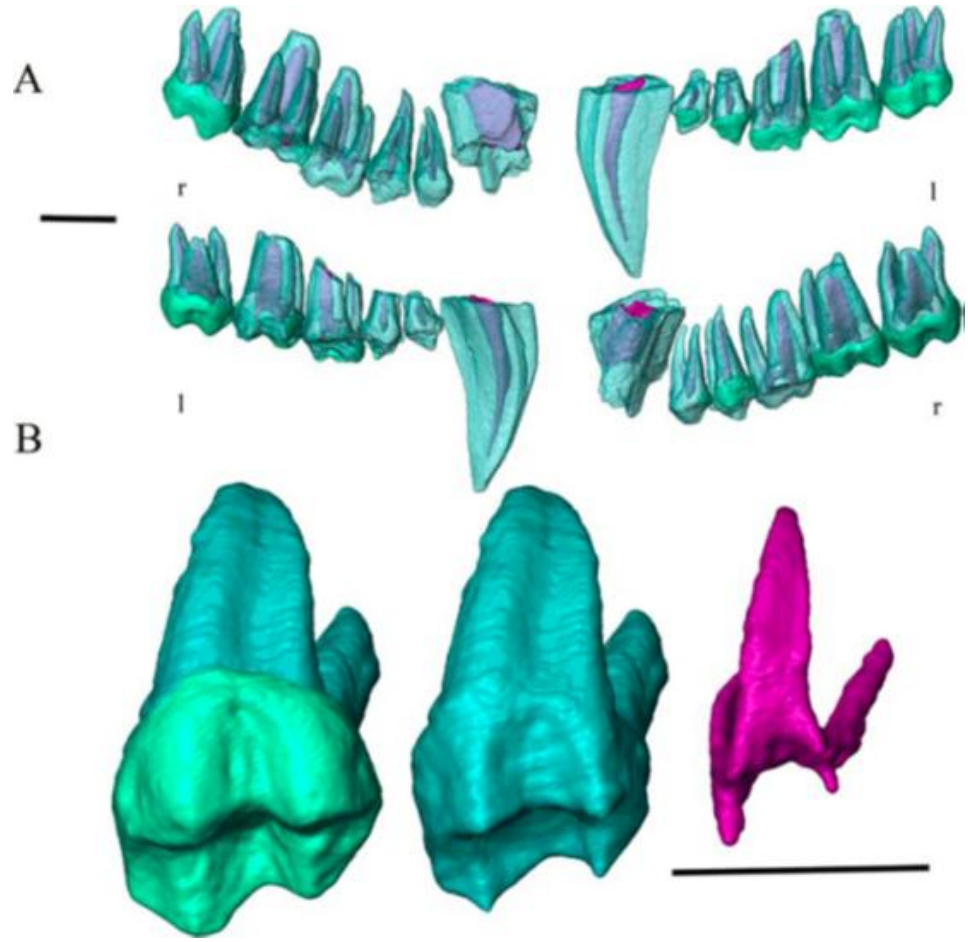

Fig. 7.17. (**A**) The virtually extracted right (**r**) and left (l) tooth rows of STS 1039 rendered in semi-transparency in buccal (upper) and lingual view (lower). (**B**) 3D rendering of the upper RM3 showing the outer enamel and dentine (*left*), the enameldentine junction (*centre*), and the pulp cavity (*right*) in occlusolingual view. *Scale bars:* 1 cm (*Courtesy*: Beaudet et al. 2015).

7.8.6 Therapsids

7.8.6.1 Scientific Question

During the Late Permian and Early Triassic, the therapsids were the dominant tetrapods. Therapsids, pelycosaurs and mammals belong to the same clade, Synapsids, a clade which possess one temporal fenestra in the skull. Therapsids were formerly also known as "mammal-like reptiles" due to their ancestry to mammals therapsids, are up to hippopotamus-sized animals and are thus of special interest for evolutionary biologists and palaeontologists. Therapsid fossils are rare and thus very valuable and the use of destructive methods to investigate the internal anatomy of therapsid skulls, that include hidden cavities which are almost completely enclosed by bony walls, is usually not considered e.g. the morphology of the inner ear labyrinth, surrounded by bones of the neurocranium, is not known. Knowledge about the internal features of the skulls of therapsids originate from a few broken fossils or well preserved natural casts of cranial cavities, which were exposed by breakage or weathering. However, a number of questions regarding the early evolution of mammals can be answered through the study of therapsids. These include the origins of the mammalian brain, hearing and masticatory apparatus, respiration, endothermy, apparatus and locomotion.

7.8.6.2 Materials and Methods

"Red Beds", an iron-rich sediment, usually fills up the relatively large and massive skulls of therapsid fossil findings. That is why non-invasive technologies which include X-rays for investigation of the internal cranial anatomy of therapsids are rarely used.

This investigation of fossil therapsid skulls focuses on neutron tomography as non-destructive analytical technique to overcome the problems mentioned earlier in the analysis of therapsid fossil findings. Due to the relative high spatial resolution obtained in the neutron tomography (NCT) data sets, NCT supported the reconstruction of the hearing apparatus

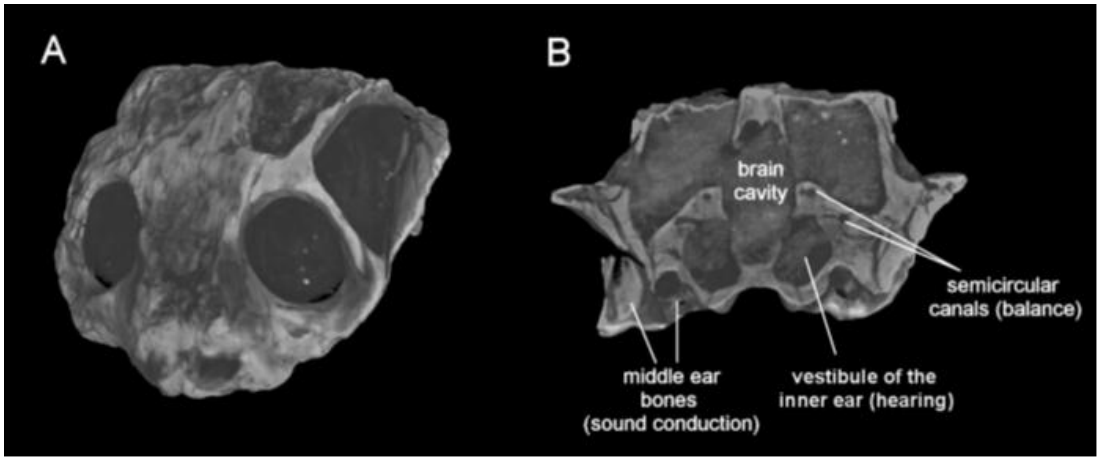

Fig. 7.18. Volume model of the skull of the anomodont Cistecephalus (BSPG 1932 I 56) from the Late Permian of South Africa. **A** Frontolateral view. **B**. Virtual section through the otic region showing the casts of the inner ears and the sound conducting bones (*Courtesy* : Laaß and Schillinger 2015).

The measurements were performed at the ANTARES facility for Neutron Imaging at the FRM II reactor of Technische Universität München.

7.8.6.3 Results

NCT was applied in order to obtain morphological data of the hearing apparatus of therapsids and specifically the middle and inner ear as well as the volumes of bones and important cavities within the skull as depicted in Figure 7.19, that support the hearing capabilities of therapsids.

Indirectly, the length of the cochlea cavity of the inner ear acts as the auditory sensory organ which is roughly correlated with the length of the basilar papilla. In general, the longer the basilar papilla, the wider the hearing range of frequencies. It was found that therapsids such as cynodonts and therocephalians, which were usually ground-dwelling animals, have often long horizontally oriented stapes that points to the supposed eardrum at the lateral side of the mandible. This supports the hypothesis that it might be an indication that these species were adapted to hear airborne sound as well as that the reflected lamina served as a sound receiver. Therefore, the suggestion is that this animal heard substrate sound by bone-conduction due to the downward sloping stapes combined with a relatively large footplate of the small anomodont Cistecephalus from the Late Permian of South Africa (Figures 7.18 and 7.19).

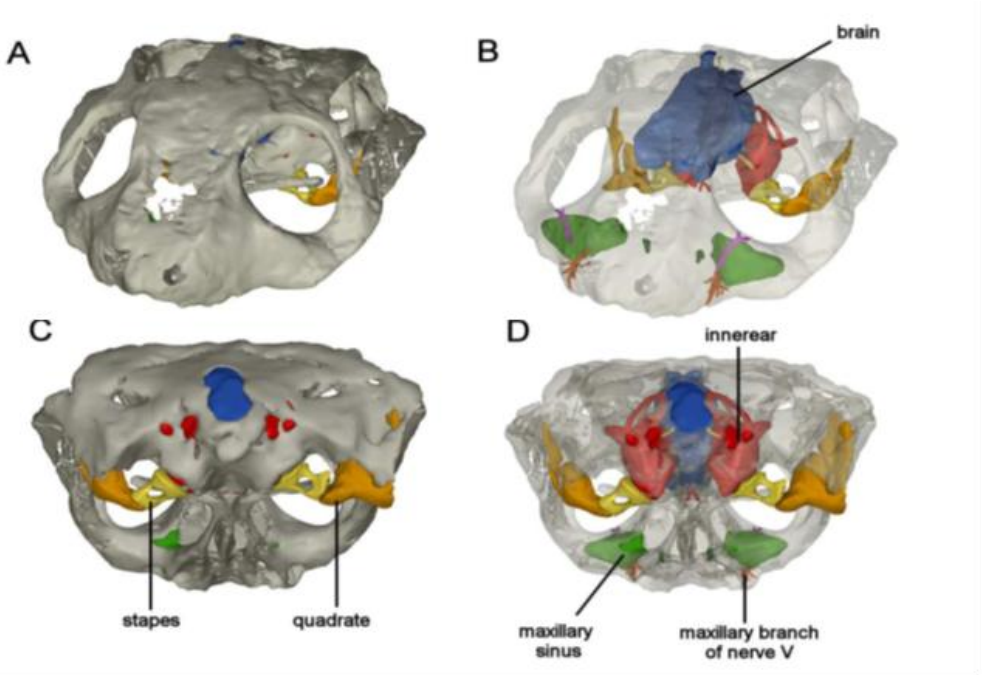

Fig. 7.19. Virtual 3D model of the Cistecephalus specimen in Figure 7.18. **A**. Frontolateral view. **B**. Frontolateral view with transparent bones showing several internal structures of interest such as the brain, the maxillary sinuses, the trigeminal nerves as well as the auditory apparatus, which is marked by different colours (*Courtesy*: Laaß and Schillinger 2015).

7.8.6.4 Conclusive Remarks Related to the Study

Neutron tomography is an excellent analytical and non-destructive probe for investigations of the auditory region of the precious and scarce therapsid fossil findings. The advantage to apply cold neutron radiation that penetrates iron-rich materials such as fossils in the range between 5 cm to 15 cm, produces good contrast between fossil bones and matrix.

The 3D-NRad created models provided important and previous inaccessible information of auditory middle and inner ear parameters and capabilities of extinct animals, their behaviour and lifestyle.

Hydrogen-containing minerals in fossil bones such as Hydroxyl-Apatite might be the reason why neutron radiation creates a good contrast between fossil bones and iron rich matrices.

7.8.7 Prehistoric Stone Slabs

7.8.7.1 Scientific Question

Several ironstone slabs, originated from the late Earlier Stone Age, exhibit some markings such as clear incisions / surface modifications on their surfaces that might be anthropogenic and thus have a high probability to be significant to understand human symbolic behavior. One of these 'incised' ironstone slabs has a series of visibly parallel incised lines which indicates that the surface modifications were inconsistent with natural processes and point to intentional modification by hominins.

It was thus necessary to determine whether the incisions represent intentional actions or were they formed through natural modifications, given the amorphous and unclear nature of these surface incisions.

7.8.7.2 Materials and Methods

Several ironstone slabs were found at the back of Wonderwerk Cave, Northern Cape Province, South Africa, that represent a late Earlier Stone Age period. Two ironstone slabs were selected to be analyzed using Neutron tomography due to grid-like patterns of deep lines on one aspect as visual inspection of the fissures in the rock have suggested the probability that these lines are only the surface expression of internal fissures (See Figure 7.20). On the other hand, the grid pattern on the surface of the slabs could also suggest being the result of hominin action. The samples are branded as External sample #23 (9.9 cm x 6.8 cm x 2.4 cm), External sample #22 and Slab BB147 (10.6 cm x 7.2 cm x 4.2 cm) (Jacobson et al. 2013).

Neutron- and X-ray radiography was performed at the South African Neutron Radiography (SANRAD) facility, being hosted by the South African Nuclear Energy Corporation SOC Ltd. (Necsa). A spatial resolution of 100 mm was achieved by rotation taking 375 projections within 360° in a field of view (FOV) of 10 cm x 10 cm.

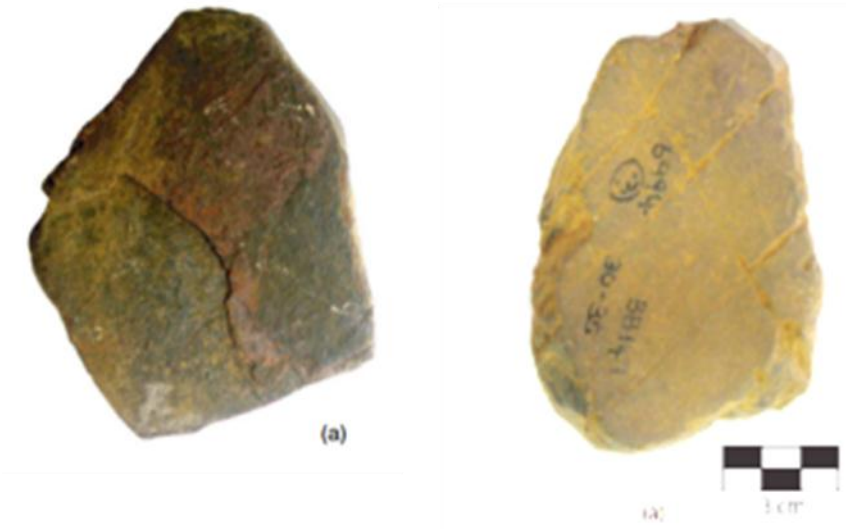

Fig. 7.20. *Left*: Slab External #23 from the slopes above Wonderwerk Cave. A photograph of the surface of the slab: no lines are visible on this surface. *Right*: Slab BB147 from Excavation 6. A photograph showing a grid of lines visible on the surface (*Courtesy*: Jacobson et al. 2013).

7.8.7.3 Results

The linear attenuation coefficients of neutrons for the sample matrix (0.19 cm^{-1}) and Fe-stone-rich area (0.73 cm^{-1}) are relatively low and thus allow easy penetration of neutrons through relatively thick samples. Neutron tomography (NT) results clearly identify fissures, both in cases where lines are visible on the surface and in cases where there is no surface expression of internal fissures. NT results of one archaeological case found lines on the surface of a slab that are not associated with internal fissures.

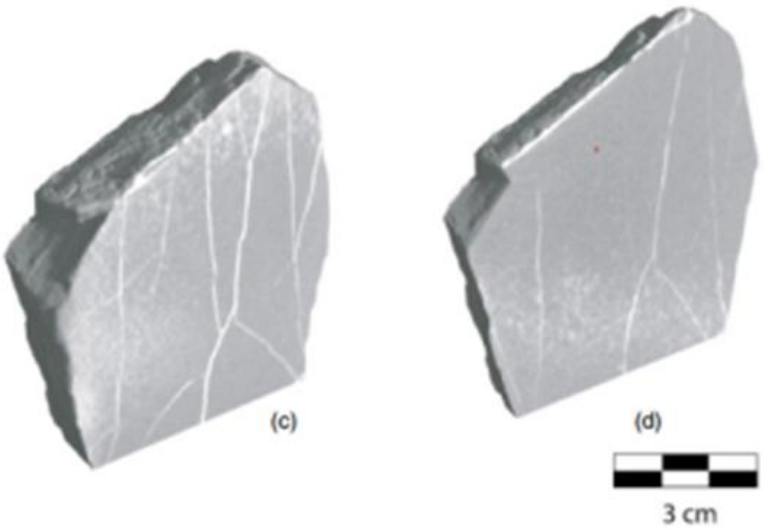

Fig. 7.21. A slice of #23 at a depth of ~5 mm, showing a dense network of fissures visible as white lines. (d) A slice at a depth of ~10 mm, showing a decrease in the number of fissure lines with depth from the surface (*Courtesy*: Jacobson et al. 2013).

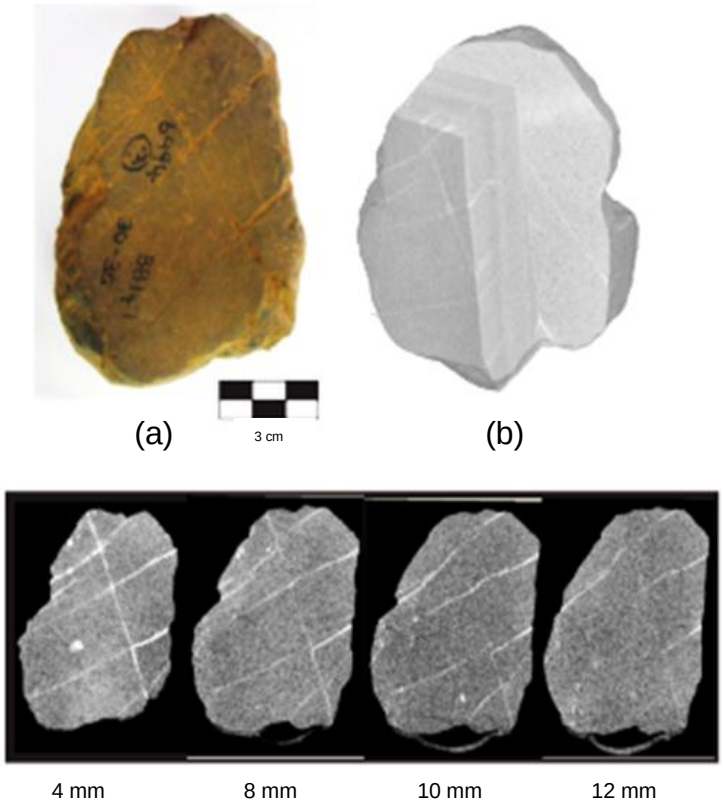

Fig. 7.22. Slab BB147 from Excavation 6. (**a**) A photograph showing a grid of lines visible on the surface. (**b**) A cutaway midway through the slab, showing that the lines continue as fissures (visible as white lines) through the slab. (**c**) Slices at 4, 8, 10 and 12 mm from the surface, showing the persistence of the grid pattern through the slab (*Courtesy*: Jacobson et al. 2013).

Sample #23 as depicted in Figure 7.21, has no lines visible on the surface while NT showed multiple, irregular internal fissures. Virtual cutaways into the NT data of the sample show that the cracks propagate from the midplane of the slab out towards the surface (Fig. 7.21 (c,d).

Visual inspection of Slab BB147 (Figure 7.22) shows a very clear pattern of deep lines regularity layout on the surface. Neutron tomography raised the possibility that the cracks could be filled with water but after the sample was dried in an oven for 2 days at 50 °C, the white lines (indicate higher neutron attenuation) were still present. NT clearly shows that the lines (cracks) on the surface of this slab extents through the entire slab. This is shown in Figure 8.22 (c) of slices taken along the plain of the face of the slab. A graphic summary of the continuation of the lines through the body of the slab is shown in Figure 8.22 (b) in three dimensions. It is concluded that NT results prove that the lines on the surface of this sample are the result of internal fissures within the ironstone and not the result of hominin intervention.

7.8.7.4 Conclusive Remarks Related to the Study

NT offers an innovative and appropriate method for a study of this kind. Given that NT provides non-destructively high-resolution 3D results of so-called impermeable materials, NT proved here

to be an effective tool to penetrate high density iron samples and distinguish surface incisions from lines that are the expression of internal fissures in the rock.

The capability of NT to create a 3D virtual reconstruction of the internal structure of dense material has further potential applications for Palaeolithic archaeology such as the possibility of examining controversial examples of modified stones. One such sample is the Tan-Tan or Berekhat Ram figurines, to determine whether the lines seen on the surface are truly the expression of internal fissures. The same method also holds promise for detecting microfractures in stone tools due to extensive usage where this kind of data could complement understandings of use-wear analysis which is limited to surface features.

7.9 Constraints of NRad in Palaeoscience Applications

National agencies controlling the movement and activities of countries regarding fossilized materials such as SAHRA (South Africa), have restrictions in the movement of fossils from South Africa to analytical facilities abroad. As neutron tomography facilities are not readily available through-out the world, such restrictions place a burden on the movements and thus the research that can be conducted. When the fossilized materials are obtainable, beam time at NRad facilities are not always available and can hinder research as palaeonsciences have to compete with other research proposals to obtain access at high profiled and quality NRad research facilities.

As with any analytical technique there is a limitation in the thickness of breccia materials that can be penetrated by neutrons. This makes it impossible to obtain research data in 3D of relative large samples which might contain a number of fossilized materials and the subsequent cutting of these breccia blocks could have a damaging effect on possible fossils imbedded in the large block.

Activation of samples (Sutton 2008) is always a possibility with high-intensity neutron bombardment that induce hazardous levels of radioactivity in some geological materials. Researchers thus have to be careful when samples contain levels of cobalt or europium; samples may thus need to be interred for months or years after NT study. Dealing with precious museum objects implies taking extra precautionary measures preventing possible damage to the samples. To this aim, the samples could initially be characterized through a preliminary Neutron Activation Analysis test measurement. This analysis is used to evaluate the concentration of trace and major elements (and their isotopes) in the sample with the aim of testing its activation rate and decay time as a function of the exposure time. In order to limit the activation level induced by the presence of critical elements and to avoid a decay time longer than a few hours, the samples were investigated for a limited neutron exposure time.

7.10 Future Prospects

The power of fast neutron radiography (MeV) was described by Berger (1962) as early as in 1962 where the absorption differences of materials are much reduced for fast neutrons while

better radiographic discrimination is possible utilizing its resonance neutron region. This is now possible as new facilities with a fast neutron radiography capability such as NECTAR and SANRAD became available (Henke et al. 2007 and Bücherl et al. 2011).

Neutron Radiography is integrated into the Development and Activities of the South African Palaeo-Scientific Community through association of a Fossil prepa-ration Laboratory located at Necsa. This proves to be a major step forward in the utilization also of Neutron Radiography as an analytical probe by the palaeoscience (Necsa annual report 2013/2014) community. The use of neutron beam facilities to support heritage studies is gaining momentum among the South African research community and a decision was made to establish a Fossil Preparation Laboratory on the Necsa site to assist the heritage research community in making even more efficient use of its beam line research facilities. This will enhance Necsa's potential contribution to knowledge generation within the scope of the newly established South African Department of Science and Technology Centre of Excellence in Palaeosciences.

The South African Nuclear Energy Corporation SOC Ltd. (Necsa) is situated within the Pelindaba complex at the North East corner of the "Cradle of Humankind". It is on the same dolomitic band that houses the fossil deposits and would have been included within the Cradle were it not a nuclear facility. Geologically it is part of the Cradle and spatially it is right next to the Cradle. The Radiation Science (RS) Department of Necsa, which is part of its R&D Division, has recently designated heritage and heritage materials studies as one of the core focus areas of its activities in its support of the National System of Innovation and Necsa's mandate to promote research in radiation sciences. Necsa thus provides access to its scientific expertize and facilities for the Cultural heritage communities to exploit its potential and capabilities. In this regard, Necsa provides capacity to exploit neutron- and micro-focus X-ray tomography scanning services (non-diagnostic) to many researchers in a variety of scientific research fields – also to the palaeosciences and archaeological sciences.

The complementary nature of neutron and X-ray tomography allows for a full understanding on a non-destructive basis of the internal information of e.g. fossil bearing rock, through the creation of detailed 3D virtual images of fossil material – critical to the scientist in evaluating also internal features of fossils e.g. morphology of the cochlea. It is foreseen that palaeontologists and palaeoarcheologists will increasingly utilize these radiation based analytical techniques to investigate critical internal detail of valuable fossilized specimens in a non-invasive manner without damage to the specimens as more international state-of-the-art neutron CT facilities are being commissioned.

7.11 Conclusion

Neutron Radiography/Tomography has, in a complementary manner with X-ray tomography, a significant role to play in answering the question of questions for mankind — the ascertainment of the place which Man occupies in nature and of his relations to the universe of things (Henke et al. 2007). Neutron Radiography is being practiced at various highly sophisticated facilities worldwide, and also plays an important but also proven significant role to advancing our understanding of various aspects of the story of life on Earth; it can reveal how plant and animal

life developed, how humans evolved and thus play a part to reveal the history of mankind (SA Strategy 2011).

The Neutron radiography technique is advantageous by being non-destructive in revealing internal details, and is being applied to study specific morphological features (e.g. trabecular details) inside fossilized specimens that is not possible using classic methods.

Breccia blocks are prioritized for preparation by surface examination and preparing of a standard 2 kg block of breccia can take up to 6 months. However, neutron radiography and tomography allows the internal details of breccia blocks to be easily visualized and can reveal the contents of a given block and thus fast-track preparation of promising fossil containing blocks. Application of neutron radiography has already stimulated new directions of research avenues in palaeontology and the future promises further exciting results and insights.

References

Abel R.L., Laurini C.R. and Richter M., A palaeobiologist's guide to 'virtual' micro-CT preparation. Palaeontologia Electronica 15 (2012), http://palaeo-electronica.org/content/pdfs/284.pdf .

Ashraf M.T. Elewa, Computational Paleontology (Google eBook);. Springer Science & Business Media, 04 Mar 2011.

Beaudet A., Braga J., de Beer F.C., Schillinger B., Steininger C., Vodopivec V. and Zanolli C. Neutron Microtomography-Based Virtual Extraction and Analysis of a Cercopithecoid Partial Cranium (STS 1039) Embedded in a Breccia Fragment From Sterkfontein Member 4 (South Africa), American Journal of Physical Anthropology (2015) Submitted for publication.

De Beer F.C., Radebe M.J., Schillinger B., Nshimirimana R., Ramushu M.A. and Modise T., Upgrading the Neutron Radiography Facility in South Africa (SANRAD): Concrete Shielding Design Characteristics, Physics Procedia 69, 115 – 123 (2015), www.doi:10.1016/j.phpro.2015.07.017.

De Beer F.C., Prevec R., Cisneros J. and Abdala F., Hidden structure of fossils revealed by neutron and X-ray tomography. In Proceedings of the 8th World Conference on Neutron Radiography (WCNR-8) held at NIST, Gaithersburg, USA, Sept 2006, Neutron Radiography 8, edited by M. Arif and R. G. Downing. Lancaster, 452-461 P. Destech Publications. 2008.

Berger, H., ""Neutron Radiography: A 1962 Progress report"."*Symposium on Physics and Nondestructive Testing*, San Antonio, Texas, 1962, 1-37.

Braga J., Thackeray J.F., Dumoncel J., Descouens D., Bruxelles L., Loubes J-M, Kahn J-L, Stampanoni M., Bam L., Hoffman J., de Beer F. and Spoor F., A new partial temporal bone of a juvenile hominin from the site of Kromdraai B (South Africa), Journal of Human Evolution 65 (2013). DOI:10.1016/j.jhevol.2013.07.013.

Braga J, Loubes J-M, Descouens D, Dumoncel J, Thackeray JF, Kahn J-L, et al., Disproportionate Cochlear Length in Genus Homo Shows a High Phylogenetic Signal during Apes' Hearing Evolution. PLoS ONE 10, e0127780 (2010), doi:10.1371/journal.pone.0127780..

Buecherl T., von Gostomski L., Breitkreutz H. and Wagner F., NECTAR—A fission neutron radiography and tomography facility, Nucl. Instr. Phys. Res. A 651, 86-89 (2011), DOI: 10.1016/j.nima.2011.01.058.

Cisneros J.C., Gomes Cabral U., De Beer F., Damiani R., Costa Fortier D. Spondarthritis in the Triassic. PLoS ONE 5 (2010): e13425. doi:10.1371/journal.pone.0013425.

Dinofossils locations, http://www.enchantedlearning.com/subjects/dinosaurs/dinofossils/locations/, Accessed 1 Nov 2015, Fossil and Fossilization, http://www.scienceclarified.com/Ex-Ga/Fossil-and-Fossilization.html Accessed 1 Nov 2015.

Franco M., Our Top 10 Stops on A Fossil Road Trip, Available at: http://adventure.howstuffworks.com/destinations/road-trips/10-stops-for-a-fossil-road-trip.htm (2011).

Gommery D. and Potze S., SAHRA Report: Bolt's Farm-Greensleeves (2010-2013), Permit renewal (2013-2016). (in collaboration with F. Sénégas and L. Kgasi), HOPE RESEARCH UNIT. Plio-Pleistocene Section, Ditsong National Museum of Natural History, Pretoria, SOUTH AFRICA, 17/06/2013. http://www.sahra.org.za/sahris/sites/default/files/additionaldocs/SAHRA%20Report%20BF-Greensleeves%2017.06.2013_0.pdf .

Grellet-Tinner G., Sim C.M., Kim D.H., Trimby P., Higa A., An S.L., Oh H.S., Kim T.J., Kardjilov N., Description of the first lithostrotian titanosaur embryo in ovo with Neutron characterization and implications for lithostrotian Aptian migration and dispersion, Gondwana Research 20, 621-629 (2011).

Henke W., Tattersall I., Hardt T., Handbook of Paleoanthropology, Volume 1, Springer Science & Business Media, 2007, ISBN 3540324747, 9783540324744.

Jacobson L., de Beer F.C., Nshimirimana R., Horwitz L.K. and Chazan M., Neutron Tomographic Assessment Of Incisions On Prehistoric Stone Slabs: A Case Study From Wonderwerk Cave, South Africa., doi: 10.1111/j.1475-4754.2012.00670.x.

Laaß M. and Schillinger B, Reconstructing the auditory apparatus of therapsids by means of neutron tomography, Physics Procedia 69, 628 – 635 (2015), doi: 10.1016/j.phpro.2015.07.089

Le Roux S.D., de Beer F.C. and Thackeray J.F., Neutron radiography of cranial bone of Sts 5 from Sterkfontein, South Africa. South African Journal of Science. 93, 176 (1997).

List of human evolution fossils, https://en.wikipedia.org/wiki/List_of_human_evolution_fossils.

List of fossil sites, https://en.wikipedia.org/wiki/List_of_fossil_sites.

Liang L., Rinaldi R. and Schober H., Neutron Applications in Earth, Energy and Environmental Sciences, (Google eBook), Springer Science & Business Media, 11 Dec 2008, https://books.google.co.za/books?isbn=0387094164 page 338.

Maropeng, http://www.maropeng.co.za/content/page/what_are_fossils Visited on 10 June 2015.

Maropeng, http://www.maropeng.co.za/news/entry/bolts_farm_the_kingdom_of_the_big_cats Visitied on 15 June 2015.

Maropeng, http://www.maropeng.co.za/content/page/the_science_of_studying_fossils Visited on 10 July 2015.

Necsa annual report 2013/2014 (Accessed 1 May 2015): http://www.necsa.co.za/Portals/1/Documents/Necsa/Necsa%20Annual%20Report%202014.pdf.

Peon E., Fuentes G., Delgado J.A., Morejon L., Almirall A. and Garcia R., Preparation And Characterization Of Porous Blocks of Synthetic Hydroxyapatite, Latin American Applied Research 34, 225-228 (2004).

PSI, http://www.psi.ch/industry/MediaBoard/neutron_imaging_e_07.pdf.

SA Strategy, The South African Strategy for the Palaeosciences. Incorporating Palaeontology, Palaeo-anthropology and Archaeology. GOVERNMENT GAZETTE, 20 SEPTEMBER 2011, GENERAL NOTICE NOTICE 657 OF 2011, No. 34624 http://www.gov.za/sites/www.gov.za/files/PALEO_STRATEGY_DST_Final_.pdf.

Schwarz D., Vontobel P.L., Eberhard H., Meyer, C.A. and Bongartz, G., Neutron tomography of internal structures of vertebrate remains: a comparison with X-ray computed tomography, Paleontol. Electronica 8 (2005), www.uv.es/pe/2005_2/**neutron**/**neutron**.pdf.

Sutton, M.D., "Tomographic techniques for the study of exceptionally preserved fossils". Proceedings of the Royal Society B: Biological Sciences 275 (1643): 1587–1593. doi:10.1098/rspb.2008.0263. PMC 2394564. PMID 18426749. (2008).

CHAPTER 5

PUBLICATION:

Proton Exchange Membrane (PEM) Water Electrolysis: Preliminary Investigations Using Neutron Radiography

The global need for the use of alternative and eco-friendly energy sources such as hydrogen based fuel cells is growing rapidly. Hydrogen fuel cells, when optimally designed, are highly efficient in converting diffusion barrier controlled chemical combustion of hydrogen directly into electricity. Neutrons can easily penetrate metals like aluminium and steel while they are strongly scattered by hydrogen, thereby allowing investigation of water distribution in fuel cells without the necessity to change the fuel cell setup and, thus, without altering the properties of the fuel cell under investigation. Continuous research to optimise the performance of fuel cells is therefore enhanced by the application of neutron radiography and tomography as non-destructive and non-invasive analytical techniques. Today, in-operando neutron radiography of fuel cells has become an important research tool, not only in the production of electricity and the visualisation of the liquid water management in the cells, but also in the reverse configuration of hydrogen electrolysis. However, not much research has been conducted into the most efficient utilisation techniques to study optimisation of the electrolysis process via neutron radiography. In this chapter, results obtained from the very first experiments performed in such a process will be presented. It revealed, inter alia, that liquid water accumulations in the porous gas diffusion layers and in the flow field channels of a fuel cell strongly affect the gas flow and, therefore, the gas supply of the catalysts. This study was the first to be undertaken by South African researchers in this field and forms a basis for continued research. Work of this nature has a clear potential to enhance the performance of alternative energy fuel systems via the utilisation of neutron radiography as an in situ investigation tool.

Available online at www.sciencedirect.com
ScienceDirect
Physics Procedia 88 (2017) 19 – 26
Physics Procedia

8th International Topical Meeting on Neutron Radiography, ITMNR-8, 4-8 September 2016, Beijing, China

PEM Water Electrolysis: Preliminary Investigations Using Neutron Radiography

Frikkie de Beer[ac65*]; Jan-Hendrik van der Merwe[b]; Dmitri Bessarabov[b]

[a] *Radiation Science Department, South African Nuclear Energy Corporation SOC Limited, P.O. Box 582, Pretoria, 0001, South Africa*
[b] *HySA Center at North-West University, Private Bag X6001, Potchefstroom, 2520, South Africa,*
[c] *School of Chemical and Minerals Engineering, North-West University, Private Bag X6001, Potchefstroom, 2520, South Africa,*

Abstract

The quasi-dynamic water distribution and performance of a proton exchange membrane (PEM) electrolyzer at both a small fuel cell's anode and cathode was observed and quantitatively measured in the in-plane imaging geometry direction (neutron beam parallel to membrane and with channels parallel to the beam) by applying the neutron radiography principle at the neutron imaging facility (NIF) of NIST, Gaithersburg, USA. The test section had 6 parallel channels with an active area of 5 cm^2 and in-situ neutron radiography observation entails the liquid water content along the total length of each of the channels. The acquisition was made with a neutron cMOS-camera system with performance of 10 sec per frame to achieve a relatively good pixel dynamic range and at a pixel resolution of 10 x 10 μm^2. A relatively high S/N ratio was achieved in the radiographs to observe in quasi real time the water management as well as quantification of water/gas within the channels. The water management has been observed at increased steps (0.2A/cm^2) of current densities until 2V potential has been achieved. These observations were made at 2 different water flow rates, at 3 temperatures for each flow rate and repeated for both the vertical and horizontal electrolyzer orientation geometries. It is observed that there is water crossover from the anode through the membrane to the cathode. A first order quantification (neutron scattering correction not included) shows that the physical vertical and horizontal orientation of the fuel cell as well as the temperature of the system up to 80°C has no significant influence on the percentage water (~18%) that crossed over into the cathode. Additionally, a higher water content was observed in the Gas Diffusion Layer at the position of the channels with respect to the lands.

Peer-review under responsibility of the organizing committee of ITMNR-8.

Keywords: Electrolysis; Neutron Radiography; NIST-NCNR; PEM Fuel Cell

65 *Corresponding author. Tel.: +27123055258
Email address: Frikkie.deBeer@necsa.co.za

Peer-review under responsibility of the organizing committee of ITMNR-8
doi: 10.1016/j.phpro.2017.06.002

1. Introduction

Recently hydrogen Proton-Exchange-Membrane (PEM) fuel cells (FC) made significant progress in several countries with roadmaps toward commercialization [USDOE, 2016; Prasad, 2016], eventually causing a growing interest in technologies for also high quality hydrogen generation. Thus, the use of PEM water electrolysis for hydrogen fuel production became a vector of interest for fuel cell deployment opportunities in sectors such as sustainable mobility, material handling, and back-up power. Hydrogen is the only energy storage concept to address energy storage in a range > 100 GWh [Waidhas, 2016]. PEM water electrolysis (PEMEL) is also considered as one of the most favourable technologies for hydrogen generation with many advantages over other available technologies such as simplicity, high current densities, solid electrolyte and high working pressures.

Water is decomposed by passing an electric current through the water into hydrogen and oxygen in the presence of suitable substances, called electrolytes. The operating principle of PEMELs is often referred to as the reversed operation of a fuel cell whereby the water is oxidized at the anode (oxygen production) to produce oxygen electrons and protons (eq-1), however, the materials and configuration thereof are typically different from PEM-FC. Optimized electrolysis plants usually operate at electrolyte temperature of 70-90^{o}C and cell voltage of 1.85-2.05 V (Zoulias et.al., 2006).

$$H_2O\ (l) \rightarrow 4H^+(aq) + 4e^- + \ O_2\ (aq) \quad (1)$$

The protons pass directly through the membrane to the cathode were they recombine and form hydrogen (eq-2).

$$2H^+ + 2e^- \ \rightarrow H_2 \quad (2)$$

Water electrolysis yield no side reactions that could generate undesired byproducts, therefore the net balance is (eq-3):

$$2H_2O \ \rightarrow (4e^-) \rightarrow O_2 + 2H_2 \quad (3)$$

Unfortunately, gas crossover occurs when either hydrogen or oxygen cross through the membrane to the other side and thus pose safety issues such as explosive gas mixtures but also lowers the efficiency of the electrolyzer and enhances degradation of the membranes. (See Fig. 1.)

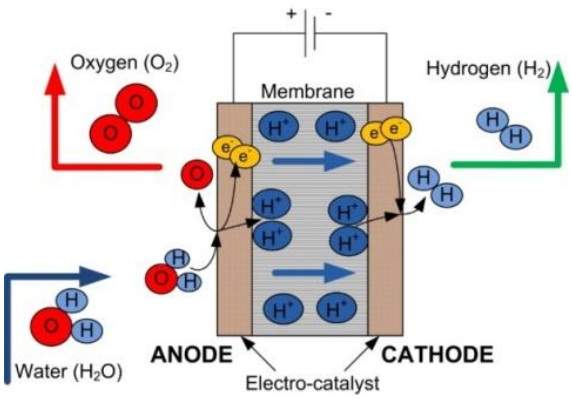

[Fig. 1. Schematic of a PEM electrolyser setup [1].

Jacobson, 2004 indicated that the water balance in a normal operating fuel cell is critical to the operation of the cell and that proper humidification of the membranes will allow optimum conduction of protons. Water entering the electrolysis system which is not transformed into ions, and water that has crossed over into the cathode and is not being removed quickly, could jeopardize the optimal functionality of the system. This is where neutrons can play a role in analyzing the effectiveness of the gas diffusion layer and water channels in removing water from the electrolyzer fuel cell.

This paper focuses on most recent preliminary studies where neutron radiography has been applied in the detection of hydrogen compounds in a working hydrogen fuel cell during the process of electrolysis. The concentration of the H2-gas being produced is actually too low to be detected via neutron radiography and all results show the water (black), which has a relatively higher neutron attenuation coefficient than the other materials in the experiment and detected within the channel areas of the electrolyzer (See Fig. 4).

In an earlier publication on the application of neutron radiography as analytic method on an electrolyzer using PEM fuel cells, Murakawa et.al [2015] focused only on the water-accumulation process in the gas diffusion layer (GDL) under the lands and channels. He concludes that the water accumulation in the GDL under the lands was larger than that under the channels during the period of early PEFC operation. However, this study focuses only on the detection and quantification of the liquid water and subsequent gas within the channels at the cathode and anode during the in-situ electrolysis process of a single working and experimental PEM fuel cell and specifically in the in-plane direction.

2. Experimental Setup

The neutron imaging facility (NIF) at the National Institute for Standards and Technology (NIST), USA and located in the NIST Center for Neutron research (NCNR) was utilized. A thermal neutron beam with intensity of 1.38 x 10^7 neutrons.cm^{-2}.sec^{-1} (maximum for the facility) at an L/D of 450 was applied. The full size of the beam was choked down by a beam limiter to a size of 2.2 cm x 2.2 cm to avoid unnecessary activation of the Fuel Cell and to expose only the area of interest (AOI) which is mainly the channels on both the anode and cathode side.

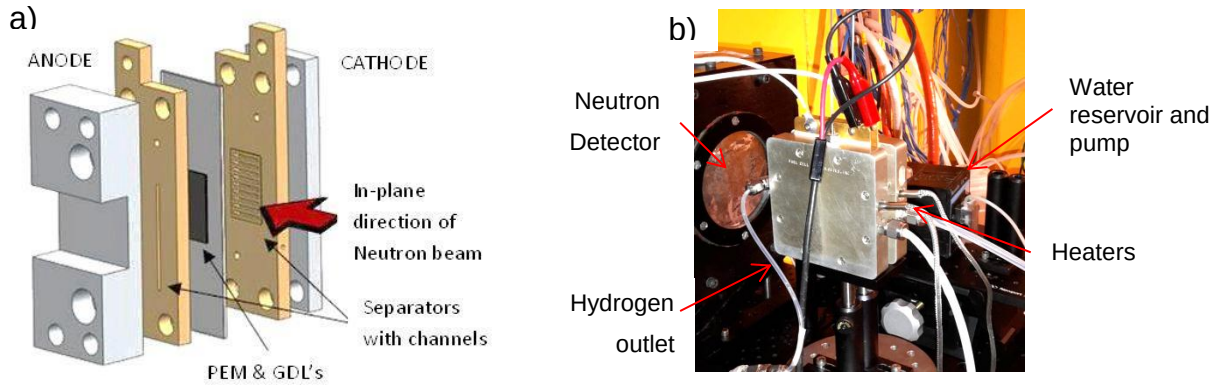

Fig. 2. a) Schematic illustration of the experimental setup and in-plane direction of the neutron beam [1]. b) Experimental set up of the electrolizer fuel cell in the NI chamber at NIST.

The electrolyzer fuel cell was aligned in its in-plane direction facing the radiation beam (Fig. 2a) in front of the camera box and as close as possible to the scintillator screen (Fig. 2b). The electrolyzer was

coupled with all the necessary utilities on the anode side of the cell such as the water inlet and access water – Oxygen removal outlet from and to the reservoir. On the cathode side the cell was equipped with an outlet for hydrogen to the outside of the NIF facility for safe release thereof into the beam port hall. The fuel cell base material has been fitted on both the anode and cathode side with 2 heating elements and an electrical DC potential (both operational from outside the NIF chamber during neutron exposure). A digitally controlled water pump was used for precise regulation of the flow of water into the anode of the electrolyzer.

The neutron radiographs were captured via a 7.9 mg/cm^2 Gadox scintillator (P43) from Lexel Imaging using a ANDOR CCD camera in 16 bit mode and cooled to -30 °C for high resolution and electronic noise free imaging. A 85 mm NIKON lens focused the image onto the 6.5 micrometer pixel size sensor to obtain an effective pixel pitch of 10 micrometer [Physics NIST, Camera accessed Jan 2017].

The sets of experiments were conducted with the electrolyzer fuel cell orientated in a vertical (see Fig.2b) and then thereafter in a horizontal position. At each orientation, three (3) sets of experiments were conducted with the fuel cell basis materials heated to Ambient = 27°C, 60°C and 80°C temperatures respectively. At each temperature setting, two (2) sets of experiments were conducted with the water flow rate at 11 ml/min and 37 ml/min. Neutron radiographs were acquired for each of these conditions described above at a rate of 1 integrated frame per 10 sec for duration of 300 sec, starting at a current density of 0 A. Similar sets of neutron radiographs were acquired thereafter with an increase of the current density in steps of 0.2 A until the potential difference of the cell reached approximately 2V. See Fig. 3. for the polarization curves of the operation of the electrolyzer at different water flow rates and fuel cell temperatures achieved in both the vertical and horizontal orientation of the cell. From these curves it is evident that the electrolyzer functions normally as expected. However, the sudden change in the slopes can be explained by the fact that in our experiments, novel and experimental catalyst-coated membranes (CCMs) based on 3M NSTF technology were used. The anode catalyst loading was considerably smaller than in conventional CCMs [Bessarabov 2015]. Due to the fact that the loading of an anode catalyst was lower than that of commercial CCMs for water electrolysis, as well as that the gas diffusional layer was not optimized, the over-potential at lower current densities was higher than in conventional PEM water electrolysis systems.

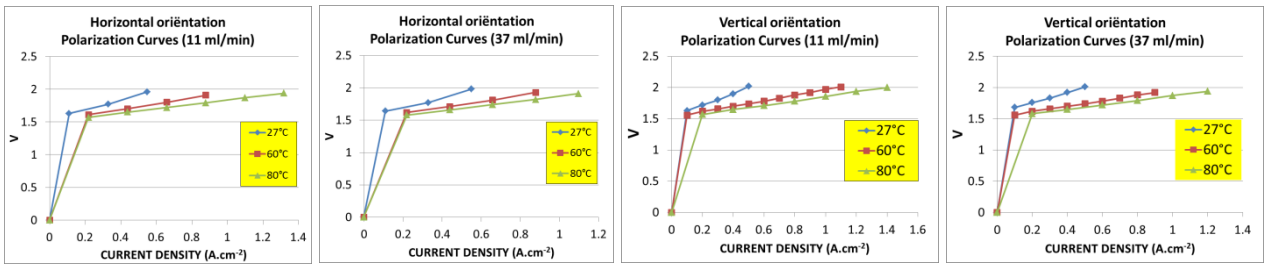

Fig. 3. Polarization curves for all the experiments conducted in a specific orientation, water flow and current density.

The illustration in Fig. 4 shows the vertical and horizontal orientations of the experimental electrolyzer fuel cell, the dimensions of the channels as well as the channels as area-of-interest (AOI) for neutron radiography.

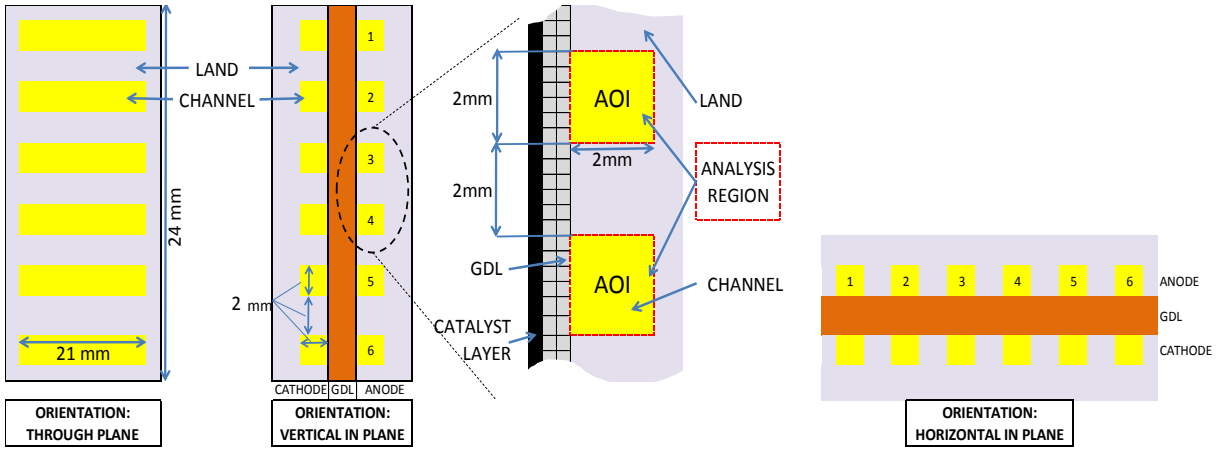

Fig. 4. Schematic diagram of the detail of the dimensions of the PEM electrolyzer fuel cell. Experiments were performed only in both the in-plane orientations (vertical & horizontal) with the channels (yellow) as main areas-of-interest.

3. Analysis Method

Qualitative:

Neutron radiographs provide a visual observation for qualitative analysis of the channels at the anode and cathode. An assessment of the water and gas content during operation at the different parameters mentioned in Section 2 were made. Each radiograph present is an accumulation of multiple radiographs being captured every 10 sec for a period of 300 sec. This visual assessment indicates the integrated information obtained in one radiograph along the 21 mm length of each of the channels. Fig. 5 shows these time-resolved radiographs (a pair) each per orientation and at different time intervals T_i.

Regular water flow patterns were observed in the vertical orientation experiments when the water was fed from the bottom of the electrolyzer into the anode [A] as shown in Fig. 5 as irregular flow was observed with no established channel water pattern when the water was fed into the system from the top. The black areas in channels represent the water (Scale bar or RIGHT indicating the percentage water in the channels in grey scale).

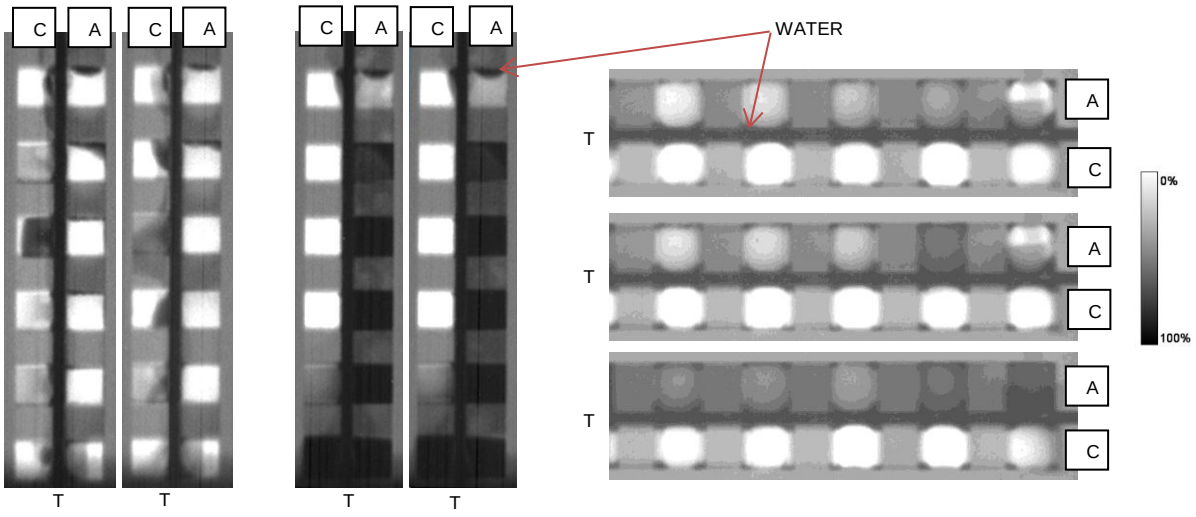

Fig. 5. LEFT: Vertical top initiated flow; MIDDLE: Vertical Bottom initiated flow; RIGHT: Horizontal flow with Anode at top.

Observation of the horizontal orientated cells shows a higher concentration of water, as expected, in the anode (the input) than the cathode [C]. Unexpectedly, water has crossed over through the membrane into the cathode which could hinder H-production and the transport thereof outwards from the system. The cathode maintains a regular pattern of water continuously over time. Interestingly, the water has accumulated (was not expected) in the corners of the channels at both the anode and cathode. The oxygen and hydrogen production in the anode and cathode respectively are located in the centre of the channels while more water, as expected, is located near the membranes.

Quantitiative:

Calibration calculations for the correct determination of the neutron attenuation of Ti (base material of the fuel cell) and water are necessary for the accurate determination of the water content within the channels of the electrolyzer. This calibration process is a first order process and does not include corrections for neutron scattering or beam hardening. From basic principles of neutron attenuation with matter it can be shown that the attenuation for water and Ti can be expressed in general as shown in eq-4:

$$\ln\left[(I_0 - I_{DC})/(I - I_{DC})\right] = \Sigma_{Ti} x_{Ti} \qquad (4)$$

With I_0 the intensity with no sample, I the intensity at a certain thickness x_{Ti} of the Ti-material, I_{DC} the dark current electronic noise of the detection system and Σ_{Ti} the linear attenuation coefficient of the medium under investigation which is an unknown for the Ti body and water within the channels.

To determine the neutron attenuation of Ti from a single radiograph (See Fig. 6.), the electrolyzer is in a non-operational state and thus without any water. The various thickness of the Ti are known to be A: 31.2 mm, B: 27.2 mm and C: 10 mm respectively. The corresponding different average pixel grey scale values (with a SD_{pixel} = 3) are displayed in a histogram. The application of eq-4 results in the graph (Fig. 6) with the slope the Σ_{Ti}.

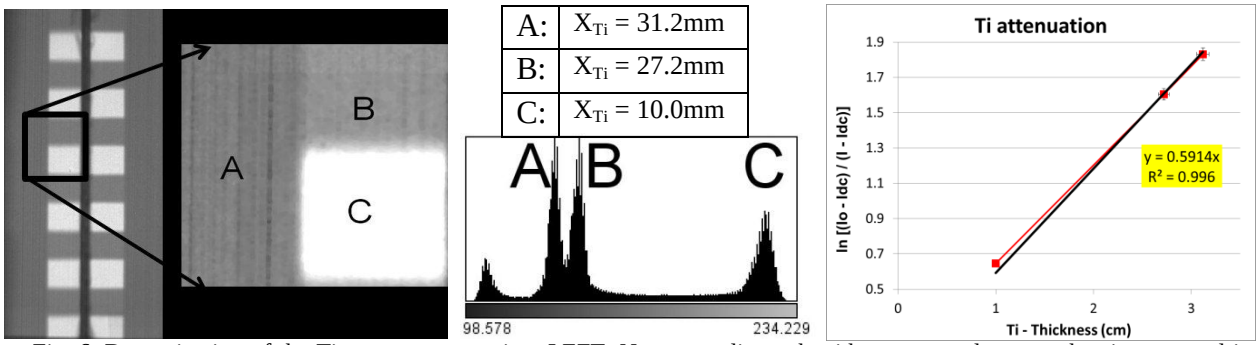

Fig. 6. Determination of the Ti neutron attenuation: LEFT: Neutron radiograph with system at dry state showing zoomed in view with the areas A,B and C. MIDDLE: Histogram with pixel values for 3 individual regions. RIGHT: Utilization of eq-4 in a graph to determine the Σ_{Ti}.

Using eg-4 to determine the thermal neutron attenuation of Ti and generating Fig. 6 RIGHT for this experiment, it is found that $\Sigma_{Ti} = 0.592_{avg} \pm 0.017$ (3% error) cm^{-1}.

To obtain the neutron attenuation coefficient for water calibration, the operating condition of the cell at 0V and 0A was used. At this condition the anode and cathode is in a dry (0%) and fully wet (100%) condition respectively knowing that the channels are either completely dry or fully filled with water. As the water is located within the channels, the attenuation of water has an offset of 0.5914 cm^{-1} for the

contribution of the Ti-material of the channel – for this experiment a wall thickness of 1 cm. The neutron attenuation for H_20 for this experimental setup was found to be Σ_{water} = 2.51 cm^{-1} using eq-5:

$$\ln\left[(I_0 - I_{DC})/(I - I_{DC})\right] = \Sigma_{Water}x_{Water} + \Sigma_{Ti}x_{Ti} \quad (5)$$

The schematic illustration as in Fig.1 shows an ideal situation with all the water, being fed into the anode, are "used or split". One should therefore expect a constant water content at the anode present, equally distributed through all the channels and with no residual water left at the anode.

4. Results and Discussion

The initial purpose of this study was to observe qualitatively the movement and behaviour of the water as well as the production and movement of oxygen and hydrogen in the anode and cathode respectively. Observation of both the anode and cathode was planned to view the behaviour of the electrolysis process. However, data being made available through neutron radiography can be used for either qualitative or quantitative analysis once the detector has a linear response characteristic. Table-1 presents the percentage water in the anode and cathode at all the different experimental parameters.

Although the membranes of the electrolyzer in the Gas-Diffusion-Layer (GDL) is hydrophilic of nature, the observation of water crossed over into the cathode is being confirmed as ~18% percent water present in both the vertical and horizontal orientations. As expected, the percentage water in the anode, the entrance of water into the system, is high and found to be ~ 44%. At the higher water flow rate of 37 ml/min, no significant difference in the amount of cross over water in the cathode for both orientations of the electrolyzer is being observed and was calculated to be in the order of ~ 19%. The experiment did not focus on the water transport process as such and thus does not reveal the tempo of the water transport through the membrane.

Table-1: Results of the experimental electrolysis process. The percentage water found in the Anode and Cathode channels for 2 x orientations of the cell: V = Vertical orientation; H = Horizontal orientation, 2 different water flow tempo of 11 and 37 ml/min, at ambient pressure and at three different temperatures (27 °C, 60 °C and 80 °C). The standard deviation of all results is ~ 2%. A = Anode; C = Cathode.

VERTICAL ORIENTATION		
	11 ml / min	
TEMP (°C)	A	C
27	37.4%	17.3%
60	35.0%	18.9%
80	40.3%	19.9%
AVG	37.5%	18.7%

V

VERTICAL ORIENTATION		
	37 ml / min	
TEMP (°C)	A	C
27	45.1%	16.2%
60	44.3%	19.8%
80	44.2%	20.2%
AVG	44.6%	18.6%

11 ml/min 37 ml/min

HORIZONTAL ORIENTATION		
	11 ml / min	
TEMP (°C)	A	C
27	32.9%	15.8%
60	33.2%	20.4%
80	32.2%	19.6%
AVG	32.8%	18.5%

H

HORIZONTAL ORIENTATION		
	37 ml / min	
TEMP (°C)	A	C
27	46.0%	22.5%
60	40.7%	19.4%
80	43.0%	21.6%
AVG	43.1%	21.1%

Additionally, the water concentration of the GDL could be observed at a low pixel resolution and found to be different within the area of the channel and the glands during operation. The background radiograph (no water as shown in Fig. 6) is being subtracted from the radiograph at any given time during the electrolysis process (those in Fig. 5) to reveal only a change in pixel grey scale value at the time, caused by the water. As no water calibration was performed for this material, only a qualitative observation could be made that indicates a higher water content in the GDL at the position of the channels rather than at the position of the lands. See Fig. 7 with water visualized as white in the resultant radiograph. Line profiles (RED at the Anode and YELLOW at the GDL) show a larger arbitrary grey scale value at the channel region indicating more water than in the lands region. This observation confirms the research of Murakawa et al., 2015 who made an in-depth study of the water content of the GDL.

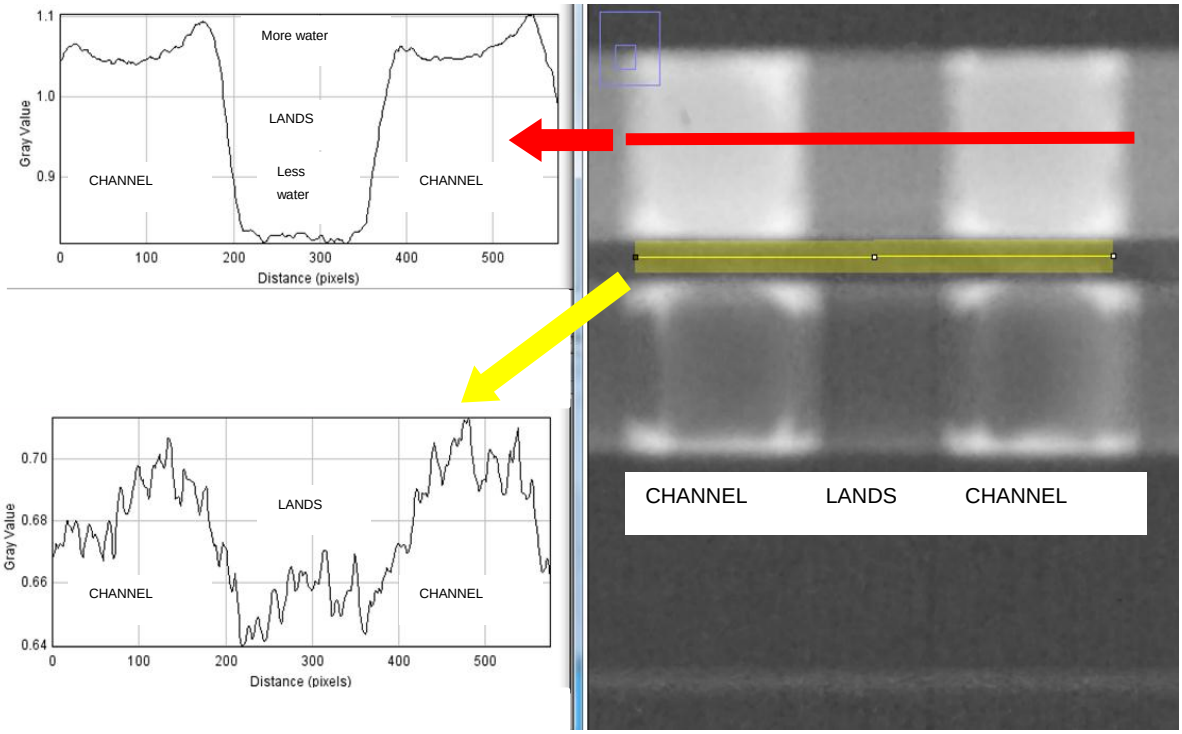

Fig. 7. TOP LEFT: A line profile at the position of the channels and land at the anode within the Ti-body of the electrolyzer. BOTTOM LEFT: A line profile at the position of the GDL spanning across the channels and land. RIGHT: Neutron radiograph at the horizontal orientation of the electrolyzer of 2 channels and 1 land indicating the positions of the line profiles.

5. Conclusion and Future

The water behaviour and management of the electrolysis process in a working fuel cell has been investigated using neutron radiography at a spatial resolution of 10 micron. Valuable insight and additional information were obtained in the internal working of the electrolyzer. No attempt was made to quantify the H production in the cathode as it is difficult to detect or quantify the different gases via neutron radiography due to their low neutron attenuation. However, a first order estimate (without correction of neutron scatter) of 19% ± 2% water in the anode and cathode for each experimental

condition could be achieved. Higher water content in the GDL at the position of the channels w.r.t. the lands were observed. Future experiments will aim to quantify the H-production rate and to look deeply into the water cross over mechanism within the membranes.

Acknowledgements

The authors want to thank: The DST-NRF for funding the trip to USA (REF: UID 96286 & UID 98290); for HySA for supplying the basic equipment; NIST for allocating neutron beam time at their NIF for the project and the staff of the NIF at NIST for their professional and excellent support; 3M USA for providing CCMs.

References

Ajay K. Prasad, A.K., Opportunities and Challenges for Commercialization of Fuel Cells, http://www.energy.udel.edu/symposium2014/7-Prasad.pdf Accessed on 5 June 2016.

Dmitri Bessarabov, Haijiang Wang, Hui Li, Nana Zhao (ed), PEM Electrolysis for Hydrogen Production: Principles and Applications., 2016, CRC Press.

Dimitrios Tsiplakides, 2012, PEM water electrolysis fundamentals. Accessed on 16 August 2016, http://research.ncl.ac.uk/sushgen/docs/summerschool_2012/PEM_water_electrolysis-Fundamentals_Prof._Tsiplakides.pdf.

Emmanuel Zoulias, Elli Varkaraki, Nicolaos Lymberopoulos, 2006, A REVIEW ON WATER ELECTROLYSIS, Accessed on 16 Aug 2016, http://www.cres.gr/kape/publications/papers/dimosieyseis/ydrogen/A%20REVIEW%20ON%20WATER%20ELECTROLYSIS.pdf.

Physics NIST, http://physics.nist.gov/MajResFac/NIF/camera.html. Accessed in Jan 2017.

Jacobson, D. 2004, Neutron Imaging Facility: PEM Fuel Cells. Accessed on 18 Aug 2016, http://physics.nist.gov/MajResFac/NIF/pemFuelCells.html.

Manfred Waidhas, Siemens AG, https://www.iea.org/media/workshops/2013/hydrogenroadmap/Session4.2WaidhasSiemens.pdf Accessed on 10 Aug 2016.

Murakawa Hideki, Katsumi Sugimoto, Nobuki Kitamura, Masataka Sawada, Hitoshi Asano, Nobuyuki Takenaka and Yasushi Saito, Visualization of water accumulation process in polymer electrolyte fuel cell using neutron radiography. Physics Procedia 69, (2015), 607 – 611.

US Department of Energy (DOE), https://www.hydrogen.energy.gov/roadmaps.html, Accessed on 10 June 2016.

CHAPTER 6

PUBLICATION:

Neutron and X-Ray Radiography/Tomography: Non-Destructive Analytical Tools for the Characterization of Nuclear Materials

Due to safety and contamination considerations, non-invasive analytical techniques for the investigation of certain materials from different phases of the nuclear fuel cycle become of considerable importance. Information can be gathered without prior sample preparation and consequential waste stream production. Neutron and X-ray radiography and tomography techniques have been successfully applied in the front end of the nuclear fuel cycle from the mining of minerals until their implementation as core materials in the assembly of nuclear fuel. Neutron radiography provides quantitative and qualitative information to determine fuel performance and has developed into an important quality control testing technique, and also for post irradiation examination (PIE) of nuclear fuel. Neutron radiography provides more comprehensive information regarding the internal condition of irradiated nuclear fuel than any other non-destructive technique. As a result, the understanding of the behaviour of nuclear fuels during irradiation and other transient conditions contributed to the development of safer and more efficient nuclear reactors. The availability of both neutron and X-ray tomography techniques in South Africa open new 3D imaging-based possibilities for research, quantitative analysis, and non-destructive evaluation. International trends are towards standardisation and utilisation of three-dimensional tomography and heading even deeper to the understanding of the performance of nuclear materials under reactor conditions. This chapter is a compilation of international activities and practical knowledge based at Necsa on the impact of neutron and X-ray radiography and tomography as analytical non-destructive techniques on important areas within the nuclear fuel cycle.

Neutron- and X-ray radiography/ tomography: non-destructive analytical tools for the characterization of nuclear materials

by F.C. de Beer*†

Synopsis

A number of important areas within the nuclear fuel cycle, both at the front-end and back-end, offer ideal opportunities for the application of non-destructive evaluation techniques. These techniques do not only provide opportunities for non-invasive testing of e.g. irradiated materials but also play an important role in the development of new materials in the nuclear sector. The advantage of penetrating radiation to be used as probe in the investigation and testing of nuclear materials makes e.g. X-ray and neutron radiography (2D) and –tomography (3D) suitable to be applied in various applications within the total nuclear fuel cycle. The unique and different interaction modes of the two radiation probes with materials provide several opportunities. Their complementary nature and analytical non-destructive character makes them most suitable for nuclear material analyses, analytic method development, and the evaluation of the performance of existing nuclear material compositions. This article gives an overview of the X-ray and neutron radiography/tomography applications in the field of nuclear material testing and highlights a few of the success stories. Several selected areas of application in the nuclear fuel cycle are discussed to illustrate the complementary nature of these techniques as applied to nuclear materials.

Keywords:
Neutron radiography; X-ray radiography; SAFARI-1; non-destructive testing

Introduction

During the development of new materials for the nuclear industry materials, testing and characterization are of outmost importance to maintain safety standards and reliability. No compromise on safety in the work place in any area within the total nuclear fuel cycle can be tolerated, and therefore most *in-situ* material characterization and testing is being conducted by certified and qualified personnel schooled in destructive- and non-destructive testing (DT and NDT) methods. Certification and qualification in NDT can be obtained through many training centres in South Africa in accordance with European-, American- and other international standards [SGS, n.d.; SAIW, n.d.; African NDT Centre, n.d.).

The testing of new methods and -materials related to the nuclear fuel cycle is essential for the continuing development and safety of nuclear related materials and processes. These fundamental research initiatives are mostly performed at laboratory scale by material- and instrument scientists, researchers and most likely post-graduate students.

Davies (2000) describes the role and value of NDT during maintenance and in-service inspection of nuclear power plants during outages and particularly the monitoring of material degradation to prevent failure. Ultrasonic testing (UT), magnetic testing (MT) and electric testing (ET) plays a major role as NDT-methods for monitoring materials degradation in situ, while atomic and nuclear physics-based methods such as positron annihilation, neutron diffraction as well as X-ray- and neutron tomography are limited to laboratory scale experimentation. However, conventional film based X-ray- and gamma-ray radiography (RT) techniques are being applied throughout many areas of material testing within the nuclear fuel cycle.

The 'nuclear fuel cycle' refers to the entire range of activities associated with the production of electricity from nuclear fusion, entailing (International Atomic Energy Agency, n.d.):

- Mining and milling: from mined uranium to yellowcake
- Conversion: from yellowcake to gas
- Enrichment: increases the proportion of the fissile isotope
- Deconversion: depleted uranium
- Fuel fabrication: UO_2 pellets – fuel pins – fuel elements
- Electricity generation: fuel burn-up
- Storage: spent fuel
- Reprocessing: spent fuel
- Radioactive waste: safe storage

The nuclear fuel cycle includes the 'front end', *i.e.* Preparation of the fuel, the 'service period' in which fuel is used in the reactor to generate electricity, and the 'back end', *i.e.* safe management of spent fuel including the reprocessing and reuse and disposal.

* *Radiation Science Department, Necsa, Pelindaba.*
† *School of Chemical and Minerals Engineering, North-West University, Potchefstroom.*
 ISSN 2225-6253. Paper received Aug. 2015 and revised paper received Aug. 2015.

The general nuclear fuel cycle is schematically depicted in Figure 1, showing the various activities in the production of energy through the nuclear fission process. Every activity requires conventional NDT techniques to be conducted to maintain the safe working and operation of the plants and facilities. The standard NDT methods applied to e.g. inspection of welds in piping, are (Willcox and Downes, n.d):

- ➢ Radiography testing (RT)
- ➢ Magnetic particle crack detection (MT)
- ➢ Dye penetrant testing (PT)
- ➢ Ultrasonic flaw detection (UT)
- ➢ Eddy current and electromagnetic testing (ET).

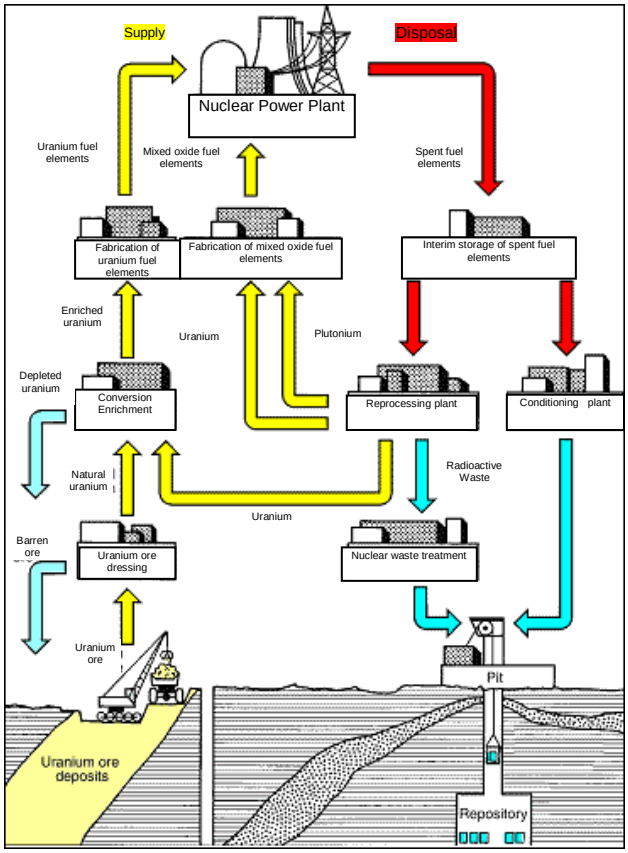

Figure 1 – Schematic depiction of the nuclear fuel cycle (Pixshark, n.d.)

This paper does not focus on the so-called conventional NDT techniques and their application in the nuclear sector, but rather on the non-conventional NDT techniques that are used as needed, and which constitute important research tools. In particular, penetrating radiation probes as realized in radiography/tomography are described with specific applications in material research. Quantitative and/or qualitative data obtained through applying these novel techniques in a laboratory environment adds value to many areas within the nuclear sector. The following specific activities, ranging from mining the ore to

security of the waste generated, and where radiography and tomography are applied, are highlighted in this paper:

- ➢ Mining and geosciences: quantification of ore deposits,
- ➢ Fuel fabrication: development and testing of new materials,
- ➢ Electricity generation: fuel rod performance; post-irradiation examination (PIE),
- ➢ Radioactive waste: safe storage, civil engineering.

Analytical methods based on penetrating radiation

Information about the internal structures of objects, for example the hydrogen content of Zr cladding, can be obtained by destructive analytical methods, e.g. cutting a fuel rod in a 2D plane for analysis by electron microscopy, or sieve analysis for particle size distribution of a soil sample. In most cases, once the sample has been destroyed, no other analytical tests are possible and the larger picture (volumetric hydrogen distribution and particle size distribution in the soil) is lost.

More valuable, unique, and in some cases more accurate results can be obtained only when three-dimensional information is available. For research purposes the most acceptable way to obtain information while maintaining the sample integrity is to apply a non-destructive test using penetrating radiation (either with X-rays, gamma rays, or neutrons). It is worthwhile to mention that the neutron, the fission product of the nuclear fuel cycle, can be used as a probe to investigate the integrity of the nuclear fuel itself. After irradiation the physical condition of fuel pellets, while still intact in the fuel pin, can be obtained only by means of radiography. This manner of non-invasive investigation keeps the sample intact, leaves the sample in its original form, and it is possible for other tests to be conducted subsequently on the real sample as if it was not touched. The non-invasive process allows for the generation of valuable qualitative information. However, when digital data is transformed into three-dimensional tomographic data (Banhard, 2008), it is possible to obtain high-resolution quantitative information of the internal structures and properties of the object. An example is the volumetric pore size distribution of voids within nuclear-encapsulating concrete matrixes, as well as their physical distribution throughout the sample (McGlinn et al., 2010). X-ray, gamma-ray, and neutron radiation are attenuated (absorbed and scattered by the sample) according to an exponential law (De Beer, Middleton, and Hilson, 2004):

$$I(E) = I_0(E)e^{\mu(E)\rho x} \qquad (1)$$

where I is the intensity of the transmitted radiation beam, I_0 the intensity of the incident radiation beam, μ the attenuation coefficient (cm^2/g) of the material under investigation for the specific radiation type, ρ the density of the sample (g/cm^3) and x the thickness of the sample (cm).

The attenuation coefficient μ expresses the total attenuation, due to both the scattering and capture processes for the incident radiation. The term μρ is also called the total absorption coefficient of the sample. We assume that the quantity μρ is linearly related to its constituents:

$$\mu\rho = \sum (\mu_i)(\rho_i)(V_i) \qquad (2)$$

where μ_i is the radiation attenuation coefficient of constituent i; ρ_i the density of constituent i; V_i the volume fraction of constituent i, and Σ the summation symbol for the i^{th} components.
Compositions of materials will thus have a different radiation attenuation property from the individual elements.

The parameters *I*(*E*), *I*0(*E*), and μ(*E*) reflect radiation energy dependency. This dependency, in a radiography context, means that materials will attenuate different radiation types by different magnitudes and thus will yield different radiological images, and also that an element has different attenuation properties at different energy levels for the same radiation type. This implies that an element can be transparent to fast neutrons (MeV energies) but can be detected easily using thermal neutrons (eV energies). An example is the thermal neutron scattering and absorption of hydrogen and boron (Domanus, 1992).

Although the basic interaction of X-rays and neutrons with the elements differs, the principle of conducting radiography to obtain a two-dimensional radiograph/image of the sample is the same. Figure 2 schematically illustrates the basic components and layout of a radiography facility.

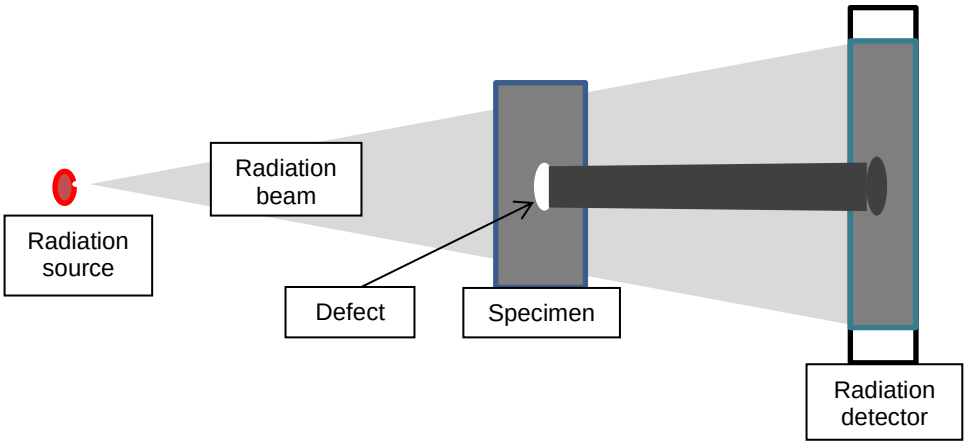

Figure 2 - Principle and layout of a 2D radiography set-up. A similar setup is used for tomography, with the sample rotating in the radiation beam (Domanus, 1992)

A source of radiation emits penetrating radiation towards a sample. For example, a sample contains either a defect, an inclusion of another material, or a void that is abnormal for the sample, or an area that differs completely in terms of composition from the basic matrix of the sample, which results in a lower or higher density at the location within the sample. The incident radiation will be attenuated (scattered

and/or absorbed) differently due to the abnormality. A sensitive area detector, with a high quantum efficiency for the detection of the specific type of penetrating radiation, registers the difference in attenuated radiation that has passed through the sample. The 2D data (image) obtained by the detector is called a radiograph and contains the integrated radiation transmitted information for the total sample in a certain orientation with respect to the source and detector configuration.

The information captured in the radiograph differs in principle for X-ray and neutron radiography/tomography. The two probes are mostly utilized within the nuclear fuel cycle as non-destructive techniques in research and for nuclear material qualification and quantification. These principles are discussed in more detail in the following paragraphs.

X-ray radiography

X-ray interaction with materials depends on the density of the sample – *i.e.* the electron cloud density (Banhard, 2008). The area detector registers a two-dimensional image (radiograph) of the object representing the internal structure density. Elements with low electron densities are not easy to resolve in a radiograph, but they are easily penetrated to reveal denser materials embedded within the sample matrix. Figure 3 presents the different X-ray attenuation coefficients (cm^{-1}) for 125 kV X-rays for the full spectrum of elements in the periodic table. It clearly shows an increase in absorption of X-rays (darker shading) at higher atomic numbers.

Attenuation coefficients for 125kV X-Rays (cm^{-1})

1a	2a	3b	4b	5b	6b	7b	8	1b	2b	3a	4a	5a	6a	7a	0
H 0.02															He 0.02
Li 0.06	Be 0.22									B 0.28	C 0.27	N 0.11	O 0.16	F 0.14	Ne 0.17
Na 0.13	Mg 0.24									Al 0.38	Si 0.33	P 0.25	S 0.30	Cl 0.23	Ar 0.20
K 0.14	Ca 0.26	Sc 0.48	Ti 0.73	V 1.04	Cr 1.29	Mn 1.32	Fe 1.57	Co 1.78	Ni 1.96	Cu 1.97	Zn 1.64	Ga 1.42	Ge 1.33	As 1.50	Se 1.23	Br 0.90	Kr 0.73
Rb 0.47	Sr 0.86	Y 1.61	Zr 2.47	Nb 3.43	Mo 4.29	Tc 5.06	Ru 5.71	Rh 6.08	Pd 6.13	Ag 5.67	Cd 4.84	In 4.31	Sn 3.98	Sb 4.28	Te 4.06	I 3.45	Xe 2.53
Cs 1.42	Ba 2.73	La 5.04	Hf 19.70	Ta 25.47	W 30.49	Re 34.47	Os 37.92	Ir 39.01	Pt 38.61	Au 35.94	Hg 25.88	Tl 23.23	Pb 22.81	Bi 20.28	Po 20.22	At	Rn 9.77
Fr	Ra 11.80	Ac 24.47	Rf	Ha													

Lanthanides	Ce 5.79	Pr 6.23	Nd 6.46	Pm 7.33	Sm 7.68	Eu 5.66	Gd 8.69	Tb 9.46	Dy 10.17	Ho 10.91	Er 11.70	Tm 12.49	Yb 9.32	Lu 14.07
*Actinides	Th 28.95	Pa 39.65	U 49.08	Np	Pu	Am	Cm	Bk	Vf	Es	Fm	Md	No	Lr x-ray

Figure 3 - Periodic table with X-ray attenuation coefficients of the elements for 125 kV X-ray energies (Grùnauer, 2005)

Neutron radiography

The interaction of neutrons with materials is totally different to that of X-rays, since neutrons, being neutral particles, interact only with the nucleus of the atom. Neutrons are not affected by even a dense electron cloud, *e.g.* of a lead atom ($\mu\rho_n$ = 0.38 cm^{-1}). The thermal neutron attenuation coefficients depicted in Figure 4 shows a totally different, and in some instances an opposite attenuation capability (grey scale) to that of X-rays (Figure 3). Hydrogen, as a highly attenuating material ($\mu\rho_n$ = 3.44 cm^{-1}), will be easy to detect and clearly visible on a neutron radiograph when embedded in *e.g.* a ZrTM ($\mu\rho_n$ = 0.29 cm^{-1}) fuel pin, which is nearly transparent to neutrons. A radiograph with low- to intermediate-energy X-rays is possible as the ZrTM tube ($\mu\rho_X$= 2.47 cm^{-1}) attenuates most of the X-ray radiation and with no photons remaining, the H ($\mu\rho_X$ = 0.02 cm^{-1}) cannot be registered/detected on the X-ray radiograph.

Tomography

Attenuation coefficients for Thermal Neutrons (cm^{-1})

1a	2a	3b	4b	5b	6b	7b	8			1b	2b	3a	4a	5a	6a	7a	0
H 3.44																	He 0.02
Li 3.30	Be 0.79											B 101.60	C 0.56	N 0.43	O 0.17	F 0.20	Ne 0.10
Na 0.09	Mg 0.15											Al 0.10	Si 0.11	P 0.12	S 0.06	Cl 1.33	Ar 0.03
K 0.06	Ca 0.08	Sc 2.00	Ti 0.60	V 0.72	Cr 0.54	Mn 1.21	Fe 1.19	Co 3.92	Ni 2.05	Cu 1.07	Zn 0.35	Ga 0.49	Ge 0.47	As 0.67	Se 0.73	Br 0.24	Kr 0.61
Rb 0.08	Sr 0.14	Y 0.27	Zr 0.29	Nb 0.40	Mo 0.52	Tc 1.76	Ru 0.58	Rh 10.88	Pd 0.78	Ag 4.04	Cd 115.11	In 7.58	Sn 0.21	Sb 0.30	Te 0.25	I 0.23	Xe 0.43
Cs 0.29	Ba 0.07	La 0.52	Hf 4.99	Ta 1.49	W 1.47	Re 6.85	Os 2.24	Ir 30.46	Pt 1.46	Au 6.23	Hg 16.21	Tl 0.47	Pb 0.38	Bi 0.27	Po	At	Rn
Fr	Ra 0.34	Ac	Rf	Ha													

*Lanthanides	Ce 0.14	Pr 0.41	Nd 1.87	Pm 5.72	Sm 171.47	Eu 94.58	Gd 1479.04	Tb 0.93	Dy 32.42	Ho 2.25	Er 5.48	Tm 3.53	Yb 1.40	Lu 2.75
**Actinides	Th 0.59	Pa 8.46	U 0.82	Np 9.80	Pu 50.20	Am 2.86	Cm	Bk	Cf	Es	Fm	Md	No	Lr neut.

Figure 4 - Periodic table with thermal neutron energy attenuation coefficients of the elements (Grünauer, 2005)

The word 'tomography' comes from the Greek words 'to cut or section' (*tomos*) and 'to write' (*graphein*) (Banhard, 2008). Tomography is also known as computer tomography (CT) or computer assisted tomography (CAT) as in diagnostic investigations in the medical field. For the purpose of this article, the following semantics are adopted: CT in general description, XCT for X-ray computer tomography, and NT for neutron tomography. CT is a radiographic inspection method that uses a computer to reconstruct an image of a cross-sectional plane (slice) through an object (ISO 15708-1). The resulting cross-sectional image is a quantitative map of the linear radiation attenuation coefficient, μ, at each point in the plane. The linear attenuation coefficient characterizes the local instantaneous rate at which the incident radiation is attenuated during the scan, by scatter or absorption, as it propagates through the object.

To obtain this 'map', the sample is radiographed and thus projection data is gathered from multiple directions through many angles of the sample. For the purpose of this article, no detailed

description of the 3D reconstruction process of the sample is presented. To put it simply, multiple 2D-projections are fed into a dedicated computer with a specialized computer algorithm to create cross-sectional planes of the sample. When these cross-sectional planes are stacked together, a full virtual three-dimensional image (tomogram) of the sample can be viewed and analyzed.

Application of radiography and tomography within the nuclear fuel cycle

In each of the following sectors of the nuclear fuel cycle, radiography and/or tomography have been applied using either X-rays or neutrons. In some areas the application was pioneered in the early second half of the 20th century by means of film techniques. The techniques applied and the description thereof is not within the scope of this article. However, the outcomes of these film-based investigations and the results obtained will be described, together with the recent digital methods in this field.

Mining

X-ray-, gamma-ray, and neutron tomography have demonstrated their potential in the earth sciences as important diagnostic tools to generate volumetric data on geological compositions, especially advances in the area borehole core investigations, as depicted in Figure 5. This aspect is being explored further with optimum resolution obtained through the application of micro-focus X-ray tomography, as CT complements conventional destructive analytical thin-sectioning of drill core samples (De Beer and Ameglio, 2011).

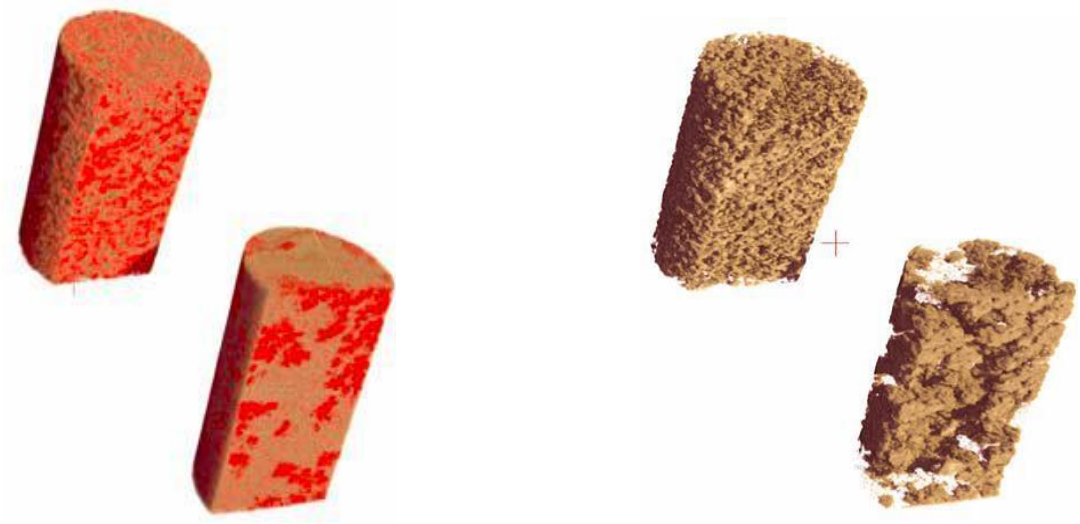

Figure 5 - Left): the grouped pyroxines mineral (coloured red) can be clearly seen in norite (top) and different concentration of feldspar are observed in anorthosite (bottom) in a thin slice. RIGHT (TOP & BOTTOM) Right: transparent corresponding neutron tomograms. The minerals shown are only pyroxenes that are present in both norite and anorthosite but at different concentrations [Archives from Necsa's Nrad and MIXRAD system]

The

raw material for nuclear fuel is uranium, which is a relatively common element that can be found throughout the world. Uranium is present in most rocks and soils, in many rivers, and in seawater. Uranium is about 500 times more abundant than gold and about as common as tin.

The largest producers of uranium are currently Australia, Canada, and Kazakhstan, with Namibia rated 5th and South Africa 11th globally (World Nuclear Association, 2015). The concentration of uranium in the ore can range from 0.03 to 20%. Conventional mining is by open cut or underground methods. Uranium ore can be produced from a mine specifically for uranium, or as a by-product from mines with a different main product such as copper, phosphate, or gold (International Atomic Energy Agency, n.d.).

Using micro-focus X-ray CT with 100 kV potential to distinguish between gold ($\mu\rho_X$ = 358 cm^{-1}) and uraninite ($\mu\rho_X$ = 283 cm^{-1}), both the minerals are easy to distinguish from the matrix minerals such as pyrite ($\mu\rho_X$ = 18.4 cm^{-1}), zircon ($\mu\rho_X$ = 45.9 cm^{-1}), and brannerite ($\mu\rho_X$ = 89.6 cm^{-1}) due to their much higher elemental densities. The use of CT as a sorting method is still a challenge, as it is difficult, at the 100 kV X-ray energy CT capability available, to distinguish between gold and uraninite (Chetty *et al.*, 2011). In a follow-up 3D micro-focus X-ray computer tomography (μXCT) study using 120 kV, the contrast and resolution of the minerals were well defined and individual minerals could be separated and distinguished from other minerals (Sebola, 2014). For the detection of uranium, 3D-CT was benchmarked against 2D mineralogical results from optical microscopy and scanning electron microscopy (SEM). Uraninite, brannerite, and uraniferous leucoxene are the uranium-bearing minerals present in the samples (from the Vaal Reef) and were quantified by μXCT-3D analysis for their sizes, shapes, and distribution with respect to other mineral components in the samples. Uraninite was found to be the major mineral, occurring mainly in the quartz matrices and also associated with carbonaceous matter as depicted in Figure 6. The uraninite and gold in the matrix occurred as rounded grains of up to 200 μm in size, as

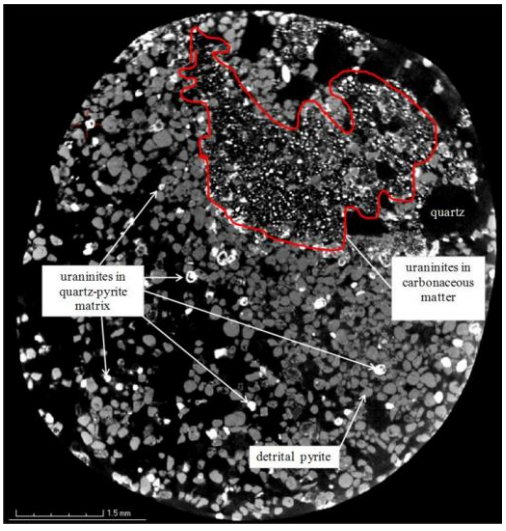

Figure 6 - X-ray CT-tomogram slice showing the distribution of uraninite grains in the quartz-pyrite matrix and the carbonaceous matter (Sebola,2014)

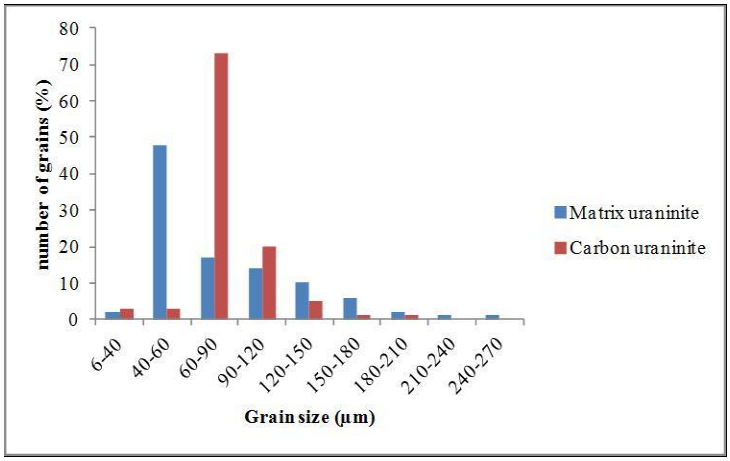

Figure 7 – Grain size distribution of uraninite in the matrix and the carbonaceous matter (Sebola,2014)

observed by 2D mineralogical techniques. CT allows for 3D grain size analyses of the uraninite grains in the total volume of the sample, and in this study also their association with matrix minerals, as depicted in Figure 7.

The CT observations supported the results acquired by conventional mineralogical techniques, suggesting that 3D μXCT can be used to complement other mineralogical techniques in obtaining 3D information. However, 3D μXCT has limitations such as spatial resolution, partial volume effect, and overlapping of mineral grey-scale values. It is therefore suggested that the technique cannot be used as an independent tool for mineral characterization, but rather in support of existing mineralogical techniques. However, valuable information is added into the nuclear value chain via 3D-CT. No sample preparation is needed other than cutting a small piece of rock for analysis. The sample integrity is maintained due to the non-destructive nature of the technique, as it provides 3D information for the total volume of the sample, including internal components. Results can be obtained within about 1 hour scan at high resolution with up to 2000 projections, providing resolution down to 6 μm (including reconstruction).

Enrichment

Enriched uranium is uranium in which the concentration of U-235 has been increased through the process of isotope separation. U-235 is the only nuclide existing in nature (in any appreciable amount) that is fissile with thermal neutrons (OECD Nuclear Energy Agency, 2003). Natural uranium is 99.284% U-238 isotope, with the U-235 isotope constituting only about 0.711%.

The very first application of neutron radiography was in the early 1960s for nuclear fuel characterization using the film technique. The use of neutron radiography in the monitoring of isotopic enrichment in fuel pellets loaded into a fuel pin has been demonstrated by Frajtag (n.d.) (Figure 8).

Figure 8 - Neutron radiograph (film) of fresh fuel pellets in a fuel pin with varying degrees of isotopic U-235 enrichment. Pellets loaded with higher enrichment appear darker (Frajtag, n.d.)

Gosh, Panakkal, and Roy (1983) investigated the possibility of monitoring plutonium enrichment in mixed oxide fuel pellets inside fuel pins using neutron radiography as early as 1983. Recently, Tremsin *et al.*, (2013) investigated the very large difference in the absorption cross sections of U-235 and U-238 isotopes, as shown in Figure 9, and deduced that very accurate non-destructive spatial mapping of the enrichment level of fuel pellets, as well as of the distribution of other isotopes in the spent fuel elements (Nd, Gd, Pu, *etc*.), can be achieved.

Additionally, information on the distribution of isotopes can then be used for the investigation of fuel burn-up rates for fuel elements placed at different rod positions in the reactor core.

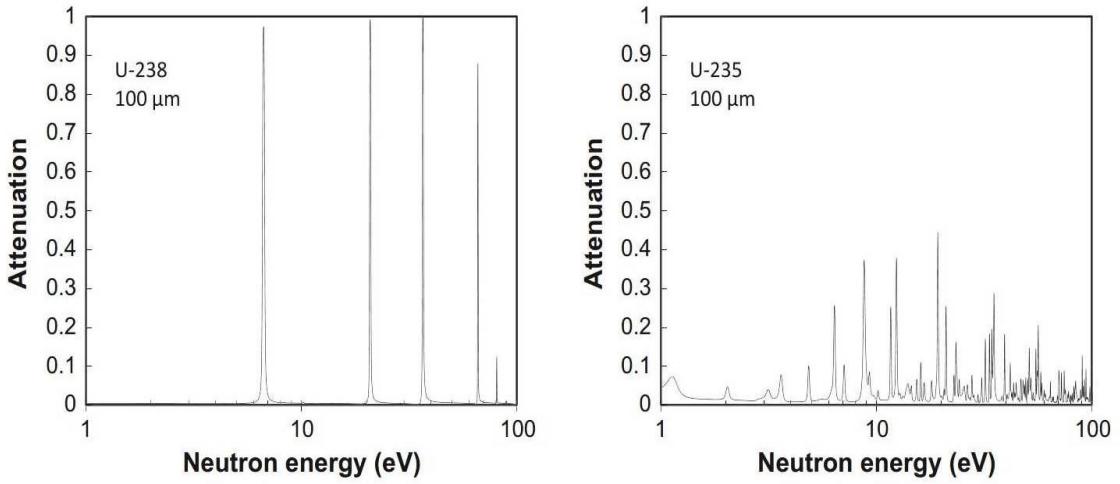

Figure 9 - Neutron attenuation of 100 micron thick U-235 and U-238 isotopes calculated from the tabulated data on the total cross sections as a function of neutron energy (Tremsin *et al*., 2013)

Large differences in transmission spectra allow very accurate mapping of isotopic distributions in the samples using either transmission radiography or neutron resonance absorption characteristics of the respective isotopes (Tremsin *et al.*, 2013). One of the attractive features of energy-resolved neutron radiography is the ability to enhance contrast, and in some cases enable quantification, as shown in Figure 10. It was observed that the contrast between the pellets of different density depends strongly on the range of neutron energies used. The more thermal part of the beam spectrum (neutron energies above 19.7 MeV) reveals the pellet with the lowest density as an object with the highest transmission. The coldest part of the neutron spectrum (neutron energies even below 6 MeV) shows the least dense pellet as the darkest in the assembly.

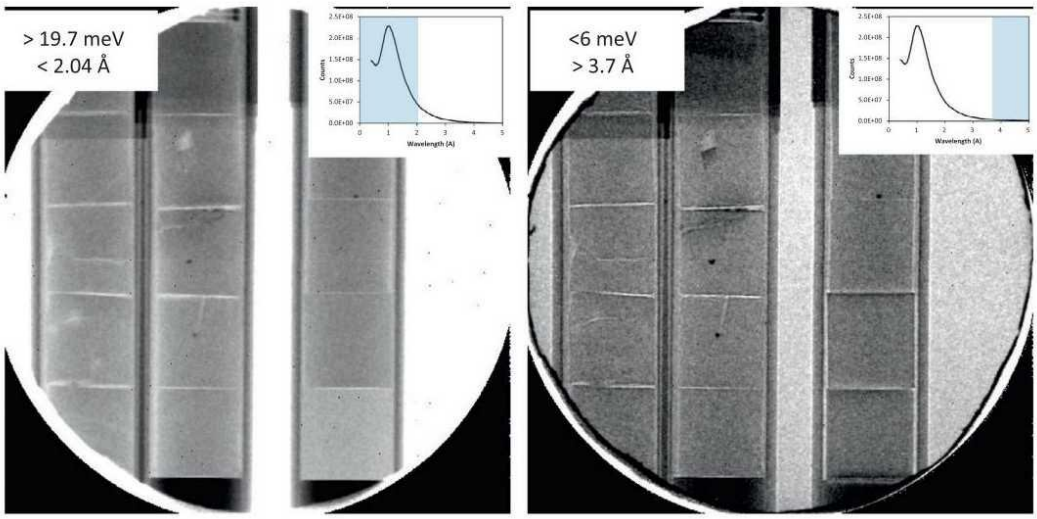

Figure 10 - Thermal neutron transmission radiographs obtained by grouping the energy resolved images of different neutron spectra. The ranges of neutron energies used to build each radiograph are shown in the respective legends (Tremsin *et al*., 2013)

Nuclear fuel fabrication and testing (I & PIE)

Nuclear fuel types range from isotopic sources in a form of salt or disks to pressurized water reactor (PWR) fuel in the form of UO2 fuel pellets inside ZrTM -cladded fuel pins. Nuclear fuel is subjected to stringent manufacturing and performance criteria which have to be verified. Nondestructive testing of the fuel ensures that other tests can be performed subsequently and that the material can still be applied in its specific environment. Some of the NDT tests are applied to characterize and/or quantify the integrity of the fuel or as quality assurance tests. X-ray radiography cannot be used for irradiated fuel inspection, whereas neutron radiography becomes possible due to the following reasons (Lehmann, Vontobel, and Hermann, 2003):

- Uranium has a very high attenuation coefficient for X-Rays (about 50 cm^{-1} at 150 keV). The diameter of fuel pellets is in the order of 10 mm and penetration by X-Rays is impossible. High-energy gamma radiation (>1 MeV) is, however, suitable for quality control of fresh fuel pellets.
- The neutron attenuation coefficient for the natural composition of uranium is low (0.8 cm^{-1}) and it is easy to transmit neutrons through thicker assemblies.
- U-235 and U-238 have very different interactions with thermal neutron beams. Due to the 60 times higher cross-section of U-235, it is very easy to distinguish between the two isotopes and to quantify the amount of the fissile isotope U-235.
- Lead is used as shielding material around fuel samples for radiation protection purposes, and thus X-ray radiography fails in transmission experiments. Neutrons, on the other hand, penetrate lead shielding with a thickness of about 15 cm and allow neutron radiography investigations.
- Additional substitutes in fuel compositions, which are in use as burnable poisons but are strong neutron absorbers (*e.g.* B, Li-6, Dy, or Gd), are easily identified with neutron methods.
- After long-term exposure, hydrogen can be found in the cladding outer region of fuel rods under some circumstances. X-ray radiography fails to visualize these material modifications because of the very low contrasts obtained for elements with low atomic numbers. Neutrons, on the other hand, have a high sensitivity for hydrogen, thus allowing quantification of the hydrogen content in cladding.

Isotopes

Characterization of isotopic sources is a demanding and difficult task due to their physical size and natural radioactivity, which makes visual inspection impossible. Hoffman (2012) investigated a small radioactive radium source using high-resolution micro-focus X-ray tomography to determine whether the sample contained a powdered form of radioactive material or whether it was solid. The source contained 20 mg of radium and was in the form of a needle with a diameter of about 1 mm and about 8 mm in length – all sealed within a glass tube.

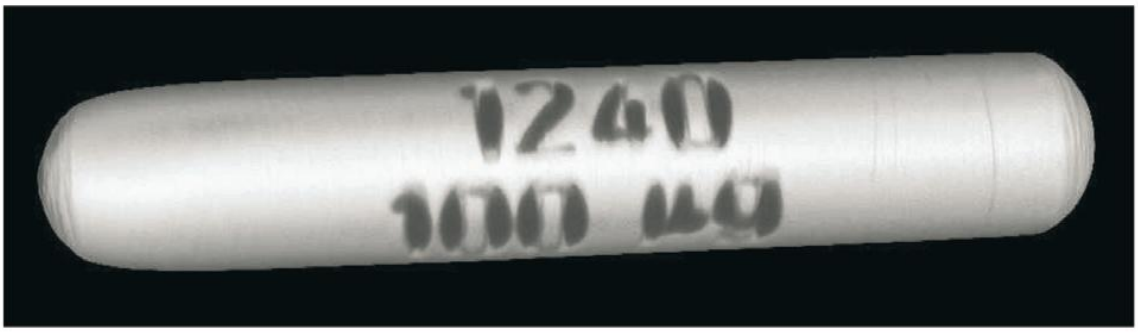

Figure 11 - µXCT of a Ra-isotope source ampule (Hoffman, 2012)

Figure 11 is an XCT tomogram of the ampoule showing its serial number clearly on the outside, while Figure 12 is a slice from the 3D tomogram revealing the position of the radioactive material inside the needle.

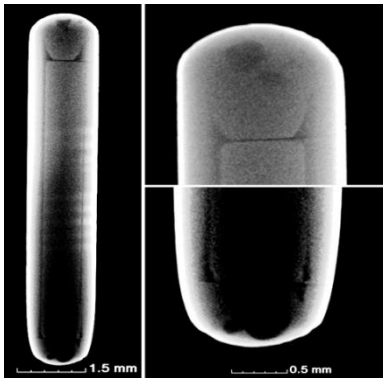

Figure 12 - Slice of µXCT tomogram with enlarged end pugs revealing Ra-isotope internal information (Hoffman, 2012)

Table-I: Quantitative information deducted from the XCT

Description: Information	Value	Unit
Needle inscription	100	µg
Official source activity	20	mCi
Contact dose rate	1.1	mSv/h
Diameter of tube	1.67	mm
Diameter of internal void	1.03	mm
Length of tube	9.72	mm
Length of internal void	7.57	mm
Wall thickness	0.34	mm
Length of salt	3.01	mm
Inner Volume	**6.31**	**mm^3**
Volume of salt	2.51	mm^3

Valuable metrology quantitative information could be deducted from the 3D tomogram of the isotope (Table I). The most important aspect for further processing of the isotope is the quantification of the volume of radioactive salt present in the needle.

Nuclear fuel

A major field of neutron radiography application is the inspection of nuclear fuel and control rods, reactor materials and components, and of irradiation devices for the testing of nuclear fuels and materials. The fuel rods are used under extreme conditions such as very high power density, temperature, pressure, and radiation level. Thermal neutron radiography investigations were conducted with the conventional film technique due to the radioactivity of the objects. The following issues are addressed through the use of neutron radiography: (a) condition of the fuel assembly, including fuel rod condition, (b) detection of leaks such as ingress of water, and (c) quality control, including functional and dimensional evaluation

and inspection of irradiation devices and components. Figure 13 shows a neutron radiograph of a fuel pin with pelletized fuel as fabricated (Domanus, 1992).

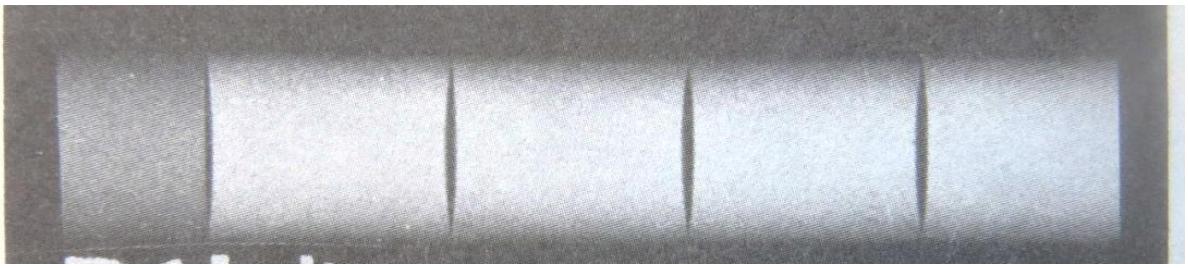

Figure 13 - Neutron radiograph of nuclear fuel prior to irradiation (Domanus, 1992)

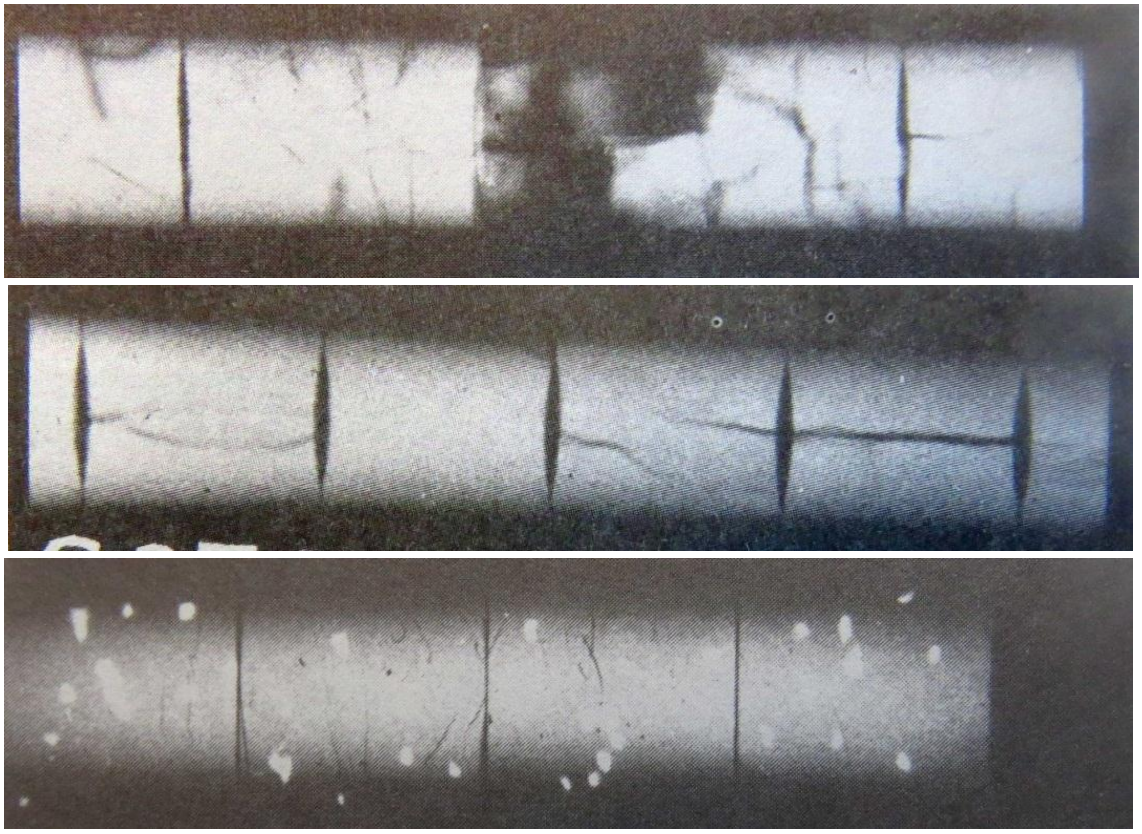

Figure 14 - Neutron radiographs (film prints) of irradiated nuclear fuel and their conditions (Domanus, 1992). Top: Random cracks in pellets Middle: Typical longitudinal cracks in pellets Bottom: Inclusions (white spots) of Pu in pellets

Due to the high radioactivity of nuclear fuel after irradiation, X-ray radiography cannot be used as an investigation technique. Investigations are done within a hot-cell laboratory set-up, which allows for the remote handling of the radioactive fuel (Klopper, De Beer, and Van Greunen, 1998). A research reactor is normally an extension of a hot cell laboratory, as neutron radiography is one of the major analytical probes in the post-irradiation examination (PIE) of nuclear fuel. Typical findings using neutron radiography as an analytical probe on irradiated fuel pins are the condition of the fuel pellets and of the ZrTM -cladding material.

Fuel pellet investigations reveal fabricated conditions such as cracks, chips, change of shape or location, voids, inclusions, corrosion, nuclear properties, and coolant. Figure 14 shows examples of these findings on film neutron radiographs.

Domanus (1992) describes a number of other fuel pellet properties revealed by neutron radiography, including centralvoids and the accumulation of Pu in the central void. Fuel rod inspections include deformed cladding, hydrides in cladding, plenum and spring, dislocated disks, condition of the bottom plug, and a picture of a melted thermocouple inside the fuel rod. Lehmann, Vontobel, and Hermann (2003) report on the extensive utilization of the NEUTRA and ICON neutron radiography (Nrad) facilities at Paul Sherrer Institute in Switzerland, where a dedicated detection station is available for the inspection of irradiated fuel assemblies. Aspects such as fuel enrichment, fuel poisoning, and hydrogen content in the fuel cladding are being addressed and investigated by neutron radiography. Due to the importance of fuel cladding investigations, the utilization and function of neutron radiography is addressed in the following paragraph.

Hydrogen embrittlement

It is well known that hydrogen agglomeration is deleterious in any material. More than a few hundred ppm hydrogen in the cladding surface of fuel rods compromises the structural stability of the cladding tube significantly, with the consequence of possible failure, especially when mechanical loading is also involved. The ability of neutrons to penetrate uranium is considerably higher than for X-rays and allows for the structures of the nuclear fuel rods to be inspected.

Furthermore, the probability of neutron interaction with hydrogen is very high, while for X-rays it is effectively zero. This allows neutron radiography to be effectively utilized for the study of even small quantities of hydrogen ingress in the cladding, which is an important mechanism for cladding embrittlement, as depicted in Figure 15.

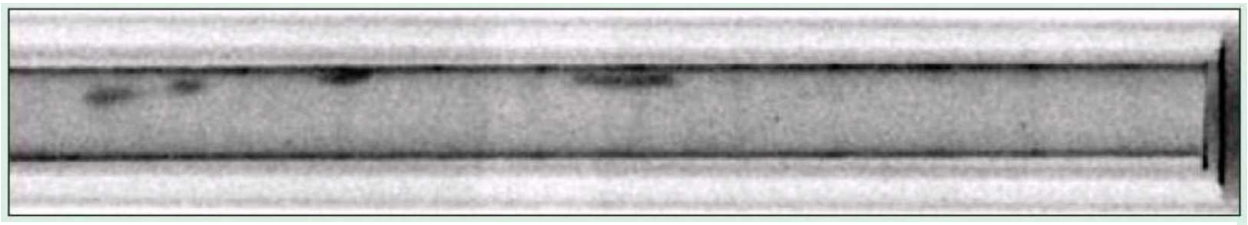

Figure 15 - Neutron radiograph of nuclear fuel and cladding material showing (black spots) hydrogen accumulation within the Zr^{TM} -tubing (Frajtag, n.d.).

Furthermore, through proper characterization and with the aid of digital radiographs, Nrad allows for the investigation of the absolute hydrogen content and its distribution. *In situ* investigations provide new information about the kinetics of hydrogen uptake during steam oxidation and of hydrogen diffusion in zirconium alloys. Nrad-studies are the only way to investigate and understand the phenomenon of hydrogen ingress in the ZrTM cladding. A linear dependence of the total macroscopic neutron cross-

section on the H/ZrTM atomic ratio, as well as on the oxygen concentration, was found, while no significant temperature dependence of the total macroscopic neutron cross-sections of hydrogen and oxygen was found, depending on zirconium and oxygen not to change their structures. Additionally, it was found that rapid hydrogen absorption takes place in the absence of the oxide layer covering the metallic surface of the ZrTM cladding (Grosse *et al.*, 2011). Figure 16 displays the results of *in-situ* Nrad

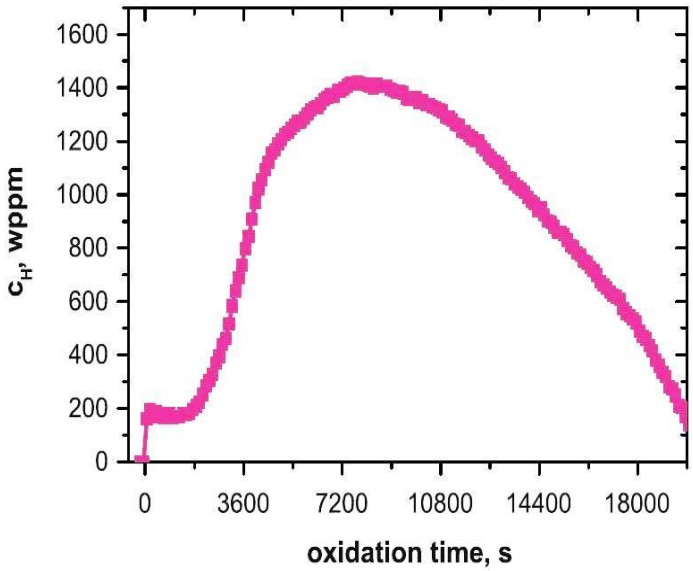

Figure 16 - Neutron radiography (Nrad) investigation: kinetics of hydrogen uptake and release during steam oxidation (Frajtag, n.d.)

investigations of hydrogen uptake during steam oxidation with the time dependence of hydrogen concentration of ZrTM-4 materials at 1273 K and higher, where a very rapid hydrogen uptake was found in the first couple of seconds after the steam flow was switched on.

At temperatures of about 1273 K a phase transformation occurs and is accompanied by a volume change and the formation of a pronounced crack structure. When the cracks are formed, the hydrogen uptake increases by nearly an order of magnitude (Grosse *et al.*, 2008; Grosse, 2010). The decrease in hydrogen concentration is due to the consumption of the ß-ZrTM phase, which contains most of the absorbed hydrogen.

Pebble bed modular reactor (PBMR) fuel

Figure 17 shows the composition of a 60 mm outer diameter high-temperature reactor (HTR) fuel pebble consisting of thousands of 0.5 mm diameter low-enriched uranium oxide fuel particles with a tri-structural isotropic (TRISO) coating, embedded in a graphitic matrix. The pebble was analyzed using the X-ray tomography technique prior to irradiation at the SANRAD facility located at the SAFARI-1 nuclear research reactor in South Africa. The aim of the investigation was to observe the homogeneity of the TRISO particles within the carbon matrix and to direct the manufacturing process to ensure the centralization of the fuel within the carbon matrix (Necsa, 2006). Figure 18 shows the misalignment of

the fuel within the carbon matrix of the fuel pebble as well as the location and identification of a TRISO particle within the fuel-free zone. The inhomogeneous distribution of the TRISO particles at the top of the fuel pebble can be clearly seen. Three-dimensional quantitative data of the misalignment of the fuel

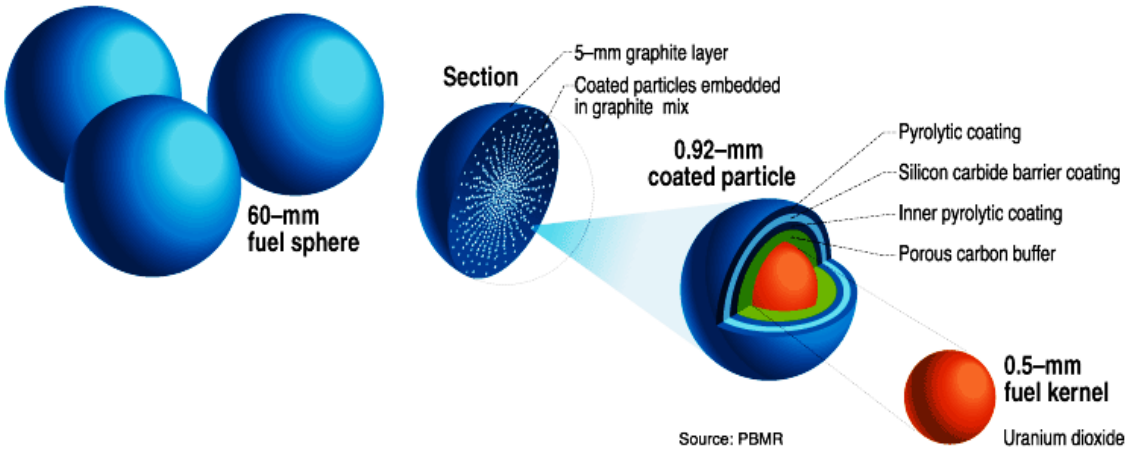

Figure 17 - Composition of PBMR-fuel (Weil, 2001)

particles becomes available in the tomograms and is presented in Figure 19, showing the extent of correction in X-, Y- and Z-directions to be introduced in the manufacturing process of the fuel pebble.

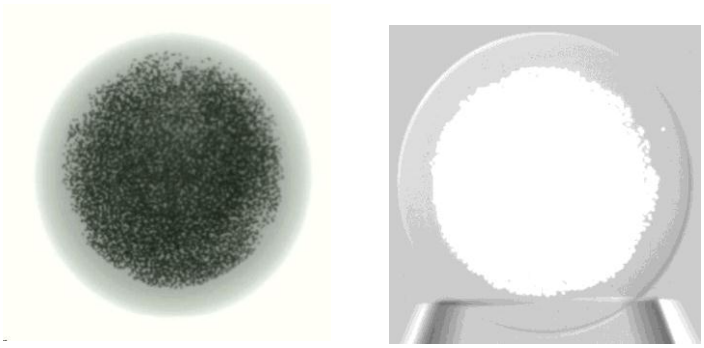

Figure 18 - X-ray tomography of a PBMR fuel pebble. Left: the non-centralized fuel sphere within the carbon matrix. Right: Location and identification of a TRISO particle inside the fuel-free zone (Necsa, 2006)

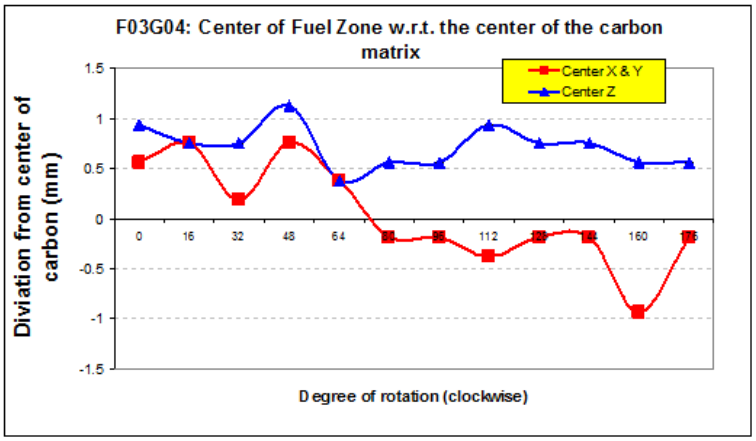

Figure 19 – Graphical presentation of the deviation of the fuel zone of a BPMR pebble from the centre of the carbon matrix in three dimensions (Necsa, 2006)

Lehmann, Vontobel, and Hermann (2003) reported the successful application of neutron tomography to the 3D scanning of PBMR fuel pebbles at the NEUTRA facility of the SINQ spallation source at PSI in Switzerland (see Figure 20). A sphere-type fuel element from the high-temperature reactor (HTR) programme was studied with neutron tomography. This sample is 6 cm in diameter and contains about 8500 individual fuel pebbles (diameter 0.5 mm). No shielding of the fresh fuel element was necessary for the tomographic inspection. The investigation was aimed at the visualization of the 3D distribution of the fuel particles in the graphite matrix in order to determine its uniformity and the fuel sphere's content of fissile material.

TRISO fuel particles are an integral part of the fuel design for current and future HTRs. A TRISO particle comprises four concentric spherical layers encasing a fuel kernel, namely the buffer (porous carbon), inner pyrolytic carbon (IPyC), silicon carbide (SiC), and outer pyrolytic carbon (OPYC) layers (see Figure 17). Each layer performs specific functions. The fuel kernel, consisting of uranium or uranium carbide, provides the fissile material and retains some of the fission products. The buffer layer, a highly porous carbon structure, provides some free volume for gaseous fission products, and protects the SiC layer from damage by high-energy fission products. The IPyC layer provides structural support for the subsequent SiC layer and prevents the chlorine compounds required for SiC deposition interacting with the fuel kernel. The SiC layer forms the main diffusion barrier for fission products. It acts as a pressure vessel, providing mechanical strength for the particle during manufacture of the nuclear fuel compact or pebble bed. The OPyC layer protects the SiC layer during fuel fabrication as the TRISO particle is pressed into a larger fuel compact or pebble.

Lowe *et al.,* (2015) examined the applicability of multiscale X-ray computer tomography (CT) for the non-destructive quantification of porosity and thickness of the various layers of TRISO particles (see Figure 21) in three dimensions, and compared this to the current destructive method involving high-resolution SEM imaging of prepared cross-sections.

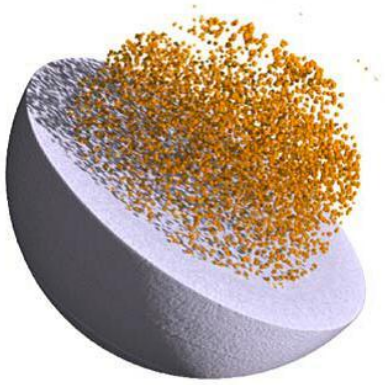

Figure 20 – Neutron tomogram generated at PSI, Switzerland showing the exact location and homogeneity of the TRISO (Lehmann, Vontobel, and Hermann, 2003)

An understanding of the thermal performance and mechanical properties of TRISO fuel requires a detailed knowledge of pore sizes, their distribution, and interconnectivity. Pore size quantification (false colour coding) and distribution in an X-ray tomogram of the SiC (D) and OPyC (E) layers within a TRISO particle is shown in Figure 22.

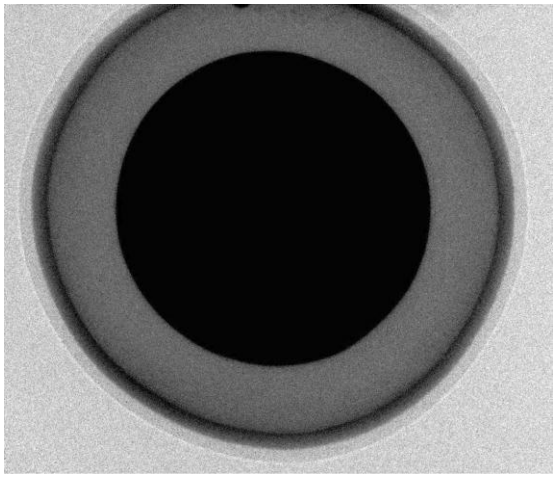

Figure 21 – Micro-focus X-ray radiograph of a TRISO particle (Necsa)

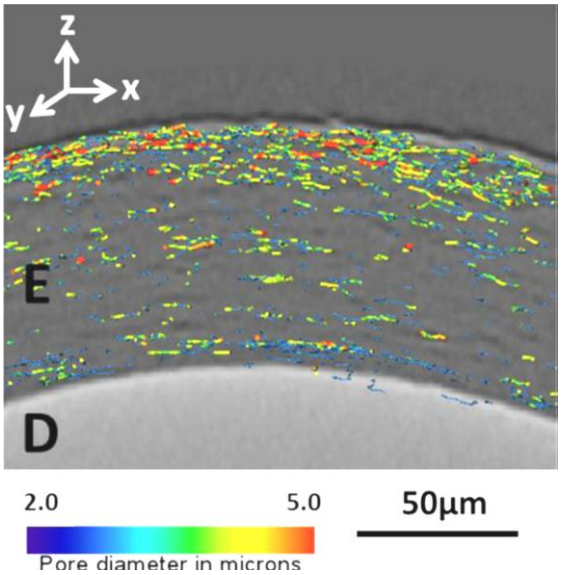

Figure 22 – Xradia VersaXRM orthoslice showing the SiC (D) and OPyC (E) layers with the pore volumes superimposed. Pore diameter is colourcoded to identify large pore clustering (Lowe et al., 2015)

Direct comparison with SEM sections indicates that destructive sectioning can introduce significant levels of coarse damage, especially in the pyrolytic carbon layers. Since it is non-destructive, multi-scale time-lapse X-ray CT opens the possibility of intermittently tracking the degradation of TRISO structure under thermal cycles or radiation conditions in order to validate models of degradation such as kernel movement. Xray CT *in situ* experimentation on TRISO particles under load and temperature could also be used to understand the internal changes that occur in the particles under accident conditions.

Research reactor control rod verification

Nrad is being applied as a verification and analytic technique at the SAFARI-1 nuclear research reactor on the control rods prior to their installation in the core of the reactor. The quality control assurance test entails the verification of the neutron attenuation cross-section of the control rod against a standard consisting of Cd. The inspection entails a visual clarification of the attenuation of the thermal neutrons by inspection of the neutron radiograph of the control rod. Additionally, due to the digital radiography capability of the neutron camera detection system, the first-order neutron transmission calculation can be made using the pixel greyscale values on the radiographs of both the standard and control rod sample. Pixel greyscale values represent a linear relationship in the neutron attenuation of materials. In this instance a dramatic decline in greyscale pixel values is seen due to the high thermal neutron absorption by

the Cd section ($\mu\rho_n$ =115.11cm^{-1}) of the control rod. Neutron radiographs of the Cd standard and a control rod are depicted in Figure 23.

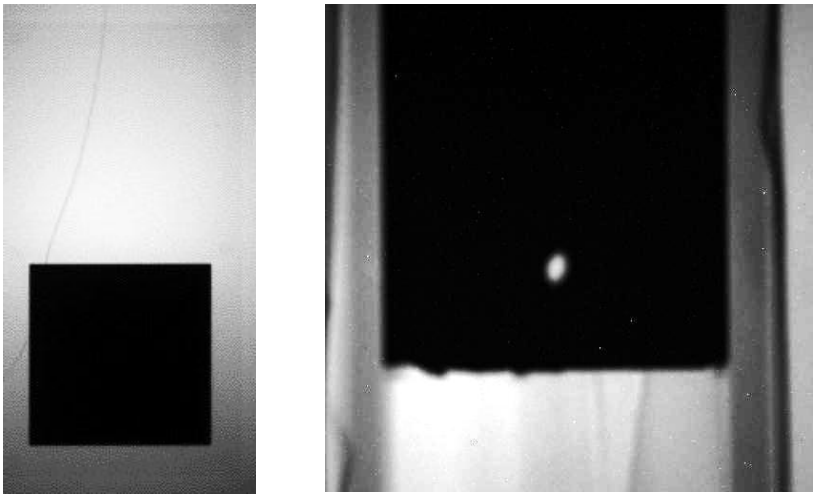

Figure 23 – Neutron radiographs of a Cd standard (left) and control rod (right) showing Cd (black) indicating high thermal neutron absorbing materials (Necsa, 2010 (a))

Radioactive waste

Low- and intermediate-level nuclear waste is normally encapsulated in in some form of barrier to protect the waste from the environment and *vice versa*. Intermediate-level nuclear waste is firstly encapsulated in a steel drum, compressed, and finally embedded normally in a concrete drum and safely stored underground in a remote location such as Vaalputs in the Karoo region in South Africa (Necsa, n.d. (b)) (see Figure 24). A site is normally chosen with low rainfall and suitable surface and groundwater conditions.

Figure 24 – Vaalputs intermediate-level waste storage site, South Africa (Necsa)

Concrete is a porous medium and the characterization of transport of water through concrete structures is well described by De Beer, Strydom and Griesel (2004) and De Beer, Le Roux and Kearsley (2005). It is especially important to understand the transport of water through concrete because nearly all concrete structures contain steel reinforcing, and in the case of nuclear waste, intermediate-level nuclear waste in compressed steel drums. When cracks in the concrete, caused by the transport of liquid through it, reach the reinforcing, an environment conductive to the corrosion of steel is created. Corrosion affects the strength of the structural members, as the steel is a major contributor to the tensile and compressive strength of the members. Severe leakage of radioactive materials into the surrounding environment is thus possible if the integrity of the concrete barrier is compromised.

Neutron radiography studies of concrete and mortars enable the direct physical visualization and quantitative detection of water inside concrete structures. The physical properties of concrete such as porosity, permeability, and sorption characteristics are obtained through applying neutron radiography as a non-destructive analytic tool. The aim of these investigations is to maximize the properties to prevent water sorption and leaching of concrete structures and optimize one of the physical properties which is sometimes neglected in the criteria to develop structures for nuclear waste encapsulation (De Beer, Strydom and Griesel, 2004; De Beer, Le Roux and Kearsley, 2005). To improve the durability of concrete, the capillary and pore size within the concrete matrix must be restricted to a minimum. This is why hydration as well as W/C ratio properties is of great importance, and thus creates an ideal opportunity for neutron radiography to play a role in obtaining the needed information in a non-destructive manner to optimize these parameters. The visualization of the sorption of water by means of neutron tomography of a laboratory-size concrete structure is depicted in Figure 25.

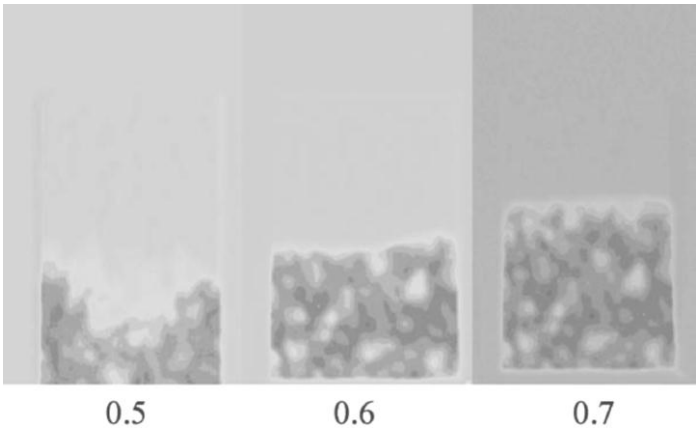

Figure 25 – Neutron radiographs showing the effect of 70%, 60%, and 50% W/C ratio on the sorptivity of water into a concrete slab (De Beer, Strydom and Griesel, 2004)

Conclusions

X-ray and neutron radiography in two or three dimensions play an important role in many dedicated areas within the nuclear fuel cycle. The advantage of these methods is their completely non-destructive nature. Visualization of the structure of samples, as well as quantitative description, is important aspects in materials research. The important roles of X-ray and neutron radiography/tomography as non-invasive analytic techniques within specific areas within the nuclear fuel cycle should not be underestimated. X-rays and neutrons are produced by very different methods, and also interact with materials in different manners. In the nuclear environment, each type of radiation has its own field of utilization due to their different characteristics, but in some instances their applications complement each other to reveal comprehensive information.

Neutron transmission analysis is a very helpful tool to obtain information on the properties of, and changes in, nuclear fuel material. Scientists and researchers in the geosciences in South Africa have, in the availability of the tomography facilities at Necsa, the capabilities to conduct quantitative analytical measurements at state-of-the-art radiation imaging facilities that compare to similar facilities elsewhere in the world.

Within the mining area, 3D computer tomography shows potential for further development, and can be already used to complement and add value to current conventional 2D mineralogical techniques. Neutron radiography analysis is able to derive the hydrogen content in fuel cladding both qualitatively and quantitatively, with high sensitivity and precision.

The results presented here illustrate how recent advances in laboratory-based X-ray CT instruments allow the examination of TRISO particles at the nano- and micro-scales in 3D. In this case study, high-resolution X-ray CT has been shown to be a viable tool for profiling the TRISO particles in two important aspects; to characterize the individual TRISO layers with variations in thickness and their subsequent interactions, thus allowing manufacturing validation as well as assisting in working towards a mechanistic understanding of fabrication and in-service issues.

The availability of these techniques in South Africa opens new possibilities for research, quantitative analysis, and non-destructive evaluation. National capacity as well as international trends shows the ability for non-destructive testing of nuclear materials utilizing penetrating X-Ray and neutron radiation in more comprehensive and unique ways than before.

References

AFRICAN NTD CENTRE. http://www.andtc.com/

BANHARD, J. 2008. Advanced Tomographic Methods in Materials Research and Engineering. Oxford University Press.

CHETTY, D., CLARK, W., BUSHELL, C., SEBOLA, P.T., HOFFMAN, J.W., NSHIMIRIMANA, R.B., and DE BEER, F.C. 2011. The use of 3D X-ray computed tomography for gold location in exploration drill cores. *Proceedings of the 10th International Congress for Applied Mineralogy (ICAM)*, Trondheim, Norway, 1-5 August 2011. pp.129–136. http://www.mintek.co.za/wpcontent/ uploads/2011/11/ch-17.pdf

DAVIES, L.M. 2000. Role of NDT in condition based maintenance of nuclear power plant components. *15th World Conference on Non-Destructive Testing*, Rome, 15-21 October 2000. http://www.ndt.net/article/wcndt00/papers/idn078/idn078.htm

DE BEER, F.C. and AMEGLIO, L. 2011. Neutron, X-ray and dual gamma-ray radiography and tomography of geomaterial – a South African perspective. *Leading Edge*, June 2011. Special Edition Africa.

DE BEER, F.C., MIDDLETON, M.F., and HILSON, J. 2004. Neutron radiography of porous rocks and iron ore. *Applied Radiation and Isotopes*, vol. 61. pp. 487–495.

DE BEER, F.C., STRYDOM, W.J., and GRIESEL, E.J. 2004. The drying process of concrete: a neutron radiography study. *Applied Radiation and Isotopes*, vol. 61, no. 4. pp. 617–623.

DE BEER, F.C., LE ROUX, J.J., and KEARSLEY, E.P. 2005. Testing the durability of concrete with neutron radiography. *Nuclear Instruments and Methods in Physics Research* A, vol. 542. pp. 226– 231.

DOMANUS, J.C. 1992. Practical Neutron Radiography. Kluwer Academic Publishers.

FRAJTAG, P. Not dated. Radiation Protection and Radiation Applications: Gamma and Neutron Radiography. http://moodle.epfl.ch/pluginfile.php/1593971/mod_resource/content/2/RRA -EPFL- FS2014-Week14a.pdf [Accessed 1 May 2015].

GHOSH, J.K., PANAKKAL, J.P., and ROY, P.R., 1983. Monitoring plutonium enrichment in mixed-oxide fuel pellets inside sealed nuclear fuel pins by neutron radiography. *NDT International*, vol. 16, no. 5, October 1983. pp. 275–276. DOI: 10.1016/0308- 9126(83)90127-X

GROSSE, M. 2010. Neutron radiography—a powerful tool for fast, quantitative and non-destructive determination of the hydrogen concentration and distribution in zirconium alloys. *Proceedings of the 6th International ASTM Symposium on Zirconium in the Nuclear Industry*, Chengdu, China, 9–13 May 2010.

GROSSE, M., VAN DEN BERG, M., GOULET, C., LEHMANN, E., and SCHILLINGER, B. 2011. I*n situ* neutron radiography investigations of hydrogen diffusion and absorption in zirconium alloys. *Nuclear Instruments and Methods in Physics Research*, vol. A651. pp. 253–257. doi: 10.1016/j.nima.2010.12.070

GROSSE, M., STEINBRUECK, M., LEHMANN, E., and VONTOBEL, P. 2008. Kinetics of hydrogen absorption and release in zirconium alloys during steam oxidation. *Oxidation of Metals*, vol. 70, no. 3. pp. 149–162.

GRÜNAUER, F. 2005. Design, optimization, and implementation of the new neutron radiography facility at FRM-II. Dr. Rer. Nat. dissertation, Faculty of Physics, Technischen Universität München.

HOFFMAN, J.W. 2012. Process description for micro-focus X-ray investigation of source at MIXRAD facility. Necsa internal report, DOC NO: RS-MFX-PRO- 12002.

INTERNATIONAL ATOMIC ENERGY AGENCY. Not dated. Getting to the Core of the Nuclear Fuel Cycle. Department of Nuclear Energy, Vienna, Austria. https://www.iaea.org/OurWork/ST/NE/NEFW/_nefwdocuments/ NuclearFuelCycle.pdf
ISO 15708-1:2002(E). Non-destructive testing — Radiation methods —Computed tomography — Part 1: Principles.

KLOPPER, W., DE BEER, F.C., and VAN GREUNEN, W.S.P. 1998. Overview of hot cell facilities in South Africa. Proceedings of the European Working Group '*Hot Laboratories and Remote Handling*'.

LEHMANN, E.H., VONTOBEL, P., and HERMANN, A. 2003. Non-destructive analysis of nuclear fuel by means of thermal and cold neutrons. *Nuclear Instruments and Methods in Physics Research* A, vol. 515, no. 3. pp. 745–759. doi:10.1016/j.nima.2003.07.059

LOWE, T., BRADLEY, R.S., YUE, S., BARII, K., GELB, J., ROHBECK, N., TURNER, J., and WITHERS, P.J. 2015. Microstructural analysis of TRISO particles using multiscale X-ray computed tomography. *Journal of Nuclear Materials*, vol. 461. pp. 29–36. http://dx.doi.org/10.1016/j.jnucmat.2015.02.034

MCGLINN, P.J., DE BEER, F.C., ALDRIDGE, L.P., RADEBE, M.J., NSHIMIRIMANA, R.B., BREW, D.R.M., PAYNE, T.E., and OLUFSON, K.P. 2010. Appraisal of a cementitious material for waste disposal: Neutron imaging studies of pore structure and sorptivity. *Cement and Concrete Research*, vol. 40. pp. 1320–1326

NECSA. 2006. RT-TVG-06/05: Test Report: X-Ray Radiography of PBMR-Fuel Spheres with Zirconium Particles. Internal report, SAMPLE NO: DFS-TF03G04. NECSA. 2010 (a). RS-TECH-REP-10004: Neutron Radiography Quality Assurance test report of neutron absorbing material in Control Rods of the SAFARI-1 Nuclear Research Reactor (Lot/Batch No: RT-LOT-10/03). Internal report.

NECSA. Not dated (b). Vaalputs. The National Radioactive Waste Disposal Facility. http://www.radwaste.co.za/vaalputs%20information%20pamflet.pdf. [Accessed 1 May 2015].

OECD NUCLEAR ENERGY AGENCY. 2003. Nuclear Energy Today. OECD Publishing. p. 25.

PIXSHARK. Not dated. http://pixshark.com/images-of-nuclear-fuels.htm

SAIW (Southern African Institute of Welding). Not dated. http://www.saiw.co.za/

SEBOLA, P. 2014. Characterisation of uranium-mineral-bearing samples in the Vaal Reef of the Klerksdorp Goldfield, Witwatersrand basin. MSc dissertation, Faculty of Science, University of the Witwatersrand, Johannesburg. http://wiredspace.wits.ac.za/handle/10539/16820?show=full http://hdl.handle.net/10539/16820

SGS SOUTH AFRICA (PTY) LTD. Not dated. http://www.sgs.co.za/en.aspx

TREMSIN, A.S., VOGEL, S.C., MOCKO, M., BOURKE, M.A.M., YUAN, V., NELSON, R.O., BROWN, D.W., and FELLER, B. 2013. Non-destructive studies of fuel pellets by neutron resonance absorption radiography and thermal neutron radiography. *Journal of Nuclear Materials*, vol. 440. pp. 633–646.

WEIL, J. 2001. Pebble-bed design returns. *Nuclear Power gets a Second Look*. IEEE Spectrum Special Report. http://spectrum.ieee.org/energy/nuclear/ pebblebed-design-returns [Accessed 20 June 2015].

WILLCOX, M. and DOWNES, G. Not dated. A brief description of NDT techniques. Insight NDT, paper T001. http://www.turkndt.org/sub/makale/ornek/a%20brief%20description%20of %20ndt.pdf

WORLD NUCLEAR ASSOCIATION. 2015. http://www.world- nuclear.org/info/Nuclear- Fuel-Cycle/Mining-of-Uranium/World-Uranium-Mining- Production/ [Accessed 13 May 2015].

CHAPTER 7

PUBLICATION:

Upgrading the Neutron Radiography Facility in South Africa (SANRAD): Concrete Shielding Design Characteristics

Radiological and conventional safety remains of utmost importance for the development of radiation facilities world-wide. Shielding becomes much more than of just radiological importance when neutron facilities are adjacent to each other, such as is the case for the NRAD and NDIFF facilities at SAFARI-1. Shielding requirements must then also take into account the reduction of parasitic radiation in order to limit the background at neighbouring instruments. These conditions are reached through designed shielding barriers, but also through planned operational procedures. Because the beam lines at SAFARI-1 are axial to the core, the spectrum consists of fast, thermal, epithermal and cold neutrons as well as primary and secondary neutron induced gamma-rays. Shielding design must therefore include due consideration of all of these radiation components. Regulations are provided by the host facility (SAFARI-1) and the National Nuclear Regulator (NNR) with respect to radiological safety of workers, but no guidelines are provided with respect to signal-to-background requirements of scientific facilities. For the upgrade of the South African NRAD facility, the radiation shielding requirements had to meet specific local radiological safety standards (25 $\mu Sv.h^{-1}$) and, in addition also had to reduce background to neighbouring beam line facilities whilst limiting construction costs. To meet the latter criterion, a self-endorsed experimental integrity standard of 1 $\mu Sv.h^{-1}$ was set as a design specification. Based on this, and consideration of the full radiation beam spectrum from the core of SAFARI-1 for the NRAD beam tube, an intensive “worst case” operational scenario via a MCNP-X process was simulated. The casted combination of high density concrete (4.2 $g.cm^{-3}$) was verified through cold and hot commissioning quality assurance tests that confirmed its casting quality as well as radiation shielding integrity. This chapter reflects the work done to achieve cost-effective, but adequate, shielding for the planned new NRAD facility as reported at the 10th World Conference on Neutron Radiography.

"It is a staggering thought that just fifty years ago man did not know the neutron existed, yet half the world is made of neutrons, The thought is staggering not so much for how unsophisticated we were in the past, but for how extremely sophisticated technology may be in the future. With this in mind, who can doubt that money and effort spent on further development of neutron radiography will be money and effort well spent."

John P Barton: Opening speech at 1st World Conference on Neutron Radiography 1981

Available online at www.sciencedirect.com
ScienceDirect
Physics Procedia 69 (2015) 115 – 123
Physics Procedia

10th World Conference on Neutron Radiography 5-10 October 2014

Upgrading the Neutron Radiography Facility in South Africa (SANRAD): Concrete Shielding Design Characteristics

F.C. de Beer[a66]*, M.J.Radebe[a], B Schillinger[b], R Nshimirimana[a], M. A. Ramushu[c], T. Modise[a]

[a]*Radiation Science, Necsa, PO BOX 582, Pretoria 0001, South Africa*
[b]*TUM, FRMII, Garching, Germany*
[c]*WITS, Johannesburg, South Africa*

Abstract

A common denominator of all neutron radiography (NRAD) facilities worldwide is that the perimeter of the experimental chamber of the facility is a radiation shielding structure which, in some cases, also includes flight tube and filter chamber structures. These chambers are normally both located on the beam port floor outside the biological shielding of the neutron source. The main function of the NRAD-shielding structure is to maintain a radiological safe working environment in the entire beam hall according to standards set by individual national radiological safety regulations. In addition, the shielding's integrity and capability should not allow, during NRAD operations, an increase in radiation levels in the beam port hall and thus negatively affect adjacent scientific facilities (e.g. neutron diffraction facilities). As a bonus, the shielding for the NRAD facility should also prevent radiation scattering towards the detector plane and doing so, thus increase the capability of obtaining better quantitative results. This paper addresses Monte Carlo neutron-particle transport simulations to theoretically optimize the shielding capabilities of the biological barrier for the SANRAD facility at the SAFARI-1 nuclear research reactor in South Africa. The experimental process to develop the shielding, based on the principles of the ANTARES facility, is described. After casting, the homogeneity distribution of these concrete mix materials is found to be near perfect and first order experimental radiation shielding characteristics through film badge (TLD) exposure show acceptable values and trends in neutron- and gamma-ray attenuation.

Selection and peer-review under responsibility of Paul Scherrer Institut.

66 Corresponding author. Tel.: +27123055258
Email address: 1958frik@gmail.com

Selection and peer-review under responsibility of Paul Scherrer Institut.
Doi:10.1016/j.phpro.2015.07.017.

Keywords: SANRAD; Neutron Radiography; Shielding Characteristics

1. Introduction

The development of any newly built, as well as any upgrade of a NRAD facility has to take into serious consideration the space available for the size of, in addition to the weight of the biological shield that forms the barrier. The radiological barrier, during operation, provides the shield between the high intensity radiation (neutrons and Gamma-rays) within the enclosure and the outside where the personnel should safely be able to work. Most of the building costs of NRAD facilities are caused by the design and construction of a radiation barrier for the safe operation of such facilities. However for many facilities, these barriers are not adequately being described in literature – e.g. the exact composition, material densities and thickness to fulfil its purpose are not reported. As an exception, the ANTARES NRAD personnel of FRMII have described the shielding of the old facility [Calzada (2005)] and the new facility [Calzada (2012), Calzada (2009)] in detail and thus emphasized the importance of adequate research and reporting of one of the most important aspects of building an NRAD facility.

This concept of using high density concrete shielding materials was developed when the first NRAD facilities were established and reported in [Aljreja (1986)]. However, not much attention was given and documented in the proceedings of the first couple of world conference gatherings about any international NRAD facility shielding properties, and if so not much detail was reported. References to "heavy concrete" or "high density concrete" [Aljreja (1986), Jacobson (2010)] and the density from 4.2 - 4.8g/cc [Pasupathy (1982), Calzada (2012)] are the only detailed descriptions of the barrier that forms the perimeter of the NRAD facilities. Limited reports found from USA-NIST and China indicated only that the shielding providing the necessary protection is a steel encased mixture of wax and steel shot [NIST-http, Tang]. There the high energy neutrons are slowed down to thermal neutrons in the wax and stopped by the material while the gamma-rays are absorbed by the steel shot.

Much attention in most papers describing NRAD facilities is given to applications of NRAD and to the infrastructure such as the neutron source, collimator composition and collimation and neutron- or gamma-ray filters to obtain a "clean and pure" neutron beam. However, it was shown with MCNP-X simulations that the composition and thickness of the shielding has a major effect on the background radiation within the NRAD facility and thus a detrimental effect on the quality of radiographs when quantitative NRAD is being performed [Hassanein (2010)].

The Monte Carlo Transport Particle Code (MCNP-X) [Briesmeister (1996)] has been extensively used for the simulation of NRAD collimators at e.g. at the Malaysian Institute for Nuclear Technology Research (MINT), Malaysia, and for example the development of new radiography facilities at NUR-3 [IAEA-TECDOC-1604(2006)], the NRAD facility at the Bhabha Atomic Research Centre (BARC), India [IAEA-TECDOC-1604(2006)] and ANTARES-II at FRMII, Germany [Calzada (2012)]. MCNP-X simulations were also successfully applied, as a first step, in the shielding design of the ANTARES

NRAD facility in Garching, Germany, [Calzada (2009), Calzada (2012), Grünauer (2005)], the NRAD facilities in Thailand [Picha], Malaysia, [IAEA-TECDOC-1604 (2006)], China (Peking University) [Wen (2011)], South Korea [Bai (2006)] and for the SANRAD facility in South Africa [Grünauer (2009)].

Proof of the integrity of the facility shielding to the national nuclear regulator (NNR) is a normal procedure. The approval by the NNR of the construction and operation also forms the basis of evaluation of the safety of the facility which is in the interest of the workers and public. Proof of the integrity of the shielding properties to provide adequate shielding is of utmost importance and it should be demonstrated by initial MCNP-X calculations, backed up and confirmed by physical experiments through foil activation and radiation dose measurements.

This paper has the intention of serving as a guideline for newly planned NRAD facilities and to show how to approach the shielding design. Experience gained from the upgrade of the SANRAD facility at the SAFARI-1 nuclear research reactor in South Africa which focused on its shielding characterization will be given here. Specific pre-casting aspects such as MCNP-X characterization, concrete development and the establishment of the final concrete mix as well as post casting examination such as tests of homogeneity of the constituents and the neutron shielding capabilities through dose meter experiments will be dealt with. Foil activation analyses and the process of implementation in radiation shielding characterization for the SANRAD facility are described in another paper within these proceeding [Radebe (2015)].

2. Upgraded NRAD facility layout

The existing (NRAD) facility, located on the beam port floor and at beam line position no. 2 at the SAFARI-1 nuclear research reactor, is being upgraded in order to achieve higher quality radiographs, to increase operating safety and to become more versatile. The design of many of its components, such as the shielding blocks and collimators, has been adopted from the FRM-II, ANTARES NRAD facility in Germany. Their only applicable fundamental safety function is shielding from radiation and the system is designed to (a) return to the fail-safe state, i.e. to close the shutters in the beam line in any unwanted or accidental condition and (b) to remain in a safe condition, i.e. not to open the shutters if certain conditions are not met – e.g. if the facility door is open.

To reach these above-mentioned conditions during operation implies that the shielding has to be

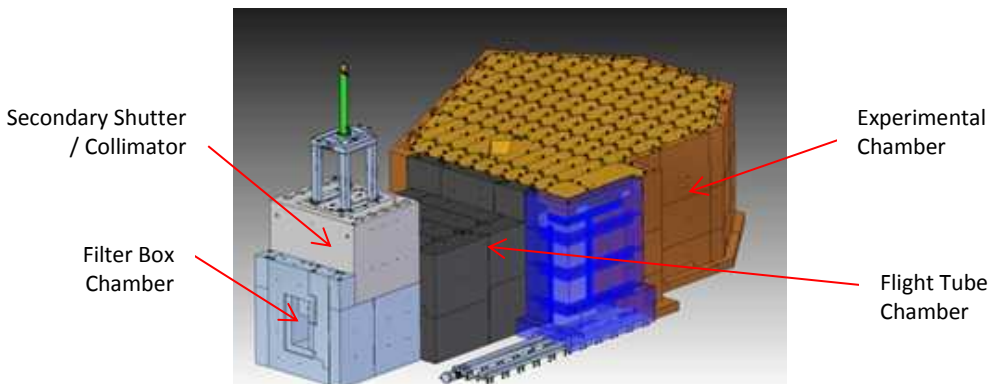

Fig.1. Model of the SANRAD facility

adequate enough to provide safe shielding and protection to personnel outside of the facility in either operational or accidental mode. Fig-1 shows the shielding layout of the proposed SANRAD facility with the shielding blocks interlacing with each other to complete the barrier for the several sections – filter box chamber, secondary shutter, flight tube chamber and experimental chamber.

The entire facility is designed for the steel boxes to interlace with each other in order to prevent radiation leakage through a straight path at any part of the shielding. Fig-2 shows the CAD-models of a number of these boxes within the facility. The multiple angles and corners of each of the boxes provide, together with the other boxes, a complete attenuation of the radiation beam.

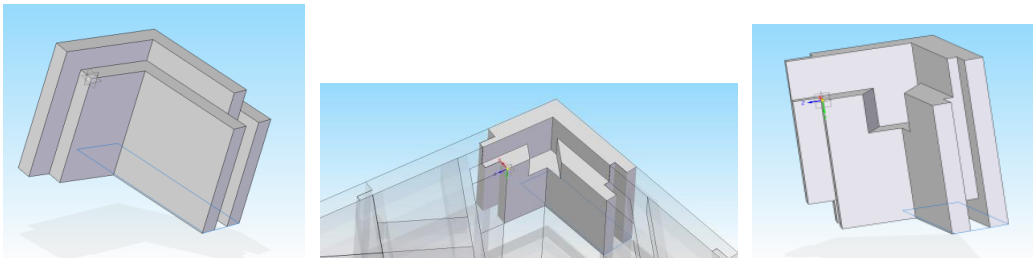

Fig. 2. Models of the steel boxes showing their interlace

The interlock design concept for the boxes adopted from the German design allows that any small shrinkage effects around the perimeter of the blocks are completely mitigated. An indirect ray path, also along the edge of a steel box, by nature, represents a weak beam of very low intensity due to the small solid angle randomly selected from a much more isotropic radiation field. This narrow beam always runs up against a high density concrete barrier that remains to be transmitted.

No concrete shrinkage through visual inspection of the cast materials, neither in a test slab nor in the cast concrete blocks could be observed or measured after 28 days of casting. The steel boxes maintained their original shape and did not bulge due to internal steel struts keeping the steel structures stable and intact. To make sure all corners of the boxes are filled with concrete mix, holes were drilled in the corners to let air escape. The concrete mix filling the corners and pouring from the hole can be observed (Fig-3 and Fig-4).

Fig. 3. Shielding steel boxes prior to casting concrete. Large enough holes at the top provided for easy concrete pouring. The laminated structures of the steel blocks are observed for optimal shielding capability when interlaced

Fig. 4. Shielding steel boxes during concrete casting process. Concrete pouring from the corner hole (left) indicating adequate filling of the corners of the boxes. Steel shot (small spherical particles) and hematite rocks (right) observed at the top of one of the boxes during pouring indicating adequate mixing and homogeneity of the concrete mix

The total radiation shielding barrier comprises, in a cross section layout (See Fig-5), firstly, a 200 mm thick borated polyethylene cover, then a 10 mm steel casing, and depending on the position of the shielding, a 1000 mm, an 800 mm or a 600 mm thick high density concrete filling with the 10 mm thick steel casing at the back. The total weight of shielding materials being put onto the beam port floor of the SAFARI-1 nuclear reactor is ~ 600 tonnes, which requires additional strengthening of the floor.

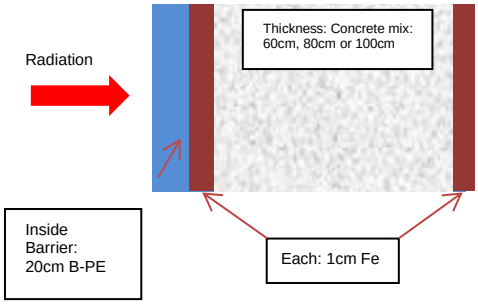

Fig. 5. Cross section of the radiation shielding barrier of the SANRAD facility

3. MCNP-X simulations to optimize radiation shielding

The initial step is to know, as accurately as possible, the neutron- and gamma-ray distribution spectrum as well as their intensities emanating from the source (reactor/isotope/spallation source). After a raw estimation of the needed shielding composition and thickness, a MCNP-X model is generated. Through many computer simulation iterations of the attenuation of primary neutron- and gamma-rays by the model, the effective material shielding composition and thickness are optimized. Optimization through MCNP-X simulations is a long and tedious process if the optimal composition of the barrier mix for best shielding properties has to be "discovered". For the South African case, the simulations for the SANRAD facility could proceed immediately as the state-of-the-art shielding composition and

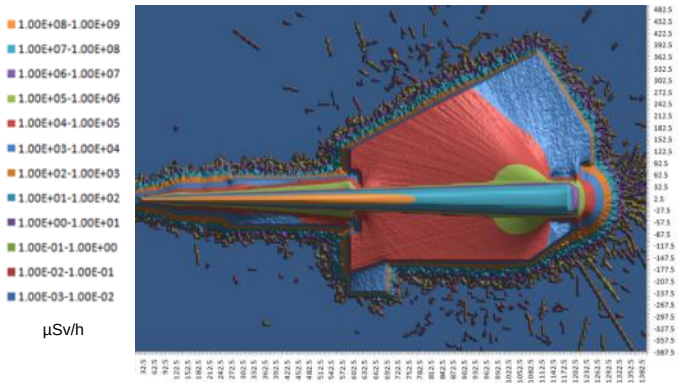

Fig.6. MCNP-X simulations showing the shielding capability for the upgraded SANRAD facility for whole neutron spectrum of SAFARI-1

thickness, as being used at the FRMII-ANTARES-I facility in Germany, were adopted. Only after the seventh MCNP-X iteration, due to changes in the shielding concept and layout of the facility, was a final design adopted [Grünauer, (2009)] and streamlined for the South African conditions as depicted in Fig-6 [Korochinsky, (2012)]. The update included an equilibrium Low Enriched Uranium (LEU) core, new internal geometry of the beam (which included the removal of the old collimator and the incorporation of the new wall coupling plate), and the latest layout and material composition of the experimental chamber. The dose rates were calculated for the worst possible case, namely at the horizontal and vertical planes that include the axis of the beam, and when the beam is fully open (no collimator and no filters), which is envisaged to need a very small fraction of the time the facility operates. For this condition both the thickness of the walls and their material composition were defined as to achieve the target of <1 μSv/h for contact dose rate with the objective of minimizing background radiation to the neighbouring beam line facility instruments (Small Angle Neutron Scattering and Neutron Powder Diffractometer). The calculations show that the contact dose rates around the whole facility (side walls and roof) meet the requirement, with the only exception being the back wall (directly exposed to the open beam) where the contact dose rate at the hottest spot does not exceed 10μSv/h. To achieve this, not only a thicker wall was designed but also a beam stopper was included in the model. The design of the beam stopper can be optimized further, but the current proposal (as modelled) is enough to meet the blue radiation area classification limit for the area outside the NRAD facility and beam port floor of 25μSv/h.

To add conservativeness to the final MCNP-X calculations, heavy concrete with density 4.0 g/cm^3 was used in the model instead of the nominal density of 4.3 g/cm^3.

Table-1.Composition of concrete mix main constituents in development for SANRAD facility.

Constituent	Simulation: Germany	Simulation: South Africa	Casted Concrete
Density(g/cc)	4.7	4.0	4.22
Hematite	60.1%	55.6%	56.8%
Colemanite	1.6%	2.3%	2.4%
Steel shot	13.6%	26.6%	36%
Water	4.9%	2.4%	3.6

Table-1 shows the mix of the main constituents that contributes to radiation attenuation namely hematite, colemanite and steel shot, the recipe of the radiation shielding of the ANTARES facility in Germany, the updated South African simulation and real casting composition.

4. Cast concrete characteristics

4.1. Physical capabilities

Taking the well-defined concrete design of the ANTARES facility as baseline and also using it in the MCNP-X calculations, an extensive research program was followed [Ramushu (2011)] to find the final mix and composition of the concrete before casting. Through casting of test samples in 8 iterations, a final mix for the South African conditions (type of cement, sand, hematite, etc.) was found to provide the best

one for the density needed for shielding, ensuring a homogeneous distribution of the particles without segregation and other concrete related parameters (e.g. slump, strength, density). A few of the important physical parameters are described in the following paragraphs.

4.2. Physical properties of cast concrete

Certain physical properties related to concrete casting play an important role in the success of the final product – even more so for an NRAD facility. For any NRAD facility, the density of the concrete plays the most important part in the attenuation of the neutron- and gamma-ray beams. Table-2 lists the main physical properties of the cast concrete blocks where cube size samples were taken from each concrete batch that had been poured into the steel containers for evaluation.

Table-2.Physical properties of the casted concrete.

Slump (mm)	28 day fcu* (MPa)	28 day Density (kg/m^3)
510	43.6 ± 1.8	4232 ± 132

**fcu is defined as a characteristic strength of concrete*

4.3. Homogeneity

A homogeneous distribution of the main constituents of the concrete mix inside the steel boxes is of absolute importance to provide the same radiation shielding capability throughout the entire shielding block - from the top, where the concrete was poured into the box, to the bottom of the box. Visual inspection was done on a cast shielding block with one side of 10 mm thick steel being removed – as shown in Fig-7. Counting of steel spheres (and spherically impressed cavities) revealed a homogeneous steel sphere distribution over the three exposed areas, to within the inherent statistical variation of sphere distribution over smaller adjacent areas (Fig-8). This shows that no discernible systematic segregation of steel spheres could be observed. The

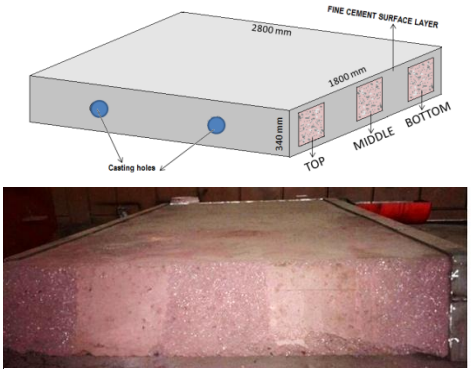

Fig. 7. TOP: Schematic of a shield block with exposed top, middle and bottom windows. BOTTOM: Photograph of the three exposed areas, showing uniform general aggregate consistency in all three exposed windows (top window is on the left)

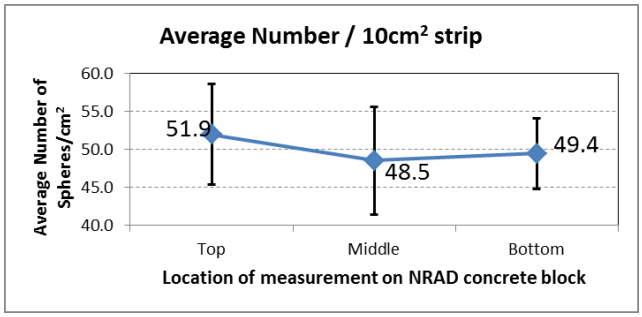

Fig. 8. Average number of steel shot balls counted at the top, middle and bottom positions of the exposed surfaces on the test concrete block in 10 cm^2 strips within each position

observation is consistent with a theoretical estimate that indicates stability against segregation for the steel balls in the used size range.

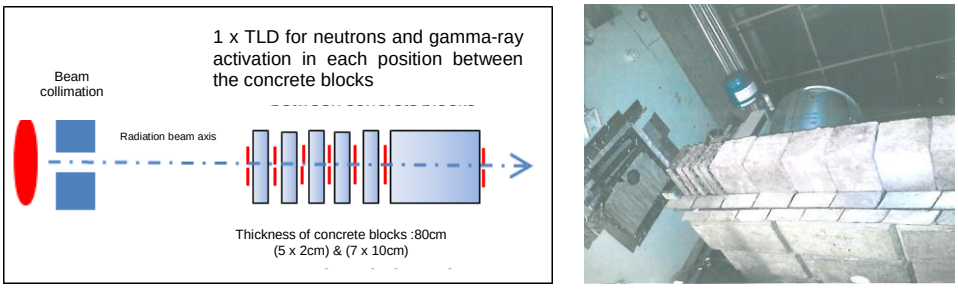

Fig. 9. Schematic- and physical layout of the experiments with the dose meters inside the NRAD experimental chamber

Table-3 lists the dose counts obtained by the neutron- and gamma TLD's. (Note: The lower gamma counts are due to Bi-filtering of the radiation beam and small cubes of material were used in the experiment – thus secondary gamma-ray generation was minimized.) The approximate neutron- and gamma-ray linear attenuation coefficients derived from the data of Table-3 are 0.112 and 0.07 respectively. Using these attenuation parameters together with arbitrary high initial values of 100000 (approximation results thus into ~200% more neutrons and ~3000% more gammas) neutron and gamma-ray counts, Fig-10 shows that for a 60 cm concrete thickness, a 99.88% and 98.5% drop of neutrons and gamma-rays counts respectively, is possible. The reason why so much more gamma-rays are simulated than what was measured is to take into account also secondary gamma-ray generation in the material upon neutron absorption for a full unfiltered white spectrum neutron beam.

Fig-10 shows that the shielding capability and requirements for neutron attenuation are met as the SANRAD concrete shielding thickness is varied from 60, 80 to 100 cm. These results were validated through foil activation measurements for neutrons using the same experimental set-up and are being reported elsewhere in these conference proceedings.

Table-3.TLD counts for neutrons and Gamma-rays.

Shielding thickness (cm)	NEUTRON TLD: (Counts)	GAMMA-RAY TLD: (Counts)
0	37233	280
2	5512	277
4	3509	78
6	3406	18
8	3276	17
10	63	19
80	14	2

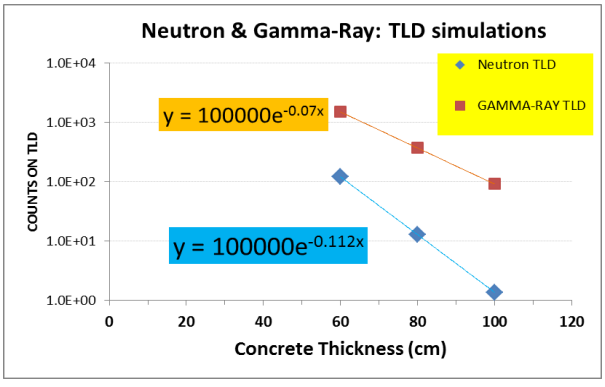

Fig. 10. Trend of attenuation of neutron- and gamma-ray radiation in laboratory concrete samples through TLD exposure and analysis

5. Conclusions

The description of the process to develop and characterize the radiation shielding for the upgraded NRAD facility has theoretically demonstrated, that the locally developed concept is completely adequate

for the safe operation of the facility i.e. that the radiation levels are far below the minimum of 10µSv/h for radiological safety. Additionally, it provides adequate shielding for minimizing background radiation at the neighbouring neutron facilities (e.g. NDIFF and SANS). This local concept is based on the internationally proven model (ANTARES at TUM in Germany) which was slightly altered to fit the experimental conditions of the SAFARI-1 research reactor and for South African concrete casting conditions.

Furthermore, the study confirmed that the final developed concrete mix used in the pouring and casting process meets all the requirements specified for structural and shielding purposes, i.e. strength and longevity. It implies that (a) the aggregates used in the mix contained no elements that will lead to radioisotopes with long half-lives, (b) the water used for casting has no mineral content that will lead to enhanced corrosion of the steel components of the mix, (c) the required minimum density of 4000 kg/m^3 as simulated in the MCNP-X calculations was exceeded, (d) the mix was of the desired slump and cohesion and that (e) the 28 day cube strength achieved is well above the desired 25 MPa limit at 43.6 MPa.

It was practically demonstrated through first order experiments with gold foils and radiological film badges on cast concrete laboratory samples from the final concrete mix, that the radiological shielding capability and requirements for neutron- and gamma-ray attenuation are met.

Prior to casting, MCNP-X simulations of the total structure were performed and the optimal shielding solution was obtained. After casting and curing, physical foil-activation and radiation dose measurements on the shielding blocks were performed. A good assessment of the shielding's capability for both neutrons and gamma-rays were obtained by these two methods.

Evaluation of the concrete mix was done prior to, during and after the pouring into cast shielding steel blocks. This was necessary as steel spheres have the highest segregation potential of all aggregates. We conclude that all materials in the Necsa shield blocks are homogeneously distributed and will therefore provide homogeneous shielding behaviour.

References

http://physics.nist.gov/MajResFac/NIF/facility.html

Aljreja, V., et al, 1987. Dedicated imaging system for real time neutron radiography, Proceedings of 2nd WCNR, Paris, France 1986, p625.

Bai, J., Shin, M.,Whang, J., 2006. 12th A-PCNDT 2006 – Asia-Pacific Conference on NDT, 5th – 10th Nov 2006, Auckland, New Zealand "A Monte Carlo Calculation for Neutron Radiography Facility Using Sealed-Tube Neutron Generator", http://www.ndt.net/article/apcndt2006/papers/p01.pdf.

Briesmeister, J., 1996. MCNP – A General Monte Carlo N-Particle Transport Code, Version 4B, Los Alamos National Lab, Los Alamos.

Calzada, E., Schillinger, B., Grünauer, F., 2005. "Construction and assembly of the neutron radiography and tomography facility ANTARES at FRM II"., NIM-A, Volume 542, Issues 1–3, 38–44.

Calzada, E., et al., 2009. "New design of the ANTARES-II facility for neutron imaging at FRM-II", NIM-A, 605, p50.

Calzada, E., et al., 2012. "Reusable shieldingmaterial for neutron- and gamma-radiation., 9th WCNR, p77.

Grünauer, F., 2005. PhD Thesis: "Design, optimization, and implementation of the new neutron radiography facility at FRM-II", http://mediatum.ub.tum.de/doc/603112/603112.pdf.

Grünauer, F., 2009. RS-RAD-REP-14001: Monte Carlo Simulations for the SAFARI Reactor and its Instruments: Part-C: Neutron radiography facility.

Hassanein, R., et al., 2010. "Correction Software Tool for Neutron tomography", Proceedings of the 8th WCNR, Gaithersburg, USA, p206.

IAEA-TECDOC-1604 Neutron Imaging:, 2006. A Non-Destructive Tool for Materials Testing Report of a coordinated research project 2003–2006.

Jacobson, D.L., et al., "Neutron Radiography and Tomography facilities at NIST to analyse in-sito PEM fuel Cell performance, "WCNR proceedings 8 (2010), Gaithersburg, USA, p50.

Korochinsky, S., *2012. RRT-NRAD001-MEM-12001:* Results from Radiological Safety Assessment for the NRAD Facilityat SAFARI-1.

Nothnagel, G., 2014. (Necsa internal report): RS-DEVELOP-REP14001: Evaluation of concrete homogeneity for the new SANRAD facility.

Pasupathy, C.S., et al., 1982. A 233U fueled reactor for NRAD, NEUTRON RADIOGRAPHY(1): Proceedings of 1st WCNR, San Diego, California, USA, p199.

Picha, R., Simaroj, N. and Sangphet, V., Designing a Transportable Neutron Radiography System http://www.lib.ku.ac.th/KUCONF/data51/KC4605035.pdf.

Radebe, J.M., et al., 2015. "Foil activation measurement and simulation of the concrete neutron shielding ability for the new upgraded SANRAD facility" This proceedings.

Ramushu, A.,2011. MES-CIV-REP-0001M. (Necsa internal report): The development of high density shielding concrete using locally sourced aggregates for the upgrade of SAFARI-1 NRAD facility.

Tang, B., Zhang,S., et al. The Design Of Neutron Radiography Facility And Its Application In SPRR-300, http://www-pub.iaea.org/MTCD/publications/PDF/te_1604_web.pdf.

Wen,W., 2011. Neutronic design and simulated performance of Peking University Neutron Imaging Facility (PKUNIFTY) , Volume 651, Issue 1, 21 September 2011, Pages 67–72.

CHAPTER 8

Conclusions and Outlook

This chapter contains a high-level summary of the development and research work presented in partial fulfilment of the requirements for a PhD by publication. This summary includes conclusions on the successes achieved with respect to the establishment of productive research facilities for radiography and tomography at Necsa and the impact these have had towards addressing key aspects of the goals of the National System of Innovation. A short outlook of future research infrastructure development envisaged at Necsa and their potential for further collaborations and research are also provided.

8.1 Conclusions

Evidence of my own research and development recently done, was provided by a Chapter in a book and three (3) peer reviewed publications included as Chapters 4 - 7 of this thesis. These articles served to show both the author's initiatives towards the development of state-of-the-art neutron radiography and tomography research infrastructure at Necsa and its utilisation in a number of key research areas of interest to the South African research communities. Apart from these articles, this thesis contains information that highlights the author's long term continuous involvement in the establishment of a radiography and tomography capability in South Africa, including neutron and complementary X-ray techniques, which are required to provide a comprehensive perspective on study objects in one location. The impact of these initiatives on research and post graduate training has also been shown.

From the contents of this thesis, it should be evident that, through the original and active participative work of the author, and his networking initiatives, the following major outcomes were achieved:

- Establishment of an unique neutron tomography research capability in South Africa, which was also (until recently) the first of its kind in the southern Hemisphere.
- Through active user group building, my own research participation and establishment of a group of competent instrument scientists, South Africa, through the Necsa facilities and activities, was put on the world map as a productive tomography user facility.
- The multidisciplinary interfaces that were established between national and international researchers using the Necsa facilities, stimulated applied research output and in this way contributed to the goals of the National System of Innovation to transform South Africa into a knowledge driven economy.
- The growing research outputs, and post graduate training achievements, provide direct evidence of the value of the established facilities and the support capabilities available to users. Figure 8.1 graphically depicts the number of peer reviewed articles on an annual basis and also shows the cumulative growth in output since commissioning of the facilities (neutrons and X-rays). The output is broken down to show how much was due to post graduate research studies. A cumulative number of 57 post graduate students (42 in the period 2012 – present) successfully completed their qualifications and derived significant benefit from 3D tomography scans performed at the Necsa facilities.

In order to achieve the outcomes summarised above, the author engaged in several bilateral research agreements with international laboratories[67] via collaborative research projects established through the International Atomic Energy Agency (IAEA).

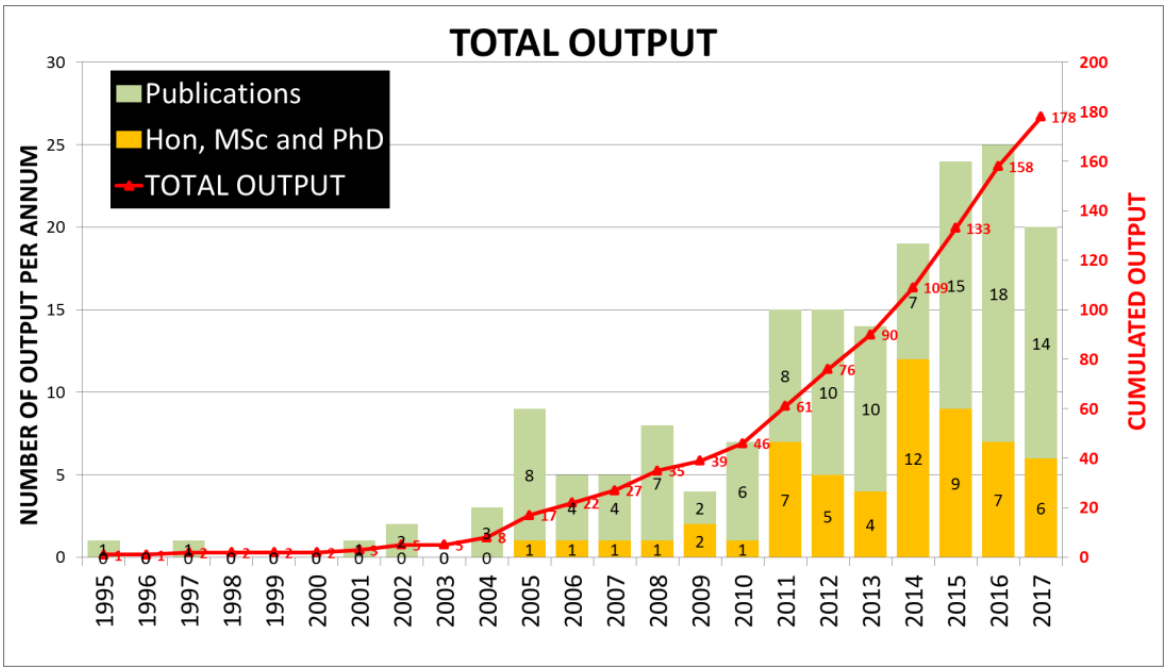

Figure 8.1: Peer reviewed publications and post graduate research output since 1995.

Due to several high quality outputs emanating from the South African facilities at Necsa and presented at international conferences of the WCNR and ITMNR series, the international community became aware of the research and development activities in South Africa. This recognition partly culminated in the election of the author to the Board of the International Society for Neutron Radiology in 2001 as Vice-President, and as President in 2008, with the honour to host the 9th WCNR in South Africa in 2010.

8.2 Future and outlook

Based on the core capabilities established so far, a realistic, positive expectation for the future of tomography and radiography at Necsa can be built. On the instrumentation side, a nano-focus X-Ray and micro-focus neutron imaging capability are realistically within reach and would add significant extra value to Necsa users from all the key research areas. This expansion will automatically extend the user base and the disciplines of research that may benefit from radiography and tomography.

67 International laboratories: Germany; Switzerland; Poland; Israel; Australia; Korea; UK.

It is envisaged that a future replacement for SAFARI-1 may very well be a multi-purpose reactor equipped with a cold neutron source, which will allow exploitation of the Bragg edge to image texture in materials, using neutron techniques currently applied at PSI (Switzerland), NIST (USA), Helmholtz-Berlin and FRMII (Germany) to name a few and shortly described in Section 2.11. In this way, a whole new area of research in a variety of research areas will open up for South African users from both academia and industry.

To improve and augment scanning services to South Africa's large and productive heritage study community, the establishment of both a mechanical and chemical fossil preparation laboratory, conveniently located nearby the X-ray and neutron tomography facilities, is currently being planned in a collaborative effort with all stakeholders in the cultural heritage community.

New research areas of high interest to South Africa, and for the rest of the world, relate to alternative energy technologies, such as fuel cells and energy storage devices. Because of the ability of neutrons to study the prevalence and movement of hydrogen and water in such devices, neutron radiography and tomography techniques promise to become important diagnostic tools for the further development of such technologies.

A holistic future vision (dream) is to establish in South Africa a regional African centre of competence in neutron and X-ray beam line science, in general, and in radiography and tomography, in particular, which will be accessible to researchers and students from African countries to perform pure and applied research.

APPENDIX 1

Historical: Nobel Prize Laurates - Important Scientists

This appendix contains a number of pictures in honour of Nobel Prize laureates and important scientists who made breakthrough discoveries and international inventions in the field of penetrating radiation, radiography and tomography and whom the candidate found inspiration.

App 1.1: Early Pioneers of X-ray and Neutron Radiation Studies.

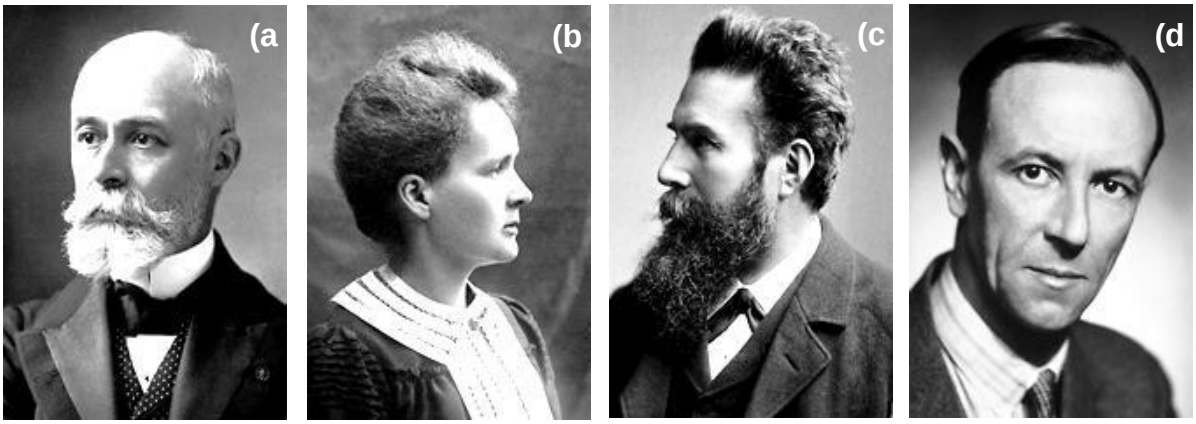

Figure App 1.1: Pioneers in radiation sciences: (a) Becquerel, (b) Curie, (c) Röntgen and (d) Chadwick.

App 1.2: Early Pioneers of Computed Tomography (CT)

Figure App 1.2: **Pioneers in aspects of Computed Tomography:**

LEFT: Johann Radon: Austrian Mathematician on Radon-transformations – the basis of CT.

MIDDLE: Allan M. Cormack: South African born Nobel Prize Laureate in Physiology or Medicine: 1979. (Cormack, 1979) – Co-inventor of the Medical CT Scanner, and

RIGHT: Britain's Sir Godfrey N. Hounsfield, Nobel Prize Laureate in Physiology or Medicine: 1979. (Hounsfield, 1979) – Co-inventor of the Medical CT Scanner.

APPENDIX 2

Relevant Achievements of the PhD Candidate

This appendix contains in tabular format a list of achievements of the author in the fields of neutron and X-ray radiography and tomography during his employment at Necsa.

App 2.1: International Conferences (Presented and Attended)

The author took the opportunity to represent Necsa and South Africa as the neutron and X-ray radiography and tomography expert at various international forums. These forums served as platforms where the author could liaise with his peers in the field of neutron and X-ray tomography, present the status of the research facilities as well as aspects of his own research.

App 2 Table 1: Summary of international forums attended and participated.

Year	City / Country	Conference	Comment (Oral / Poster presentation is standard)
1999	Osaka, Japan	6th WCNR	1st International Conference attended by the author. Introduction to the international scientific community on neutron radiography.
2001	Penn State College, Pennsylvania, USA	4th ITMNR	Met Harold Berger: Pioneer in NRAD
2002	Rome, Italy	7th WCNR	- Session Chairman - Elected member of ISNR Board - Elected Vice-President ISNR - Met John Barton: Pioneer in NRAD
2004	Munchen, Germany	5th ITMNR	- Session Chairman - Serve member ISNR Board
2005	Sydney, Australia	ICNS	
2006	Cairo, Egypt	4th AFNDT	
	Washington DC, USA	8th WCNR	- Session Chairman - Elected President ISNR - Restart International Newsletter on NR
	Oak-Ridge, USA	IAN-2006	
	Munchen, Germany	1st NEUWAVE	
2007	Perth, Australia	ASEG	Presenting as winner of best Lecture at South African Geological Association (SAGA-2007)
2008	Cape Town, South Africa	AAPG	Session Chairman
	Kobe, Japan	6th ITMNR	- Session Chairman - Chairman ISNR Board
2010	Budapest, Hungary	19th IMA	
	Kwa-Maritane, South Africa	9th WCNR	- Host and Chairman of WCNR-9 - Session Chairman - Chairman ISNR Board - Presenting Honorary Membership in Neutron Radiography to J.P Barton, H. Berger and H. Kobayashi
2011	Rabat, Morocco	IAEA-RRT	
2012	Munich, Germany	4th NEUWAVE	
	Kingston, Canada	7th ITMNR	- Session Chairman - Serve member of ISNR Board

Year	City / Country	Conference	Comment (Oral / Poster presentation is standard)
	Durban South Africa	18th WCNDT	- Session Chairman - Exhibition Tomography in NDT
	Cape Town, South Africa	6th ISPT	
	Toronto, Canada	SAfA	
2013	Garching, Germany	1st NINMACH	Session Chairman
	Ghent, Belgium	ICTMS-1	Session Chairman
2014	Grindelwald, Switzerland	10th WCNR	- Session Chairman - Serve member ISNR Board
	Sandton, Johannesburg	21st IMA	Session Chairman
2016	Abingdon, UK	8th NEUWAVE	
	Beijing, China	8th ITMNR	- Session Chairman - Serve member ISNR Board
2017	Vienna, Austria	1st ICARST	Session Chairman
	Lund, Sweden	ICTMS-3	Session Chairman
2018	Sydney, Australia	11th WCNR	- Session Chairman - Serve member ISNR Board

- AAPG: American Association of Petroleum Geologists International Conference and Exhibition
- AFNDT: African Regional and 1st Exhibition on Non-Destructive Testing
- ASEG: Australian Society of Exploration Geophysicists
- IAEA – RRT: International Conference on Research Reactors: Safe Management and Effective Utilization
- IAN: Imaging and Neutrons
- ICARST: International Conference on Applications of Radiation Science and Technology
- ICNS: International Conference on Neutron Scattering
- ICTMS: International Conference on Tomography of Materials and Structures
- IMA: International Mineralogical Association
- ISPT: International Symposium on Process Tomography
- ITMNR: International Topical Meeting on Neutron Radiography
- NEUWAVE: Workshop on Neutron Wavelength Dependent Imaging
- NINMACH: International Conference on Neutron Imaging and Neutron Methods in Archaeology and Cultural Heritage Research
- SAfA: Society of Africanist Archaeologists
- WCNR: World Conference on Neutron Radiography

App 2.2: Rewards and Achievements

App 2 Table 2: Summary of international forums attended and participated.

YEAR	INSTITUTION	AWARD / ACHIEVEMENT
1995	South African Institute for Non-Destructive Testing (SAINT)	Receiving Reisener award for best lecture at SAINT evening meeting.
2003	Necsa Chairman's Award	Establishing and commissioning the 1st Neutron Tomography capability in South Africa, Africa and Southern Hemisphere.
2004	International Society for Neutron Radiology (ISNR)	Elected Vice President of the ISNR at WCNR-7 in Rome, Italy.
2007	South African Geological Association (SAGA)	Best oral presentation at bi-annual SAGA conference.
2008	International Society for Neutron Radiology (ISNR)	Elected President of the ISNR at WCNR-8 in Gaithersburg, USA.
	DST-NRF-rated: C3 researcher	Evaluated C3 category rated researcher.
2010	International Society for Neutron Radiology (ISNR)	Chairing and hosting 9th World Conference on Neutron Radiography in South Africa (WCNR-9).
2011	Necsa Chairman's Award (DInaledi Awards for Innovator and Activator)	Elected President of the International Society for Neutron Radiology (ISNR) and chairing and hosting the 9th World Conference on Neutron Radiography (WCNR-9) in South Africa.
2013	Imaging with Radiation Conference (IMGRAD)	- Establishing with University of the Witwatersrand (WITS) and Stellenbosch University (SUN) the National IMGRAD* Conference series in South Africa. - Chairing and Hosting 1st IMGRAD Conference in South Africa.
2015	DST-NRF-rated: C3 Researcher	Re-evaluated C3 category rated researcher.
2016	SAINT	Receiving H Rohloff Trophy for best research project for 2016 in non-destructive testing in South Africa.
2017	Suid Afrikaanse Akademie vir Wetenskap en Kuns.	Sertifikaat vir beste voordrag by 17th Suid Afrikaanse Akademie vir Wetenskap en Kuns: Studentesimposium.

* IMGRAD: Imaging with Radiation Conference

App 2.3: Equipment and Research Incentive Funding

App 2 Table 3: Summary of international forums attended and participated in.

YEAR	INSTITUTION	AWARD	AMOUNT
2008 – 2020	National Research Foundation	DST-NRF C3 Rated Researcher: Incentive Funding	R40k annually Total: R520k
2010	National Equipment Fund (DST-NEP)	Micro-Focus X-ray tomography facility: (Principle applicant: Dr. Andrew Venter)	R2.3M
2010	DST-NRF KIC	Hosting Radiation Imaging School before WCNR-9	R50k
2011	DST-RISP equipment fund	Neutron radiography facility: (Principle applicant: Dr. Andrew Venter)	R13.8M
2013	DST-NRF KIC	Hosting 1st IMGRAD national conference at Necsa	R50k

App 2.4: Chairman and Host of the 9th World Conference on Neutron Radiography (WCNR-9) at Kwa-Maritane, Pilansberg, South Africa (2010)